
Electronic Thesis and Dissertation Repository

10-15-2012 12:00 AM

Monotonic and Cyclic Behaviour of Steel Fibre-Reinforced and FRP-Steel Fibre-Reinforced Helical Pulldown Micropiles

Mahmoud Meckkey M. El Sharnouby
The University of Western Ontario

Supervisor

M. Hesham El Naggar
The University of Western Ontario

Graduate Program in Civil and Environmental Engineering

A thesis submitted in partial fulfillment of the requirements for the degree in Doctor of Philosophy

© Mahmoud Meckkey M. El Sharnouby 2012

Follow this and additional works at: <https://ir.lib.uwo.ca/etd>



Part of the [Civil Engineering Commons](#), [Computational Engineering Commons](#), [Construction Engineering and Management Commons](#), and the [Geotechnical Engineering Commons](#)

Recommended Citation

El Sharnouby, Mahmoud Meckkey M., "Monotonic and Cyclic Behaviour of Steel Fibre-Reinforced and FRP-Steel Fibre-Reinforced Helical Pulldown Micropiles" (2012). *Electronic Thesis and Dissertation Repository*. 902.

<https://ir.lib.uwo.ca/etd/902>

This Dissertation/Thesis is brought to you for free and open access by Scholarship@Western. It has been accepted for inclusion in Electronic Thesis and Dissertation Repository by an authorized administrator of Scholarship@Western. For more information, please contact wlsadmin@uwo.ca.

**MONOTONIC AND CYCLIC BEHAVIOUR OF STEEL FIBRE-REINFORCED
AND FRP-STEEL FIBRE-REINFORCED HELICAL PULLDOWN MICROPILES**

(Spine title: Monotonic and Cyclic Behaviour of Helical Pulldown Micropiles)

(Thesis format: Integrated-Article)

by

Mahmoud Meckkey El Sharnouby

Graduate Program in Engineering Science
Department of Civil and Environmental Engineering

A thesis submitted in partial fulfillment
of the requirements for the degree of
Doctor of Philosophy

The School of Graduate and Postdoctoral Studies
The University of Western Ontario
London, Ontario, Canada

© Mahmoud Meckkey El Sharnouby 2012

THE UNIVERSITY OF WESTERN ONTARIO
SCHOOL OF GRADUATE AND POSTDOCTORAL STUDIES

CERTIFICATE OF EXAMINATION

Supervisor

Dr. M. Hesham El Naggar

Supervisory Committee

Examiners

Dr. Ashraf A. El Damatty

Dr. Pawel M. Kurowski

Dr. Alan J. Lutenegger

Dr. Abouzar Sadrekarimi

The thesis by

Mahmoud Meckkey El Sharnouby

entitled:

**Monotonic and Cyclic Behaviour of Steel Fibre-Reinforced and FRP-
Steel Fibre-Reinforced Helical Pulldown Micropiles**

is accepted in partial fulfilment of the
requirements for the degree of
Doctor of Philosophy

Date _____

Chair of the Thesis Examination Board

ABSTRACT

Helical piles are a deep foundation system that can be used to support pipelines, telecommunication and transmission towers, and low- and medium-rise buildings. Advantages of helical piles include: short installation time with minimal noise and vibration levels; can be installed with ease in limited accessibility site; and onsite quality control by measurement of installation torque.

The main objective of the current research is to assess the performance of steel fibre-reinforced helical pulldown micropiles (RHPM), and fibre-reinforced polymer-steel fibre-reinforced pulldown micropiles (FRP-RHPM) under axial and lateral monotonic and cyclic loading conditions.

The research methodology involved conducting full scale field testing on: one plain helical pile, 12 RHPM and 12 FRP-RHPM. Piles were subjected to axial static and one-way cyclic loading, and lateral static and two-way cyclic loading. The axial test results were then used to calibrate a three-dimensional finite element model. To calibrate the lateral test results, moment-rigidity curves for the tested piles were generated through three-dimensional finite element models. Along with test results, these curves were used to calibrate a finite difference model.

The experimental investigation under axial loads shows that these pile systems behave as composite pile systems. The grout shaft significantly improves the helical pile axial performance. Cyclic loads resulted in degradation of the shaft resistance, however,

resulted in an improvement of the lead section resistance. The overall pile cyclic response was found to stabilize after a few cycles of loading. Finally, the cyclic loading was found to improve the axial capacity of these systems.

The experimental investigation under lateral loads shows that the grout shaft and/or the FRP sleeve significantly improve the plain helical pile lateral performance and ductility. Two-way cyclic loading resulted in overall degradation in pile stiffness and capacity.

A design procedure for FRP-RHPM and RHPM under axial compression loading conditions is presented. For the lateral direction, a series of design charts that can be used in conjunction with available numerical programs to design such systems are provided.

In general, the RHPM and FRP-RHPM are viable foundation options for axial and lateral monotonic and cyclic loading applications.

Key words: Helical piles, Pulldown micropile, FRP, Steel-fibres, Full-scale field testing, Axial and lateral testing, monotonic and cyclic loading, Load transfer mechanism, Pile capacity, Numerical modelling.

CO-AUTHORSHIP STATEMENT

All the field testing, numerical modeling, interpretation of results and writing the draft and the final thesis were carried out by the candidate himself, under the supervision of Dr. M. Hesham El Naggar. The supervisor's contribution consisted of providing advice throughout the research program and reviewing the draft and the final thesis and publications results from this research.

ACKNOWLEDGMENTS

I would like to express my appreciation and gratitude to the people without whom this thesis would have not been completed.

First, I would like to thank my supervisor Dr. M. Hesham El Naggar for his guidance, support, patience, and continuous encouragement throughout the research period. I have learned a lot from you during the past 6 years. I will never forget those years. Thank you.

I would like to express my appreciation to EBS Engineering and Construction Ltd., and specially Dino Vito, for funding the experimental program, providing the materials and installing the piles.

I am very grateful to Paul Sunseth. Your support, understanding and advice throughout and after this program made me simply want to do the work. I couldn't ask for a better project manager and a mentor.

Thanks for the administrative staff in the structural and geotechnical lab at the University of Western Ontario for their help and advice. Special thanks to Wilber Logan, Melody Richards, Whitney Barrett and Stephanie Laurence.

To my parents, I would have not been who I am without you. You taught me faith and love. You showed me how to succeed. I am proud to be your son.

Finally, thanks to my wife. Your patience, understanding and support are unforgettable. Your love and encouragement are what made this thesis come true. I look forward to continue this journey with you.

TABLE OF CONTENTS

CERTIFICATE OF EXAMINATION	ii
ABSTRACT.....	iii
CO-AUTHORSHIP statement.....	v
ACKNOWLEDGMENTS	vi
Table of Contents	viii
LIST OF TABLES	xiii
LIST OF FIGURES	xiv
LIST OF APPENDICES.....	xviii
LIST OF ABBREVIATIONS, SYMBOLS, NOMENCLATURE	xix
CHAPTER 1	1
1 INTRODUCTION	1
1.1 Helical Piles.....	1
1.2 Helical pulldown® micropiles (HPM) and Steel fibre-reinforced helical pulldown micropiles (RHPM).....	1
1.3 Fibre reinforced-polymer- helical pulldown micropiles (FRP-HPM) and Fibre reinforced polymer-steel fibre-reinforced helical pulldown micropiles (FRP-RHPM)..	2
1.4 Research Objectives	3
1.5 Thesis Outline	4
1.6 Original contributions	6
1.7 References	7

CHAPTER 2	8
2 Literature Review.....	8
2.1 Introduction	8
2.2 Helical piles.....	9
2.3 Installation and termination criteria	11
2.4 Modified helical piles.....	11
2.5 Helical piles under axial monotonic loads	18
2.6 Helical piles under axial cyclic loads.....	27
2.7 Helical piles under lateral monotonic loads	29
2.8 Helical piles under lateral cyclic loads.....	30
2.9 Summary	30
2.10 References	31
CHAPTER 3	37
3 Field investigation of axial monotonic and cyclic performance of reinforced helical pulldown micropiles.....	37
3.1 Introduction	37
3.2 Site Investigation.....	40
3.3 Test Pile Description, Installation and Instrumentation	41
3.4 Field Test Set-up	48
3.5 Testing Procedure.....	49

3.6	Test Results-Stage 1-A.....	51
3.7	Axial Results-Stage I-B.....	56
3.8	Load transfer mechanism in lead section	60
3.9	Axial Capacity of Tested Piles.....	68
3.10	Conclusions	72
3.11	References	75
CHAPTER 4		84
4	Axial monotonic and cyclic performance of FRP-steel fibre-reinforced helical pulldown micropiles (FRP-RHPM)	84
4.1	Introduction	84
4.2	Objectives of Study	90
4.3	Site Investigation.....	91
4.4	Test Pile Description, Installation and Instrumentation.....	92
4.5	Field Test Set-up	97
4.6	Testing Procedure.....	98
4.7	Axial Compression Results	100
4.8	Performance of FRP-RHPM Subjected to Cyclic Loading.....	106
4.9	Monotonic Performance of FRP-RHPM after Cyclic Loading.....	112
4.10	Ultimate Capacity of Test Piles	117
4.11	Prediction of Ultimate Capacity	119

4.12	Conclusions	122
4.13	References	125
CHAPTER 5		134
5	Numerical investigation of axial monotonic performance of reinforced helical pulldown micropile (RHPM) and FRP-steel fibre-reinforced helical pulldown micropiles (FRP-RHPM)	134
5.1	Introduction	134
5.2	Pile Description and Soil Conditions	135
5.3	Geometry and Model Discretization	139
5.4	Boundary conditions	140
5.5	Interaction modelling	141
5.6	Material model	141
5.7	Loading and solution steps	141
5.8	Limitations	142
5.9	Verification of FE model.....	142
5.10	Parametric Study.....	146
5.11	Design Method for Axial Compressive Loading.....	155
5.12	Conclusions	160
5.13	References	161
CHAPTER 6		168

6	Field investigation of lateral monotonic and cyclic performance of steel fibre-reinforced helical pulldown micropiles (RHPM) and fibre glass-reinforced polymer-fibre reinforced helical pulldown micropiles (FRP-RHPM).....	168
6.1	Introduction	168
6.2	Site Investigation.....	172
6.3	Test Pile Description and Installation	173
6.4	Field Test Set-up	177
6.5	Monotonic behaviour of RHPM	182
6.6	Cyclic Behaviour of RHPM.....	187
6.7	Monotonic behaviour of FRP-RHPM	193
6.8	Comparison between behaviour of FRP-RHPM and RHPM.....	201
6.9	Ultimate capacity prediction	203
6.10	Development of Design charts	211
6.11	Conclusions	217
6.12	References	219
	CHAPTER 7	225
7	SUMMARY, CONCLUSIONS AND RECOMMENDATIONS.....	225
7.1	Summary and Conclusions.....	225
7.2	Recommendations for future research.....	228
	APPENDICES	230
	Curriculum Vitae	232

LIST OF TABLES

Table 3-1. Soil profile and SPT count established from boreholes.	80
Table 3-2. Summary of geotechnical properties of soil from BH-1 and BH-2.....	81
Table 3-3. Cyclic tests results for Stages I-A and I-B.	82
Table 3-4. Pile capacity and torque factors for tested piles.	83
Table 4.1. Soil profile and SPT count established from boreholes.....	130
Table 4.2. Summary of geotechnical properties of soil from BH-1 and BH-2.....	131
Table 4.3. Cyclic load test results.	132
Table 4.4. Observed ultimate capacities of test piles.....	133
Table 5.1. Material properties for pile components.....	165
Table 5.2. Range of soil parameters used for calibration of RHPM and FRP-RHPM. ..	165
Table 5.3. Soil properties used for the parametric study.	166
Table 5.4. Comparison between computed and predicted ultimate capacity for lead section in sand.....	167
Table 6.1. Test results for RHPM and FRP-RHPM.....	223
Table 6.2. Soil properties used in LPILE Plus (Ensoft Inc. 2011).....	224

LIST OF FIGURES

Figure 2.1. Typical helical pile assembly; lead section and two extensions.....	10
Figure 2.2. Typical schematic of HPM or RHPM.	13
Figure 2.4. Possible failure mechanisms for helical piles under compression: (a) Individual bearing; and (b) cylindrical shear failure.....	21
Figure 2.5. Schematic of piles failure components for compressive loading; after Livneh and El Naggar (2008).....	24
Figure 3.1. (a) Schematic of plain helical pile. (b) Schematic of reinforced pulldown micropiles and positions of strain gauges.	44
Figure 3.2. (a) Strain gauge installation. (b) Strain gauge protection through tape.....	47
Figure 3.3. Full view of axial load test set-up.....	49
Figure 3.4. Cyclic load test protocol.....	51
Figure 3.5. Results for Stage I-A: (a) load vs. displacement; (b) cyclic load vs. displacement (average cyclic load of 200 kN); (c) cyclic vs. displacement (average cyclic load of 270 kN).	55
Figure 3.6. Test results for Stage I-B: (a) cyclic load vs. displacement; (b) Load vs. displacement; (c) shaft resistance vs. applied load for RHPM-10.....	59
Figure 3.7. Loads at displacement equal to 13 % of shaft diameter for Stages I-A and I-B.	60
Figure 3.8. Measured load transfer in lead section and % resistance of helices; (a), (b) plain helical pile; (c), (d) RHPM-4; (e) RHPM-6; (f), (g) RHPM-10; (h) RHPM-10 during cyclic loading. (Note: G = Gauge).	67
Figure 4.1. (a) FRP-RHPM test pile profile after installation; (b) FRP-RHPM during installation and components.....	96
Figure 4.2. Full view of axial and cyclic test set-up.	98
Figure 4.3. Test loading protocol for Piles 1 to 5; and for Piles 6 to 13.....	100

Figure 4.4. Initial static load displacement response, Phase I.	101
Figure 4.5. Shaft resistance vs. applied load for FRP Pile 1, Phase I.	103
Figure 4.6. (a) Measured load transfer in lead section for FRP Pile 1; (b) Measured load transfer in lead section for plain pile; (c) Helix resistance vs. displacement for plain pile.	106
Figure 4.7. Cyclic load-displacement response after large static loading (Phase I).	108
Figure 4.8. Cyclic test results for piles with no prior large static load (Phase II): (a) cyclic load-displacement response; (b) shaft resistance vs. applied load; (c) measured load at gauges vs. applied load for FRP Pile 6.	111
Figure 4.9. Full load-displacement response for Phase I.	113
Figure 4.10. (a) Full load-displacement response for Phase II; (b) Full load-normalized displacement (% of shaft diameter) response for Phase II (c) Shaft resistance vs. applied load.	115
Figure 4.11. FRP Pile 6: Measured load at gauges vs. applied load (Phase II).	117
Figure 5.1. Dimensions and schematic of test piles used for FE verification: (a) Schematic of plain helical pile; (b) RHPM test pile profile; (c) FRP-RHPM test pile profile.	138
Figure 5.1. Typical finite element mesh.	140
Figure 5.3. Comparison between computed and test load-displacement curves for plain helical pile.	143
Figure 5.4. Comparison between computed and test load-displacement curves for: (a) RHPM; (b) FRP-RHPM.	145
Figure 5.6. Schematic of pile dimensions and soil type along pile depth used for FE analysis.	147
Figure 5.7. Load-normalized displacement (% of shaft diameter) response for RHPM for grouted shaft in Soft, Medium and Stiff clay and lead section in: (a) Loose Sand; (b) Medium sand; (C) Dense sand.	149

Figure 5.8. Computed load-normalized displacement (% of shaft diameter) response for RHPM; shaft in soft clay and lead section in loose, medium and dense sand.....	150
Figure 5.9. Contours of axial strains at 25 mm pile head displacement for RHPM with shaft embedded in soft clay and lead section in (a) dense sand; (b) medium sand; (c) loose sand.	152
Figure 5.10. Load displacement curves for SS 175 (plate thickness 9.5 mm) and for SS 225 (plate thickness = 13 mm) for RHPM with shaft in soft clay and lead section in (a) loose sand; (b) medium sand; (c) dense sand.....	154
Figure 6.1. (a) Plain pile configurations; (b) RHPM test pile profile after installation; (c) FRP-RHPM test pile profile after installation.	176
Figure 6.2 (a) Lateral test set-up; first set-up; (b) Lateral test set-up; second set-up.	180
Figure 6.3. Cyclic test set-up.	181
Figure 6.4. Cyclic test protocol.....	182
Figure 6.5. Load-displacement response for RHPM.	183
Figure 6.6: (a) Gap opening behind the pile-RHPM, static test; (b) Radial cracks profile at end of static test-RHPM.....	186
Figure 6.7. Cyclic load vs. displacement for RHPM 7.	188
Figure 6.8. Cyclic load vs. displacement for first cycle at 5,10,15 and 20 kN for RHPM 7.	189
Figure 6.9. Load displacement for first and last cycle for (a) 10 kN; (b) 15 kN; (c) 20 kN; and (d) 25 kN [() = no. of cycles].	191
Figure 6.10. Static and backbone curves for RHPM.	192
Figure 6.11. Load-displacement response for RHPM 3 and 5.....	194
Figure 6.12. Gap opening at end of testing, FRP-RHPM static test.	195
Figure 6.13. Cyclic load vs. displacement for FRP-RHPM 8.....	196

Figure 6.14. Load displacement for first and last cycle for (a) 10 kN, (b) 15 kN, (c) 20 kN, (d) 25 kN, and (e) 30 kN [() = no. of cycles].	198
Figure 6.15. Static and backbone curves for FRP-RHPM.	199
Figure 6.16. Load-displacement response for FRP-RHPM for piles with no prior lateral cyclic load (LC) and piles with prior lateral cyclic load.	200
Figure 6.17. Load-displacement response for FRP-RHPM 6 and RHPM 2.	202
Figure 6.18. Cyclic load displacement for FRP-RHPM, RHPM and plain pile at last cycle of loading.	203
Figure 6.19. Typical finite element mesh, (a) RHPM, and (b) FRP-RHPM.	206
Figure 6.20. Fibre-reinforced grout model: (a) in compression; (b) in tension.	208
Figure 6.21. Computed M-EI for RHPM and FRP-RHPM test piles.	209
Figure 6.21 Comparison between computed and experimental results for (a) RHPM 3; (b) FRP-RHPM 5.	211
Figure 6.22. M-EI charts for 152.4 mm (6 in.), 178.8 mm (7 in.) and 203.2 mm (8 in.) grout shaft diameters for: (a) SS 175; (b) SS 225; (C) SS 225.	213
Figure 6.23. Computed load-displacement curves for RHPM with different shaft configurations.	214
Figure 6.24. M-EI charts for 140 mm (5.5 in.), 125 (5 in.) and 116 (4.5 in.) FRP pipe diameter for: (a) SS 175; (b) SS 225; (C) SS 225.	216
Figure 6.25. Computed load-displacement for different FRP-RHPM configurations.	217
Figure A.1. Installation torque versus depth for SS 225 piles used for pre-drilling. Pile numbers correspond to same pile numbers in Chapter 3.	230
Figure A.2. Installation torque versus depth for SS 200 reaction piles.	231
Figure A.3. Installation torque versus depth for RHPM.	231

LIST OF APPENDICES

APPENDIX A.....	230
-----------------	-----

LIST OF ABBREVIATIONS, SYMBOLS, NOMENCLATURE

A_h	projected bearing area of one helix
A_s	steel shaft cross-sectional area
C	soil cohesion
A_{shaft}	surface area of the soil-shaft interface
C_a	adhesion along the pile-soil interface
C_u	undrained shear strength of the soil
D	helix diameter
d_t	tensile damage parameter for steel fibre-reinforced grout
E_{FRP}	FRP tube elastic modulus
E_g	steel fibre-reinforced grout elastic modulus in compression
E_s	steel elastic modulus
E_t	steel fibre-reinforced grout elastic modulus in tension
FEM	Finite Element Model
FHWA	Federal Highway Administration
FRP	fiber reinforced polymer

FRP-HPM	Fibre-reinforced polymer-helical pulldown micropile
FRP-RHPM	Fibre-reinforced polymer-steel-fibre reinforced helical pulldown micropile
f_c'	steel fibre reinforced grout compressive strength
f_t	steel fibre reinforced grout tensile strength
f_{bu}/f_{cu}	biaxial to uniaxial compressive ratio of the steel fibre reinforced grout
f_{yFRP}	yield stress of the FRP material
f_{ys}	yield stress of steel material
f_{utFRP}	ultimate strength of the FRP material
f_{uts}	ultimate strength of the FRP material
G	shear modulus
K_c	ratio of the second stress invariant on the tensile meridian to that on the compressive meridian for a given value of the first stress invariant
K_o	in-situ coefficient of lateral earth pressure
K_t	an empirical torque factor
K_{taper}	pile taper coefficient
L	pile length

l	length between the uppermost and lower most helices
LDT	Linear Displacement Transducers
N_q	bearing capacity factor
N_c	bearing capacity factor
N_{60}	corrected number of blows at 70% hammer input energy
n	number of piles in a pile group
P-HSP	plain helical screw pile
Q_{bearing}	bearing resistance of one helix
Q_c	group efficiency factor
Q_g	ultimate capacity of a pile group
Q_{lead}	ultimate resistance of a lead section
Q_{shaft}	shaft resistance along the pile-soil interface
Q_s	shaft resistance along the cylindrical failure surface
Q_u	ultimate resistance of a plain helical piles, RHPM or FRP-RHPM
q	unit bearing capacity below one helix
RHPM	reinforced helical pulldown micropile

SCC	self consolidating concrete
T	average installation torque over the last 1 m
α	adhesion coefficient
α_{taper}	taper angle
μ_c	coefficient of friction between hardened grout and steel or FRP
δ	angle of friction along the taper surface
ϕ	internal friction angle of soil
γ	unit weight of the soil
γ'	effective unit weight of the soil
γ_{sub}	submerged unit weight of the soil
σ_v'	vertical effective stress at a point along the pile shaft
τ	soil shear strength along the cylindrical failure surface
ν_g	steel fibre-reinforced grout Poisson's ratio
ν_{FRP}	FRP Poisson's ratio
ν_s	steel Poisson's ratio

ε	field measured strain
ε_{cu}	steel fibre-reinforced grout ultimate strain
ζ	natural logarithm of the ratio between the pile radius and radius at which shear stress becomes negligible

INTRODUCTION

1.1 Helical Piles

Helical piles are a deep foundation system that can be used to support pipelines, telecommunication and transmission towers, and low- and medium-rise buildings. They can be used for both underpinning of deficient foundations of existing buildings and for supporting new foundations. With recent changes of building codes stipulating increased seismic forces, there is an increasing demand for a retrofitting tool that can be reliably used to upgrade the seismic resistance of existing foundations.

The segmented helical (screw) pile (HSP) consists of relatively small galvanized central square shaft (SS) or rounded shaft (RS) fitted with one or more (up to 4) helices. The SS sizes range from 42 mm to 57 mm and RS sizes range from 73 mm to 114.3 mm. The first segment of a pile (lead section) contains the helices and is installed to the desired depth by adding extensions connected onsite using bolted couplings. The helices diameters range between 150 mm to 400 mm, and have a standard pitch of 76 mm (3").

1.2 Helical pulldown® micropiles (HPM) and Steel fibre-reinforced helical pulldown micropiles (RHPM)

A Helical Pulldown® Micropile (HPM) consists of a helical pile installed with a grout column surrounding the pile central shaft along the extensions. This pile system was first introduced by Vickars and Clemence (2000) who demonstrated that the addition of a grout column to helical piles results in a considerable increase in the ultimate axial

capacity and performance of the pile. The naming of this pile system stems from its installation method. The fact that the grout is poured by gravity and it surrounds a central steel shaft renders the shaft system as a Type A micropile, according to the FHWA micropile design and construction implementation manual (Armour et al., 2000).

The RHPM tested in this study differs from the HPM in that the grout mix contains steel fibres that are added during construction. The main advantage of addition of such fibres is that they provide ductility and therefore energy dissipation to the material which are favorable characteristics for structures to resist earthquake, wind and impact loads (de Oliveira Junior et al., 2010; Abbas and Mohsin, 2010).

1.3 Fibre reinforced-polymer- helical pulldown micropiles (FRP-HPM) and Fibre reinforced polymer-steel fibre-reinforced helical pulldown micropiles (FRP-RHPM)

The use of FRP composite materials in construction has increased significantly in the past few years. Their features include: light weight (i.e. 1/4 to 1/8 of steel), corrosion resistance, minimum maintenance and environmental resistance. These features render them an attractive option for deep foundations.

A composite helical-FRP-grout pile system was first investigated by Abdelghany and El Naggar (2010) [FRP-HPM: no steel fibres added to the grout mix]. They reported some difficulty during installation of the FRP tubes as a result of the soil resistance; additional torque was required to install the tubes, and in some cases the embedment depth was limited as the maximum torque was reached. The piles offered slight improvement over

the helical piles. They concluded that the FRP-HPM is a viable foundation option and should be explored further.

In this study, an innovative installation method was employed that resulted in successful installation of the FRP tube in stiff clay soil. In addition, steel-fibres were added to the grout mix, producing a composite pile system namely, FRP-steel-fibre reinforced helical pulldown micropile (FRP-RHPM).

1.4 Research Objectives

The main objective of this research is to develop an effective piling system that can significantly improve the capacity, and overcome the drawbacks of helical piles, resulting in a pile system that can be effectively used for both static and cyclic loading applications. The specific objectives of this research program are:

- 1-Study the constructability of the RHPM compared to HPM, and to develop an efficient technique/apparatus for the installation of the FRP-RHPM.
- 2-Introduce modifications to the structural components of RHPM and FRP-RHPM in order to improve their performance under axial and lateral loading conditions.
- 3-Understand the load-displacement curves of RHPM and FRP-RHPM and evaluate the capacity of these pile types under axial compression loads, considering the load transfer mechanism within the lead section (i.e. individual bearing or cylindrical shear).

4-Investigate the performance of RHPM and FRP-RHPM under axial cyclic loading, examine the effect of cyclic loading on their axial performance, and determine the load sharing mechanism between the shaft and lead section during and post cyclic loading.

5-Develop a three-dimensional finite element model that can simulate the axial behaviour of these pile systems. Utilize the developed model to conduct a parametric study to characterize the behaviour of the investigated pile systems in different soil conditions.

6-Develop a design procedure for the RHPM and FRP-RHPM, based on the results of the experimental program and the FE analysis.

7-Develop an economical testing apparatus that can enable testing two piles simultaneously under monotonic and two-way cyclic lateral loading conditions.

7-Evaluate the load-displacement curves and capacity of test piles under lateral loads.

8-Investigate their suitability for cyclic loading applications.

9-Develop design curves that can be used in conjunction with other existing methods to estimate the lateral capacity of such pile systems.

1.5 Thesis Outline

This thesis has been produced in accordance with the guidelines of the School of Graduate and Postdoctoral Studies. Substantial parts of this thesis have been published, accepted or submitted in peer-reviewed journal and international conferences.

Chapter 2 provides a brief review of previous studies conducted on helical piles, RHPM and FRP-RHPM.

In Chapter 3, the performance of RHPM pile is investigated under axial monotonic and cyclic loads, through full-scale field testing. In chapter 4, a novel installation technique that minimizes soil disturbance is employed for the construction of FRP-RHPM. The results of full-scale axial testing on fibre-reinforced polymer-steel fibre-reinforced pulldown micropiles (FRP-RHPM) subjected to axial one-way cyclic and monotonic loads are presented.

Chapter 5 presents the development and verification of a numerical simulation of the axial monotonic behaviour of plain helical piles, reinforced helical pulldown micropiles (RHPM) and FRP-steel fibre-reinforced helical micropiles (FRP-RHPM). In addition, a design procedure is suggested.

Chapter 6 introduces the components of a specially designed and manufactured dual-testing system that allows testing two piles under static and cyclic loading simultaneously. In addition, it describes a field study of the lateral monotonic and cyclic behaviour of RHPM and the novel FRP-RHPM. Moreover, it presents design curves for both pile systems that can be used in lateral loading applications.

Chapter 7 provides a summary of the research work, conclusions, and recommendations for future research.

1.6 Original contributions

This research explores the suitability of using the RHPM and FRP-RHPM as candidate foundation systems for seismic retrofitting of existing foundations as well as for an efficient foundation option for new construction. The specific contributions are:

1-Developing a new installation technique and components of a novel foundation system, the FRP-RHPM, which proved to be feasible, even in hard soil conditions. The addition of steel-fibres as part of the pile construction contributed to the lateral resistance, and maintained the structural integrity of the system.

2- Evaluating the performance characteristics of these pile systems under axial and lateral monotonic and cyclic loading conditions, based on a considerable number of pile load tests.

3- Establishing a design procedure for RHPM and FRP-RHPM under axial loading conditions.

4- Providing design charts to be used in conjunction with available methods to estimate their lateral resistance.

5- Lastly, this research provides engineers in practice with a data base and analysis tools that facilitate achieving a feasible design with confidence.

1.7 References

Abbas, A., and Mohsin, S.S. 2010. Numerical modeling of fibre-reinforced concrete. In proceedings the international Conference on Computing in Civil and Building Engineering.

de Oliveira Junior, L.A., dos Santos Borges, V.E., Danin, A.R., Machado, V.R., de Lima Araujo, D., El Debs, M.KH., Rodrigues, P.F. 2010. Stress-strain curves for steel-fibre reinforced concrete in compression. *Revista Materia*. 15(2): 260-266.

Abdelghany, Y., and El Naggar, M.H. 2010. Full-scale experimental and numerical analysis of instrumented helical screw piles under axial and lateral monotonic and cyclic loadings-A promising solution for seismic retrofitting. In Proceedings of the 6th International Engineering and Construction Conference. American Society of Civil Engineers, Cairo, Egypt.

O'Neill, M.W., and Reese, L.C. 1999. Drilled shafts: construction procedures and design methods. Federal Highway Administration, FHWA-IF-99-025, Washington D.C.

Vickers, R.A., and Clemence, S.P. 2000. Performance of helical piles with grouted shafts. In Proceedings of Sessions of Geo-Denver 2000 - New Technological and Design Developments in Deep Foundations. American Society of Civil Engineers, GSP 100, v 288, pp. 327-341.

LITERATURE REVIEW**2.1 Introduction**

Piles are structural members that transfer loads to competent soil layers below ground surface where shallow foundations are not adequate. They can generally be classified according to their material: timber, concrete (cast-in-place; precast), steel (pipe pile; H-section), or composite piles. Pile can also be classified according to their method of installation: driven (precast; cast-in-situ), bored, or screwed (helical piles), etc. Moreover, piles can be categorized based on the ground displacement during installation: large displacement (close ended steel pipes; tapered steel piles), small displacement (helical piles; H-sections), or non-displacement (bored piles).

Piles can be subjected to axial, compression or tension loads, lateral loads, and/or moments. Under axial loading, piles carry their loads through end bearing, shaft friction or a combination of both. The load transfer depends on the pile and soil properties along the shaft and below the pile. Under lateral loading, piles transfer their loads through bearing on the surrounding soil.

In this chapter, a description of helical piles and their installation technique is provided. This is followed by the description of the innovative modified helical pile types along with their installation methodology. The literature review also covers the performance of helical piles under axial and later monotonic and cyclic loading conditions.

2.2 Helical piles

Helical piles are a deep foundation system that can be used in light and medium structural loads. They are installed using mechanical torque with minimal noise and vibration levels. They are suitable for applications involving expansive soils and ad-freeze conditions and are advantageous in limited access installations. One of their greatest advantages is that they offer onsite quality control by monitoring installation torque. Helical piles can be used for both underpinning of deficient foundations of existing buildings and for supporting new foundations using pile caps. With recent changes of building codes stipulating increased seismic forces, there is an increasing demand for a retrofitting tool than can be reliably used to upgrade the seismic resistance of existing foundations. The segmented helical piles are examined in this study as a candidate for seismic retrofitting of existing foundations, which can also provide an efficient foundation option for new construction.

The segmented helical (screw) pile (HSP) consists of relatively small galvanized central square shaft (SS) or rounded shaft (RS) fitted with one or more (up to 4) helices. SS sizes range from 42 mm to 57 mm and RS sizes from 73 mm to 114.3 mm. The first segment (lead section) contains the helices and is installed to the desired depth by adding extensions connected onsite using bolted couplings. The helices diameters range between 150 mm to 400 mm. For multi-helix lead sections, larger diameter helices are placed near the top followed by smaller diameter helices at a spacing of about three times the helix diameter. Helices have standard pitch of 76 mm (3"). A schematic of a typical helical pile is shown in Figure 2.1.

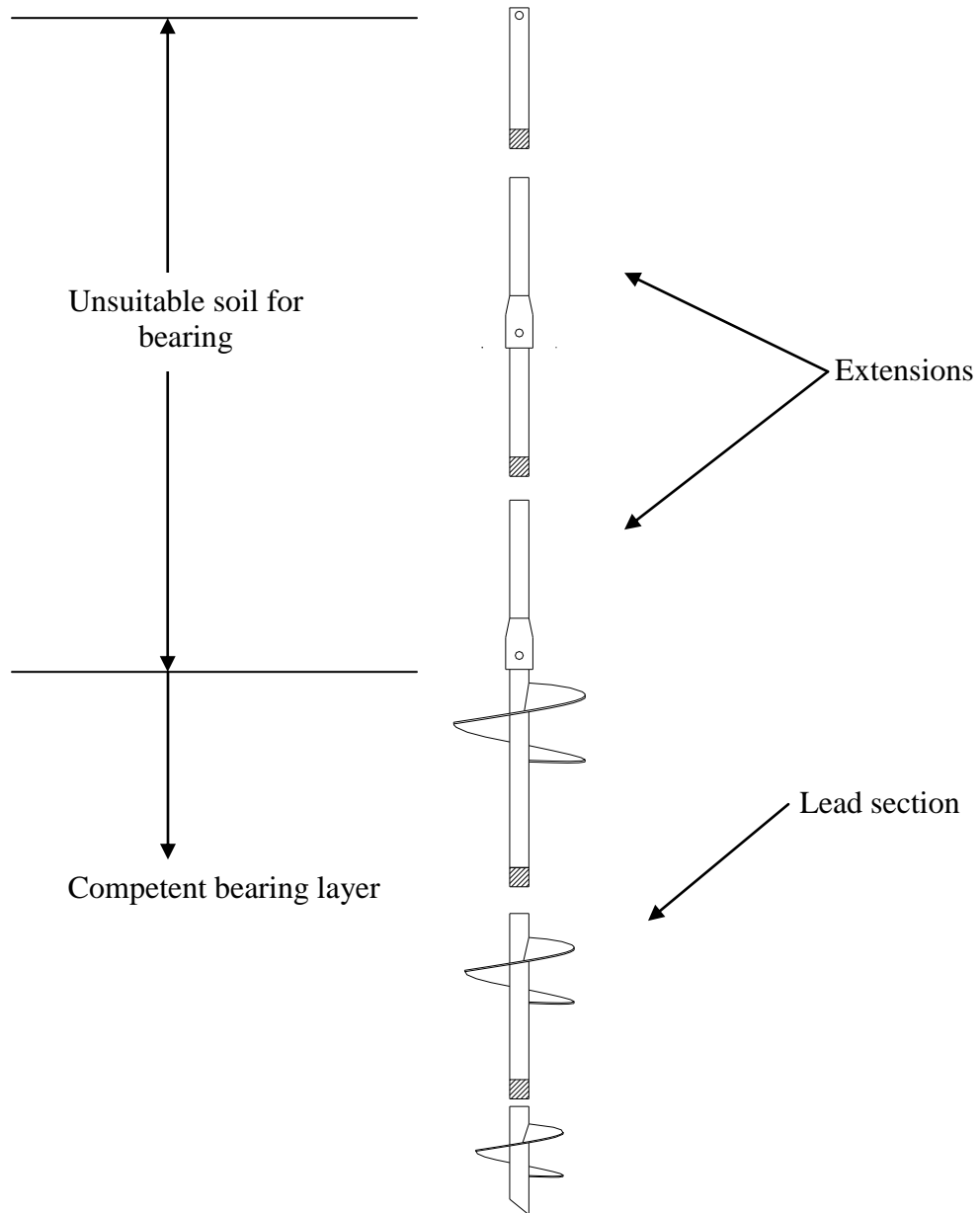


Figure 2.1. Typical helical pile assembly; lead section and two extensions.

2.3 Installation and termination criteria

The plain helical pile is installed in the ground through mechanical rotation accompanied with axial force. The helix geometry is of a true ramped spiral with a uniform pitch. This geometry provides a downward force that pulls the pile in during rotation. The lead section is installed first, and then the necessary number of extensions is connected on-site until the lead section reaches a competent soil layer (See Figure 2.1). However, each pile category has a torque rating, which is defined as the maximum torque that can be applied during installation, and measured torque during installation should not surpass the respective torque rating. The choice of the pile dimensions may depend in part on the anticipated torsional resistance during installation.

2.4 Modified helical piles

2.4.1 HPM

The axial capacity of helical piles under compression can be limited by the buckling capacity of its shaft, especially for long piles and/or piles installed in weak soils. Vickers and Clemence (2000) introduced the Helical Pulldown[®] Micropile (HPM). It consists of a helical pile installed with a grout column surrounding the pile central shaft along the extensions. The helical micropile has a grout shaft diameter of less than 300 mm, and is reinforced by the steel shaft (extension) of the helical pile. Vickers and Clemence (2000) demonstrated that the addition of a grout column to helical piles results in a considerable increase in the ultimate axial capacity and performance of the pile. A schematic of HPM is shown in Figure 2.2.

Abdelghany (2008) and El Naggari and Abdelghany (2007a, 2007b), examined several modifications to the HPM installed in clayey soils under axial loading conditions. These modifications include: enhanced grout mix, using steel fibre reinforcement in the grout mix; and encasing part of the grout column with relatively rigid fibre reinforced polymer tubes. A brief description of the modifications attempted is below.

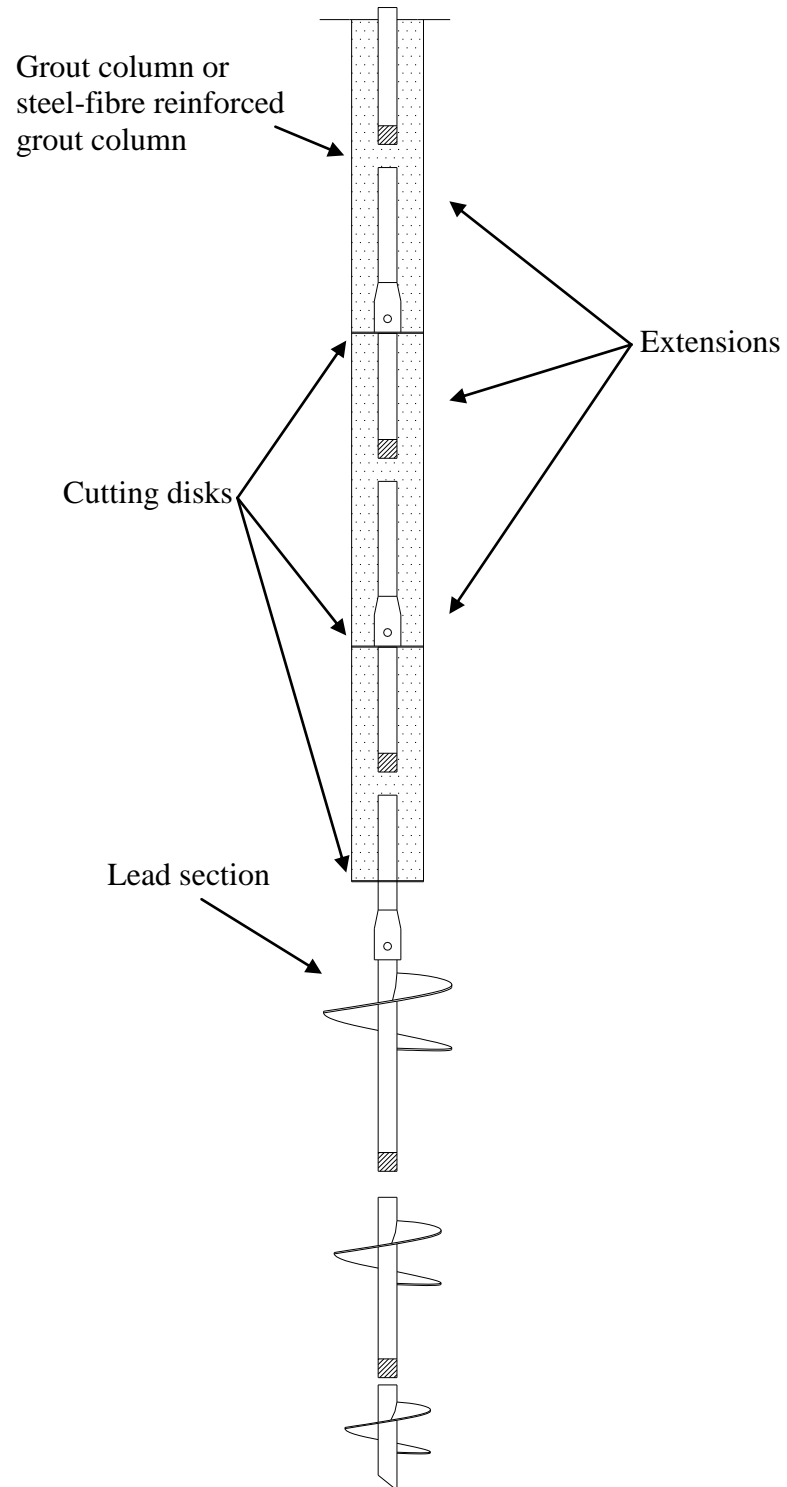


Figure 2.2. Typical schematic of HPM or RHPM.

2.4.2 Steel fibre-reinforced helical pulldown micropiles (RHPM)

The steel fibre-reinforced helical pulldown micropile is a modification to the HPM by adding steel fibres to the grout mix. The installation procedure is primarily the same as the HPM, as shown in Figure 2.2. The main advantage of addition of such fibres is that they provide ductility and therefore energy dissipation to the material which are favorable characteristics for structures to resist earthquake, wind and impact loads (de Oliveira Junior et al 2010; Abbas and Mohsin 2010). Despite the increased use of steel fibre-reinforced concrete/grout in structural application, its use did not extrapolate yet from structural applications to foundation engineering. Expanding their use to foundation engineering, given the low associated cost, may result in a better performing foundations and more economical design.

2.4.3 Fibre reinforced grouted helical screw piles FRP-HPM

The use of FRP composite materials in construction has increased significantly in the past few years. FRP materials are made of a polymer matrix reinforced with fibreglass (or other fibres). Their features include: light weight (i.e. 1/4 to 1/8 of steel), corrosion resistance, minimum maintenance and environmental resistance. These features render them an attractive option for deep foundations.

Iskander et al. (2001) provided a detailed parametric study on drivability of FRP composite piling using wave equation analysis. They looked at long term performance, driveability of FRP piles relative to steel piles, effect of piles properties on drivability. They concluded that the driveability of FRP material depends on the specific weight and the elastic modulus of the composite section. They also recommended that durability of

FRP piling should be investigated. Ashford and Jakrapiyanun (2001) compared the drivability of FRP piles to piles of conventional material. They found that the drivability of FRP piles compared well with steel and precast pre-stressed piles.

Other investigators looked at the performance of FRP-concrete filled piles under compression and lateral loads. Pando et al. (2000) conducted full scale tests on piles consisting of FRP tubes filled with concrete and pre-stressed piles. They found that while piles display similar behaviour in compression, the lateral capacity of FRP-concrete filled piles were less than pre-stressed concrete piles.

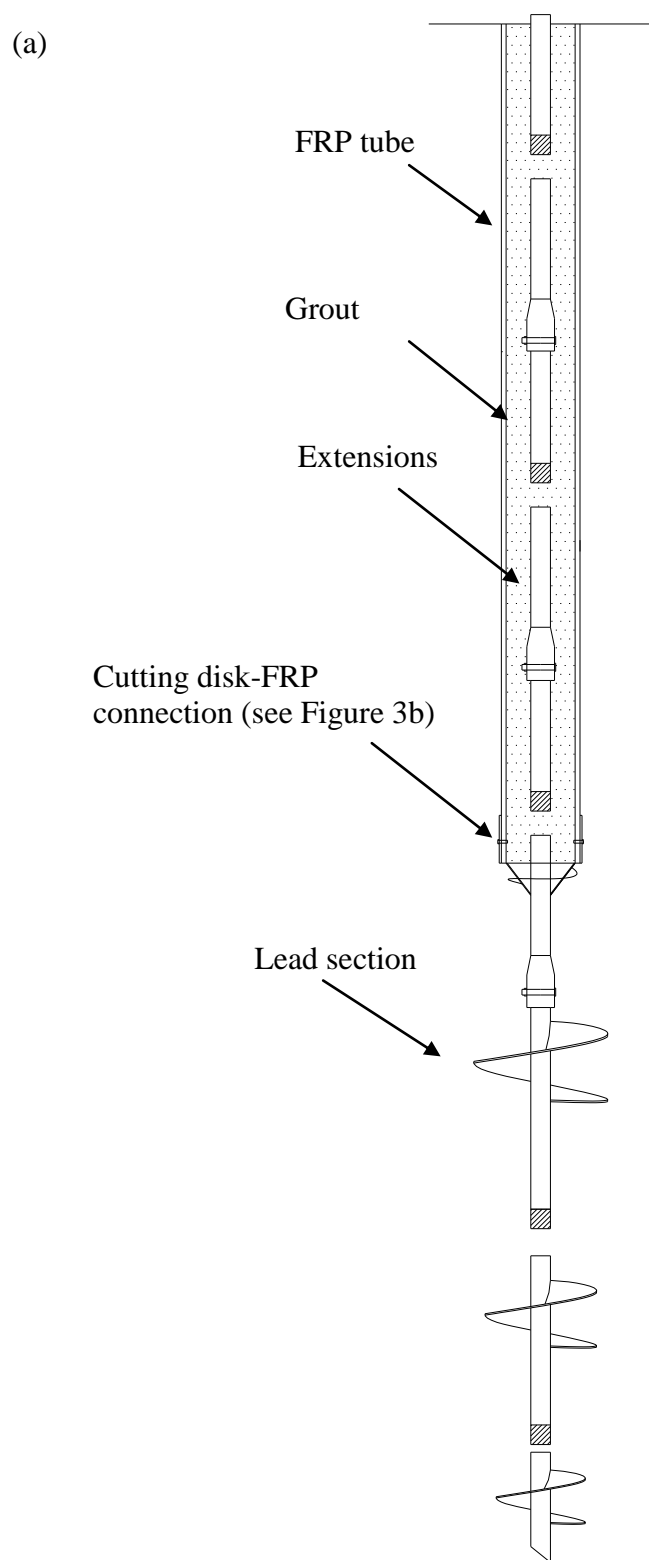
Sakr et al. (2004a) developed a novel technology for the construction of FRP piles. A toe driving technique was developed to install empty FRP tubes into the soil followed by casting self-consolidating concrete (SCC) into the tubes. They found that the toe driving technique was very suitable for installing FRP piles in dense soils. They also found that the axial uplift capacity of FRP-SCC piles and steel piles were comparable. However, the lateral capacity of FRP-SCC piles was less than that of steel piles. Sakr et al. (2004b) stated that the FRP-self-consolidating concrete piles are an attractive option for deep foundation industry.

More recently, Guades et al. (2012) conducted a review on the driving performance of FRP composite piles. They found that driving hammers used, resistance offered by the soil, and the impact strength of the pile materials are the main factors affecting the driving performance of FRP composite piles. They concluded that FRP hollow piles, just

like other composite piles, provide significant advantages over traditional piles in hard environments.

Given the advantages of FRP-concrete piles, along with those of helical piles, a composite helical-FRP-grout pile system was first investigated by Abdelghany (2008) and Abdelghany and El Naggar (2010). It consists of the HPM and an FRP tube infilled with grout mix (see Figure 2.3a). The lead section was first installed. Afterwards, the FRP was seated on a specially manufactured cutting disk that was designed to accommodate the FRP tube. The tube was bolted to the cutting disk (see Figure 2.3b) which allowed the FRP tube to rotate with the same rate of penetration as the steel central shaft. The Tube and the central shaft were connected to the driving machine through two collars. More details on the installation procedure can be found in Abdelghany (2008). A schematic of typical profile of FRP-HPM is shown in Figure 3a and a photo of the cutting disk-FRP connection is shown in Figure 2.3b.

They reported some difficulty during installation of the FRP tubes as a result of the soil resistance; additional torque was required to install the tubes, and in some cases the embedment depth was limited as the maximum torque was reached. The piles offered slight improvement over the helical piles. The fact that the FRP-HPM didn't offer a considerable increase in the performance was attributed to the disturbance within the inter-helix zone (and disturbance along the FRP tube) caused by the additional torque required for installation of the FRP tube. They concluded that the FRP-HPM is a viable foundation option and should be explored further.



(b)



Figure 2.3. (a) Typical schematic of FRP-HPM; and (b) Cutting disk – FRP tube connection above top helix; after Abdelghany (2008).

2.5 Helical piles under axial monotonic loads

2.5.1 Theoretical capacity

The axial capacity of helical piles can be evaluated considering two load transfer mechanisms: individual helix bearing or the cylindrical shear methods. The individual bearing method considers the pile capacity as the sum of the individual bearing capacity of each helical plate, as shown in Figure 2.4a. The cylindrical shear method assumes that the load is transferred to the soil through a cylinder of a soil mass that is enclosed between the upper and lower helices, and bearing of the upper helix for tension loading or lower helix for compression loading, as shown in Figure 2.4b, such as:

$$[2.1] Q_u = \sum_1^n Q_{bearing}$$

or

$$[2.2] Q_u = Q_{bearing} + Q_s$$

$$[2.3] Q_{bearing} = A_h(qN_q)$$

$$[2.4] Q_s = \tau l \pi D$$

where Q_u is the ultimate capacity, Q_b is the bearing capacity of one helix, Q_s is the shaft resistance along the cylindrical failure surface, n is the number of helices, A_h is the projected bearing area, q is the unit bearing capacity below the helix, N_q is the bearing capacity factor., τ is the soil shear strength, l is the length between the uppermost and lower most helices and D is the helix diameter.

The failure mechanism depends primarily on the helix spacing ratio, defined as ratio of helix spacing to helix diameter, and soil conditions. Kulhawy (1985) stated that if the helices are widely spaced, anchor capacity is that of several single plates. On the other hand, several studies showed that cylindrical failure surface develops between the helices, especially in clayey soil. Examples for these studies include: Mooney et al. (1985), El Naggar and Abdelghany (2007a, 2007b), Livneh and El Naggar (2008),

Merifield and Smith (2010), Narashima Rao and Prasad (1993). They conducted model scale tests, full scale tests, finite element modelling, and upper bound solutions. Spacing ratios were as large as 4.5. All studies found that the cylindrical failure surface develop between the helices, except for Narashima Rao and Prasad (1993) who concluded that for spacing ratios larger than 1.5, failure surface is not cylindrical.

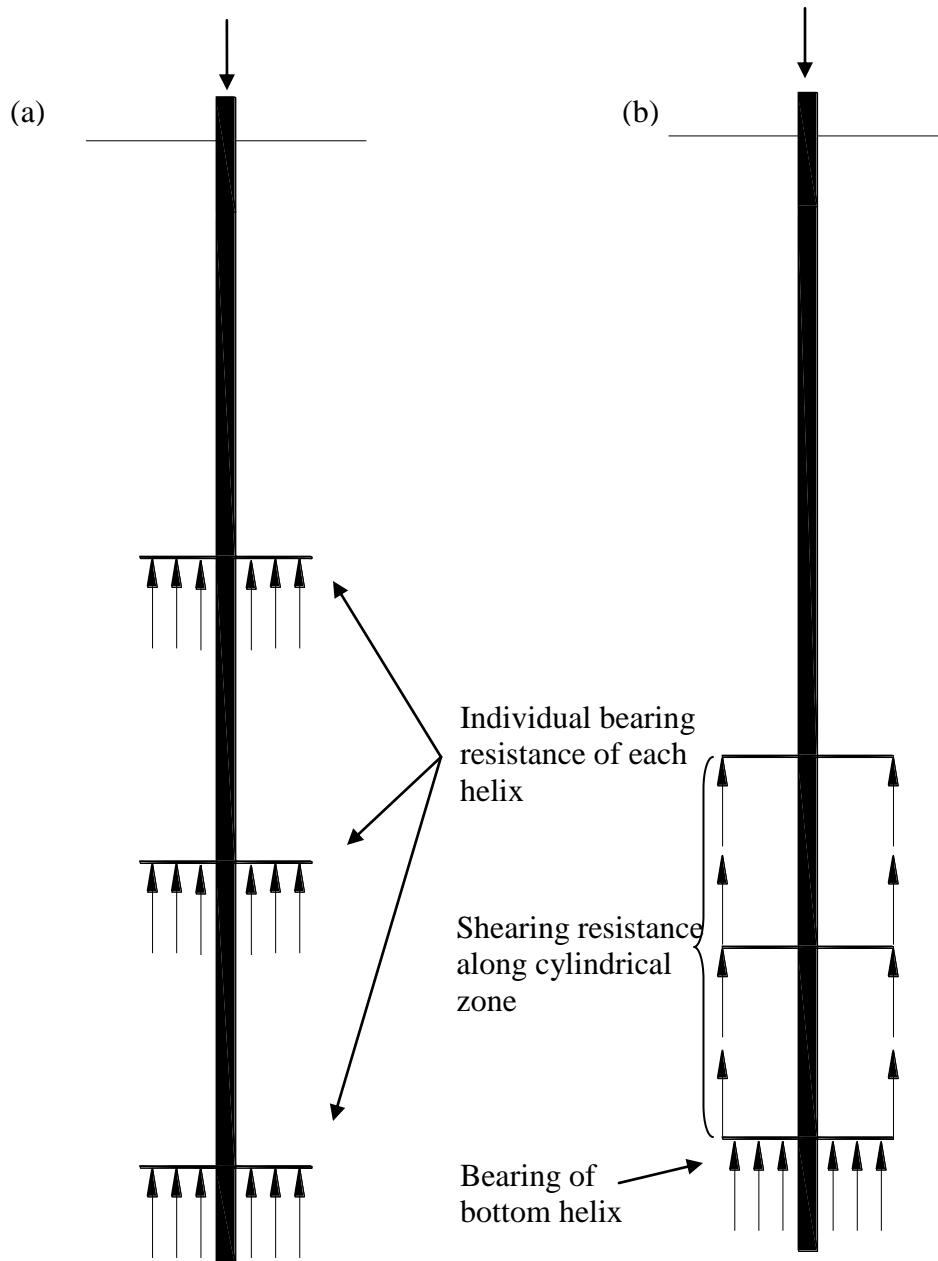


Figure 2.4. Possible failure mechanisms for helical piles under compression: (a) Individual bearing; and (b) cylindrical shear failure.

Livneh and El Naggar (2008), based on field testing and three-dimensional finite element modelling of helical piles in sand and clay, observed that the ultimate capacity consist of the shear resistance along a tapered cylindrical zone and bearing of the bottom helix against the underneath soil. The tapered cylindrical zone is composed of two parts; the first one has a taper angle of 5.33° and located between the upper and intermediate helices and the second has a taper angle of 2.12° and is located between the intermediate and bottom helices, as shown in Figure 2.5. Livneh and El Naggar (2008) suggested that the approach proposed by El Naggar and Sakr (2000) for computing the compressive capacity of tapered piles in sand to be used to calculate the capacity of the inter-helix tapered cylindrical zone. The ultimate capacity of a plain pile, Q_u , as:

$$[2.5] Q_u = Q_{bearing} + (Q_{shaft})_{\alpha=5.53} + (Q_{shaft})_{\alpha=2.12}$$

$$[2.6] Q_{shaft} = \int_0^1 K_t K_s \sigma'_v \tan(\delta) p dz$$

$$[2.7] Q_{bearing} = A_h (cN_c + q'N_q)$$

where, Q_u is the ultimate compression capacity; Q_{shaft} is the ultimate skin friction along the tapered surface at $\alpha = 5.33^\circ$ and $\alpha = 2.12^\circ$; $Q_{bearing}$ = ultimate bearing capacity; K_{taper} is the pile taper coefficient, K_s is the coefficient of lateral earth pressure; σ'_v is the vertical effective stress; δ is the angle of friction along the taper surface; and A_h is the area of the bottom helix; and N_c and N_q are the bearing capacity factors.

The value of K_t is computed based on several factors such as the factor S_r , that is the pile settlement to diameter ratio ($S_r = U_p/D$):

$$[2.8] K_{taper} = A + \frac{B S_r}{\sigma_v}$$

A, B and M can be obtained as:

$$[2.9a] A = \frac{\tan(\alpha + \delta) \cot(\delta)}{1 + 2 \epsilon \tan(\alpha) \tan(\alpha + \delta)}$$

$$[2.9b] B = \frac{4G \tan(\alpha) \tan(\alpha + \delta) \cot(\delta)}{[1 + 2 \epsilon \tan(\delta) \tan(\alpha + \delta)] k_s}$$

where G is the shear modulus ; α_{taper} is the taper angle; and ζ is equal to $\ln(r_1/r_m)$, where r_m is the mean radius and r_1 is a radius at which the shear stress becomes negligible and is taken to be equal to $2.5L(1-\nu)$, where L represents the length of the taper part.

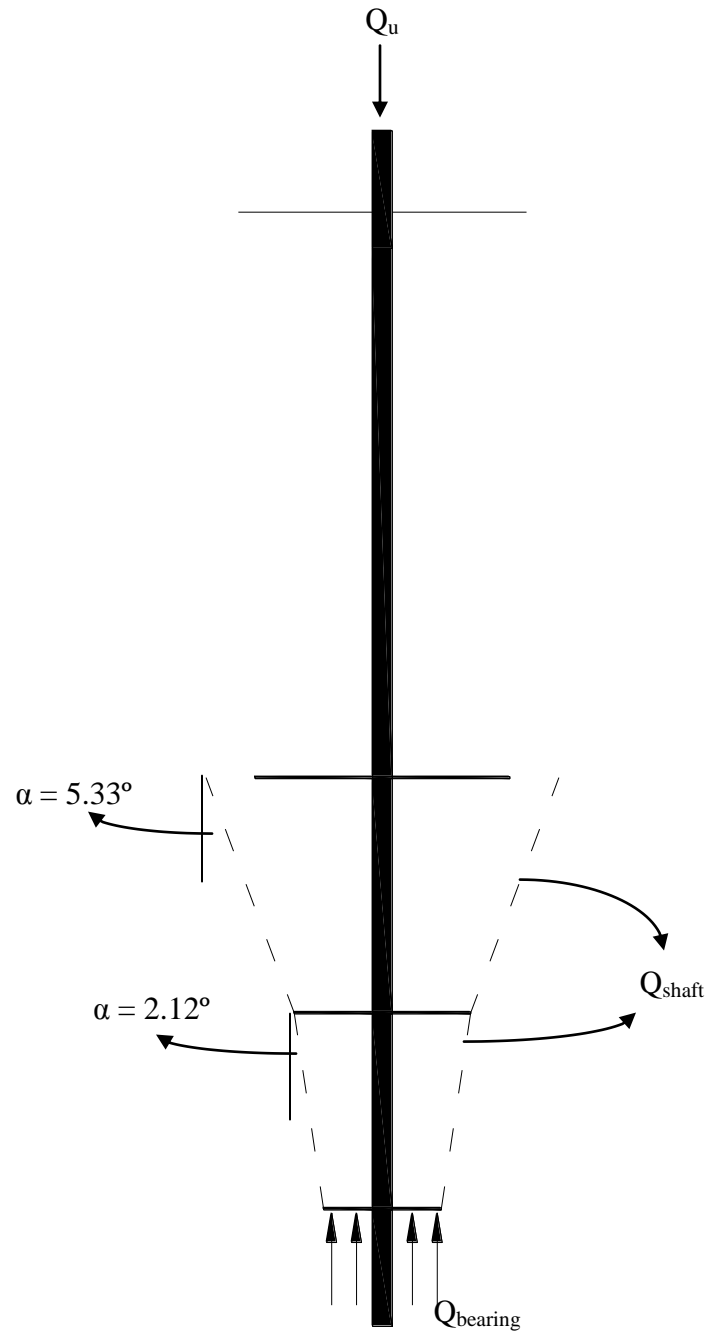


Figure 2.5. Schematic of piles failure components for compressive loading; after Livneh and El Naggar (2008).

Fewer investigations were conducted on helical piles in sand. Mitsch and Clemence (1985) conducted laboratory tests on piles in sand with spacing ratio of 3, and concluded that shear failure takes place along the interface boundary between the helices. The Canadian Foundation Manual (BiTech, 2006) specifies that, for the individual bearing method to be applicable, helices should be placed at least three times the largest helix diameter. Sakr (2009) based on field testing results of single and double helix piles, suggested that individual bearing method is more suitable for piles in oil sands with spacing ratio of 3. Cerato and Victor (2009) compared the measured uplift capacity of helical anchors with both design methods, and concluded that the cylindrical shear method significantly underpredicted the uplift capacity of most tested anchors. Lutenecker (2011) performed tests on double-, triple and quadruple-helix screw anchors with helix spacing to diameter ratios varying from 1.5 to 3 (0.75 to 4.125 for triple helix anchors). He found that the transition from cylindrical shear behaviour to individual plate behaviour of cylindrical multihelix anchors with a fixed number of helical plates in sand occurs at a spacing of about 3.

2.5.2 Capacity by torque correlation

Helical piles are installed by means of mechanical torque. The installation torque has been commonly used as a practical means to predict the screw anchor ultimate capacity through an empirical correlation factor. Livenh and El Naggar (2008) discussed that the rationale behind this method is that installation torque is a measure of the energy required to overcome the shear strength of the soil and hence directly related to pile capacity. A number of theoretical correlations between installation torque and uplift capacity were

developed by several investigators including: Ghaly et al. (1991); Perko (2009); Tsuha and Aoki (2010).

Hoyt and Clemence (1989) introduced an empirical factor K_t that depends on screw pile shaft diameter where,

$$[2.10] \quad Q_u = T \times K_t$$

where T is the average installation torque over the last 1 m (3 ft), and K_t is an empirical torque factor. K_t values are 33 m^{-1} (10 ft^{-1}) for all square shaft anchors and round shaft anchors less than 89 mm, 23 m^{-1} for 89 mm round-shaft anchors, and 9.8 m^{-1} for anchors with 219 mm diameter extension shafts. The Canadian Foundation Manual (CFEM, 2006) recommends for pipe shaft anchors of 90 mm diameter a torque correlation factor of 33 m^{-1} , with this value decreasing to 10 m^{-1} for shaft diameters approaching 200 mm. A.B Chance (2007) reported that K_t may range from 10 to 66 m^{-1} depending on soil conditions, helical pile geometric configuration, and loading direction (compression or tension). For piles in dense sand (field N-Value of 30), Livneh and El Naggar (2008) found K_t values of 61.5 to 62.1 m^{-1} for piles under compression loading and 24.3 to 32.7 m^{-1} for piles under tensile loading. Abdelghany (2008) reported values of K_t between 20 - 28 m^{-1} for piles installed in clayey till. For piles installed in oil sands, Sakr (2009) reported K_t values of 23.6 m^{-1} for piles loaded in compression and 11 m^{-1} for piles loaded in tension. It is worth noting that the calculated K_t -value depends on the interpretation of load test results (i.e. determination of ultimate capacity from load test data).

2.6 Helical piles under axial cyclic loads

Various types of structures are required to withstand cyclic loads. These loads can be one way compression or tension (repeated loads) or of alternating manner. Several studies (Hanna et al. (1978); Andreadis et al. (1981); Hanna and Al-Mosawe (1981); Clemence and Smithling (1983); Cerato and Victor (2009); Buhler and Cerato (2010)) have focused on the behaviour of helical piles or embedded anchors under sustained uplift cyclic loading (and to a lesser degree on alternating loads), and its effect on the post-cyclic static behaviour. These studies were geared towards simulating wind-type loading on wind turbines and transmission towers. As such, the cyclic loading duration was of a long term, i.e., 1 hr to 500 hrs (large number of cycles). Hanna et al. (1978) observed that the displacement of an anchor during sustained-repeated (one-way) uplift cyclic loading depends primarily on the load range during cyclic loading; higher load range requires smaller number of cycles to cause failure. While failure didn't occur during testing, they observed that the displacement per cycle decreases, but never ceases, and that the size of the hysteresis loop decrease with the number of cycles. Andreadis et al. (1981) demonstrated experimentally that repeated application of loads reduced the anchor resistance and resulted in non-recoverable movements. On the other hand, other studies reported that repeated cyclic uplift loading improves the static performance of the pile and increases its post-cyclic capacity (e.g. Hanna et al. (1978); Hanna and Al-Mosawe (1981); Andreadis et al. (1981); Cerato and Victor (2009); Buhler and Cerato (2010)).

Meanwhile, Clemence and Smithling (1983) observed degradation in the performance of pre-stressed under cyclic loading that resulted in anchor failure. They found that the

number of cycles to failure depends on the cyclic displacement amplitude. The anchor that was subjected to relatively larger displacement amplitudes of 1.78 mm (0.07 inches) failed after 120 cycles, while the anchor subjected to 0.68 mm (0.027 inches) displacement amplitude failed after 1200 cycles. They observed reduction in horizontal stresses during cyclic loading that indicated loosening of the sand during loading until the active horizontal state of stress was reached which was followed by anchor failure.

Less attention was given to the behaviour of helical piles in compression, and even less for helical piles under one-way cyclic compression loading. The load transfer mechanism and resistance during and after cyclic loading may differ from that under tensile loading conditions. When helical piles are used to support new construction or retrofitting existing structures, loading conditions include axial compression and one way cyclic compression (sustained cyclic compression loading).

El Naggar and Abdelghany (2007a) investigated the performance of plain helical piles, and helical pulldown® micropiles installed in clay under 15 slow cycles of loading over a span of 8 hrs. The mean cyclic load level was 100 kN (1/3 of the estimated ultimate capacity) and the amplitude was +/- 30 kN. They found that the stiffness remained almost constant during cyclic loading for all three test piles. They observed that for the plain pile, post-cyclic static capacity was reduced by 5% to 10%. Meanwhile the axial capacity of the helical pulldown® micropile displayed a variation of +/-18% of its axial capacity. Abdelghany (2008) attributed the capacity increase for some piles to the cyclic loading effect on reducing the disturbance caused during installation.

2.7 Helical piles under lateral monotonic loads

The square shaft pile requires less installation torque and can be constructed in hard soil conditions compared to the round shaft pile. However, the square shaft is more susceptible to buckling. In addition, the square shaft has a limited surface area with the surrounding soil which limits its lateral resistance. El Naggar and Abdelghany (2007a) found that the lateral resistance of square shaft helical piles to be negligible. As such, round square shafts have received more attention in the literature.

Puri et al (1984) looked at various test data of piles in sand and clay. They concluded that helical anchors can develop significant resistance to lateral loads. Perko (2009) carried out L-PileTM analysis, using the p-y curves approach, considering several pile types and found that the helical piles offer lateral capacity of the same order of magnitude as micropiles and small diameter drilled shaft piles having comparable diameters and installed in similar soil conditions. Prasad and Rao (1996) examined the behaviour of model scale piles in clayey soils. They found that the lateral capacity increases with increasing embedment depth and soil shear strength.

Several attempts have been made to study the effect of the helical plates on the pile's lateral resistance. Puri et al (1984) based on full-scale and model test data concluded that the helices play a minor role in the lateral resistance if the extension is more than a certain limiting value. Similarly, Sakr (2009) conducted full-scale lateral tests on piles installed in oil sand. He observed that piles with one and two helices behaved similarly. He concluded that the helices had a minor effect on the lateral resistance. Meanwhile, Prasad and Rao (1996), and Mital et al. (2010) found that helical piles offer more lateral

resistance than that of single straight pile without plates, with resistance increasing with number of plates. A theoretical model was developed from both studies that attributed the capacity increase to the bearing resistance on the bottom of the plates, uplift resistance on the top of the helices and frictional resistance on their surface. The disagreement between the above studies may be due to the difference in soil-pile interaction and depth of the helices relative to the depth of the active soil resisting zone, as well as if piles are behaving as rigid short piles where rotation activates the resistance on top and bottom of the plates, or as long piles where rotation doesn't take place considerably.

2.8 Helical piles under lateral cyclic loads

Helical piles behaviour under cyclic loading has received much less attention in the literature, and focused on behaviour under one-way cyclic loads. Prasad and Rao (1994) carried out one way sustained cyclic load model tests on helical piles embedded in clay and reported that helical piles performed better at relatively high cyclic load levels than piles without helical plates that had the same geometric dimensions. More recently, Abdelghany and El Nagggar (2010) conducted one-way sustained lateral cyclic tests plain helical piles and HPM including the RHPM. They concluded that for all tested piles, the lateral capacity degraded due to the cyclic loading, with the RHPM presenting the most favorable performance during cyclic loading.

2.9 Summary

In this chapter, definition of various innovative types of helical piles is provided. A literature review on the performance of helical piles and modified helical piles is presented. The literature review revealed that there is very little research conducted on

the performance of RHPM. In addition, FRP-HPM piles are viable foundation options, however, the installation method need to be modified in order to utilize the advantages of such composite system. In addition, the performance of plain helical piles with cylinder shafts under lateral loading was reported to be insignificant; the modified helical piles behaviour under lateral load was found to be superior, however more research is required. Finally, the literature survey revealed that more research is needed for the behaviour of helical and modified helical piles under cyclic loads.

2.10 References

A. B. Chance Co. 2007. Chance Civil Construction Technical Design Manual, Hubbell Power Systems Inc., Centralia, MO, USA.

Abbas, A., and Mohsin, S.S. 2010 Numerical modeling of fibre-reinforced concrete. In proceedings the international Conference on Computing in Civil and Building Engineering.

Abdelghany, Y. 2008. Monotonic and cyclic performance of helical screw piles. PhD thesis, The University of Western Ontario, Canada.

Abdelghany, Y., and El Naggar, M.H. 2010. Full-scale experimental and numerical analysis of instrumented helical screw piles under axial and lateral monotonic and cyclic loadings-A promising solution for seismic retrofitting. *In* Proceedings of the 6th International Engineering and Construction Conference. American Society of Civil Engineers, Cairo, Egypt.

Andreadis, A., Harvey, R.C., and Burley, E. 1981. Embedded anchor response to uplift loading. *Journal of the Geotechnical Engineering Division, ASCE*, 107(1), 59-78.

Ashford, S. A., Jakrapiyanun, W. 2001. Drivability of glass FRP composite piling. *Journal of Composites for Construction*, 5(1): 58-60.

El Naggar, M.H, and Abdelghany, Y. 2007a. Helical screw piles capacity for axial cyclic loadings in cohesive soils. *In Proceeding of the 4th International Conference on Earthquake Geotechnical Engineering*, Thessaloniki, Greece.

Buhler, R., and Cerato, A.B. 2010. Design of dynamically wind-loaded helical piers for small wind turbines. *Journal of Performance and Construction Facilities, ASCE*, 24(4), 417-426.

Canadian Foundation Engineering Manual. 2006. Fourth edition. Canadian Geotechnical Society, 488 p.

Cerato, A.B., and Victor, R. 2009. Effects of long-term dynamic loading and fluctuating water table on helical anchor performance for small wind tower foundations. *Journal of Performance and Construction Facilities, ASCE*, 23(4), 251-261.

Clemence, S.P., and Smithling, A.P. 1984. Dynamic uplift capacity of helical anchors in sand. *Civil Engineering for Practicing and Design Engineers*, 2 (3), 345-367.

de Oliveira Junior, L.A., dos Santos Borges, V.E., Danin, A.R., Machado, V.R., de Lima Araujo, D., El Debs, M.KH., Rodrigues, P.F. 2010 Stress-strain curves for steel-fibre reinforced concrete in compression. *Revista Materia*. 15(2): 260-266.

El Naggar, M.H., and Abdelghany, Y. 2007b. Seismic helical screw foundation systems. *In Proceedings of the 60th Canadian Geotechnical Conference*, Ottawa, ON, pp. 21-24.

El Naggar, M.H., and Sakr, M. 2000. Evaluation of axial performance of tapered piles from centrifuge tests. *Canadian Geotechnical Journal*, 37: 1295-1308.

Ghaly, A., Hanna, A., and Hanna, M. 1991. Installation torque of screw anchors in dry sand. *Soils and Foundations*, 31(2): 77-92.

Guades, E. , Aravinthan, T., Islam, M., and Manalo, A. 2012 A review on the driving performance of FRP composite piles. *Composite Structures*, 94(6): 1932-1942.

Hanna, T. H., Sivapalan, E., and Senturk, A. 1978. Behaviour of dead anchors subjected to repeating and alternating loads. *Ground Engineering*, 11(3), 28-32, 34, 40.

Hanna, T.H., and Al-Mosawe, M.J. 1981. Performance of prestressed anchors under slow repeated loadings. *In Proceedings of the 10th International Conference on Soil Mechanics and Foundation Engineering*, Stockholm, Sweden. pp. 127-132.

Hoyt, R. M., and Clemence, S.P. 1989. Uplift capacity of helical anchors in soil. *In Proceedings of the 12th International Conference on Soil Mechanics and Foundation Engineering*, Rio de Janeiro, Br. 13-18 August 1989, Vol. 2, pp. 1019-1022.

Iskander, M. G., Hanna, S, and Stachula, A. 2001. Drivability of FRP composite piling. *Journal of Geotechnical and Geoenvironmental Engineering*, 127(2): 169-176.

Kulhawy, FH. 1985. Uplift behaviour of shallow soil anchors-an overview. ASCE, pp. 1-25.

Livneh, B., and El Naggar, M.H. 2008. Axial testing and numerical modeling of square shaft helical piles under compressive and tensile loading. *Canadian Geotechnical Journal*, 45(8): 1142-1155.

Lutenegger, A.J. 2011. Behavior of multi-helix anchors in sand. *In* Proceeding of the 2011 Pan-Am CGS Geotechnical conference. Canadian Geotechnical Society, Toronto, Ontario, paper no, 126.

Merifield, R.S., and Smith, C.C. 2010. The ultimate uplift capacity of multi-strip anchors in undrained clay. *Computers and Geomechanics*, 37(4): 504-514.

Mittal, S., Ganjoo, B., & Shekhar, S. 2010. Static Equilibrium of Screw Anchor Pile Under Lateral Load in Sands. *Geotechnical Geological Engineering*, 28: 717-725.

Mooney, J.S., Adamczak, S.Jr., and Clemence, S.P. 1985. Uplift capacity of helical anchors in clay and silt. *In* Proceedings, Uplift Behavior of Anchor Foundations in Soil, Proceedings of a Session held in conjunction with the ASCE Convention, Detroit, MI, pp. 48-72, American Society of Civil Engineers, New York, NY, USA.

Narashima Rao, N.S., and Prasad, Y.V.S.N. 1993. Estimation of uplift capacity of helical anchors in clay. *Journal of Geotechnical Engineering*, 119 (2): 352-357.

Tsuha, C. de H.C., and Aoki, A. 2010. Relationship between installation torque and uplift capacity of steel helical piles in sand. *Canadian Geotechnical Journal*, 47(6): 635-647.

Pando, M., Lesko, J., and Case, S. Preliminary development of a durability model for concrete filled FRP piles. 2001. *In Proceedings*, International SAMPE Symposium and Exhibition, v 46 II, pp 1597-1611.

Perko, H.A. 2009. *Helical piles: a practical guide to design and installation*. John Wiley & Son, Inc., Hoboken, N.J.

Prasad, Y., & Narasimha Rao, S. 1996. Lateral Capacity of Helical Piles in Clays. *Journal of Geotechnical Engineering*, 938-941.

Puri, V.K., Stephenson, R.W., Dziedzic, E., and Goen, L. 1984. Helical anchor piles under lateral loading. *Laterally Loaded Deep Foundations: Analysis and Performance (STP 835)*, American Society for Testing and Materials, pp. 194-213.

Sakr, M., El Naggar, M.H., and Nehdi, M. (2004a). Load transfer of fibre-reinforced polymer (FRP) composite tapered piles in dense sand. *Canadian Geotechnical Journal*, 41(1), 70-88.

Sakr, M., El Naggar, M.H., and Nehdi, M. (2004b). Novel toe driving for thin-walled piles and performance of fiberglass-reinforced polymer (FRP) pile segments. *Canadian Geotechnical Journal*, 41(2), 313-325.

Sakr, M. 2009. Performance of helical piles in oil sand. *Canadian Geotechnical Journal*, 46(9): 1046-1061.

Vickers, R.A., and Clemence, S.P. 2000. Performance of helical piles with grouted shafts. *In Proceedings of Sessions of Geo-Denver 2000 - New Technological and Design Developments in Deep Foundations*, GSP 100, v 288, pp. 327-341.

***FIELD INVESTIGATION OF AXIAL MONOTONIC AND
CYCLIC PERFORMANCE OF REINFORCED HELICAL
PULLDOWN MICROPILES**

3.1 Introduction

A helical (screw) pile (HSP) is a deep segmented foundation system that consists of relatively small galvanised central shaft fitted with one or more helices. The central shaft can be square (SS), round (RS) or combination of square and round shafts (SS/RS), depending on soil and loading conditions. Shaft sizes range from 42 mm to 57 mm. First segment (lead section) contains the helices and is installed to the desired depth by adding plain extensions connected onsite through bolted couplings. Number of helices varies from one up to four, and their diameters range between 150 mm to 400 mm. For multi-helix lead sections, diameter of helices decreases with depth. Helices have standard pitch of 76 mm (3") and a spacing of about three times the helix diameter.

Helical piles are used in wide range of foundation applications: buried pipe lines, telecommunication and transmission towers, machine foundations, and commercial and residential buildings. Advantages of helical piles include: short installation time with minimal noise and vibration levels; suitability for applicability in expansive soils and ad-freeze conditions; can be installed with ease in limited accessibility site; and onsite

*A version of this chapter has been published in the Canadian Geotechnical Journal, Vol. 49, no. 5, pp: 560-573, and a version of part of this chapter has been published in the 14th Pan-American Conference on Soil Mechanics and Geotechnical Engineering, Paper no. 336.

quality control by measurement of installation torque. Helical piles are widely used for underpinning of deficient foundations and soil remediation, especially in urban areas. They are connected to new foundations using pile caps, and to existing foundation using specialized connectors.

There are two methods for predicting the compressive and tensile ultimate capacity of helical piles: the individual bearing; and the cylindrical shear. The individual bearing method considers the pile capacity as the sum of the individual bearing capacity of each helical plate. The cylindrical shear method assumes that the load is transferred to the soil through a cylinder of a soil mass that is enclosed between the upper and lower helices, and bearing of the upper helix for tension loading or lower helix for compression loading. Surveyed literature indicates that failure mechanism depends primarily on the spacing ratio, defined as ratio of helix spacing to helix diameter, and soil conditions. Kulhawy (1985) stated that if the helices are widely spread, anchor capacity is that of several single plates. The Canadian Foundation Manual (BiTech, 2006) specifies that, for the individual bearing method to be applicable, helices should be placed at least three times the largest helix diameter. Several researchers studied helical piles in clay including, Mooney et al. (1985), El Naggar and Abdelghany (2007a, 2007b), Livneh and El Naggar (2008), Merifield and Smith (2010), Narashima Rao and Prasad (1993). They conducted model scale tests, full scale tests, finite element modelling, and upper bound solutions. Spacing ratios was as large as 4.5. All studies found that the cylindrical failure surface develop between the helices, except for Narashima Rao and Prasad (1993) who concluded that for spacing ratios larger than 1.5, failure surface is not cylindrical. Fewer studies investigated

the load transfer mechanism of helical piles in sand. Sakr (2009) based on field testing results of single and double helix piles, suggested that individual bearing method is more suitable for piles in oil sands with spacing ratio of 3. Mitsch and Clemence (1985) conducted laboratory tests on piles in sand with spacing ratio of 3, and concluded that shear failure takes place along the interface boundary between the helices. Tappenden et al. (2009) based on full-scale tests on instrumented helical pile with circular shaft with a spacing ratio of 1.5 found that the cylindrical shear model provide a close estimation of the pile ultimate capacity under compression load.

Axial capacity of helical piles under compression can be limited by the buckling capacity of its shaft, especially for long piles and/or piles installed in weak soils. Vickers and Clemence (2000) introduced the Helical Pulldown[®] Micropile or grouted-helical pile (HPM). It consists of a helical pile installed with a grout column surrounding the pile central shaft along the extensions. The naming of the pile as a helical micropile comes from the fact that the grout shaft diameter is less than 300 mm, and is reinforced by the steel shaft (extension) of the helical pile. Vickers and Clemence (2000) demonstrated that the addition of a grout column to helical piles results in a considerable increase in the ultimate axial capacity and performance of the pile.

While the above investigations showed that the grout shaft contributes significantly to the pile resistance, it is only used as means of overcoming buckling potential, and providing additional corrosion protection. This can be attributed to the lack of sufficient field data for these modified helical piles under axial loading conditions. In addition, there is an

increasing demand for a retrofitting tool than can be used to upgrade the cyclic resistance of existing foundations. Abdelghany (2008) and El Naggar and Abdelghany (2007a, 2007b), experimented several modifications to the HPM installed in clayey soils under axial loading conditions. These modifications include: enhanced grout mix, using steel fibre reinforcement in the grout mix; and encasing part of the grout column with relatively rigid fibre reinforced polymer tubes. While the number of tests on each modified helical pile was limited, the results indicated that in all cases, the axial compressive capacity increased compared to the plain helical pile.

The main objective of the current research is to assess the performance of plain helical piles, RHPM piles, and RHPM piles with the grout shaft encased in a fibre reinforced polymer tube under axial and lateral monotonic and cyclic loading conditions. This paper deals with Stage I, where the performance of RHPM pile is investigated under axial monotonic and cyclic loads, through full-scale field testing. The specific objectives of this test program were to (i) understand the load-displacement curves and evaluate their axial capacities under compression; (iv) investigate their load transfer mechanism; and (iii) to examine the effect of cyclic loading on their axial performance.

3.2 Site Investigation

The experimental program was carried out at the environmental site of the University of Western Ontario, located about 8 km north of London, Ontario. Two boreholes, 16.6 m apart within the tests area, were performed to a depth of 8.8 m. Standard penetration test was performed for each borehole using an automatic hammer. Borehole logs and SPT counts are provided in Table 3.1.

The site consisted of stiff to very stiff clayey silt till underlain by dense sand. Traces of gravel and cobbles were observed during sampling, which is also manifested in spikes of the SPT counts due to the gravel within the till layer. Retrieved samples showed that the till layer was fissured, especially at shallow depth. The ground water table was found at an elevation of 3.7 m and 4.1 for BH-1 and BH-2, respectively.

Samples retrieved at BH-1 from depths 1.5-2 m (undisturbed), 3.6 to 4.25 m (disturbed), and 6.6 to 7.25 m (disturbed) were subjected to sieve and hydrometer analysis, and consistency tests. The sample at 1.5-2 m depth was subjected to undrained consolidated test. The results of lab tests are presented in Table 3.2.

3.3 Test Pile Description, Installation and Instrumentation

Helical piles are installed by applying mechanical torque at the pile head. The applied torque is recorded during installation every 305 mm (1 ft) and is commonly used as a quality control measure on site. As one of the objectives of this study was to investigate the load transfer mechanism for lead sections fully embedded in sand, and due to hard soil conditions, the location of each test pile was pre-drilled by using round corner square SS 225 (57.15 mm) helical piles. Helices had diameters of 254 mm, 203 and 152 mm (with the largest helix being the upper one.), and the same pitch and spacing as those of test piles. This is a common practice for cases where hard soil conditions exist and the use of SS 175 (test piles) is more economical.

The plain helical pile was the SS 175 (44.5 mm) square shaft helical pile, which consisted of a lead section with three helices, with 305 mm, 254 mm and 203 mm diameters

attached to it, and a number of extensions, as shown schematically in Figure 3.1a. The helix pitch is 76 mm and the spacing between the helices is about three times the helix diameter. The helices have true helical shape and therefore, they do not auger into the soil but rather screw into it with minimal soil disturbance. During installation of the lead section, fluid-like grout was poured in for lubrication. Round square extension segments were 44.5 mm and were assembled onsite through couplings. The piles were installed such that the lead section lies within the sand layer to investigate the load transfer mechanism in sand. One lead section and three extensions were used to locate the lead section within the sand layer.

A schematic of the reinforced helical pulldown micropile (RHPM) is shown in Figure 3.1b. It consisted of two main parts: a plain helical pile; and a steel fibre-reinforced grout column surrounding all or part of the extensions; the steel fibres were 0.5 mm in diameter and 30 mm long. After the lead section and first extension were installed, 152.4 mm (6") diameter hole was created by attaching a cylindrical conical disk to the end of first and second extensions. The hole was filled with fibre-reinforced grout during, thus creating a grout column that extends along the second and third extensions. The void created at the ground surface due to the installation process was filled with relatively flowable grout by gravity. It should be noted that very flowable grout was used as a lubricant during the installation of the lead section for the RHPM but not for the plain pile. As the grout used to fill the shaft void was poured in by gravity, it can be classified as a Type A micropile according to the FHWA micropile design and construction implementation manual (Armour et al. 2000). Compression and splitting tensile lab tests were conducted on the

grout mix. The average compressive and tensile strength of three specimens, after 28 days, were found to be 47 MPa and 6.5 MPa, respectively. All piles were tested after 28 days.

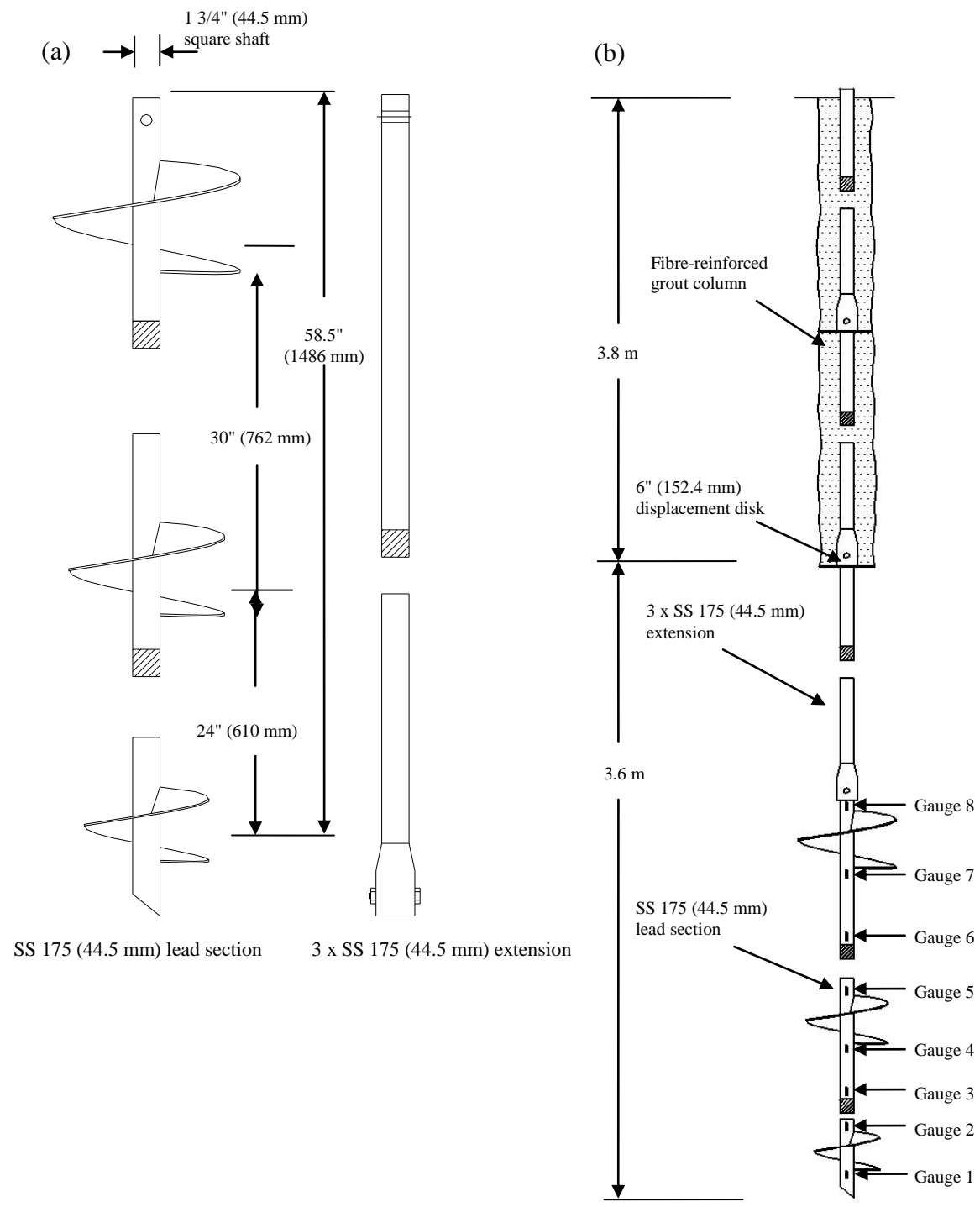
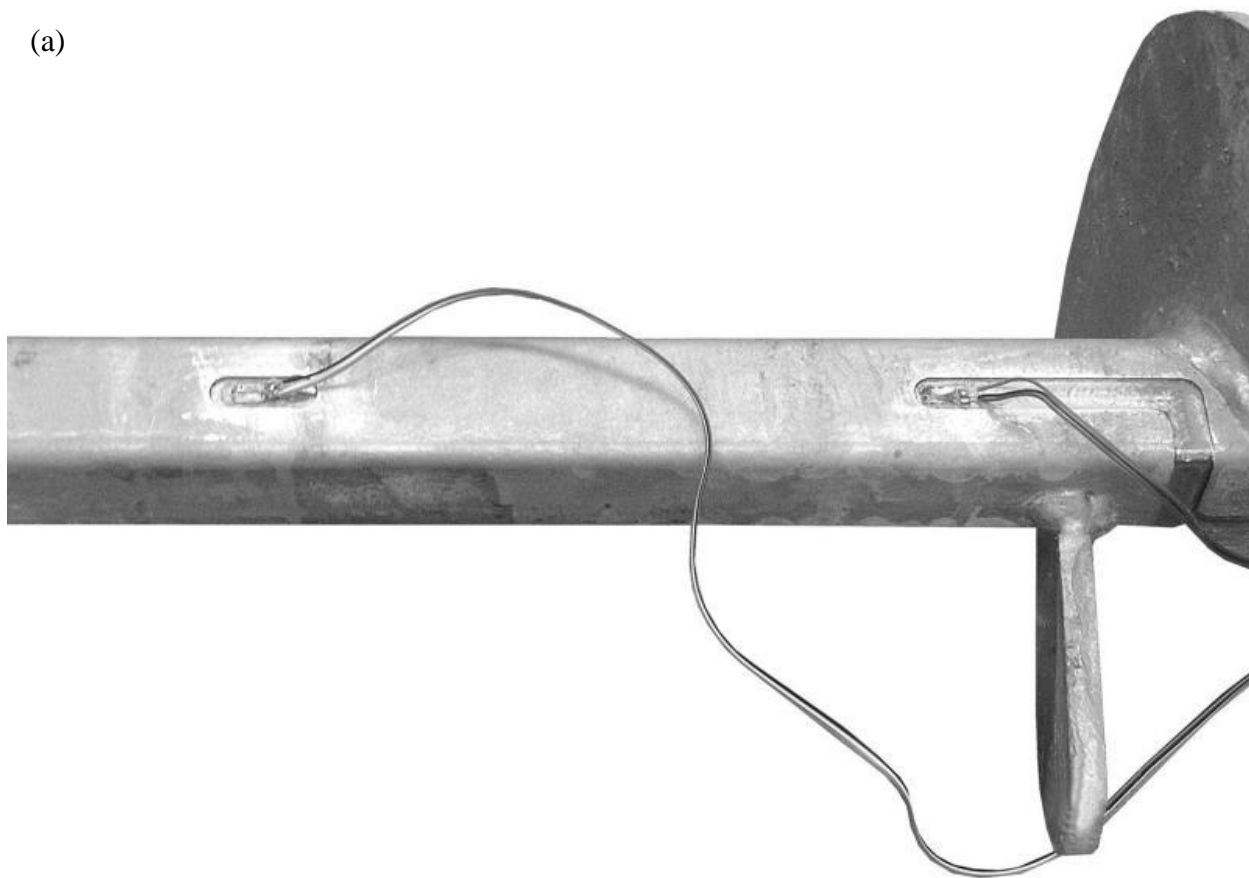


Figure 3.1. (a) Schematic of plain helical pile. (b) Schematic of reinforced pulldown micropiles and positions of strain gauges.

One plain helical pile and 13 RHPM piles were installed for this study. The depth of piles ranged from 7 m to 7.5 m, and the length of the grout column ranged between 3.4 and 3.9 m (Figure 3.1b).

In order to define the load transfer mechanism, end bearing or cylindrical shaft, and to evaluate the contribution of the shaft and lead section, the lead sections were instrumented with eight strain gauges. Six gauges were installed on the shaft just before and after the helices, and the remaining two at mid distance between each two helices, as shown schematically in Figure 3.1b. To protect the gauges during installation, they were placed inside specially made grooves on the lead section shaft (see Figure 3.2a), and then covered by a layer of coating. The lead section was wrapped in a few layers of tape to protect the gauges wires during installation, as shown in Figure 3.2b. On site, the lead wires were extended along the extensions and wrapped in layers of tape during installation (see Figure 3.2b). Channels within the cutting disks were made so that gauges wires can be passed through and extended at the cutting disks locations.

(a)



(b)



Figure 3.2. (a) Strain gauge installation. (b) Strain gauge protection through tape.

3.4 Field Test Set-up

3.4.1 Field test set-up

Figure 3.3 shows the load test set-up. It comprised a main steel reaction beam, centered over the test pile, and two secondary reaction beams. The secondary beams were tied to four reaction piles (square shaft SS 200 (50.8 mm) helical piles) using threaded rods and couplings. Reaction piles were installed at a rectangular arrangement of 3 x 3.6 m (> 10 and 20 times the largest helix diameter and shaft diameter, respectively). Same arrangement was applied for test piles. For each test, reaction piles were installed to equal torque in order to ensure similar response from all four piles. The loading plate was manufactured such that it rests on the pile head from one side, and threads into the load cell from the other side. Load was applied using a hydraulic jack that was centered over the load cell. Any gap between the hydraulic jack and main beam was filled by steel plates. Axial displacements were measured using four LDTs at the corners of the loading plates, and mounted on steel reference beams (SS 175 extensions). The load cell, LDTs, and strain gauges were connected on site to a data acquisition system.



Figure 3.3. Full view of axial load test set-up.

3.5 Testing Procedure

The testing program comprised two stages: I-A and I-B. The objective of stage I-A was to investigate the axial compression behaviour of RHPM piles. The objective of Stage I-B was to investigate the cyclic performance of the RHPM piles at an average cyclic load of at least the working load found in Stage I-A, and to examine the effect of cyclic load on the axial compression behaviour of RHPM piles. Stage I-A included testing of one plain helical pile and 6 RHPM piles, and Stage I-B included testing 6 RHPM piles.

The piles were tested under monotonic compression loads following the guidelines of ASTM D-1143 (2007) quick load test method. The applied load was increased in increments of 30 kN every 4 minutes. In Stage I-A (prior to cyclic loading), piles were tested up to a displacement of 25mm or higher than 8% of the average helix diameter. After cyclic loading, for all test piles, the load was increased until continuous jacking was required to maintain the load, a considerable displacement was reached or until the load approached the capacity of the load cell (or the reaction system).

3.5.1 Cyclic Testing

Figure 3.4 shows the cyclic loading protocol. The cyclic load tests involved one-way compression loading. All piles were subjected to 15 cycles of loading; each cycle was applied over a period of 2 minutes. The maximum and minimum cyclic load was taken as 130% and 70% of the average cyclic load, respectively. The average cyclic load was taken as 300 kN, i.e., maximum cyclic load of 390 kN and minimum of 210 kN.

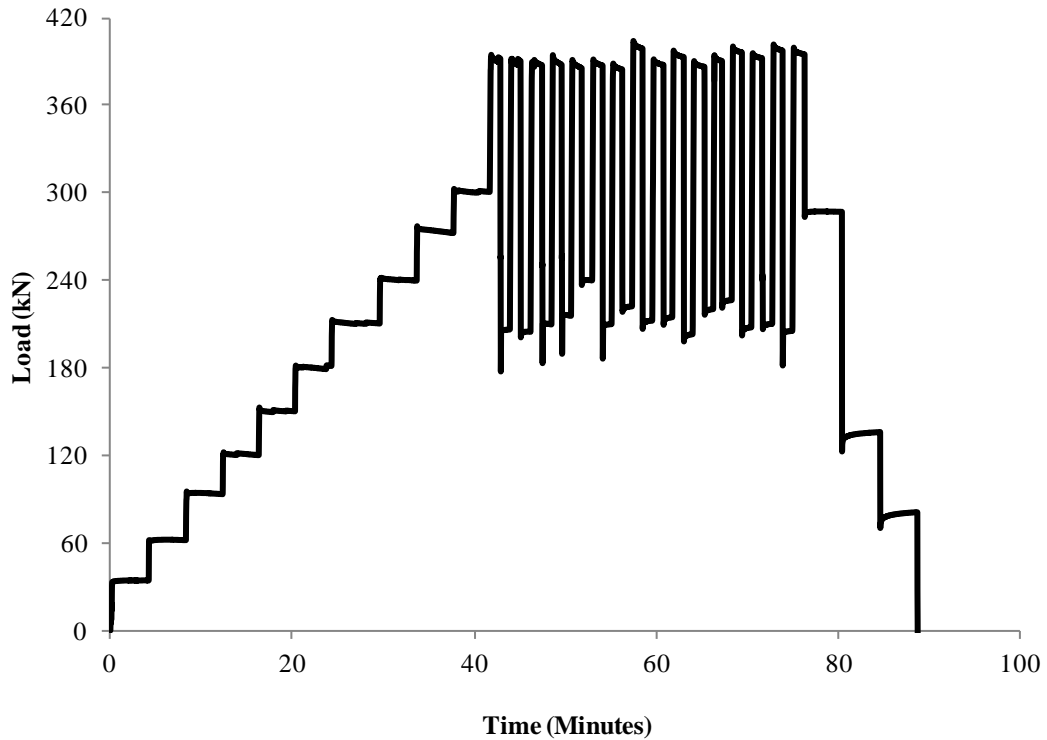


Figure 3.4. Cyclic load test protocol.

3.6 Test Results-Stage 1-A

As indicated above, piles were initially loaded to a minimum displacement of about 8% of the average helix diameter. The piles were then subjected to cyclic loading, followed by axial loading until the load approached the maximum allowable capacity of the load cell (890 kN). The cyclic and second compression tests were performed, in most cases, one day to two weeks after the first compression test. The displacement after the initial compression test was measured for one day for a few piles, and it was found that the residual displacement decreased by about 0.1 to 0.3 mm.

Figure 3.5a shows the load displacement responses for two test piles in Stage I-A. All other piles had similar trends. In general, the pile response can be characterized by the typical three branches, initial linear branch, transitional non-linear branch and near-linear branch with a slowly decreasing stiffness. The pile response was linear up to a displacement of about 2 mm (1.3 % of the shaft diameter). The transitional non-linear segment was up to a displacement of 10 mm to 12.5 mm (6.5% to 8% of the shaft diameter). The piles were loaded up to 850 kN at displacements ranging from 34 mm to 55 mm. The variation in the performance can be highly attributed to the site conditions; cobbles and boulders of a size up to 1 m in diameter were found upon excavation in the vicinity of the piles after testing.

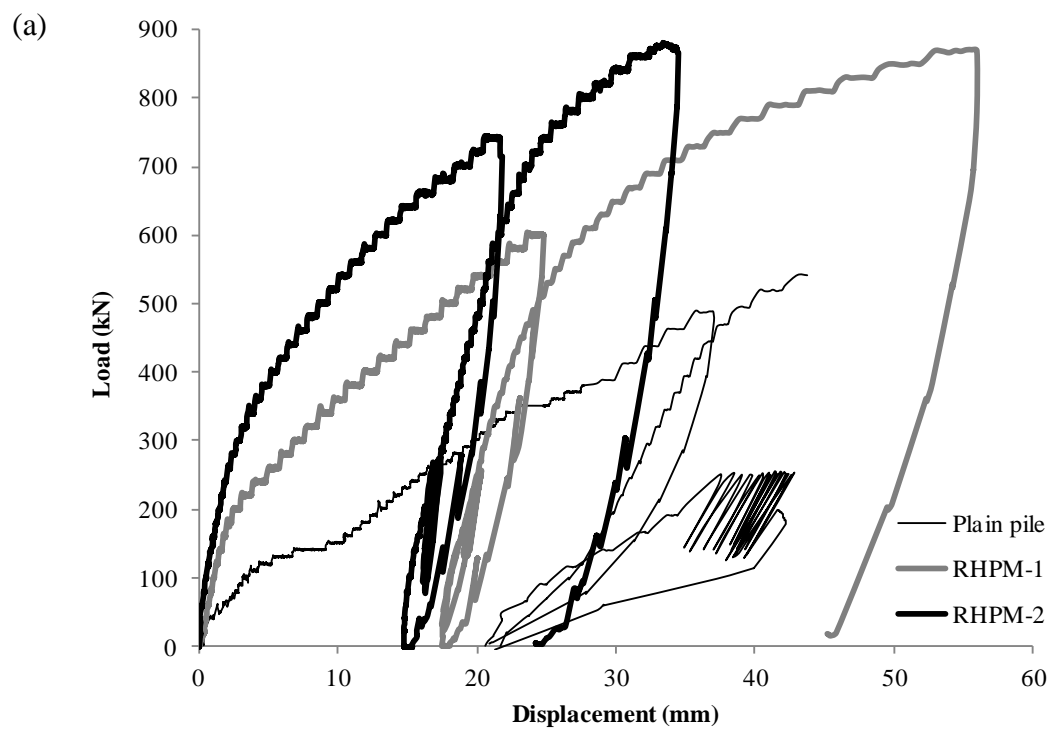
Figure 3.5a shows the axial response of the plain helical pile, installed to the same depth as the RHPM piles. As can be seen, the RHPM piles had higher stiffness and resistance at all times; the increase was significant at low displacement levels. At higher displacement levels, i.e. 20 mm (or 13% of the shaft diameter), the RHPM piles had a resistance of 180% to 250% of that of the plain pile. These results show that grout column significantly improved the performance and resistance of the helical pile.

The contribution of the grout shaft can be evaluated (approximately) using these results. The steel shaft friction for the plain pile is expected to be neglected because the installation process results in a cylindrical void that is slightly larger than the pile cross section. At low displacement levels, i.e. 1.3 % of the shaft diameter, the shaft resistance was 72% to 80% of the total resistance. Within the initial linear branch, the contribution

of the grout shaft was fairly constant and ranged between 61% and 70% of the total resistance. As the load increased, the shaft resistance, in percentage, gradually decreased; at a displacement of about 20% the shaft diameter, the grout shaft contribution ranged from 36% to 50%. These observations show that the pile resistance stems from both the shaft resistance and the lead section, and that at working load levels, a significant portion of that resistance is due to the shaft resistance. Similar observations were reported for helical pulldown® micropiles (no steel fibre reinforcement) by Lutenecker (2010).

Figure 3.5b shows the cyclic response of Pile 1 where the average cyclic load was 200 kN, while Figure 3.5c shows the cyclic response of Pile 4 where the average cyclic load was 270 kN (values of displacement are relative to residual displacement). It can be observed from Figures 3.5b and 3.5c that the piles didn't experience stiffness degradation during cyclic loading. It can also be observed that the cyclic displacement per cycle decreased with the number of cycles, indicating stabilization of the pile system. The displacement due to cyclic loading ranged from 0.1 mm to 0.45 mm (0.07% to 0.3% of the shaft diameter) as shown in Table 3.3. The observed behaviour of these piles during cyclic loading may be explained by the densification of the sand layer in the vicinity of the helices during cyclic loading where after few cycles; the sand is compacted such that the displacement increase with additional cycles becomes considerably small. Another possible interpretation of the observed behaviour is the shakedown phenomenon; after few cycles, the sandy soil has reached a state of equilibrium where loading ceased to induce permanent (plastic) strains and the sand experienced only elastic strain.

Comparing the second compression test after cyclic loading with that before cyclic loading, it seems that the response of the piles after cyclic loading follows that of before cyclic loading. This suggests that the axial stiffness and capacity were probably not affected by cyclic loading. A possible explanation to the observed performance is sand densification during initial loading and cyclic loading.



(b)

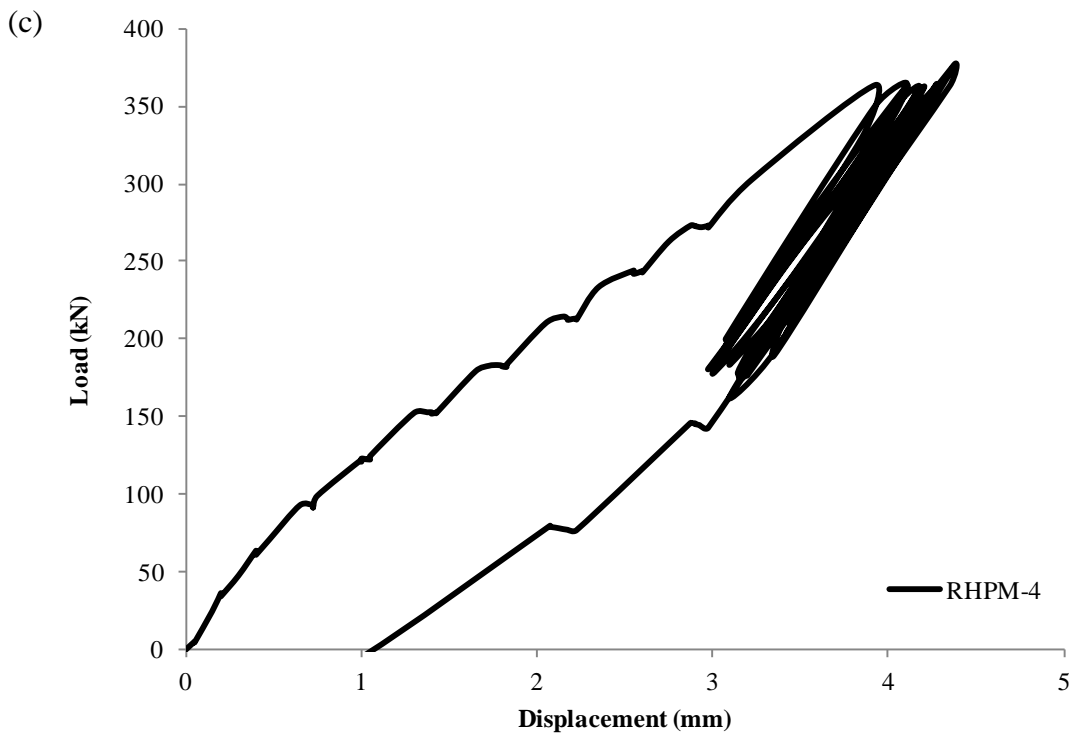
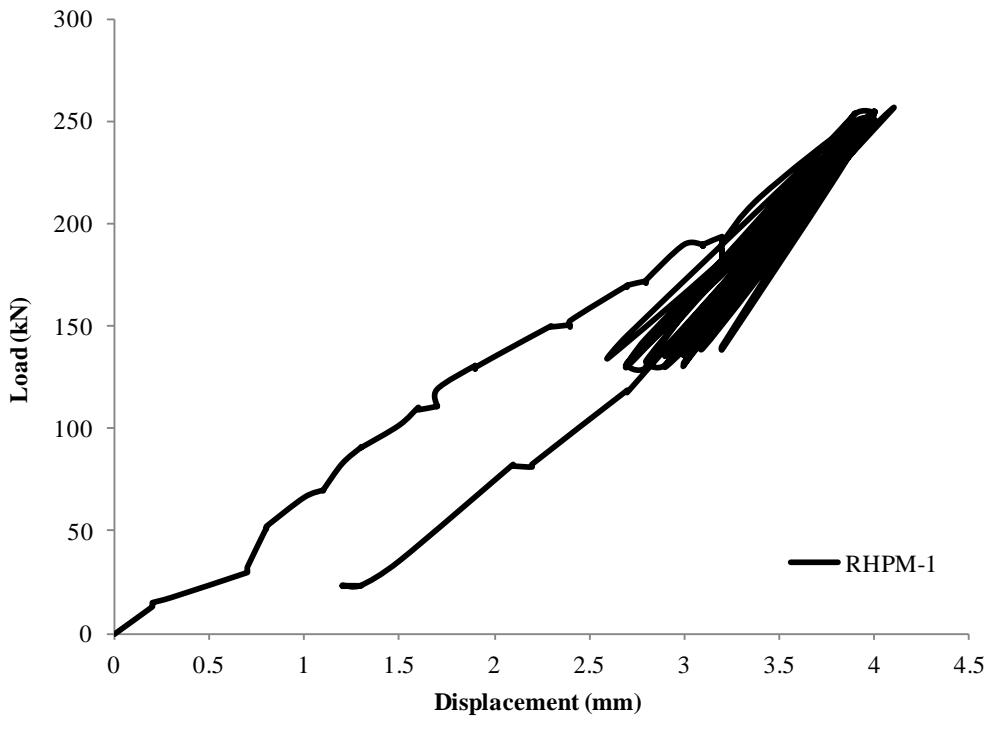


Figure 3.5. Results for Stage I-A: (a) load vs. displacement; (b) cyclic load vs. displacement (average cyclic load of 200 kN); (c) cyclic vs. displacement (average cyclic load of 270 kN).

3.7 Axial Results-Stage I-B

In stage I-A, the cyclic load range was less than the maximum load applied to the piles during axial compression loading. As reported above, the piles experienced small displacements during cyclic loading. In stage I-B, piles were loaded such that the average cyclic load is equal to the maximum monotonic load that the pile was subjected to (300 kN). The maximum and minimum cyclic loads were 130% and 70% of the average cyclic load, respectively.

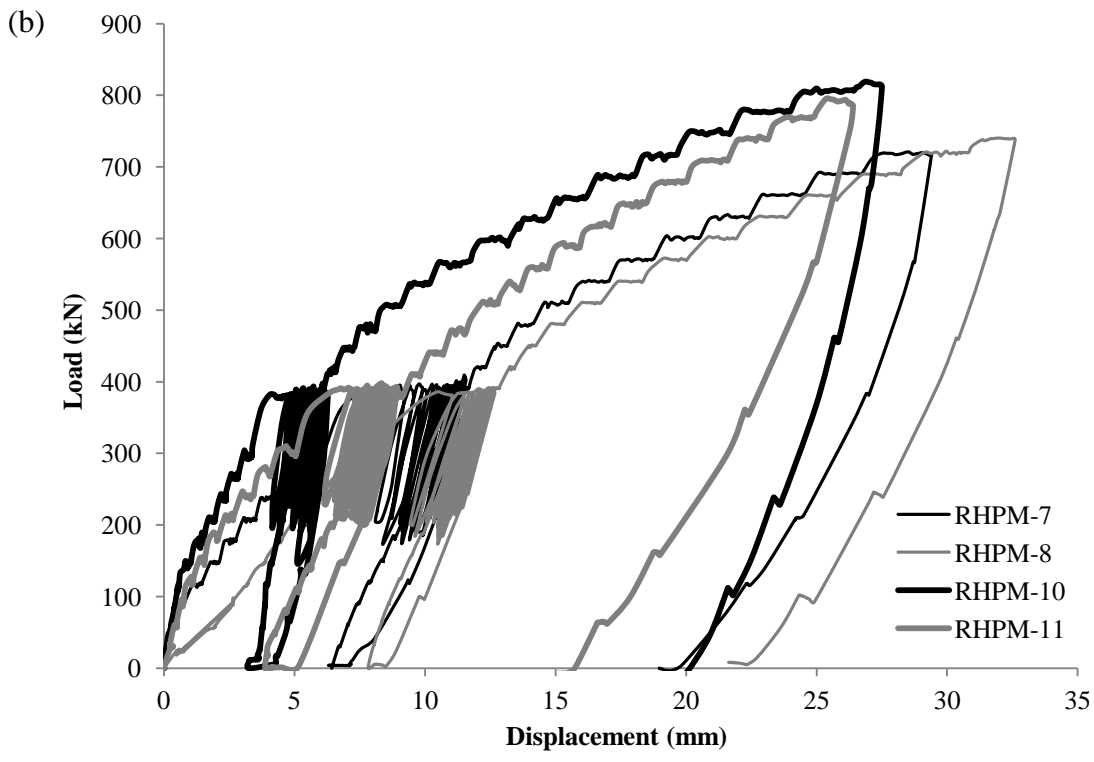
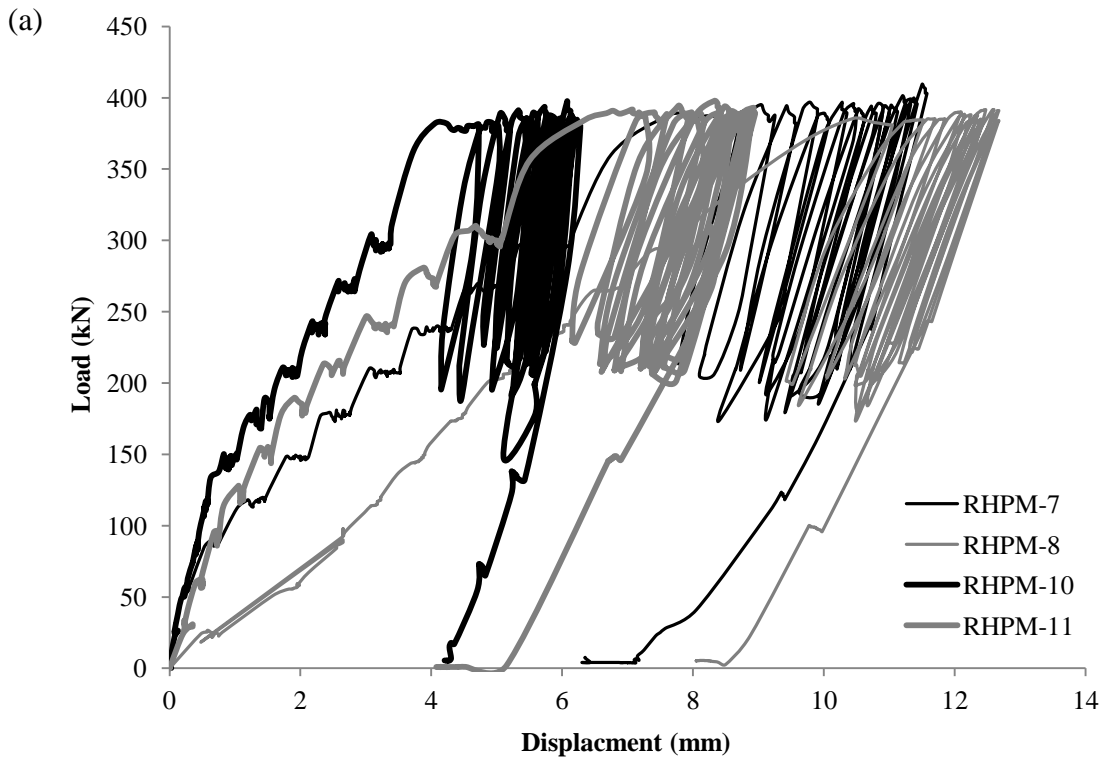
Figure 3.6a shows the cyclic load-displacement response for piles tested in Stage I-B. The response of all other piles tested within Stage I-B was similar to the presented results. In general, the piles' behaviour was similar to those reported above. The piles almost did not experience any stiffness degradation during cyclic loading. It can be observed that piles with higher initial stiffness had higher load-unload stiffness during cyclic loading. Also, the value of displacement increase during each cycle decreased with cyclic loading; this indicates the pile system stabilized under the applied cyclic loading. In addition, as can be seen from Table 3.3, all piles had almost the same displacement increase during cyclic loading; the increase ranged from 1.4 mm to 2.7 mm (0.92% to 1.77% of the shaft diameter).

Figure 3.6a shows that piles tested in Stage I-A had a displacement increase during cyclic loading less than 25% of that experienced by piles tested in Stage I-B. This can be attributed to the loading history of piles tested in Stage I; where the cyclic loading range was less than the maximum axial load the piles were subjected to prior to cyclic loading.

In addition, the fact that these piles were subjected to relatively high axial loads prior to cyclic loading may have resulted in densification of the sand below the helices.

Figure 3.6b shows the full load displacement curves of the piles under cyclic loading and compression loads. After cyclic loading, the non-linear (transitional) and near-linear branched can be observed, where the piles response seem to follow the same trend as for the case of compressive loading prior to cyclic loading.

Figure 3.6c shows the shaft resistance during loading of RHPM-10 (based on readings of Gauge 8, refer to Figure 3.2b). The shaft resistance before cyclic loading was about 80 % while it was 75 % at the end of cyclic loading, indicating that the displacement during cyclic loading was due to a slight degradation in the shaft resistance. As the final compression load was applied, the shaft resistance increased with a decreasing percentage from 75% to 67% at a corresponding total displacement of about 7 % of the shaft diameter. At this displacement level, the shaft appears to have reached its maximum resistance. With further load increase, the shaft resistance was constant at 380 kN (resistance was decreasing in percentage). At a load of 750 kN, with corresponding displacement of 13% of the shaft diameter, the shaft resistance was 50% of the total resistance. These results suggest that the cyclic loading had no effect on the performance of these piles. In all cases, the piles sustained load levels varying from 740 kN to 820 kN at displacements varying from 27 mm to 32 mm.



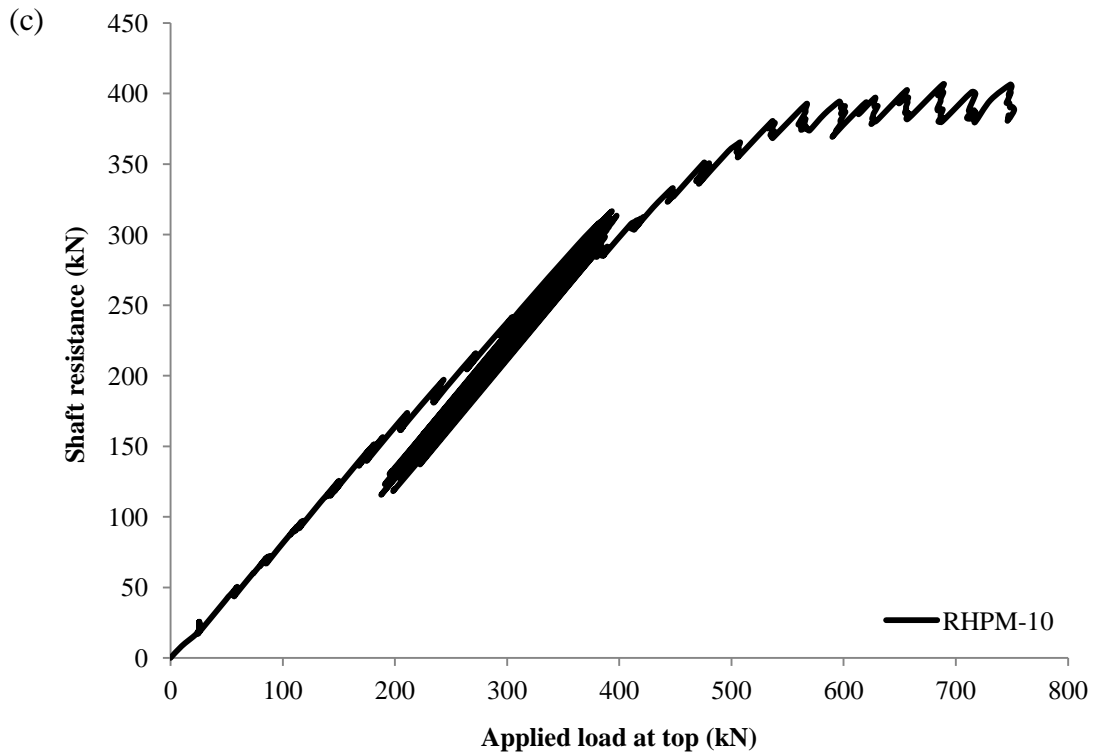


Figure 3.6. Test results for Stage I-B: (a) cyclic load vs. displacement; (b) Load vs. displacement; (c) shaft resistance vs. applied load for RHPM-10.

The loads corresponding to 20 mm displacement (13% of shaft diameter) for both test stages are plotted in Figure 3.7. It is noted from Figure 3.7 that piles tested in Stage I-B withstood, in general, equal or higher loads than those tested in Stage I-A. In addition, inspecting Figures 3.5a and 6b, it is noted that the range of stiffness for piles tested in Stage I-B is higher than that of piles tested in Stage I-A. This observation suggests that the applied cyclic load didn't have a negative effect, if not positive, on the axial performance of these piles.

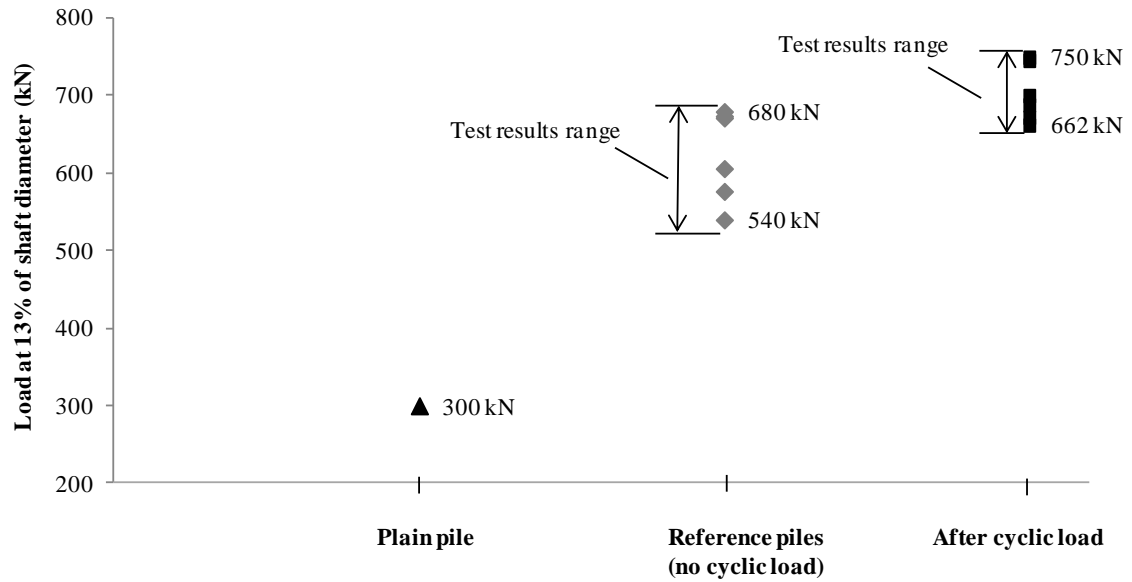


Figure 3.7. Loads at displacement equal to 13 % of shaft diameter for Stages I-A and I-B.

3.8 Load transfer mechanism in lead section

To evaluate the load transfer mechanism, strain gauges were mounted on the lead section before and after, and at the mid distance between each helix. It is noted, however, that due to hard installation conditions, several gauges were damaged. The axial force, P , at the location of the each gauge was calculated as:

$$[3.1] P = E_s A_s \varepsilon$$

Where E_s is the steel shaft modulus of elasticity, A_s is the steel shaft cross-sectional area and ε is the measured strain.

Figure 3.8 shows the measured axial forces from the gauge readings. Examining the load measurements at the gauges (Figures 3.8a to 8g), it can be seen that significant reduction occurred in the load measured below each helix compared to that measured above the

respective helix. Meanwhile, minimal or no reduction was measured between the helices. In addition, the reduction above and below each helix increased in value (and in percentage in some cases) as the load increased. For instance, inspecting Figures 3.8a and b (the plain pile), it can be seen that at a load of 240 kN, the loads above and below the mid helix were 118 kN and 75 kN, respectively; at 366 kN these loads were 238 kN and 108 kN. For RHPM-10 (Figures 3.8f and g), at a load of 410 kN, the loads above and below the first helix were 114 kN and 79 kN, respectively; at 746 kN, the respective loads were 377 and 227 kN. It is noted that the load measured at Gauges 6 and 7 for the plain pile (Figure 3.8a and b), both located between the top two helices, were almost identical. Meanwhile, some load loss was observed between Gauges 7 and 5 (Gauge 5 located just above the second helix) for Pile 6 (Figure 3.8e). This can be explained by the fact that the lubricant grout used during the installation of the lead section for Pile 6 provided an added resistance in the interhelix zone. While for the plain pile, no lubricant grout was used.

These observations show that under axial monotonic loading, the load transfer within the lead section was through individual bearing. It can also be noted from the figures that at low load levels, the distribution of load resistance between the helices was not equal. For instance, the top helix of the plain pile (Figure 3.8a and b) had a more significant contribution to the resistance up to an applied load of 150 kN. As the load increased, the top helix offered constant resistance, and the mid and lead helices' resistance increased with increase in applied load. Similarly, the lead helix of Pile 4 (Figure 3.8c) developed greater resistance than the other two helices until loads transferred to lead section reached

about 50 kN, after which redistribution of resistances occurred. The above observations can be attributed to the effect of installation disturbance on the sand condition at the vicinity of each helix. At low load levels, at the helix where installation disturbance was less pronounced, the resistance was relatively higher. As load increased, installation effect was lessened and resistance of the other two helices was mobilized. As in-situ conditions (before installation) were similar for the three helices, they developed similar resistances at higher load levels.

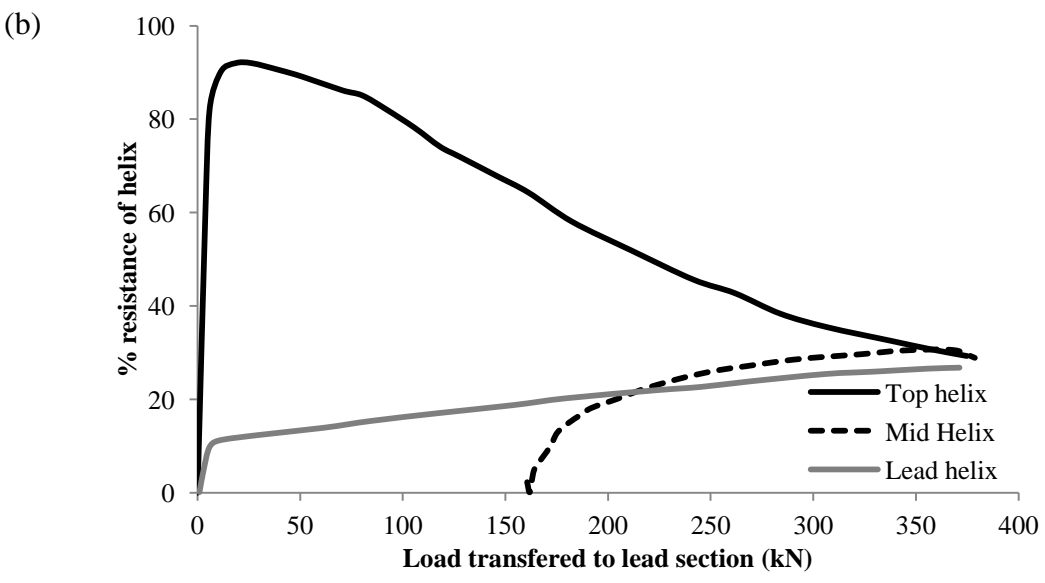
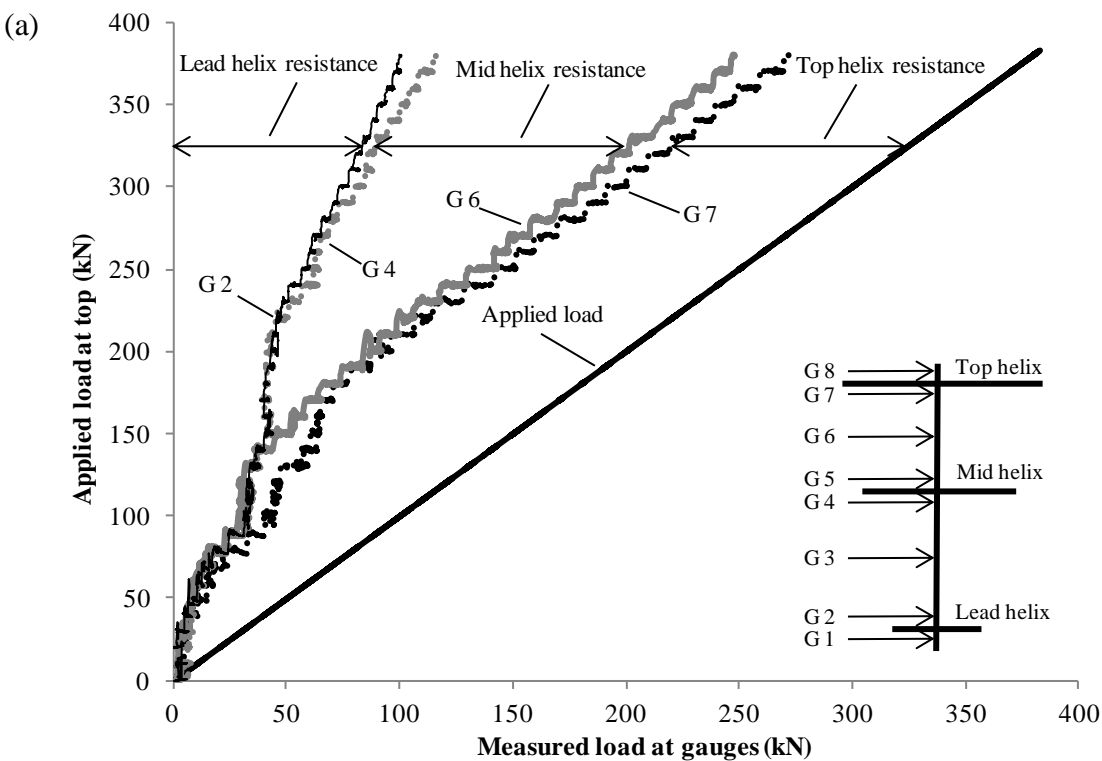
In addition, the redistribution of load share between the helices may be due to excessive stresses occurring underneath one of the helices. Figure 3.8a and b shows that the resistance of the first helix proportionally increased with loading until it reached 115 kN, after which, the resistance remained constant, and the other two helices began to have a more significant contribution to the load resistance. In fact, calculating the ultimate resistance considering strength parameters and bearing capacity factors based on Bowles (1996) and Prakash and Sharma (1990), after Mayerhof (1976) (see detailed calculations in next section) provide an estimated ultimate resistance of the first helix of about 130 kN. This shows that the maximum bearing pressure underneath the first helix was reached, and that a plastic zone may have developed, resulting in load re-distribution between the three helices. These observations are in-line with the findings of Sakr (2009). He observed that one-helix and two-helix piles offered almost identical behaviour at early stages of loading (i.e. one helix was providing almost all the resistance), and at higher loading levels, the two-helix pile offered a stiffer response, indicating that at relatively low load levels one helix was almost solely resisting the applied load, and that at higher

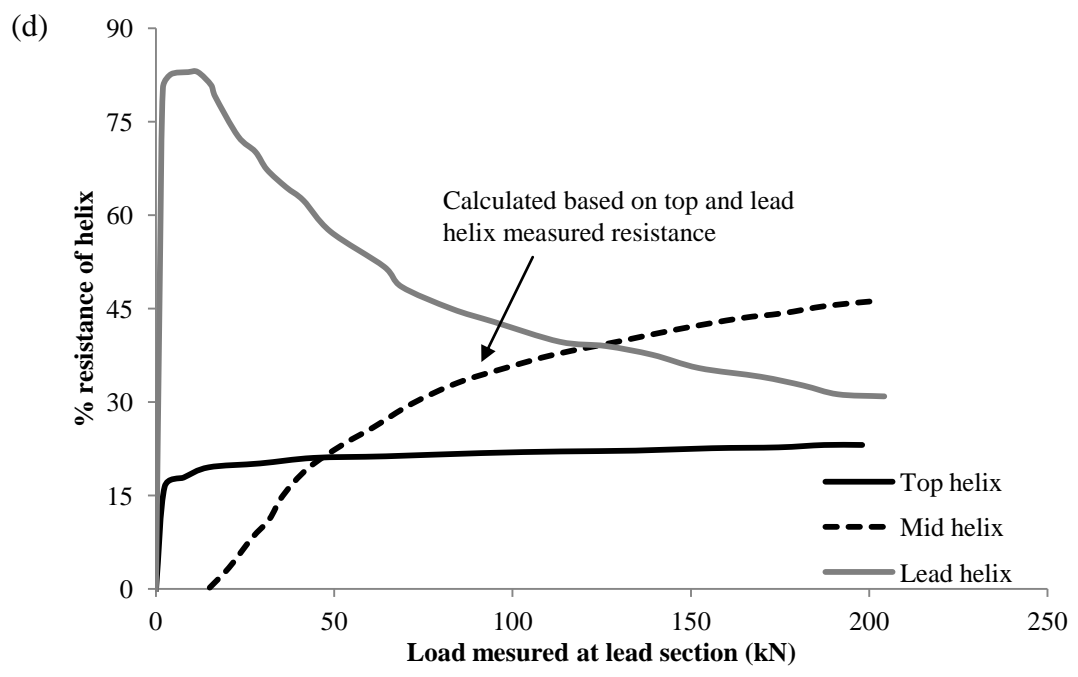
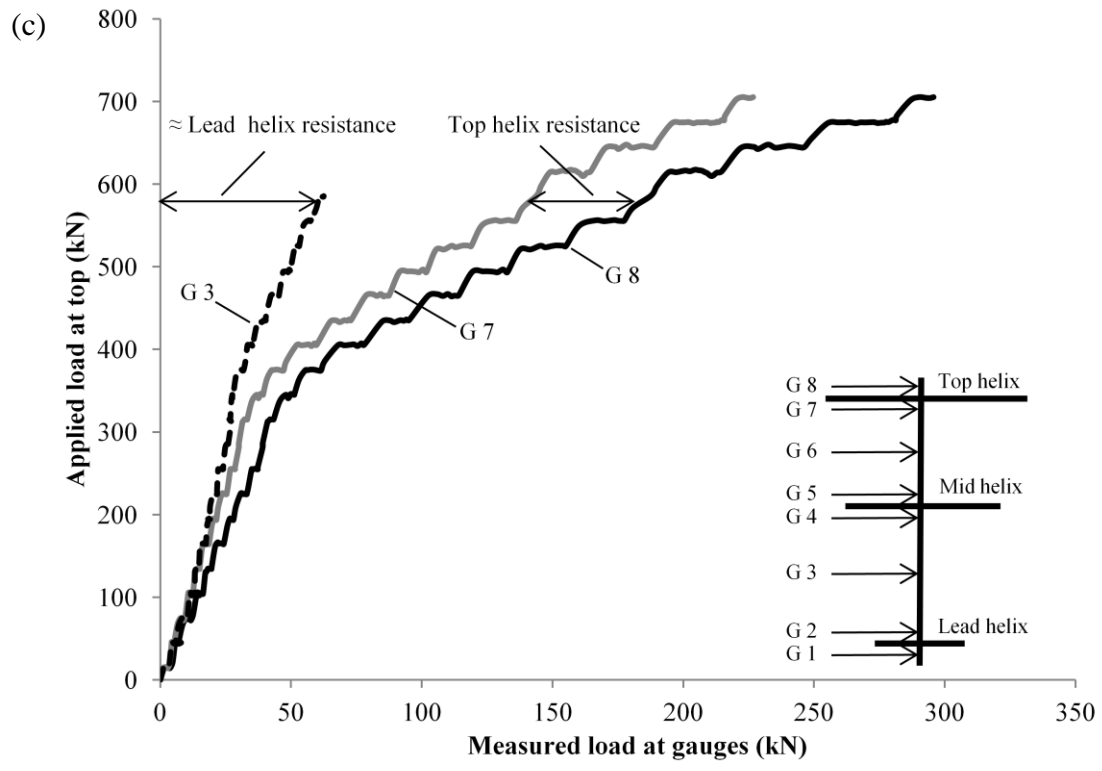
loads the load resistance share was redistributed. It should be noted that the measured top helix resistance for Pile 10 (Figure 3.8f and g) was up to 150 kN; the flowable grout used during installation may have strengthened the soil in the vicinity of the helix.

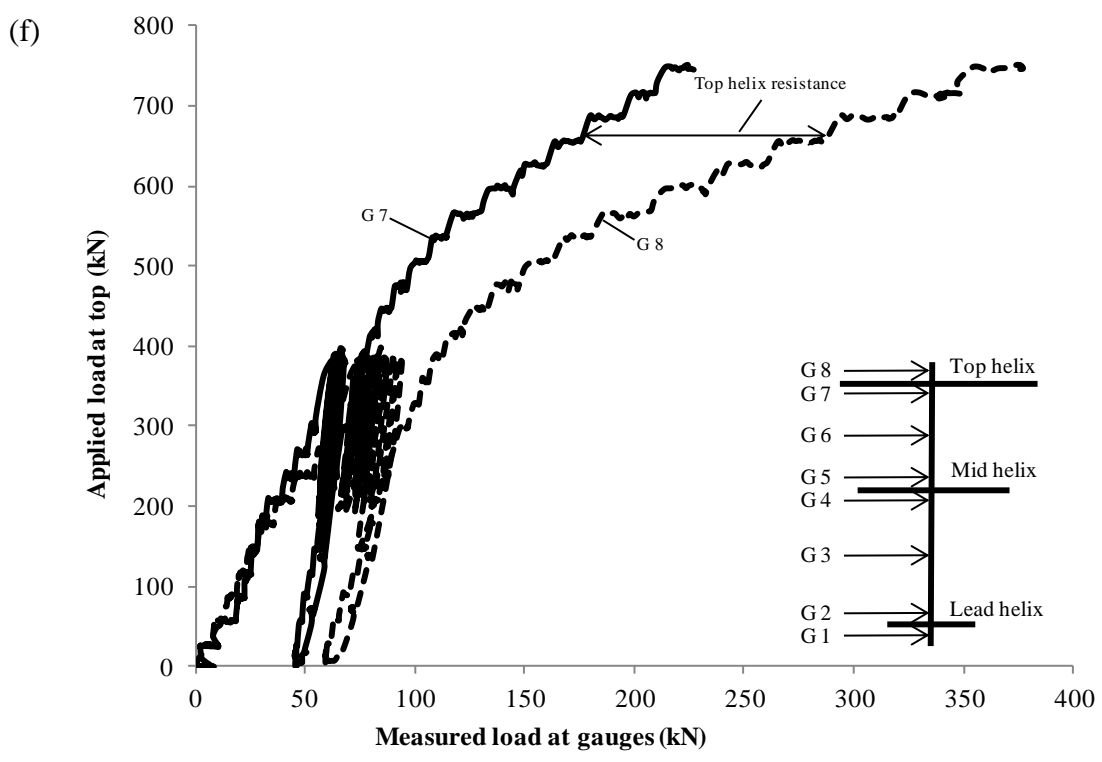
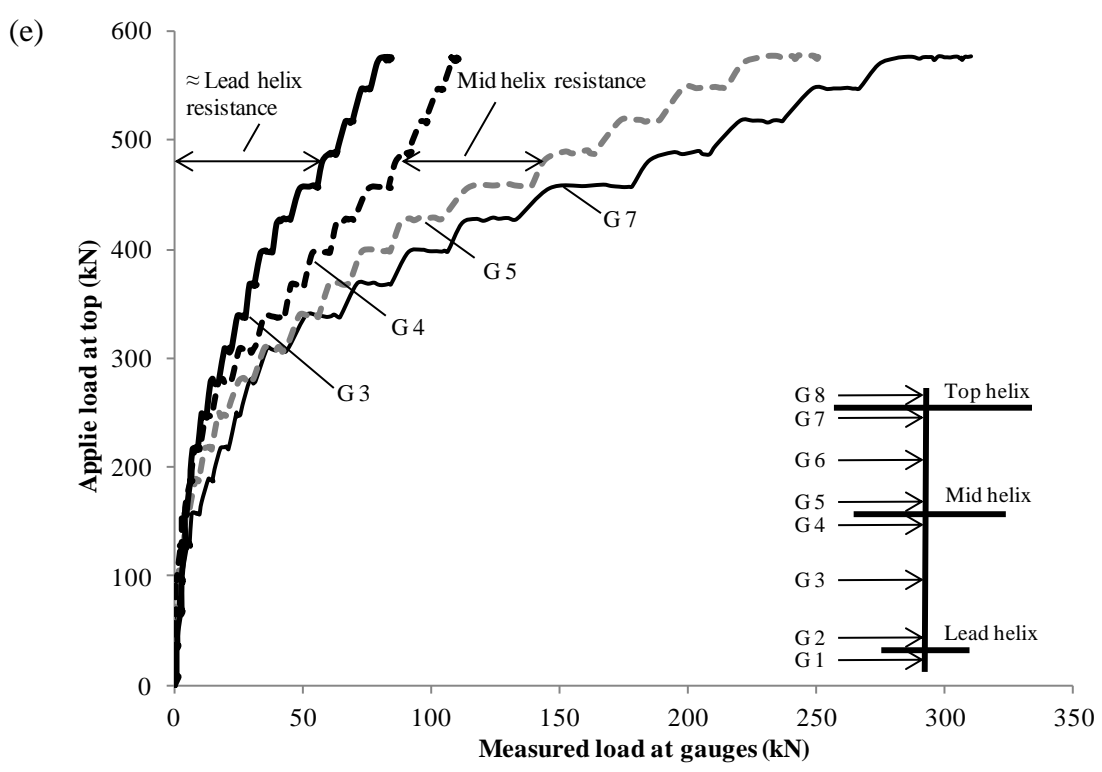
The axial forces measured above and below the first helix during cyclic loading for Pile 10 are shown in Figure 3.8e. As can be seen, the axial load transferred to the lead section increased during cyclic loading (Gauge 8). As mentioned before (Figure 3.6e), the load increase demonstrates the cyclic degradation in the shaft resistance. This degradation was compensated in part by the increase in resistance of the first helix. The load measured during cyclic loading increased from 74 kN to 94 kN and from 62 kN to 68 kN, a 75% load reduction by the top helix. Inspecting Figures 3.8f and g, it can be seen that unlike before cyclic loading where the top helix had minimal contribution to the load resistance, after cyclic loading the first helix contribution significantly increased; this can be explained by the effect of cyclic load on compacting the soil at the vicinity of the helix. This observation can be of importance for design of helical piles under cyclic loads; soil condition in the vicinity of the top helix may have a significant influence in the pile's cyclic performance.

The results also show that during cyclic loading, increase in the load transferred to the lead section was largely accommodated by the first helix. This demonstrates that using this composite system of a helical pile and a micropile can be advantageous for cyclic loading applications as the reduction in the shaft resistance may be accommodated by the

lead section. In addition, it may be advantageous to use multiple-helices (compared to a single helix) to further improve the cyclic performance of this pile system.







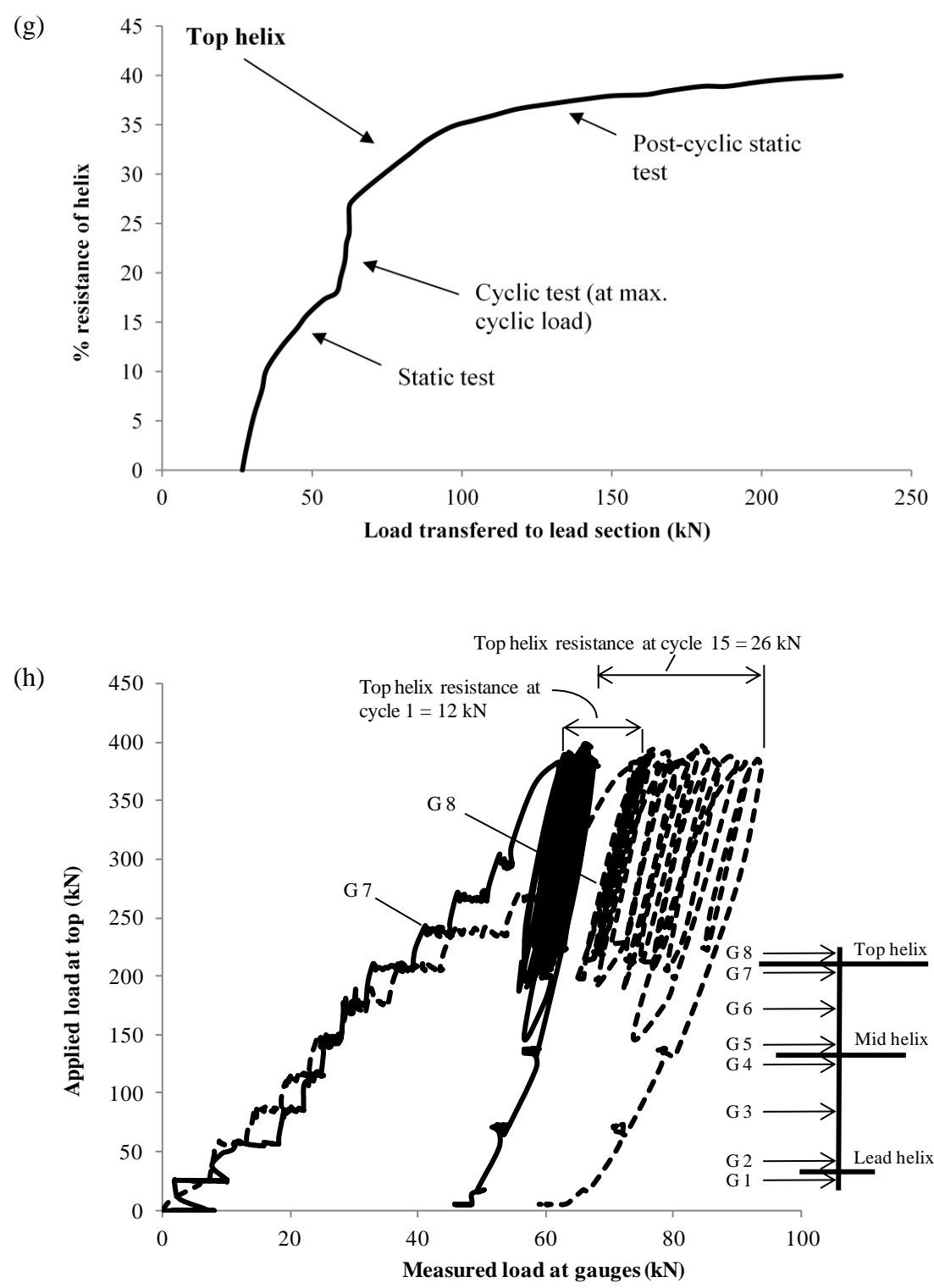


Figure 3.8. Measured load transfer in lead section and % resistance of helices; (a), (b) plain helical pile; (c), (d) RHPM-4; (e) RHPM-6; (f), (g) RHPM-10; (h) RHPM-10 during cyclic loading. (Note: G = Gauge).

3.9 Axial Capacity of Tested Piles

There are several methods available for defining the failure load of a pile. Some methods define the failure load as the load corresponding to a settlement limit. This settlement limit is usually a predefined value or a percentage of the pile diameter. Other methods define the failure load as the intersection of the initial tangent and the tangent of the final portion of the load displacement curve. Terzaghi (1942) defined the ultimate load as the load corresponding to a displacement of 10% of the pile diameter. For cast-in-place piles, O'Neill and Reese (1999), consider the ultimate pile capacity to be the load corresponding to 5% of the pile toe diameter. Butler and Hoy (1977) suggested the ultimate pile capacity as the load defined by the intersection between the tangents of the initial portion and the final portion sloping 0.05 in./ton (12.7 mm/100 kN). Also, the load corresponding to a pile head displacement of 25.4 mm (1 inch) is commonly used in practice.

A suitable failure criterion should take into account the unique geometry characteristics of helical piles where lead sections consist of multiple plates. Sakr (2008) found, for helical piles with two helices in oil sands, that the estimated capacities of these piles were in reasonable agreement with the 10% failure criterion (10% of helix diameter). Livneh and El Naggar (2008) defined the ultimate compressive load for helical piles with three helices as the load associated with a displacement of 8% of the largest helical diameter plus the elastic deflection of the pile. In this study, the ultimate capacity was calculated based on two different criteria: Livneh and El Naggar's and as the load corresponding to 25.4 mm (inch) displacement. It should be noted that the 10% of the average helix diameter criterion would yield the same results as the limiting 25.4 mm method. Axial

capacities are shown in Table 3.4 where it can be seen that the capacity based on Livneh and El Naggar's criterion was higher by 14% than the 25.4 mm limit criterion, for the plain helical pile, and by 4% to 5% for the RHPM.

The ultimate capacity of the reinforced helical pulldown micropile can be estimated as the sum of the shaft capacity and lead section capacity. The shaft capacity can be calculated using the recommended nominal grout-to-grout bond nominal strength in FHWA 2000 (Armour et al. 2000). For type A micropile, the nominal strength ranges from 50 kPa to 120 kPa. For test piles, using the aforementioned values, the predicted shaft strength ranges from 93.4 kN to 224 kN.

The capacity of the lead section can be calculated as the sum of the ultimate capacities of each helix (plate); the capacity of each helix can be calculated as:

$$[3.2] \quad Q_h = A_h(qN_q)$$

where A_h is the projected bearing area, q is the unite bearing capacity below the helix. and N_q is a bearing capacity factor.

The in-situ angle of internal friction of sand was estimated from the SPT results based on Bowels (1996). Prakash and Sharma (1990), after Mayerhof (1976), provide an estimation of the bearing capacity factor, N_q , based on installation method. Taking the installation method as drilled shaft (in order to ensure conservative design), $N_q = 22, 26$ and 35 for top, mid and bottom helices, respectively. The estimated bearing capacity for the lead section was found to be 354 kN.

The estimated ultimate capacity of the RHPM piles was found to range from 447.4 kN to 578 kN. The measured ultimate capacities are shown in Table 3.4; they are higher than the range of the calculated values by 4% to 39% using the 25.4 mm limiting displacement criterion, and higher by 16% to 43% using Livneh and EL Naggar's criterion. The difference between the measured and estimated ultimate capacities is mainly from the shaft friction component of the ultimate capacity. It appears that using the higher end of the range provided in the FHWA 2000 for nominal grout-to-grout bond strength (Armour et al. 2000) is more appropriate for estimating shaft friction for RHPM installed in stiff clay.

These results indicate that the pile capacity can be conservatively estimated based on the capacity of the shaft as a type A micropile, and individual bearing of the helices within the lead section.

3.9.1 Installation Torque-Compressive Ultimate Capacity Relationship

Helical piles are installed by means of mechanical torque. The installation torque has been commonly used as a practical means to predict the screw anchor ultimate capacity through an empirical correlation factor. Livneh and El Naggar (2008) discussed that the rationale behind this method is that installation torque is a measure of the energy required to overcome the shear strength of the soil and hence directly related to pile capacity. In addition to the empirical correlation method, a number of theoretical correlations between installation torque and uplift capacity were developed by several investigators including, Ghaly et al. (1991); Perko (2009); Tsuha and Aoki (2010). However, the empirical correlation factor remains to be widely used in practice; it doesn't require detailed

knowledge of soil properties or strength parameters, i.e. it can be easily applied on-site for ultimate capacity estimation.

Hoyt and Clemence (1989) introduced an empirical factor K_t that depends on screw pile shaft diameter where,

$$[3.3] \quad Q_u = T \times K_t$$

where T is the average installation torque over the last 1 m (3 ft), and K_t is an empirical torque factor. K_t values are 33 m^{-1} (10 ft^{-1}) for all square shaft anchors and round shaft anchors less than 89 mm, 23 m^{-1} for 89 mm round-shaft anchors, and 9.8 m^{-1} for anchors with 219 mm diameter extension shafts. The Canadian Foundation Manual (CFEM, 2006) recommends for pipe shaft anchors of 90 mm diameter a torque correlation factor of 33 m^{-1} , with this value decreasing to 10 m^{-1} for shaft diameters approaching 200 mm. A. B. Chance Co. (2007) reported that K_t may range from 10 to 66 m^{-1} depending on soil conditions, helical pile geometric configuration, and loading direction (compression or tension). For piles in dense sand (field N-Value of 30), Livneh and El Naggar (2008) found K_t values of 61.5 to 62.1 m^{-1} for piles under compression loading and 24.3 to 32.7 m^{-1} for piles under tensile loading. Abdelghany (2008) reported values of K_t between 20 - 28 m^{-1} for piles installed in clayey till. For piles installed in oil sands, Sakr (2008) reported K_t values of 23.6 m^{-1} for piles loaded in compression and 11 m^{-1} for piles loaded in tension. It is worth noting that the calculated K_t value depends on the interpretation of load test results (i.e. determination of ultimate capacity from load test data).

Table 3.4 presents the ultimate capacities and torque factors (based on average installation torque). For the plain helical piles, K_t is found to be 38 m^{-1} which is in a close agreement with the reported literature. For RHPM piles, K_t varies between 59.9 and 77.2 m^{-1} for piles tested in Stage I-A and between 63.6 and 77.4 m^{-1} for those tested in Stage I-B. These torque values are higher than those reported in the Canadian Foundation Manual (2006) by at least a factor of 1.8. This can be attributed to the increased resistance provided by the grout shaft.

Table 4.3 shows the torque factors calculated based on the lead section resistance only. The lead section capacity was estimated from the measured total capacity minus the shaft friction. The shaft friction was calculated assuming bond strength of 120 kPa (highest applicable value) as per the FHWA (Armour et al. 2000). As can be seen, the torque factor ranged from 40.8 m^{-1} to 58.6 m^{-1} .

3.10 Conclusions

In this study, a full scale experimental program was conducted to evaluate the axial monotonic and cyclic performance of reinforced helical pulldown micropiles. Based on the experimental results, the following conclusions can be drawn:

1-The load-displacement curves of RHPM piles display the typical trend consisting of an initial branch, followed by a transitional branch than a near-linear branch.

2-The results show significant shaft contribution to the total resistance. The shaft contribution ranged from 72% to 80% at working load levels and from 36% to 50% at relatively high load levels.

3-The load transfer mechanism for the lead section is through individual helices bearing.

4- The pile performance during cyclic loading largely depends on the cyclic performance of the grout shaft. The displacement during 15 cycles of one-way cyclic loading was found to be less than 1.77% of the shaft diameter with no degradation in load-unloading stiffness, demonstrating good performance during cyclic loading.

5-Strain gauge measurements during cyclic loading suggest that shaft resistance decrease is accommodated by the lead section, where bearing of the first helix dissipating the excess load transferred to the lead section. This shows that for cyclic loading applications, it is favourable to use multi-helix lead sections instead of single helix lead sections.

6-One way cyclic loading with average and maximum cyclic loading more than 40% and 54% of the ultimate capacity slightly improved the ultimate axial stiffness and axial capacity of tested piles.

7-The torque correlation factor was found to be 33 m^{-1} for plan helical pile and ranged from 59.9 to 77.7 m^{-1} for the RHPM piles. Application of recommended torque factors in the Canadian Foundation Manual for pipe shaft anchors may be over-conservative.

8-The shaft friction ultimate resistance can be estimated by adapting typical design correlations for type A micropile. The bearing capacity can be estimated by considering the sum of individual bearing resistance for the helical plates.

9- The RHPM pile is a viable foundation system for axial monotonic and one-way cyclic applications.

3.11 References

A. B. Chance Co. 2007. Chance Civil Construction Technical Design Manual, Hubbell Power Systems Inc., Centralia, MO, USA.

Abd Elaziz, A.Y., and El Naggar, M.H. 2012. Axial behaviour of hollow core micropiles under monotonic and cyclic loadings. *Geotechnical Testing Journal*, ASTM, 35(2):249-260.

Abdelghany, Y. 2008. Monotonic and cyclic performance of helical screw piles. PhD thesis, The University of Western Ontario, Canada.

Armour, T., Groneck, P., Keeley, J., and Sharma, S. 2000. Micropile design and construction guidelines- implementation manual. Federal Highway Administration FHWA-SA-97-070, Washington, D.C.

ASTM International. 2007. Standard test method for deep foundations under static axial compressive load. Designation D 1143/D 1143M, West Conshohocken, PA, USA.

Bowels, J.E. (1996). *Foundation analysis and design*. The McGraw-Hill Companies, Inc., NY.

Butler, H.D., and Hoy, H.E. 1977. Users manual for the Texas quick-load method for foundation load testing. Federal Highway Administration, Washington, D.C.

Canadian Foundation Engineering Manual. 2006. Fourth edition. Canadian Geotechnical Society, 488 p.

El Naggar, M.H, and Abdelghany, Y. 2007a. Helical screw piles capacity for axial cyclic loadings in cohesive soils. *In* Proceeding of the 4th International Conference on Earthquake Geotechnical Engineering, Thessaloniki, Greece.

El Naggar, M.H., and Abdelghany, Y. 2007b. Seismic helical screw foundation systems. *In* Proceedings of the 60th Canadian Geotechnical Conference, Ottawa, ON, pp. 21-24

Ghaly, A., Hanna, A., and Hanna, M. 1991. Installation torque of screw anchors in dry sand. *Soils and Foundations*, 31(2): 77-92.

Hoyt, R. M., and Clemence, S.P. 1989. Uplift capacity of helical anchors in soil. *In* Proceedings of the 12th International Conference on Soil Mechanics and Foundation Engineering, Rio de Janerio, Br. 13-18 August 1989, Vol. 2, pp. 1019-1022.

Kulhawy, FH. 1985. Uplift behaviour of shallow soil anchors-an overview. ASCE, pp. 1-25

Livneh, B., and El Naggar, M.H. 2008. Axial testing and numerical modeling of square shaft helical piles under compressive and tensile loading. *Canadian Geotechnical Journal*, 45(8): 1142-1155.

Lutenegger, A. J. 2010. Shaft resistance of grouted helical micropiles in clay. *In* Proceedings of the 10th International Workshop on Micropiles, IWM, Washington, D.C., USA, pp. 22-25.

- Mayerhof, G.G. 1976. Bearing capacity and settlement of pile foundations. *Journal of the Geotechnical Engineering Division, ASCE*, 102(GT3), pp. 225-244.
- Merifield, R.S., and Smith, C.C. 2010. The ultimate uplift capacity of multi-strip anchors in undrained clay. *Computers and Geomechanics*, 37(4): 504-514.
- Mitsch, M.P., and Clemence, S.P. 1985. The uplift capacity of helix anchors in sand. *ASCE*, 37(4): 26-47.
- Mooney, J.S., Adamczak, S.Jr., and Clemence, S.P. 1985. Uplift capacity of helical anchors in clay and silt. *In Proceedings, Uplift Behavior of Anchor Foundations in Soil, Proceedings of a Session held in conjunction with the ASCE Convention, Detroit, MI*, pp. 48-72, American Society of Civil Engineers, New York, NY, USA.
- Narashima Rao, N.S., and Prasad, Y.V.S.N. 1993. Estimation of uplift capacity of helical anchors in clay. *Journal of Geotechnical Engineering*, 119 (2): 352-357.
- O'Neill, M.W., and Reese, L.C. 1999. Drilled shafts: construction procedures and design methods. Federal Highway Administration, FHWA-IF-99-025, Washington D.C.
- Perko, H.A. 2009. *Helical piles: a practical guide to design and installation*. John Wiley & Son, Inc., Hoboken, N.J.
- Prakash, S., and Sharma, H.D 1990. *Pile foundations in engineering practice*. John Wiley & Sons, Inc., NY.

Sakr, M. 2009. Performance of helical piles in oil sand. *Canadian Geotechnical Journal*, 46(9): 1046-1061.

Tappenden, K., Segoo, D., and Robertson, P. 2009. Load transfer behavior of full-scale instrumented screw anchors. *In Proceedings of Geo-Florida 2009-Contemporary topics in deep foundations*, ASCE, GSP 185, pp. 472-479.

Terzaghi, K. 1942. Discussion of the progress report of the committee on the bearing value of pile foundations. *In Proceedings, Earth and Foundations*, American Society of Civil Engineers, Vol. 59, No. 8, pp. 1363-1372.

Tsuha, C. de H.C., and Aoki, A. 2010. Relationship between installation torque and uplift capacity of deep helical piles in sand. *Canadian Geotechnical Journal*, 47(6): 635-647.

Vickers, R.A., and Clemence, S.P. 2000. Performance of helical piles with grouted shafts. *In Proceedings of Sessions of Geo-Denver 2000 - New Technological and Design Developments in Deep Foundations*, GSP 100, v 288, pp. 327-341.

Table 3-1. Soil profile and SPT count established from boreholes.

Soil layer	Depth (m)	N-Value
BH-1		
Compact brown silty sand and gravel.	0-1	31
Very stiff to hard, brown becoming grey at 3 m (10 ft) depth, clayey silt to silty clay till. W.T. at 3.7 m depth.	1-1.8	43
	1.8-2.6	24
	2.6-3.3	47
	3.3-4	18
	4-5.9	22
Compact to dense sand, trace of some silt	5.9-7.9	32
Compact, grey silt	7.9-8.8	18
BH-2		
Very stiff to hard, brown becoming grey at 3 m (10 ft) depth, clayey silt to silty clay till. W.T. at 4.1 m depth.	0-1	21
	1-1.8	28
	1.8-2.6	8
Compact to dense sand, trace of some silt	5.6-6.4	30
	6.4-7.1	36
	7.1-7.9	42
	7.9-8.8	22

Table 3-2. Summary of geotechnical properties of soil from BH-1 and BH-2.

BH-1			
Depth, m	1.8	3.9	7
Gravel content (%)	7.3	0 (very small fraction)	1.4
Sand content (%)	54	66.2	86
Silt-clay content (%)	38.7 (72.5 % silt and 27.5 clay)	33.8 (62 % silt and 38 clay)	12.6
Specific gravity	2.69	2.77	2.67
Moisture content (%)	10.7	-	-
Liquid limit	28.7	35.7	-
Plastic Limit	12.8	16.6	-
Plasticity index	15.9	19.1	-
Undrained shear strength, (kPa)	100	-	-
BH-2*			
Depth (m)	3.0	3.8	4.2
Undrained shear strength, C_u (kPa)	86	183	174

*See Abd Elaziz and El Naggar (2012), C_u from undrained unconsolidated tests.

Table 3-3. Cyclic tests results for Stages I-A and I-B.

Pile NO.	Displacement before cyclic load (residual displacement)	Displacement after cyclic load	Increase in displacement	% of grout diameter	% of average helix diameter
Stage I-A, average cyclic 200 kN					
Plain pile	16.9 (37.5)	21.8	4.9	-	1.93
RHPM-1	3.9 (17.475)	4	0.1	0.07	0.04
RHPM-2	2.3 (15.475)	2.6	0.3	0.20	0.12
Stage I-A, average cyclic 270 kN					
RHPM-3	3.925 (14.05)	4.275	0.35	0.23	0.14
RHPM-4	3.97 (21.4)	4.36	0.39	0.26	0.15
Stage I-A, average cyclic 300 kN					
RHPM-6	4.85 (12.7)	5.2	0.35	0.23	0.14
Stage I-B, average cyclic 300 kN					
RHPM-7	8.7	11.4	2.7	1.77	1.06
RHPM-8	11.1	12.7	1.6	1.07	0.64
RHPM-9	9.8	11.4	1.7	1.10	0.66
RHPM-10	4.7	6.1	1.4	0.92	0.55
RHPM-11	7.3	9.0	1.7	1.10	0.66
RHPM-12	6.8	8.7	1.8	1.21	0.72

Table 3-4. Pile capacity and torque factors for tested piles.

Pile No.	Ultimate capacity, load at 25.4 mm (kN)	Ultimate capacity, load at elastic displacement + 8% of largest helix (kN)	Average Installation torque (kN.m) [lb.ft]	K_T (m⁻¹) [ft⁻¹] based on total pile capacity	K_T (m⁻¹) [ft⁻¹] based on lead section capacity
Plain pile	360	412	10.58 (7800)	38 (11.5)	
RHPM-1	600	669	10.85 (8000)	61.6 (18.7)	55 (16.6)
RHPM-2	800	838	10.85 (8000)	77.2 (23.4)	58.6 (17.7)
RHPM-3	755	790	10.85 (8000)	72.8 (22.1)	54 (16.4)
RHPM-4	704	734	10.85 (8000)	67.6 (20.5)	48.8 (14.8)
RHPM-5	620	650	10.85 (8000)	59.9 (18.2)	40.8 (12.4)
RHPM-6	709	739	10.85 (8000)	68.1 (20.6)	49.2 (14.9)
RHPM-7	690	720	10.85 (8000)	66.4 (20.1)	47.4 (14.4)
RHPM-8	659	690	10.85 (8000)	63.6 (19.3)	44.6 (13.5)
RHPM-9	740	775	10.85 (8000)	71.4 (21.6)	52.6 (15.9)
RHPM-10	805.9	840	10.85 (8000)	77.4 (23.5)	49.3 (14.9)
RHPM-11	794.9	830	10.85 (8000)	76.5 (23.2)	57.8 (17.5)
RHPM-12	761.7	800	10.85 (8000)	73.7 (22.3)	55 (16.7)

*** AXIAL MONOTONIC AND CYCLIC PERFORMANCE OF FRP-
STEEL FIBRE-REINFORCED HELICAL PULLDOWN
MICROPILES (FRP-RHPM)**

4.1 Introduction

Helical piles are a deep foundation system that can be used to support pipelines, telecommunication and transmission towers, and low- and medium-rise buildings. They are installed using mechanical torque with minimal noise and vibration levels. They are suitable for applications involving expansive soils and ad-freeze conditions and are advantageous in limited access installations. One of their greatest advantages is that they offer onsite quality control by monitoring installation torque. Helical piles can be used for both underpinning of deficient foundations of existing buildings and for supporting new foundations using pile caps. With recent changes of building codes stipulating increased seismic forces, there is an increasing demand for a retrofitting tool than can be reliably used to upgrade the seismic resistance of existing foundations. The segmented helical piles are examined in this study as a candidate for seismic retrofitting of existing foundations, which can also provide an efficient foundation option for new construction.

The segmented helical (screw) pile (HSP) consists of relatively small galvanized central square shaft (SS) or rounded shaft (RS) fitted with one or more (up to 4) helices. SS sizes range from 42 mm to 57 mm and RS sizes from 73 mm to 114.3 mm. The first segment

*A version of this chapter has been accepted for publication in the Canadian Geotechnical Journal (in press).

(lead section) contains the helices and is installed to the desired depth by adding extensions connected onsite using bolted couplings. The helices diameters range between 150 mm to 400 mm. For multi-helix lead sections, larger diameter helices are placed near the top followed by smaller diameter helices at a spacing of about three times the helix diameter. Helices have standard pitch of 76 mm (3").

The axial capacity of helical piles under compression can be limited by the buckling capacity of its shaft, especially for long piles and/or piles installed in weak soils. Vickers and Clemence (2000) introduced the Helical Pulldown[®] Micropile (HPM). It consists of a helical pile installed with a grout column surrounding the pile central shaft along the extensions. In addition, a casing can be installed surrounding the grout column; most commonly used casings are made of PVC or steel. The type of casing used depends on soil and loading conditions (e.g. recent fills, soft soil conditions, high lateral loads). The helical micropile has a grout shaft diameter of less than 300 mm, and is reinforced by the steel shaft (extension) of the helical pile. Vickers and Clemence (2000) demonstrated that the addition of a grout column to helical piles results in a considerable increase in the ultimate axial capacity and performance of the pile. Similarly, Abdelghany and El Naggar (2010), Lutenecker (2010), and El Sharnouby and El Naggar (2012) reported that the grouted shaft results in a considerable increase in the pile axial capacity.

4.1.1 Static capacity of helical piles

The axial capacity of helical piles can be evaluated considering two load transfer mechanisms: individual helix bearing or the cylindrical shear methods. The individual bearing method considers the pile capacity as the sum of the individual bearing capacity

of each helical plate. The cylindrical shear method assumes that the load is transferred to the soil through a cylinder of a soil mass that is enclosed between the upper and lower helices, and bearing of the upper helix for tension loading or lower helix for compression loading. The failure mechanism depends primarily on the helix spacing ratio, defined as ratio of helix spacing to helix diameter, and soil conditions. Kulhawy (1985) stated that if the helices are widely spaced, anchor capacity is that of several single plates. On the other hand, several studies showed that cylindrical failure surface develop between the helices, especially in clayey soil. For example, Mooney et al. (1985), El Naggar and Abdelghany (2007a, 2007b), Livneh and El Naggar (2008), and Merrifield and Smith (2010) conducted model and full scale tests as well as numerical and analytical solutions considering helical spacing ratios as large as 4.5. They concluded that the failure mechanism is dominated by cylindrical shear failure. However, Narashima Rao and Prasad (1993) who concluded that for spacing ratios larger than 1.5, the cylindrical shear failure didn't mobilize.

Fewer studies investigated the load transfer mechanism of helical piles in sand. Mitsch and Clemence (1985) conducted laboratory tests on piles in sand with spacing ratio of 3, and concluded that shear failure takes place along the interface boundary between the helices. The Canadian Foundation Manual (BiTech, 2006) specifies that, for the individual bearing method to be applicable, helices should be placed at least three times the largest helix diameter. Sakr (2009) based on field testing results of single and double helix piles, suggested that individual bearing method is more suitable for piles in oil sands with spacing ratio of 3. Cerato and Victor (2009) compared the measured uplift

capacity of helical anchors with both design methods, and concluded that the cylindrical shear method significantly underpredicted the uplift capacity of most tested anchors. Lutenecker (2011) performed tests on double-, triple and quadruple-helix screw anchors with helix spacing to diameter ratios varying from 1.5 to 3 (0.75 to 4.125 for triple helix anchors). He found that the transition from cylindrical shear behaviour to individual plate behaviour of cylindrical multihelix anchors with a fixed number of helical plates in sand occurs at a spacing of about 3. El Sharnouby and El Naggar (2012) carried out full scale testing on instrumented three-helix piles. They found that for helical piles installed in dense sand, the load transfer is dominated by individual bearing.

4.1.2 Review on cyclic behaviour of helical piles

Various types of structures are required to withstand cyclic loads. These loads can be one way compression or tension (repeated loads) or of alternating manner. Several researchers (Hanna et al., (1978); Andreadis et al. (1981); Hanna and Al-Mosawe (1981); Clemence and Smithling (1983); Cerato and Victor (2009); Buhler and Cerato (2010)) have focused on the behaviour of helical piles or embedded anchors under sustained uplift cyclic loading (and to a lesser degree on alternating loads), and its effect on the post-cyclic static behaviour. These studies were geared towards simulating wind-type loading on wind turbines and transmission towers. As such, the cyclic loading duration was of a long term, i.e., 1 hr to 500 hrs (large number of cycles). Hanna et al. (1978) observed that the displacement of an anchor during sustained-repeated (one-way) uplift cyclic loading depends primarily on the load range during cyclic loading; higher load range requires smaller number of cycles to cause failure. While failure didn't occur during

testing, they observed that the displacement per cycle decreases, but never ceases, and that the size of the hysteresis loop decrease with the number of cycles. Andreadis et al. (1981) demonstrated experimentally that repeated application of loads reduced the anchor resistance and resulted in non-recoverable movements. On the other hand, other studies reported that repeated cyclic uplift loading improves the static performance of the pile and increases its post-cyclic capacity (e.g. Hanna et al. (1978); Hanna and Al-Mosawe (1981); Andreadis et al. (1981); Cerato and Victor (2009); Buhler and Cerato (2010)).

Meanwhile, Clemence and Smithling (1983) observed degradation in performance of pre-stressed under cyclic loading that resulted in anchor failure. . They found that the number of cycles to failure depends on the cyclic displacement amplitude. The anchor that was subjected to relatively larger displacement amplitudes of 1.78 mm (0.07 inches) failed after 120 cycles, while the anchor subjected to 0.68 mm (0.027 inches.) displacement amplitude failed after 1200 cycles. They observed reduction in horizontal stresses during cyclic loading, indicating loosening of the sand during loading until the active horizontal state of stress was reached which was followed by anchor failure.

Less attention was given to the behaviour of helical piles in compression, and even less for helical piles under one-way cyclic compression loading. The load transfer mechanism and resistance during and after cyclic loading may differ from that under tensile loading conditions. When helical piles are used to support new construction or retrofitting existing structures, loading conditions include axial compression and one way cyclic compression (sustained cyclic compression loading).

El Naggar and Abdelghany (2007a) investigated the performance of plain helical piles, and helical pulldown® micropiles installed in clay under 15 slow cycles of loading over a span of 8 hrs. The mean cyclic load level was 100 kN (1/3 of the estimated ultimate capacity) and the amplitude was +/- 30 kN. They found that the stiffness remained almost constant during cyclic loading for all three test piles. They observed that for the plain pile, post-cyclic static capacity was reduced by 5% to 10%. Meanwhile the axial capacity of the helical pulldown® micropile displayed a variation of +/-18% of its axial capacity. Abdelghany (2008) attributed the capacity increase for some piles to the cyclic loading effect on reducing the disturbance caused during installation. El Sharnouby and El Naggar (2012) conducted full scale testing on steel fibre-reinforced helical pulldown micropiles (RHPM) with their helical plates situated in sand and the grout shaft embedded in clayey till soils. They observed no degradation in the stiffness of the pile during 15 cycles of loading spanned over 30 minutes, and reported an increase in the pile post-cyclic capacity.

4.1.3 Previous studies on fibre reinforced polymer-helical pulldown micropile (FRP-HPM)

The use of FRP composite materials in construction has increased significantly in the past few years. FRP materials are made of a polymer matrix reinforced with fibreglass (or other fibres). Their features include: light weight (i.e. 1/4 to 1/8 of steel), corrosion resistance, minimum maintenance and environmental resistance. These features render them an attractive option for deep foundations. Sakr et al. (2004a) conducted large scale laboratory testing on FRP-concrete piles and found that their performance is comparable

to that of steel piles. Sakr et al. (2004b) stated that the FRP-self-consolidating concrete piles are an attractive option for deep foundation industry.

Given the advantages of FRP-concrete piles, along with those of helical piles, a composite helical-FRP-grout pile system was first investigated by Abdelghany and El Naggar (2010). They conducted full-scale tests on helical piles sleeved with FRP tubes along the top 3 m of the pile. The FRP tube was installed in stiff to very stiff clayey soils (SPT values of 21 to 36 along the tube depth). They reported some difficulty during installation of the FRP tubes as a result of the soil resistance; additional torque was required to install the tubes, and in some cases the embedment depth was limited as the maximum torque was reached. The piles offered slight improvement over the helical piles. The fact that the FRP-HPM didn't offer a considerable increase in the performance was attributed to the disturbance within the inter-helix zone (and disturbance along the FRP tube) caused by the additional torque required for installation of the FRP tube. They concluded that the FRP-HPM is a viable foundation option and should be explored further.

4.2 Objectives of Study

The primary objectives of this study are to (i) develop an effective piling system that can significantly improve the capacity, and overcome the drawback, of helical piles; (ii) develop an efficient technique/apparatus for the installation of the FRP-RHPM (iii) understand the load-settlement curves and use them to evaluate the piles axial capacity under compression; (iv) investigate the developed pile performance under cyclic loading; (v) examine the effect of cyclic loading on their axial performance; (vi) investigate the

load sharing mechanism between the shaft and lead section under static and cyclic loads; and (vii) investigate the load transfer mechanism within the lead section, individual bearing or cylindrical shear.

4.3 Site Investigation

The experimental program was carried out at the environmental site of the University of Western Ontario, London, Ontario. Two boreholes were conducted within the tests area, 16.6 m apart, to a depth of 8.8 m. Standard penetration tests was performed for each borehole using an automatic hammer. Borehole logs and SPT counts are provided in Table 4.1. The site consisted of stiff to very stiff clayey silt till underlain by dense sand. Traces of gravel and cobbles were observed during sampling, which was also manifested in spikes of the SPT counts due to the gravel within the till layer. Retrieved samples showed that the till layer was fissured, especially at shallow depth. The ground water table was found at an elevation of 3.7 m and 4.1 for BH-1 and BH-2, respectively.

Samples retrieved at BH-1 from depths 1.5-2 m (undisturbed), 3.6 to 4.25 m (disturbed), and 6.6 to 7.25 m (disturbed) were subjected to sieve and hydrometer analysis, and consistency tests. The sample at 1.5-2 m depth was subjected to undrained consolidated test. The results of lab tests are presented in Table 4.2.

4.4 Test Pile Description, Installation and Instrumentation

4.4.1 Components

The tested composite pile system (Figure 4.1) was comprised of: a lead section, three extensions, a pile-sleeve coupling, and a cylindrical FRP tube (sleeve) that surrounded part of the pile shaft, infilled with steel fibre-reinforced grout column. The details of the lead section are as follows: 1.5 m long; 44.5 mm square shaft; 3 attached helices (diameters = 305 mm, 254 mm and 203 mm); 76 mm helix pitch, helix spacing 3 times helix diameter. Extensions were 44.5 mm square shafts, each was 2.1 m long. The FRP tube was 3.3 m long, a nominal outside diameter of 140 mm and wall thickness of 7.62 mm. The pile was installed such that the lead section was situated entirely within the dense sand, while the shaft (FRP shaft) was situated within the stiff clayey silt till, as shown in Figure 4.1a.

To evaluate the improvements that the FRP-RHPM offers over the plain helical pile, one instrumented plain helical pile with the same lead section and extension configurations was installed to the same depth and tested under axial and cyclic loading conditions.

In order to evaluate the load transfer mechanism, end bearing or cylindrical shaft, including the individual contribution of the pile shaft (FRP tube) and lead section during axial static and cyclic loading, the lead sections were instrumented with eight strain gauges as shown in Figure 4.1a. Six gauges were installed on the shaft of the lead section just before and after the helices, and the remaining two at mid distance between each two helices.

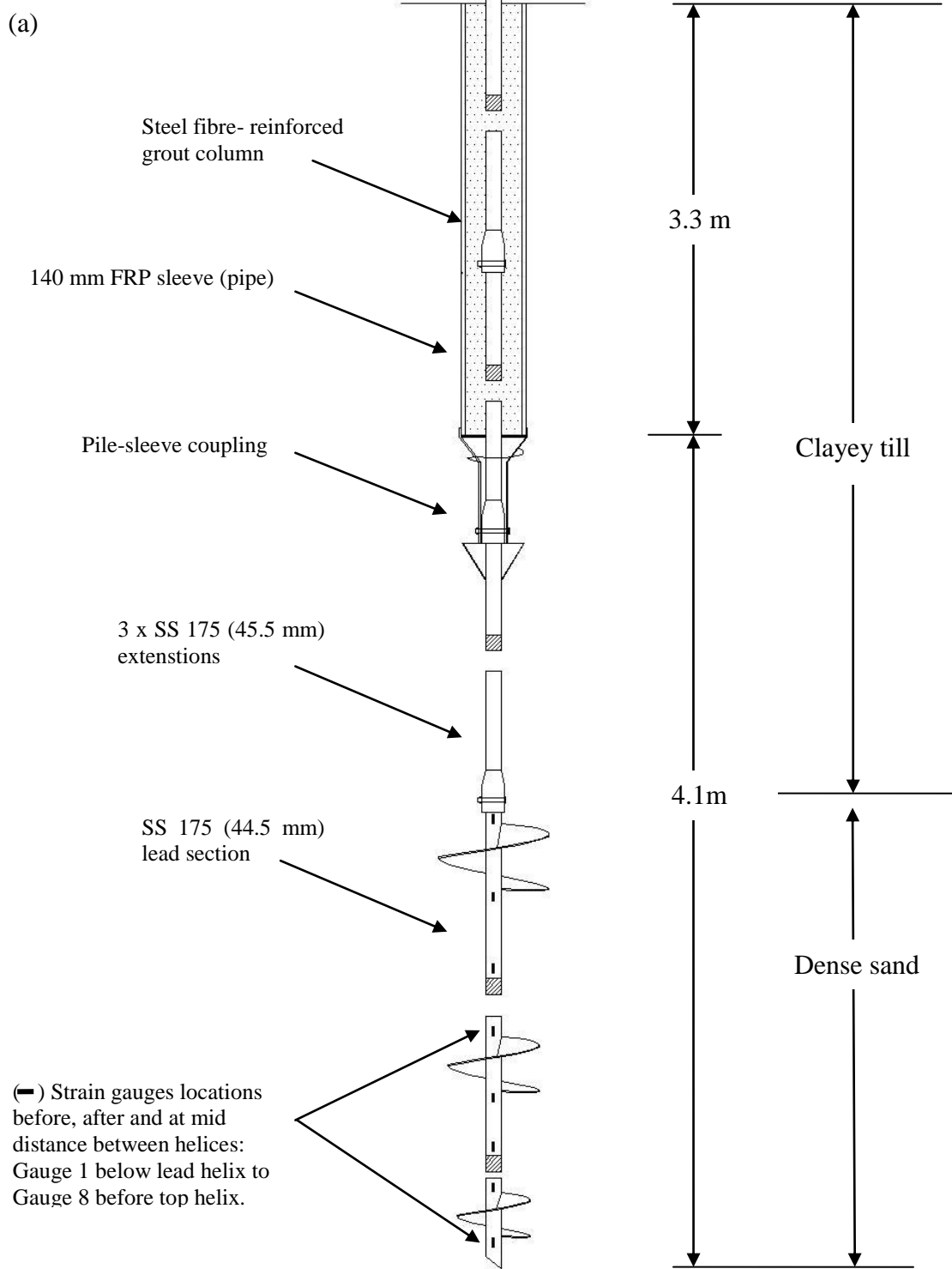
4.4.2 Novel installation technique

An innovative installation technique for constructing the FRP-RHPM was developed to overcome the installation difficulties associated with excessive friction along the FRP tube. Figure 4.1b shows a schematic of the pile during installation, along with the components used for installation, a pile-sleeve coupling and an installation adaptor. The pile-sleeve coupling consisted of an elevation tube specially manufactured to accommodate the 3.3 m tube length, an installation helix to facilitate pile installation, and an annular seating that the FRP tube rests on. The Installation adaptor comprised of an annular sleeve coupling, installation tube, annular driving cap and a conventional square shaft driving tool.

The pile was constructed by first installing the lead section and the first extensions. A soil displacement conical disk and the pile-sleeve coupling were then mounted on the pile shaft (See Figure 4.1b). The FRP tube was then placed encasing the extension, seated on a tube seating from one side. From the other side, the installation adaptor (shown in Figure 4.1b) was placed, having an annular seat that fits onto the FRP tube. Pile installation was then resumed; the pull-down force generated from the lead section along with axial downward force by the installation machine pushed the FRP tube downwards. The tube was then filled with steel-fibre reinforced grout under gravity. It should be noted that prior to pile installation, a hole having slightly smaller diameter than that of the FRP tube and same length was pre-drilled.

The proposed installation technique, unlike currently used methods, allowed the FRP tube to rotate relative to the installation components from sides, the pile-sleeve coupling

and the installation adaptor. This mechanism provided minimal resistance along the FRP profile during installation, and minimized the stresses developed within the FRP tube and hence preserving its structural integrity.



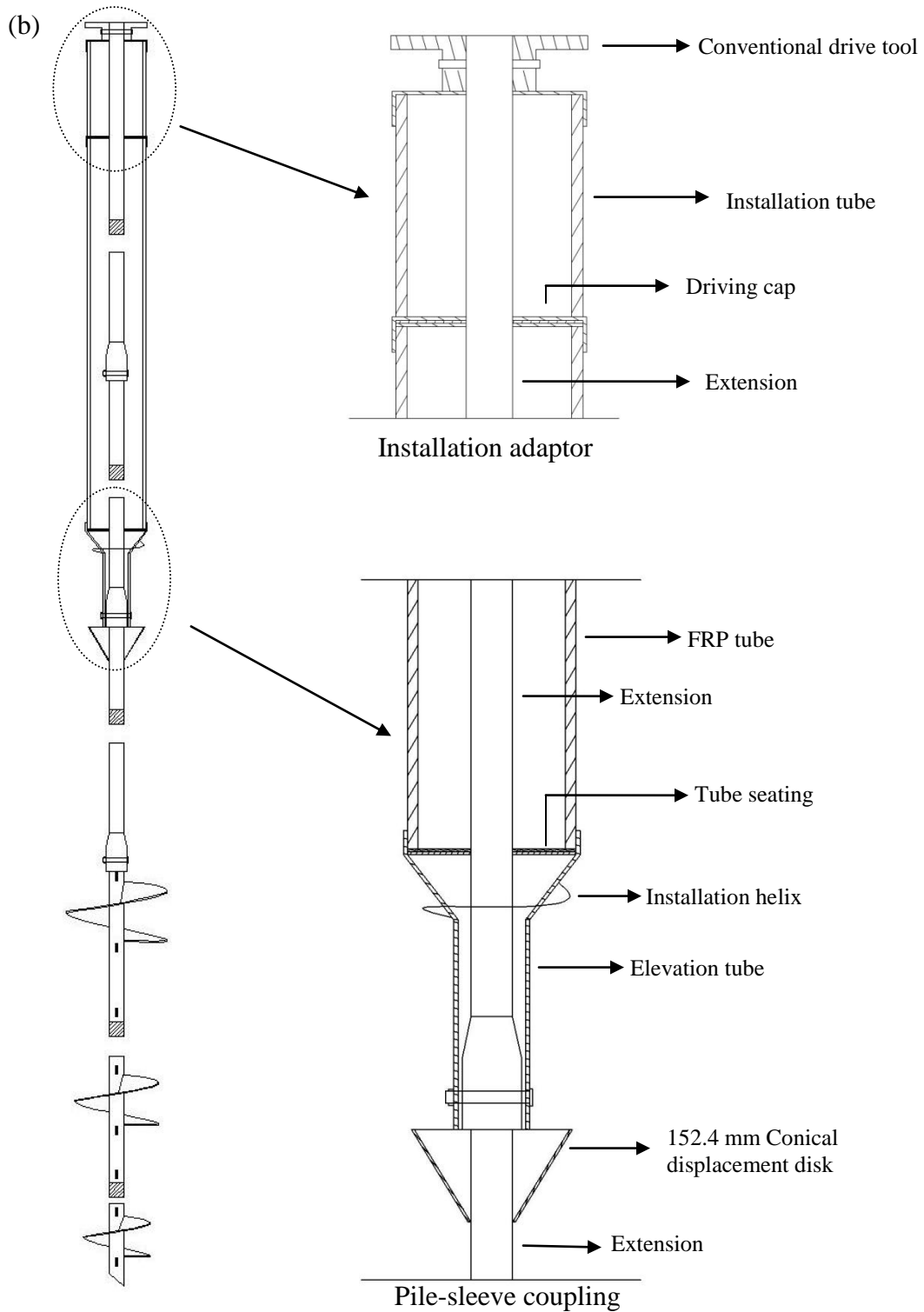


Figure 4.1. (a) FRP-RHPM test pile profile after installation; (b) FRP-RHPM during installation and components.

4.5 Field Test Set-up

Figure 4.2 shows a full view of the load test set-up. It comprised a main steel reaction beam, centered over the test pile, and two secondary reaction beams. The secondary beams were tied to four reaction piles (helical piles with 50.8 mm square shaft) using threaded rods and couplings. ASTM D-1143 (2007) specifies a minimum clear distance between test piles and reaction piles of five times the largest pile diameter but not less than 2.8 m. In addition, Elsherbiny (2011) found that interaction between helical piles is minimal if spacing is more than four times the largest helix diameter. Therefore, reaction piles were installed at a rectangular arrangement of 3 x 3.6 m (> 10 times the largest helix diameter). For each test, reaction piles were installed to equal torque in order to ensure similar response from all four piles. The loading plate was manufactured such that it rests on the pile head from one side, and threads into the load cell from the other side. The load was applied using a hydraulic jack that was centered over the load cell. Any gap between the hydraulic jack and main beam was filled by steel plates. Axial displacements were measured using four linear displacement transducers (LDTs) at the corners of the loading plates, and mounted on steel reference beams (helical pile extensions). The load cell, LDTs, and strain gauges were connected on site to a data acquisition system.



Figure 4.2. Full view of axial and cyclic test set-up.

4.6 Testing Procedure

The objective of the testing program is to identify the performance characteristics of the FRP-RHPM under static and cyclic loading, and to determine the effect of the cyclic loading on the pile capacity. The monotonic compression loads followed the guidelines of ASTM D-1143 (2007) quick load test method. The applied load was increased in increments of 30 kN every 4 minutes (or less if constant displacement was observed for more than 30 seconds). The cyclic loading involved fifteen cycles of one-way compression cyclic loading completed in 30 min (0.008 Hz). The loading program included two phases of testing. The first phase (Phase I) involved 5 piles subjected to the following testing stages, as shown in Figure 4.3:

- i) Static (monotonic) loading up to maximum displacement at the pile head of not less than 13% of the diameter of the FRP tube. This was done to ensure that the ultimate capacity could be fully mobilized (Livneh and El Naggar2008).
- ii) Fifteen cycles of one-way compression cyclic loading were completed in 30 min. The mean cyclic load applied was equal to the pile estimated design capacity, 300 kN, and the cyclic load amplitude was 90 kN (i.e. cyclic load varied between 70% and 130% of the design capacity).
- iii) Final static (monotonic) loading up to a maximum displacement of 25 mm (1 in) or the capacity of the testing equipment was reached.

The plain (control) pile was tested following the same steps. The first static loading was carried up to 490 kN (maximum displacement of 37 mm). The cyclic load ranged from 140 kN to 250 kN, followed by final static loading until failure was reached.

The second phase (Phase II) of testing involved 8 piles, and was designed to examine the cyclic performance of the piles without prior excessive loading. The testing procedure was as follows (see Figure 4.3):

- i) Piles were subjected to static loading to a maximum of 300 kN.
- ii) Fifteen cycles of one-way compression cyclic loading were completed over 30 min. The average cyclic load was taken as equal to the pile estimated design capacity, 300 kN, and the cyclic load amplitude was 90 (i.e. cyclic load varied between 70% and 130% of the design capacity).

- iii) Final static loading, where the applied loads were increased until continuous jacking was required to maintain the load, a considerable displacement was reached or until the load approached the capacity of the load cell (or the reaction system).

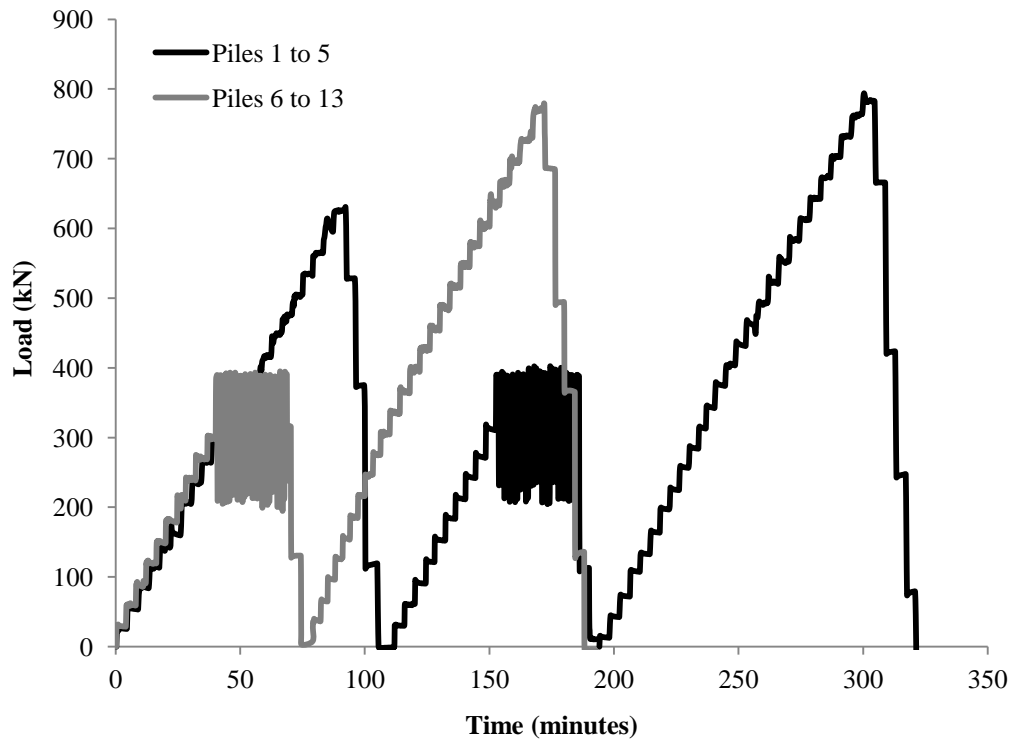


Figure 4.3. Test loading protocol for Piles 1 to 5; and for Piles 6 to 13.

4.7 Axial Compression Results

4.7.1 Initial axial static results

Figure 4.4 shows the load-settlement curves for two FRP-RHPM, which represent the upper bound and lower bound of observed behaviour of all tested FRP-RHPM piles (i.e. load-settlement curves for other piles fall between these two curves). The load-settlement curves feature the typical trends of a conventional pile load test curve, i.e., a linear branch,

followed by a transitional branch, followed by a semi-linear branch until maximum load is reached. The results of the plain helical pile are also shown in Figure 4.4. It can be noted from Figure 4.4 that the addition of the FRP tube and grout reinforcement significantly improved the performance of the helical pile throughout the loading range. For example, the maximum load sustained by the FRP-RHPM piles at 20 mm settlement was between 570 kN and 640 kN, while the plain pile carried only 320 kN. Similarly, at a relatively low settlement of 2.5 mm (corresponding to expected design load capacity), the lower bound FRP-RHPM demonstrated an increase in load capacity of 65%.

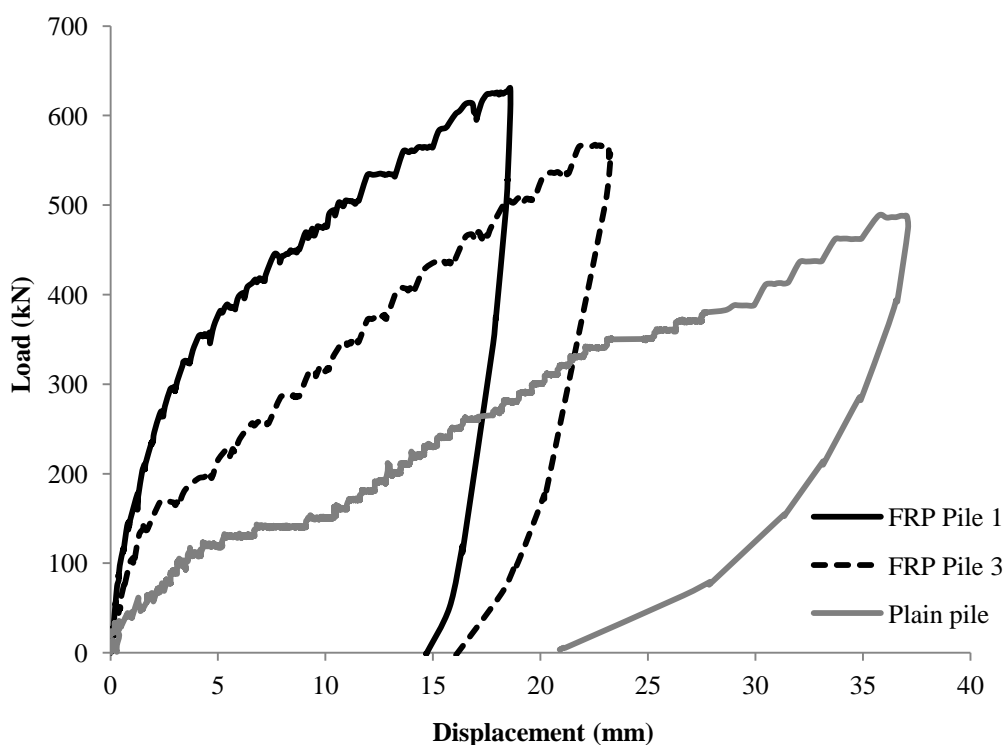


Figure 4.4. Initial static load displacement response, Phase I.

4.7.2 Load sharing between FRP shaft and lead section

The load transferred to the lead section was evaluated from the measurements of the strain gauge attached to the pile shaft above the top helix. The FRP shaft resistance was then calculated as the applied force minus the force transferred to the lead section. It is assumed that the steel shaft resistance, for the ungrouted part, is negligible. The shaft resistance for FRP Pile 1 is presented in Figure 4.5. Inspecting Figures 4.4 and 4.5, it can be seen that the changes in slope of the resistance curve (hardening behaviour) corresponds closely to the transition from one loading branch to another. The percentage contribution of the shaft to the applied load was highest at low load levels, and decreased with loading. At settlement of about 1 mm, the FRP shaft carried about 70% of the applied load. As the settlement reached about 5 mm, the FRP shaft load has increased, but its share of the applied load was approximately 59%; after which the resistance increased, but with a gradually decreasing share of the applied load. This trend continued as the pile head settlement increased, with the shaft resistance providing only 50% of the 600 kN applied at pile head settlement of 14 mm. Similar observations were made from test results of other FRP-RHPM. From these observations, it may be concluded that the lead section contributes to the pile load carrying resistance from early stages of loading. In addition, the slope of loading branches can serve as an indication to the hardening/softening behaviour of the shaft-soil interface.

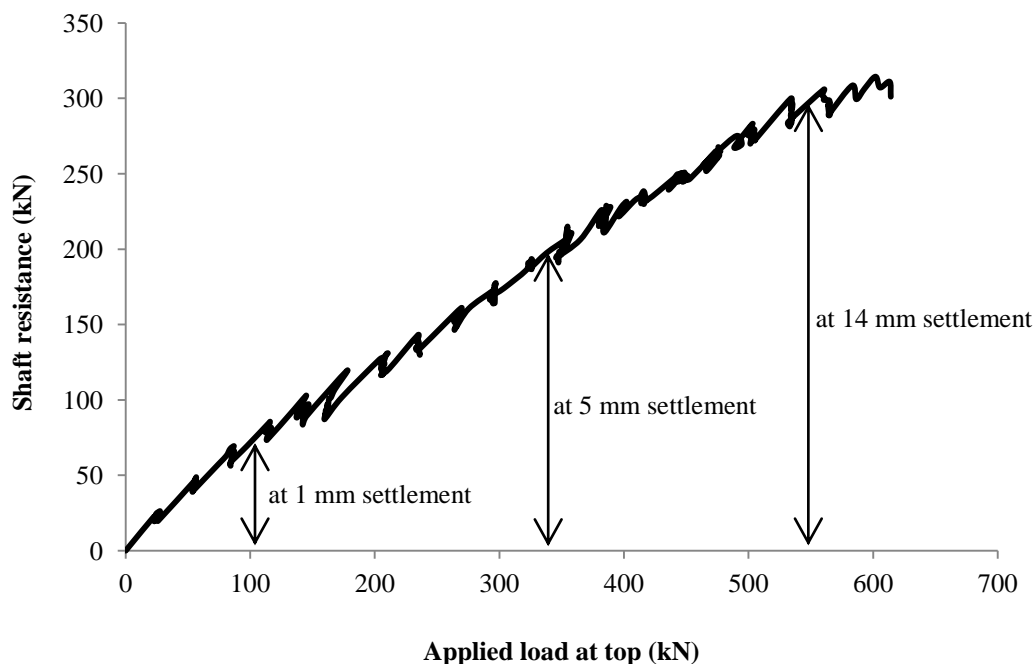


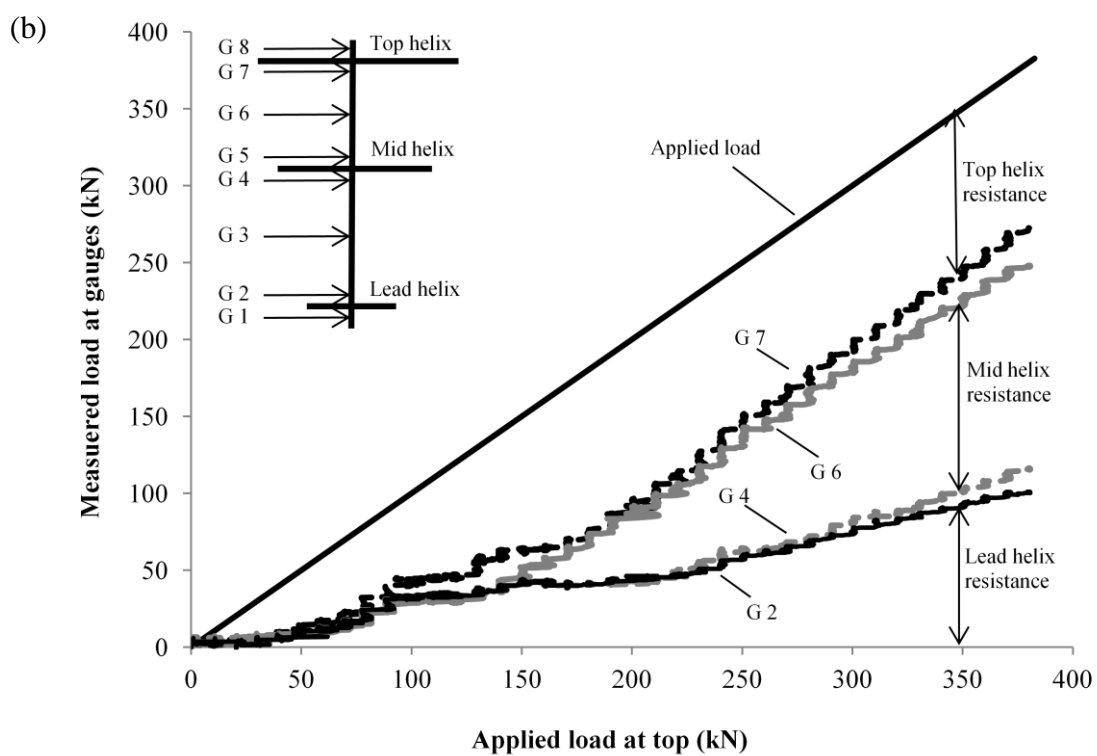
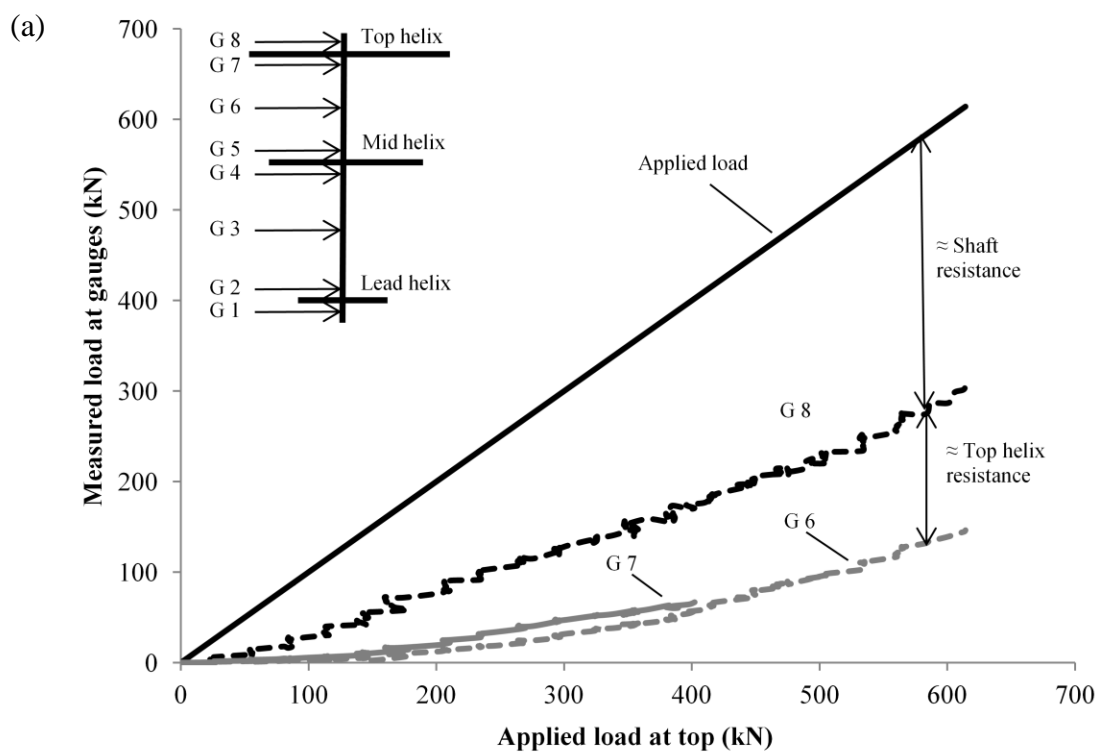
Figure 4.5. Shaft resistance vs. applied load for FRP Pile 1, Phase I.

4.7.3 Load transfer mechanism in lead section

The strain readings of strain gauges attached to the shaft of the lead section above and below each helix and at mid distance between helices were used to evaluate the load transfer mechanism within the lead section. It should be noted, however, that due to hard installation conditions, several strain gauges were damaged. The readings from FRP Pile 1 and the plain pile are shown in Figure 4.6. As can be noted from Figure 4.6a for FRP Pile 1, the load measured below the top helix (Gauge 7) was significantly reduced compared to the load measured above the helix (Gauge 8). At the same time, the loads measured at Gauges 6 and 7, both located between the first two helices, were almost identical. The same pattern was observed for the plain pile (Figure 4.6b); at Gauge 7 (just below the top helix) and Gauge 4 (just below the second helix), a reduction of 40% and 60% of the load measured above each helix, respectively (it is assumed that the load

above the top helix equals the applied load), respectively. Meanwhile, gauges located between the helices such as Gauges 6 and 7, and Gauges 2 and 4 had almost identical load measurements. These results demonstrate that the load transfer mechanism was through individual bearing of each helix.

Figure 4.6c shows the resistance of each helix versus measured displacement at pile top. Inspecting Figure 4.6c It can be seen that that at low displacement levels (<2.5 mm), the top helix contributed significantly to the load transfer compared to the other two helices. With load increase, the lead helix contribution increased. Up to a displacement of 10.5 mm, the applied load was resisted by the top and the bottom helix, with no apparent contribution from the mid helix. As the displacement level reached 23 mm (8.5% of the average helix diameter), the three helices shared the load equally. These observations are in agreement with the findings of El Sharnouby and El Naggar (2012a). They reported that the unequal load share between the helices at low load levels followed by redistribution of the load share at higher load levels can be attributed to installation effects and/or development of plastic zones underneath one of the helices.



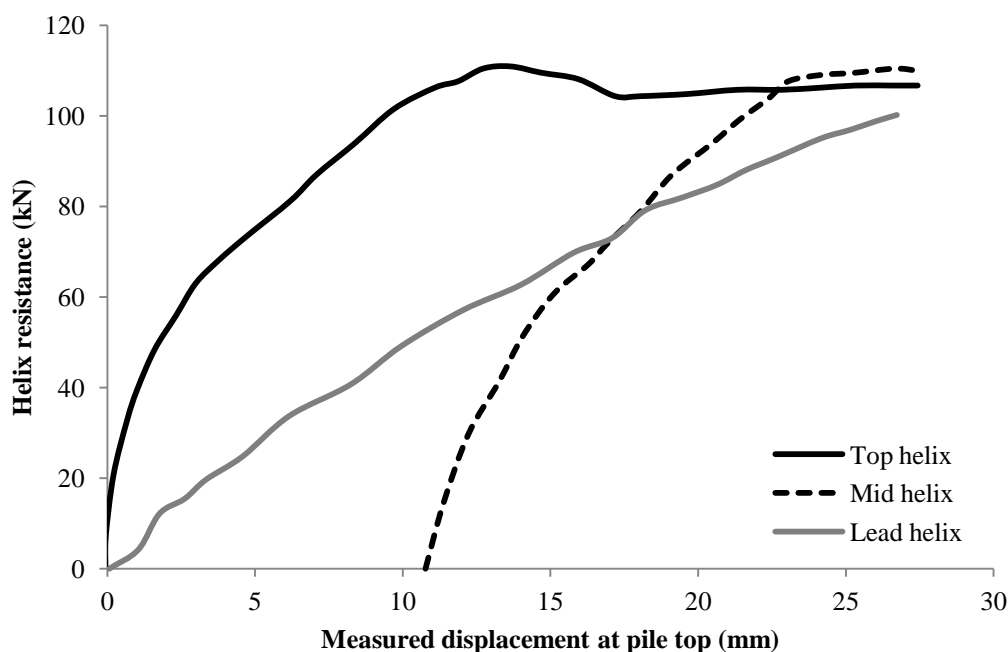


Figure 4.6. (a) Measured load transfer in lead section for FRP Pile 1; (b) Measured load transfer in lead section for plain pile; (c) Helix resistance vs. displacement for plain pile.

4.8 Performance of FRP-RHMP Subjected to Cyclic Loading

The cyclic loading program included two sets of testing. In the first set of loading (Phase I), the piles were loaded up to a maximum pile-head settlement not less than approximately 13% of the FRP tube diameter. After unloading the piles, they were then subjected to cyclic loading. In the second set (Phase II), the piles were subjected to cyclic loading first, followed by monotonic loading until the considerable displacement was reached. The results of both sets are examined below.

4.8.1 Cyclic loading with prior larger static load

Figure 4.7 shows the cyclic load-settlement response of the plain pile and FRP Piles 1 and 3 (other FRP-RHMP exhibited similar responses). The response curves demonstrate

very clearly the superiority of the FRP-RHMP relative to the plain pile in terms of reduced cyclic settlement as well as reduced residual settlement after unloading. The settlement during cyclic loading for the plain pile was 3 mm, while the settlement for both FRP Piles 1 and 3 was only 0.2 mm (93 % reduction), despite the fact that the cyclic loading range was higher for the FRP-RHMP.

The rate of settlement increase for the plain pile reduced as the number of loading cycles increased, probably due to compaction of sand underneath the helices. It can also be noted that the pile recovered 95% of the displacement upon unloading (i.e. elastic settlement). Similarly, the FRP piles 1 and 3 recovered 91% to 100% of the displacement upon unloading. However, the shape of the hysteretic loop was pinched in shape and its size progressively decreased as the number of load cycles increased resulting in a marginal residual settlement at the end of 15 cycles of loading. . This performance confirms the feasibility of using FRP-RHMP for foundations subjected to cyclic loading (e.g. wind turbine foundations and foundations in seismic areas).

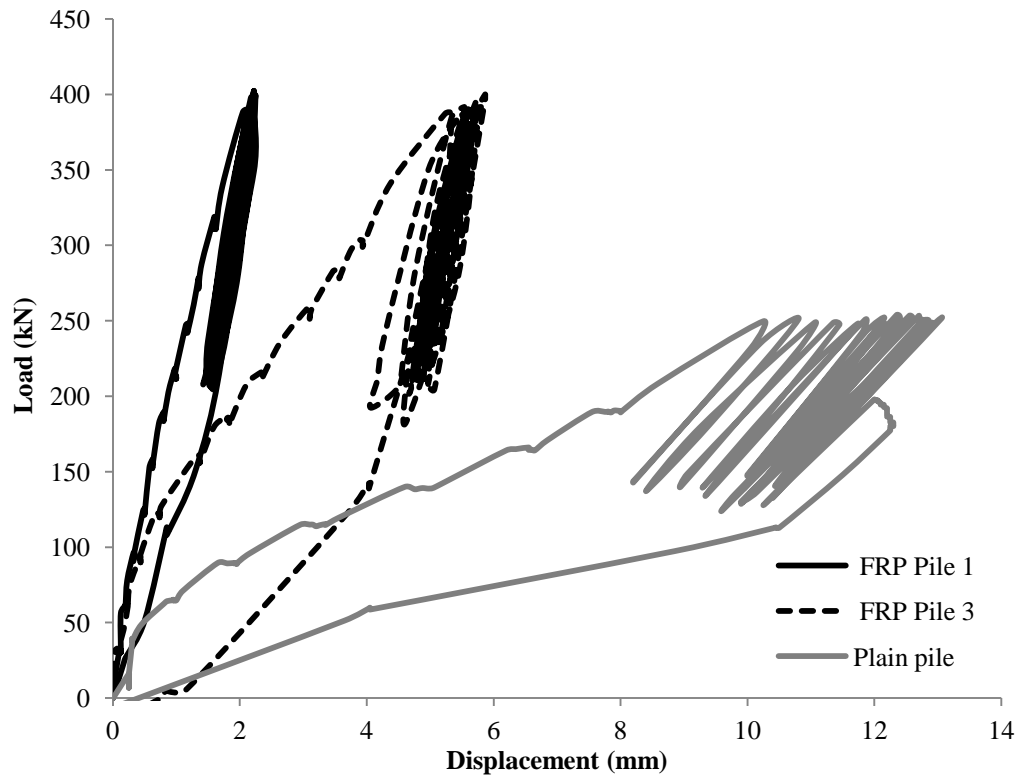


Figure 4.7. Cyclic load-displacement response after large static loading (Phase D).

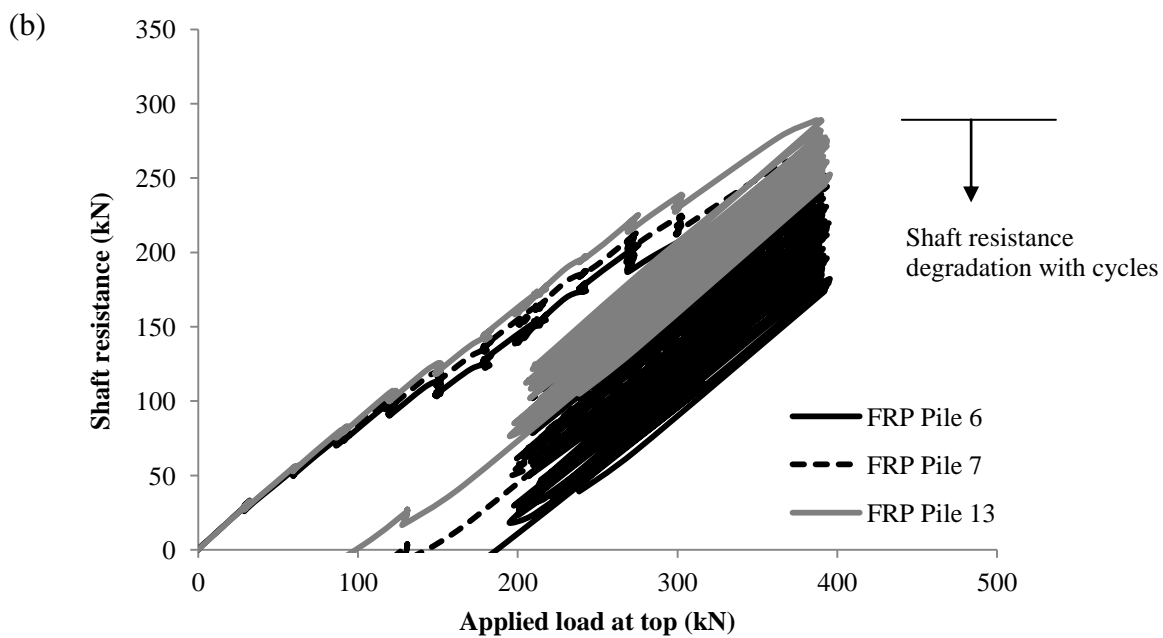
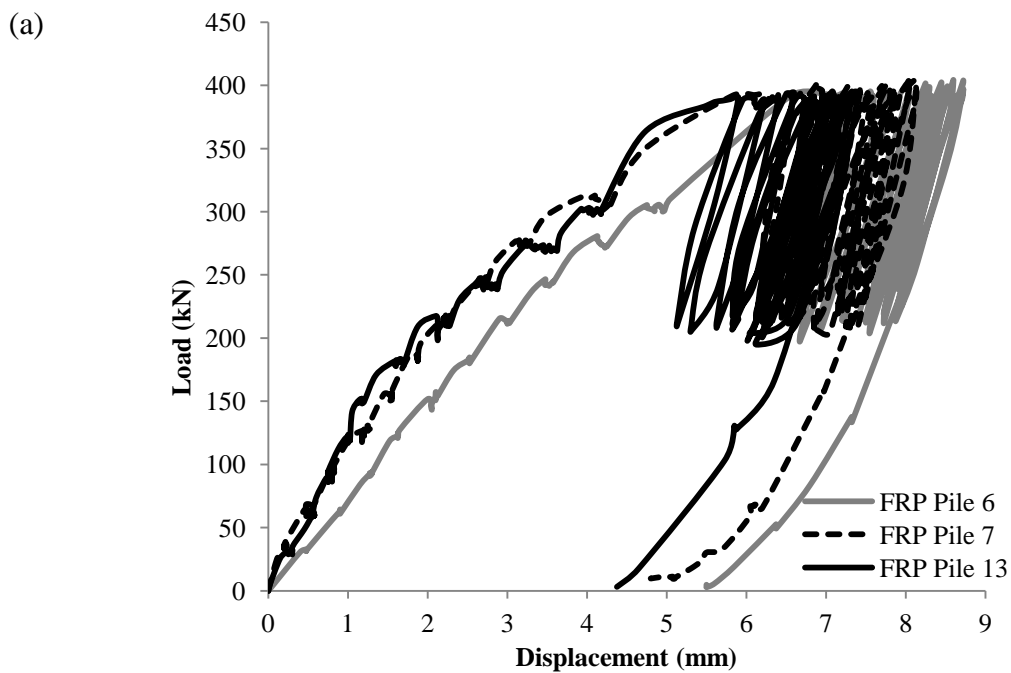
4.8.2 Cyclic behaviour of FRP-RHPM with no prior larger static load

Figure 4.8a shows the cyclic load-settlement response of three FRP-RHPM piles. The response curves of all other piles are bounded with these results. The loading and unloading stiffness values were close, and fairly constant throughout the cyclic loading. The cyclic settlement was highest in the first few cycles and decreased during subsequent cycles, indicating that the pile was stabilizing as the cyclic loading progressed. The size of the hysteretic loops decreased as the number of load cycles increased, and shifted right word (i.e. increased cumulative settlement), which resulted in permanent settlement upon unloading.

The variation of the shaft resistance during cyclic loading for the three piles is shown in Figure 4.8b. As can be noted, the load carried by the shaft-soil interface increased up until the start of cyclic loading. During cyclic loading, the shaft resistance suffered degradation with each loading cycle. The rate of degradation was almost uniform throughout loading. For the piles discussed in Figure 4.8, the lead section carried 62.5% to 75% of the applied load at the beginning of loading, decreasing to 47.5% to 62.5% after the cyclic loading was completed. The stiffness, however, did not degrade as the cyclic loading progressed.

Figure 4.8c shows the load transfer within the lead section during cyclic loading for FRP Pile 6: the load measured above the top helix (Gauge 8), between the top and second helices (closer to the top helix, Gauge 6), and just above the lead helix (Gauge 2). It can be noted from Figure 4.8c that the load transfer during cyclic loading was similar to that during monotonic loading, i.e., through individual helix bearing. The load measured during cyclic loading increased from 150 kN to 210 kN, 54 to 75 kN, 30 to 35 kN at Gauge 8, 6 and 2, respectively. This increase in helix resistance compensated for the degradation in shaft resistance; the top, mid, and lead helices provided 65%, 15%, and 5% of the load increase, respectively. This maybe an important design consideration when estimating the cyclic response of helical piles with multiple helices, i.e. the soil in the vicinity of the top helix may have a considerable influence on the pile's cyclic response. Also, all helices provided additional increase in capacity, which means the cyclic resistance increased as the number of helices increased. Buhler and Cerato (2010)

made similar observation as they found that 3-helix piles had greater dynamic resistance than 2-helix piles.



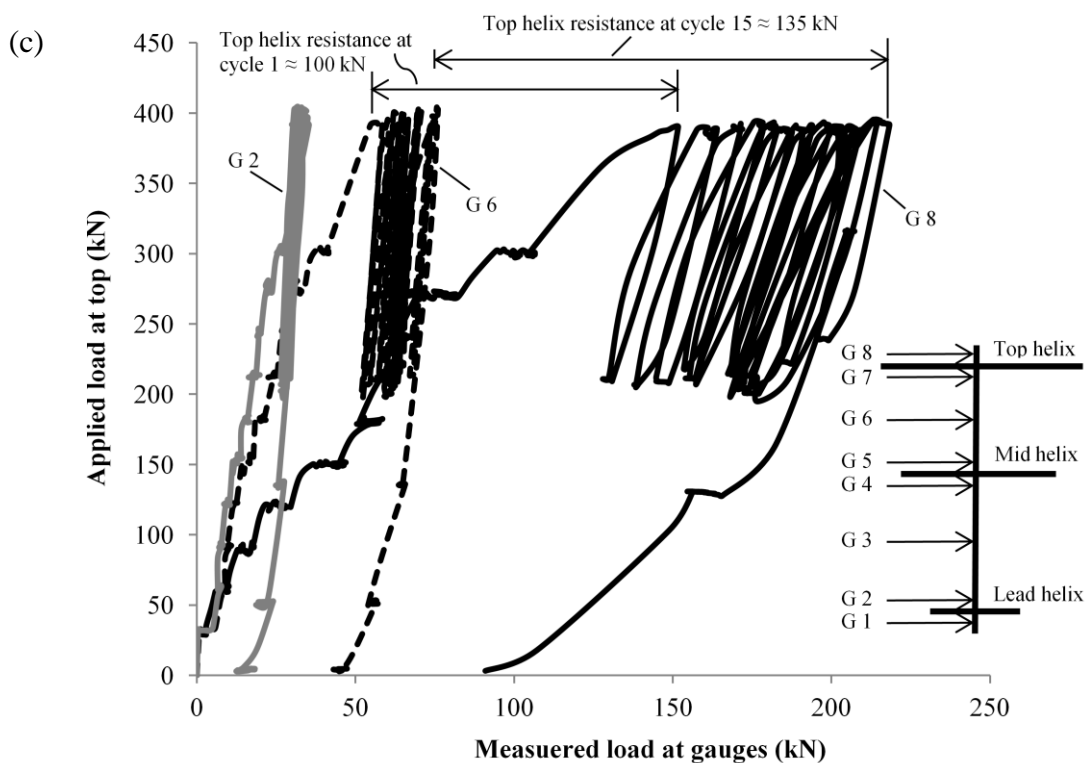


Figure 4.8. Cyclic test results for piles with no prior large static load (Phase II): (a) cyclic load-displacement response; (b) shaft resistance vs. applied load; (c) measured load at gauges vs. applied load for FRP Pile 6.

4.8.3 Comparison of pile performance under cyclic loading for Phase I and II

Table 4.3 shows the cyclic loading results for all piles. The piles that were subjected to cyclic loading without prior large static load (Piles 6 to 13) displayed a satisfactory performance, with a maximum displacement of 2.9 mm (2.13% of the FRP tube diameter) and no degradation of stiffness. When cyclic loading was preceded by a large static load (Piles 1 to 5), the piles exhibited even superior performance; the maximum cyclic displacement was less than 0.6 mm (0.41% of the FRP tube diameter). These results suggest that for piles designed to sustain cyclic loads with a range below the static design load, the cyclic displacement is expected to be minimal and can be ignored. It may

also be concluded that if the FRP-RHPM is subjected to cyclic loading with mean cyclic load of $0.43Q_u$ and cyclic load amplitude of $0.13Q_u$, the performance is satisfactory.

4.9 Monotonic Performance of FRP-RHPM after Cyclic Loading

4.9.1 Behaviour after cyclic loading with prior larger static load

Figure 4.9 shows the full load-displacement response for FRP Piles 1 and 3, and the plain pile. The FRP-RHPM followed the original load-settlement curves upon reaching highest previous load level (with 2.3-2.5 mm shift due to cyclic loading), indicating no degradation in the axial stiffness/performance after cyclic loading. The ultimate load reached after cyclic loading were 838 kN and 813 kN at displacements of 34 and 44 mm, for piles 1 and 3, respectively. The plain pile behaved similarly, with 1.0 mm shift; its ultimate load of 540 kN was reached at at 43.5 mm displacement. Its failure was due to buckling in the uppermost extension, which was verified by extracting the pile.

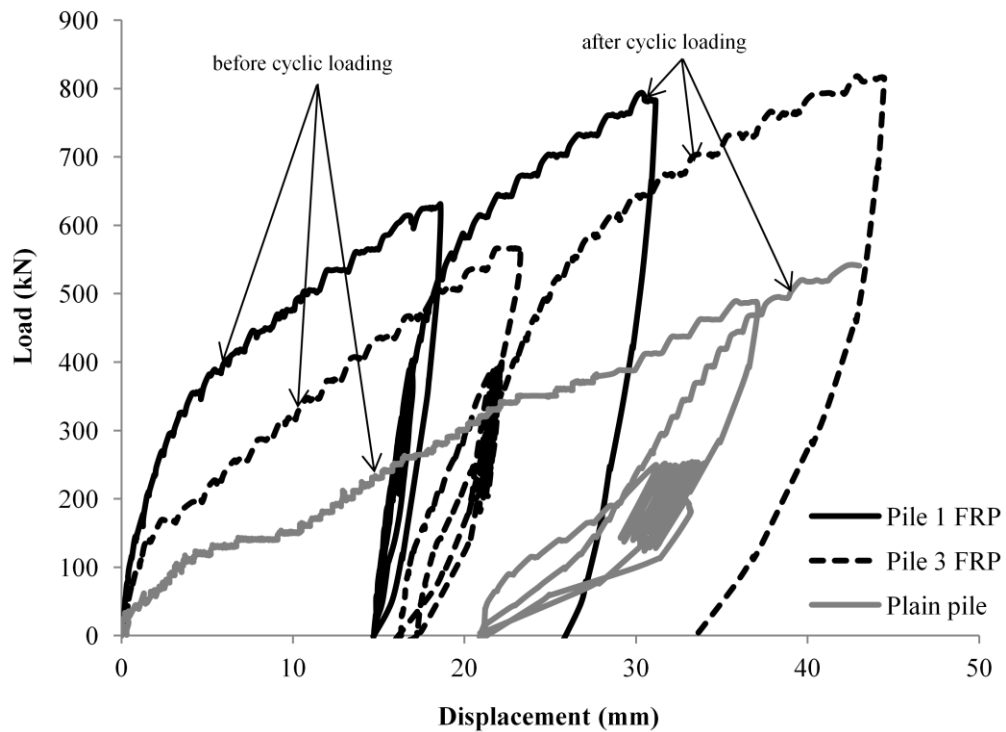
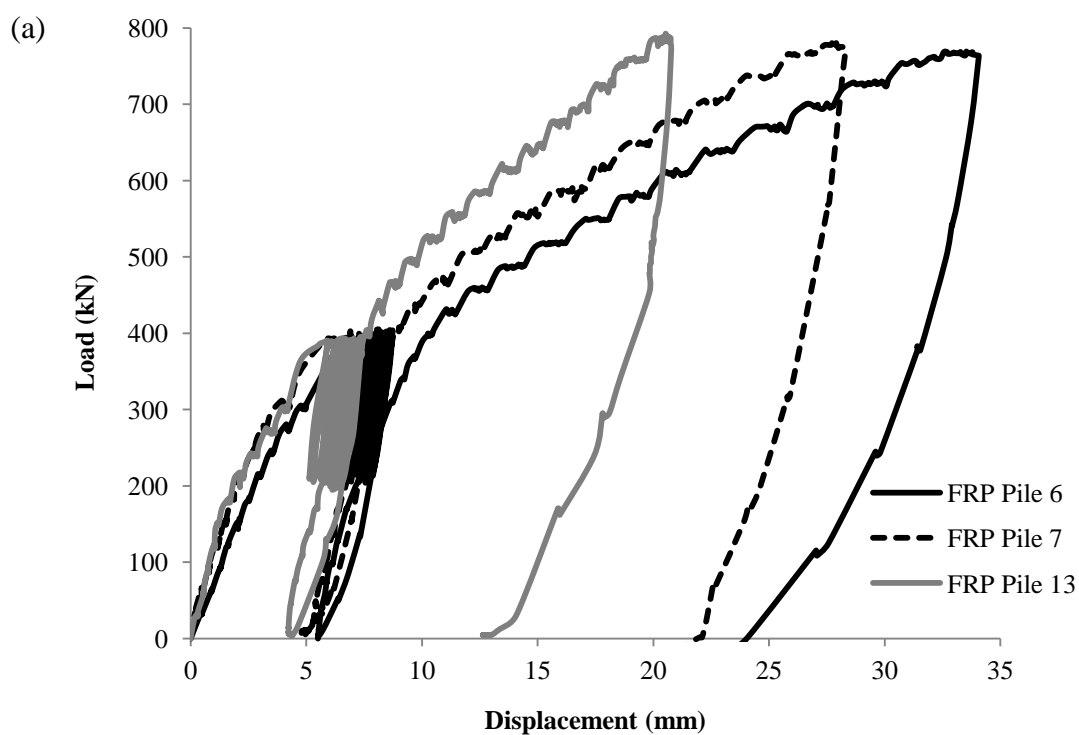


Figure 4.9. Full load-displacement response for Phase I.

4.9.2 Behaviour after cyclic loading with no prior larger load

Figure 4.10a and b shows the full load-displacement response of three FRP-RHPM piles, tested in Phase II. The maximum pile settlement reached at the end of cyclic loading with maximum cyclic load of 400 kN was 1.5 mm. The load-displacement curves demonstrated transitional and semi-linear branches as the load progressed to the ultimate value. Figure 4.10c shows the measured shaft resistance, which explains the variation in piles responses. The shaft resistance of Pile 13 displayed almost linear behaviour to the end of loading. The shaft of Pile 7 experienced slippage at an applied load of 500 kN; the shaft load decreased from 290 kN to 220 kN as the applied load increased from 500 kN to 780 kN and the settlement increased from 9% to 20% of pile sleeve diameter (FRP tube diameter). The shaft of Pile 6 displayed a softer response after yielding, with a maximum

shaft resistance of 250 kN when the applied load reached 740 kN. These observations show that the performance and ultimate capacities of the piles were influenced significantly by the soil-shaft interface conditions. In addition, the results demonstrate the inherent variability in clayey till characteristics, which should be taken into account for the piles geotechnical design.



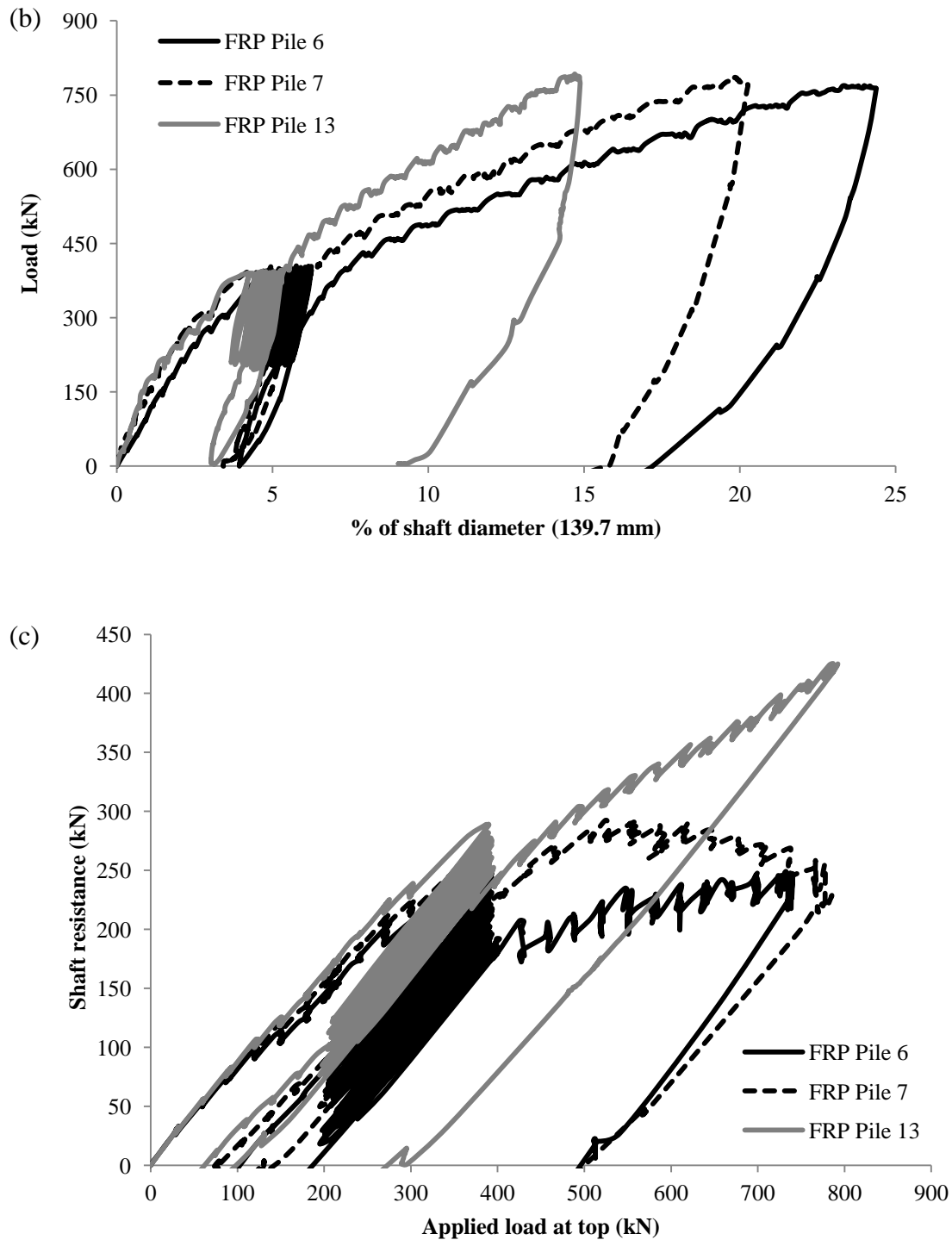


Figure 4.10. (a) Full load-displacement response for Phase II; (b) Full load-normalized displacement (% of shaft diameter) response for Phase II (c) Shaft resistance vs. applied load.

4.9.3 Effect of cyclic loading with no prior larger static load on load transfer mechanism in lead section

Figure 4.11 shows the load measured above the top helix (Gauge 8) and between the first two helices (Gauge 6) for Pile 6. As can be noted from Figure 4.11, the load measured above the top helix increased at a higher rate compared to the load measured between the first two helices. This indicates that the load carried by the top helix continued to increase to the end of loading. Figure 4.11 also shows an increase in the load transferred to the mid and lead helices at about 500 kN. While data of the load values above and below the mid helix were not available from the tests, Figure 4.11 demonstrates that the load transfer after cyclic loading was of individual bearing, with the top helix share of the applied load increasing from 30% before cyclic-loading to 50% after cyclic loading. This was probably due to the densification of sand in the vicinity of the top helix during cyclic loading.

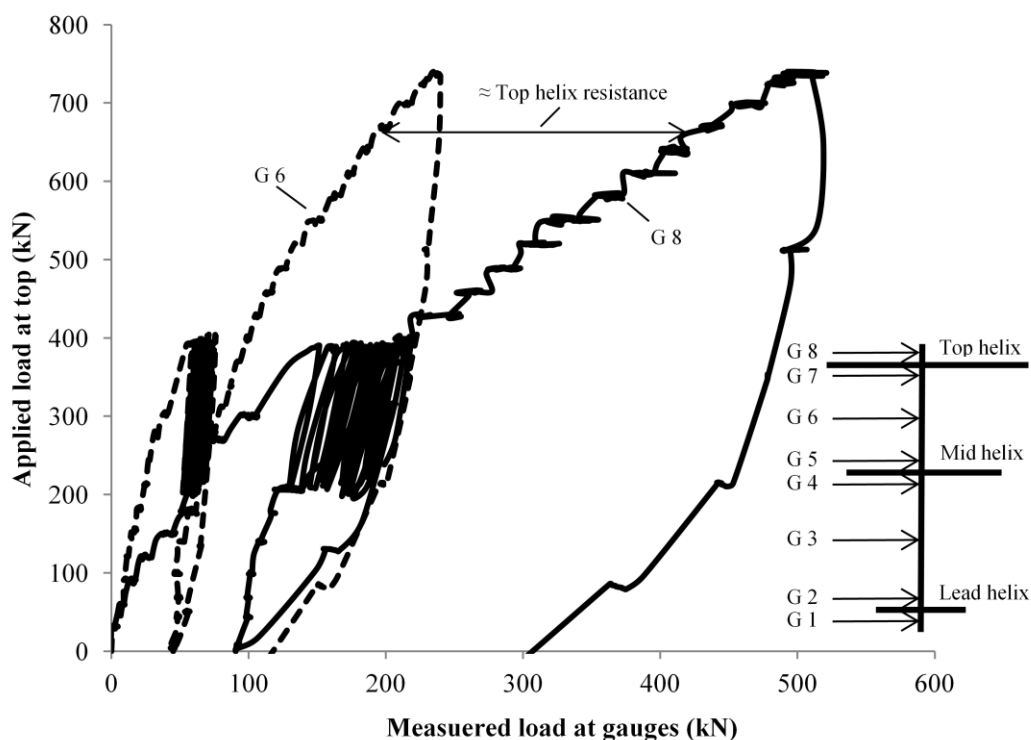


Figure 4.11. FRP Pile 6: Measured load at gauges vs. applied load (Phase II).

4.10 Ultimate Capacity of Test Piles

The failure (ultimate) load of a pile is usually defined as the load that corresponds to a specified settlement, usually as a percentage of the pile diameter. Other methods define the failure in terms slope change of the load-settlement curve (e.g. the load corresponding to the point of intersection of the initial tangent and the tangent of the final portion of the load-settlement curve). Terzaghi (1942) defined the ultimate load as the load corresponding to a settlement of 10% of the pile diameter. Also, the load corresponding to a pile head settlement of 25.4 mm (1 in.) is commonly used in practice.

A suitable failure criterion should account for the unique geometry characteristics of helical piles where lead sections consist of multiple plates. Livneh and El Naggar (2008)

defined the ultimate compressive load for helical piles with three helices as the load associated with a settlement of 8% of the largest helical diameter plus the elastic deflection of the pile. In this study, the ultimate capacity was calculated based on two different criteria: Livneh and El Naggar's and as the load corresponding to 25.4 mm (1 in) displacement. It should be noted that 25.4 mm settlement is equal to 10% of the average helix diameter. The elastic deflection was calculated based on the elastic modulus and cross sectional area of steels haft, grout column and the FRP tube, such that:

$$[4.1] EA_{equivalent} = EA_{steel\ shaft} + EA_{grout\ shaft} + EA_{FRP\ sleeve}$$

where A is the cross-sectional area for the respective sections and $E_{grout} = 30.8$ GPa is the grout elastic modulus, $E_s = 200$ GPa, the steel elastic modulus, and $E_{FRP} = 12.7$ GPa is the FRP tube elastic modulus,. The length considered was conservatively taken as the FRP tube length (3 m).

The axial capacities for piles tested in Phase I are shown in Table 4.4. The capacity evaluated considering the Livneh and El Naggar's (2008) criterion was within 7% of the 25.4 mm limit criterion. It is also noted that the axial capacity of FRP-RHPM was 150% to 175% of the plain pile. Due to the negligible effect of cyclic loading, the pile capacity values reported herein can be considered as the static capacity of the pile. The average ultimate capacity evaluated considering the Livneh and El Naggr's was found to be 700 kN.

The ultimate capacity of piles tested in Phase II is also reported in Table 4.4. The capacity of piles tested after cyclic loading increased by about 15%. This clearly indicates

that the cyclic loading enhanced the piles performance. These results are in agreement with the observations made by Hanna et al. (1978) and Hanna and Al-Mosawe (1981). This behaviour can be explained as follows. The pile installation initially caused disturbance, which resulted in loosening the sandy soil in the vicinity of the helices. Upon applying cyclic loading, the sand was compacted, and hence improving the performance. It should be noted though, that for higher cyclic loading levels, softening behaviour may take place due to strain localization. It can be concluded that FRP-HRPM piles installed in similar soil conditions of the test site would perform satisfactorily during cyclic loading events, e.g. earthquakes, and that their axial capacity would increase. A conservative approach to design, though, would be considering the axial capacity for cyclic loading conditions the same as for static loading conditions.

4.11 Prediction of Ultimate Capacity

The ultimate capacity of the FRP-RHPM can be estimated as the sum of the shaft resistance along the pile-soil interface, Q_{shaft} , and the capacity of the lead section, Q_{lead} , i.e.:

$$[3.2] Q_u = Q_{shaft} + Q_{lead}$$

Based on the measured load transfer mechanism, the capacity of the lead section can be calculated as the sum of the ultimate capacities of each helix (plate) given by:

$$[3.3] \quad Q_{lead} = \sum_1^n Q_{bearing}$$

$$[3.4] \quad Q_{bearing} = A_h(qN_q)$$

where A_h is the projected bearing area, q is the unit bearing capacity below the helix, and N_q is the bearing capacity factor.

The in-situ angle of internal friction of sand was estimated from the SPT results based on Bowles (1996). Prakash and Sharma (1990), after Meyerhof (1976), provide an estimation of the bearing capacity factor, N_q , based on installation method. Taking the installation method (conservatively) as similar to drilled shafts, $N_q = 22, 26$ and 35 for top, mid and bottom helices, respectively. The estimated bearing capacity for the lead section was found to be 354 kN. Estimating the bearing resistance via the SPT count using Meyerhof's (1976) method as cited by the Canadian Foundation Manual (CFEM 2006), yields a bearing resistance of 474 kN. Considering Decourt's (1995) method recommended in the CFEM, the bearing resistance was calculated as 670 kN. The measured ultimate capacity for the plain pile at a displacement = elastic displacement + 8% largest helix diameter was 412 kN. Clearly, the Decourt's method overpredicted the ultimate capacity at elastic displacement + 8% largest helix diameter, and should be used with caution, while the aforementioned two methods provide reasonable estimates for the ultimate capacity of the plain helical pile.

The shaft friction, Q_{shaft} , for piles in clay can be estimated as:

$$[3.5] Q_{shaft} = c_a A_{shaft} = \alpha c_u A_{shaft}$$

where c_a is the adhesion, α is the adhesion coefficient, c_u is the cohesion and A_{shaft} is the surface area of the soil-shaft interface. The adhesion can be calculated using several methods including the recommended grout-to-ground bond nominal strength in FHWA 2000 (Armour et al. 2000). For type A micropile, the nominal strength (adhesion) ranges from 50 kPa to 120 kPa. Considering the aforementioned values, the predicted shaft strength for test piles ranges from 65.5 kN to 157.5 kN. For driven piles in clays with undrained shear strength less than 100 kPa, the CFEM provides an estimation of the adhesion coefficient based on the undrained shear strength. Considering the undrained shear strength of 86 kPa (see Table 4.2), the shaft side resistance is estimated to be 57.5 kN. On the other hand, estimating the side resistance via the SPT count and Decourt's (1995) method yields a side resistance of 123 kN.

Comparing the estimated side resistance values with the observed values shows that the aforementioned methods are conservative in estimating the shaft resistance of FRP-RHPM installed in overconsolidated clay.

The total ultimate capacity of the pile calculated using Equation 2 ranged from 411.5 kN to 631.5 kN. The upper limit is 10% less than the measured axial capacity of piles (with cyclic loading with prior larger static load) and 22% less than the ultimate capacity of piles tested after cyclic loading with no prior larger static load. This suggests that the ultimate capacity of FRP-RHPMs, considered for static applications and for cyclic applications, and installed in similar soil conditions, can be conservatively estimated

using available conventional methods used in practice. Similar observations were made by Cerato and Victor (2009); they found that the individual bearing method to underpredict the uplift post-cyclic capacity for helical piles. They suggested that this may be due to the densification of the soil during the dynamic testing.

4.12 Conclusions

A full scale experimental program was conducted to evaluate the axial performance characteristics of FRP-steel fibre-reinforced helical pulldown micropiles (FRP-RHPM). Piles were tested under static and one-way cyclic loadings. The cyclic loading consisted of 15 cycles with mean cyclic load of 43% of the ultimate capacity and cyclic load amplitude of about +/- 13% of the ultimate capacity. Based on the experimental results, the following conclusions can be drawn:

1-The tested FRP-RHPM performed as a composite foundation system. The load-displacement curves of this pile system display the typical trend of conventional piles consisting of an initial branch, followed by a transitional branch followed by a near-linear branch.

2-The cyclic and post cyclic performance of the pile depends on the initial level of static loading:

- i) Where cyclic loading range below the maximum initial static load, loading and unloading stiffness values remain constant throughout cyclic loading with different values at beginning of testing and converging to similar values as loading proceeds. The cyclic displacement is significantly small and occurs within

the first one or two cycles. Also, no or negligible permanent displacement due to cyclic loading would occur. Post-cyclic axial stiffness is not affected by the cyclic loading.

ii) Where maximum cyclic loading was higher than the maximum initial static load:

- The pile performance during 15 cycles of loading was found to be satisfactory. The displacement per cycle decreased with number of cycles. No notable degradation in the stiffness was observed, with the loading and unloading stiffnesses of similar values throughout the cyclic loading.
- Uniform stable degradation of the pile shaft resistance was observed. The degradation was counter balanced by the stiffening effect from the lead section. It appears that the cyclic loading densifies the sandy soil in the vicinity of the helices, reducing the disturbance due to installation.
- The top helix (top most) contributed more significantly to the cyclic loading resistance compared to other helices. This may be of important consideration for cyclic design of helical piles.

4-Cyclic loading may considerably improve the axial performance and capacity by up to 15% for pile installed in similar soil conditions.

5-The load transfer mechanism within the lead section with helices spaced at about three times the helix diameter under static loading, cyclic loading, and post-cyclic static conditions is through individual bearing of each helix. For piles under relatively high

static loads (and no previous cyclic loads), all helices have equal distribution of the applied load. For piles under post-cyclic static loads, the top helix share is more than 50%.

6-The pile ultimate capacity for axial static or cyclic loading applications can be conservatively estimated using the conventional available methods. However, more research is required to examine the effect of higher cyclic loading range on the pile ultimate capacity and performance.

In general, the FRP-RHPM pile was shown to be a viable foundation system for axial monotonic and one-way cyclic loading applications.

4.13 References

Abd Elaziz, A.Y., and El Naggar, M.H. 2012. Axial behaviour of hollow core micropiles under monotonic and cyclic loadings. *Geotechnical Testing Journal*, ASTM, 35 (2), 249-260.

Abdelghany, Y. 2008. Monotonic and cyclic performance of helical screw piles. PhD thesis, Western University, Canada.

Abdelghany, Y., and El Naggar, M.H. 2010. Full-scale experimental and numerical analysis of instrumented helical screw piles under axial and lateral monotonic and cyclic loadings-A promising solution for seismic retrofitting. *In Proceedings of the 6th International Engineering and Construction Conference*. American Society of Civil Engineers, Cairo, Egypt.

Andreadis, A., Harvey, R.C., and Burley, E. 1981. Embedded anchor response to uplift loading. *Journal of the Geotechnical Engineering Division*, ASCE, 107(1), 59-78.

Armour, T., Groneck, P., Keeley, J., and Sharma, S. 2000. Micropile design and construction guidelines-implementation manual. Federal Highway Administration FHWA-SA-97-070, Washington, D.C.

ASTM International. 2007. Standard test method for deep foundations under static axial compressive load. Designation D 1143/D 1143M, West Conshohocken, PA, USA.

Bowels, J.E. 1996. Foundation analysis and design. The McGraw-Hill Companies, Inc., NY.

Buhler, R., and Cerato, A.B. 2010. Design of dynamically wind-loaded helical piers for small wind turbines. *Journal of Performance and Construction Facilities*, ASCE, 24(4), 417-426.

Canadian Foundation Engineering Manual. 2006. Fourth edition. Canadian Geotechnical Society, 488 p.

Cerato, A.B., and Victor, R. 2009. Effects of long-term dynamic loading and fluctuating water table on helical anchor performance for small wind tower foundations. *Journal of Performance and Construction Facilities*, ASCE, 23(4), 251-261.

Clemence, S.P., and Smithling, A.P. 1984. Dynamic uplift capacity of helical anchors in sand. *Civil Engineering for Practicing and Design Engineers*, 2 (3), 345-367.

Decourt, L. 1995. Prediction of load-settlement relationship for foundations on the basis of the SPT-T. *Ciclo de Conferencias Internacionales*, Loenardo Zeevaert, UNAM, Mexico, pp. 85-104.

El Naggar, M.H., and Abdelghany, Y. 2007a. Helical screw piles capacity for axial cyclic loadings in cohesive soils. *In Proceeding of the 4th International Conference on Earthquake Geotechnical Engineering*. Thessaloniki, Greece, paper 1567.

El Naggar, M.H., and Abdelghany, Y. 2007b. Seismic helical screw foundation systems. *In Proceedings of the 60th Canadian Geotechnical Conference*. Ottawa, ON, pp. 21-24

El Sharnouby, M.M and El Naggar, M.H. 2012. Field investigation of axial monotonic and cyclic performance of reinforced helical pulldown micropiles. *Canadian Geotechnical Journal*, 49 (5), 560-573.

Elsherbiny, Z.H. 2011. Axial and lateral performance of helical pile groups. M.E.Sc thesis. The University of Western Ontario, Canada.

Hanna, T.H., and Al-Mosawe, M.J. 1981. Performance of prestressed anchors under slow repeated loadings. *In Proceedings of the 10th International Conference on Soil Mechanics and Foundation Engineering*, Stockholm, Sweden. pp. 127-132.

Hanna, T. H., Sivapalan, E., and Senturk, A. 1978. Behaviour of dead anchors subjected to repeating and alternating loads. *Ground Engineering*, 11(3), 28-32, 34, 40.

Kulhawy, F.H. 1985. Uplift behaviour of shallow soil anchors-an overview. ASCE, pp. 1-25

Livneh, B., and El Naggar, M.H. 2008. Axial testing and numerical modeling of square shaft helical piles under compressive and tensile loading. *Canadian Geotechnical Journal*, 45(8): 1142-1155.

Lutenegger, A.J. 2010. Shaft resistance of grouted helical micropiles in clay. *In Proceeding of the 10th International Workshop on Micropiles*. International Society of Micropiles, Washington, D.C., USA, pp. 22-25.

Lutenegger, A.J. 2011. Behavior of multi-helix anchors in sand. *In* Proceeding of the 2011 Pan-Am CGS Geotechnical conference. Canadian Geotechnical Society, Toronto, Ontario, paper no, 126.

Meyerhof, G.G. 1976. Bearing capacity and settlement of pile foundations. *Journal of the Geotechnical Engineering Division, ASCE*, 102(GT3), pp. 225-244.

Merifield, R.S., and Smith, C.C. 2010. The ultimate uplift capacity of multi-strip anchors in undrained clay. *Computers and Geomechanics*, 37(4): 504-514.

Mitsch, M.P., and Clemence, S.P. 1985. The uplift capacity of helix anchors in sand. *ASCE*, 37(4): 26-47.

Mooney, J.S., Adamczak, S.Jr., and Clemence, S.P. 1985. Uplift capacity of helical anchors in clay and silt. *In* Proceedings, Uplift Behavior of Anchor Foundations in Soil, Proceedings of a Session held in conjunction with the ASCE Convention, Detroit, MI., American Society of Civil Engineers, New York, USA, pp. 48-72.

Narashima Rao, N.S., and Prasad, Y.V.S.N. 1993. Estimation of uplift capacity of helical anchors in clay. *Journal of Geotechnical Engineering*, 119 (2): 352-357.

Prakash, S., and Sharma, H.D 1990. *Pile foundations in engineering practice*. John Wiley & Sons, Inc., NY.

Sakr, M., El Naggar, M.H., and Nehdi, M. (2004a). Load transfer of fibre-reinforced polymer (FRP) composite tapered piles in dense sand. *Canadian Geotechnical Journal*, 41(1), 70-88.

Sakr, M., El Naggar, M.H., and Nehdi, M. (2004b). Novel toe driving for thin-walled piles and performance of fiberglass-reinforced polymer (FRP) pile segments. *Canadian Geotechnical Journal*, 41(2), 313-325.

Sakr, M. 2009. Performance of helical piles in oil sand. *Canadian Geotechnical Journal*, 46(9): 1046-1061.

Terzaghi, K. 1942. Discussion of the progress report of the committee on the bearing value of pile foundations. *In Proceedings, Earth and Foundations. American Society of Civil Engineers*, Vol. 59, No. 8, pp. 1363-1372.

Vickers, R.A., and Clemence, S.P. 2000. Performance of helical piles with grouted shafts. *In Proceedings of Sessions of Geo-Denver 2000 - New Technological and Design Developments in Deep Foundations. American Society of Civil Engineers, GSP 100, v 288, pp. 327-341.*

Table 4.1. Soil profile and SPT count established from boreholes.

Soil layer	Depth (m)	N-Value
BH-1		
Compact brown silty sand and gravel.	0-1	31
Very stiff to hard, brown becoming grey at 3 m (10 ft) depth, clayey silt to silty clay till. W.T. at 3.7 m depth.	1-1.8	43
	1.8-2.6	24
	2.6-3.3	47
	3.3-4	18
	4-5.9	22
Compact to dense sand, trace of some silt	5.9-7.9	32
Compact, grey silt	7.9-8.8	18
BH-2		
Very stiff to hard, brown becoming grey at 3 m (10 ft) depth, clayey silt to silty clay till. W.T. at 4.1 m depth.	0-1	21
	1-1.8	28
	1.8-2.6	8
Compact to dense sand, trace of some silt	5.6-6.4	30
	6.4-7.1	36
	7.1-7.9	42
	7.9-8.8	22

Table 4.2. Summary of geotechnical properties of soil from BH-1 and BH-2.

BH-1			
Depth, m	1.8	3.9	7
Gravel content (%)	7.3	0 (very small fraction)	1.4
Sand content (%)	54	66.2	86
Silt-clay content (%)	38.7 (72.5 % silt and 27.5 clay)	33.8 (62 % silt and 38 clay)	12.6
Specific gravity	2.69	2.77	2.67
Moisture content (%)	10.7	-	-
Liquid limit	28.7	35.7	-
Plastic Limit	12.8	16.6	-
Plasticity index	15.9	19.1	-
Undrained shear strength, (kPa)	100	-	-
BH-2*			
Depth (m)	3.0	3.8	4.2
Undrained shear strength, C_u (kPa)	86	183	174

*See Abd Elaziz and El Naggar (2012), C_u from undrained unconsolidated tests.

Table 4.3. Cyclic load test results.

Pile NO.	Displacement before cyclic loading (mm)	Displacement after cyclic loading (mm)	Increase in displacement (mm)	% of average helix diameter	% of pipe diameter
Plain	10.2	13.2	3	1.2	N/A
1	16.8	16.9	0.2	0.06	0.11
2	21.6	21.8	0.2	0.08	0.14
3	21.5	22.1	0.6	0.22	0.41
4	20.9	21.1	0.2	0.07	0.13
5	23.2	23.6	0.4	0.16	0.29
6	6.6	8.7	2.2	0.85	1.56
7	5.8	8.1	2.3	0.91	1.67
8	4.3	6.0	1.7	0.68	1.25
9	10.7	13.3	2.6	1.01	1.87
10	6.2	9.2	2.9	1.15	2.13
11	7.0	9.6	2.6	1.02	1.88
12	5.5	7.4	1.9	0.75	1.38
13	3.9	6.5	2.6	1.02	1.88

Table 4.4. Observed ultimate capacities of test piles.

Pile NO.	Load at 25.4 mm (kN)	Load at elastic displacement + 8% largest helix diameter (kN)
Phase I		
Plain	360	412
1	700	720
2	700	710
3	600	620
4	750	780
5	620	665
Average capacity, Phase I	674	700
Ave % increase over plain pile	87%	70%
Phase II		
6	670	700
7	740	770
8	925*	975*
9	700	720
10	700	740
11	800	810
12	865	900
13	851*	900*
Average capacity, Phase II	778	814
Ave % increase over Phase I	15%	14%

*From extrapolation

**NUMERICAL INVESTIGATION OF AXIAL MONOTONIC
PERFORMANCE OF REINFORCED HELICAL PULLDOWN
MICROPILE (RHPM) AND FRP-STEEL FIBRE-REINFORCED
HELICAL PULLDOWN MICROPILES (FRP-RHPM)**

5.1 Introduction

Axial capacity of helical piles under compression can be limited by the buckling capacity of its shaft, especially for long piles and/or piles installed in weak soils. Vickers and Clemence (2000) introduced the Helical Pulldown[®] Micropile or grouted-helical pile (HPM). It consists of a helical pile installed with a grout column surrounding the pile central shaft along the extensions. Since then, several modification have been introduced to this pile system including the addition of steel fibres to the grout column, namely, steel fibre-reinforced helical pulldown micropile and a FRP casing surrounding the grouted column, namely, FRP-steel fibre-reinforced helical micropiles (FRP-RHPM). Chapters 3 and 4 presented the results of a full scale investigation on the axial performance of RHPM and FRP-RHPM. The shafts of these piles were embedded in stiff clay soil and the lead section in medium dense sand. The experimental program confirmed that the grouted column (RHPM) and cased grouted column (FRP-RHPM) contributed significantly to the pile's resistance and that these pile system perform as composite piles with satisfactory performance under axial loads.

In this Chapter, a three-dimensional finite element (FE) model was developed using the computer program ABAQUS (Haibitt et al., 2011). The FE model simulates the RHPM

and FRP-RHPM under axial compression loads. The model was calibrated using the experimental results presented in Chapters 3 and 4. The purpose of the FE model was to gain a comprehensive understanding of the load transfer mechanism, and the state of stress and strain within the pile and soil medium. The calibrated model was used to conduct a parametric study in order to examine the behaviour of RHPM and FRP-RHPM in different soil conditions. Based on the experimental results and the FE analysis, a design procedure is suggested.

5.2 Pile Description and Soil Conditions

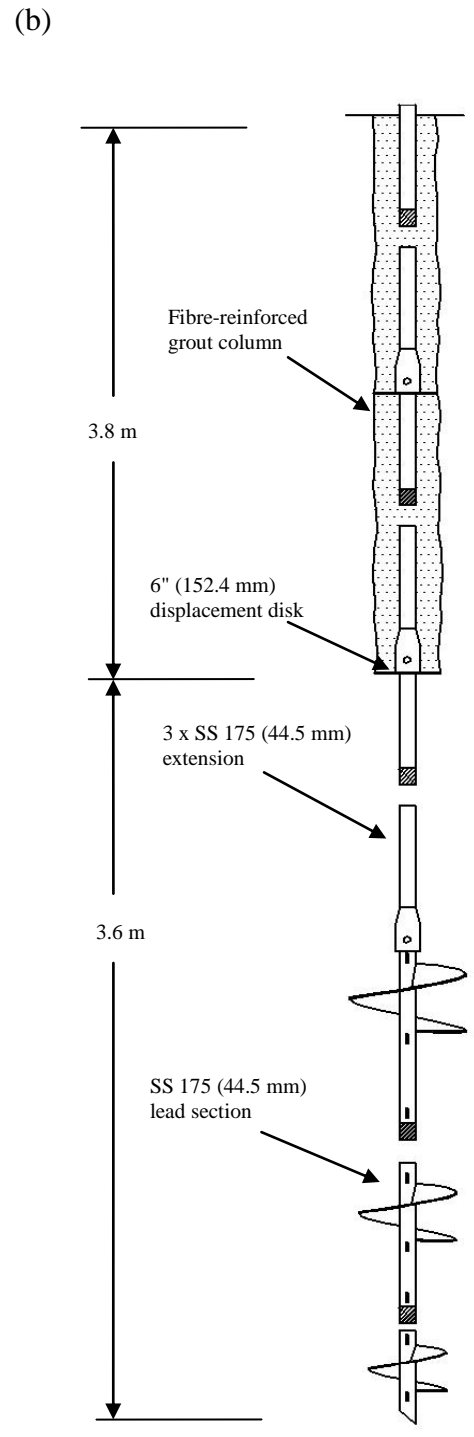
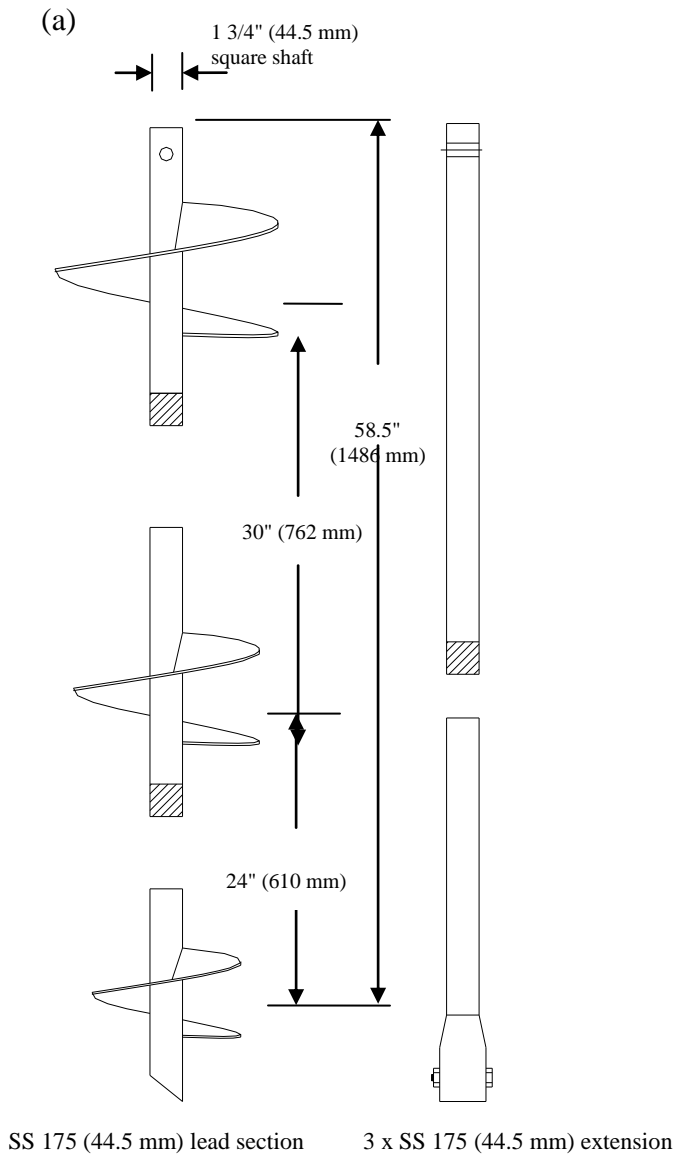
The configuration of piles in the testing program, which was used for the FE analysis validations are as follows. The plain helical pile was the SS 175 (44.5 mm) square shaft helical pile, which consisted of a lead section with three helices, with 305 mm, 254 mm and 203 mm diameters attached to it, and a number of extensions, as shown schematically in Figure 5.1a. The helix pitch is 76 mm and the spacing between the helices is about three times the helix diameter.

The reinforced helical pulldown micropile (RHPM) consisted of two main parts, as shown in Figure 5.1b: a plain helical pile, with a lead section and three extensions; and a steel fibre-reinforced grout column surrounding the top two extensions. The plain pile was the SS 175 (44.5 mm). The diameter of the grouted grouted column was 152.4 mm (6") diameter and extended for 3.8 m.

The FRP-steel fibre-reinforced helical micropile (FRP-RHPM) was comprised of: plain helical pile, and a cylindrical FRP tube (sleeve) that surrounded part of the pile shaft,

infilled with steel fibre-reinforced grout column. The plain pile was the SS 175 (44.5 mm). The FRP tube was 3.3 m long, a nominal outside diameter of 140 mm and wall thickness of 7.62 mm. A schematic of the FRP-RHPM is shown in Figure 5.1c.

All piles were installed such that the lead section was situated entirely within the dense sand, while the shaft (FRP shaft) was situated within the stiff clayey silt till, as shown in Figure 5.1b and c. More details on all pile systems, installation procedure and in-situ soil conditions can be found in Chapters 3 and 4).



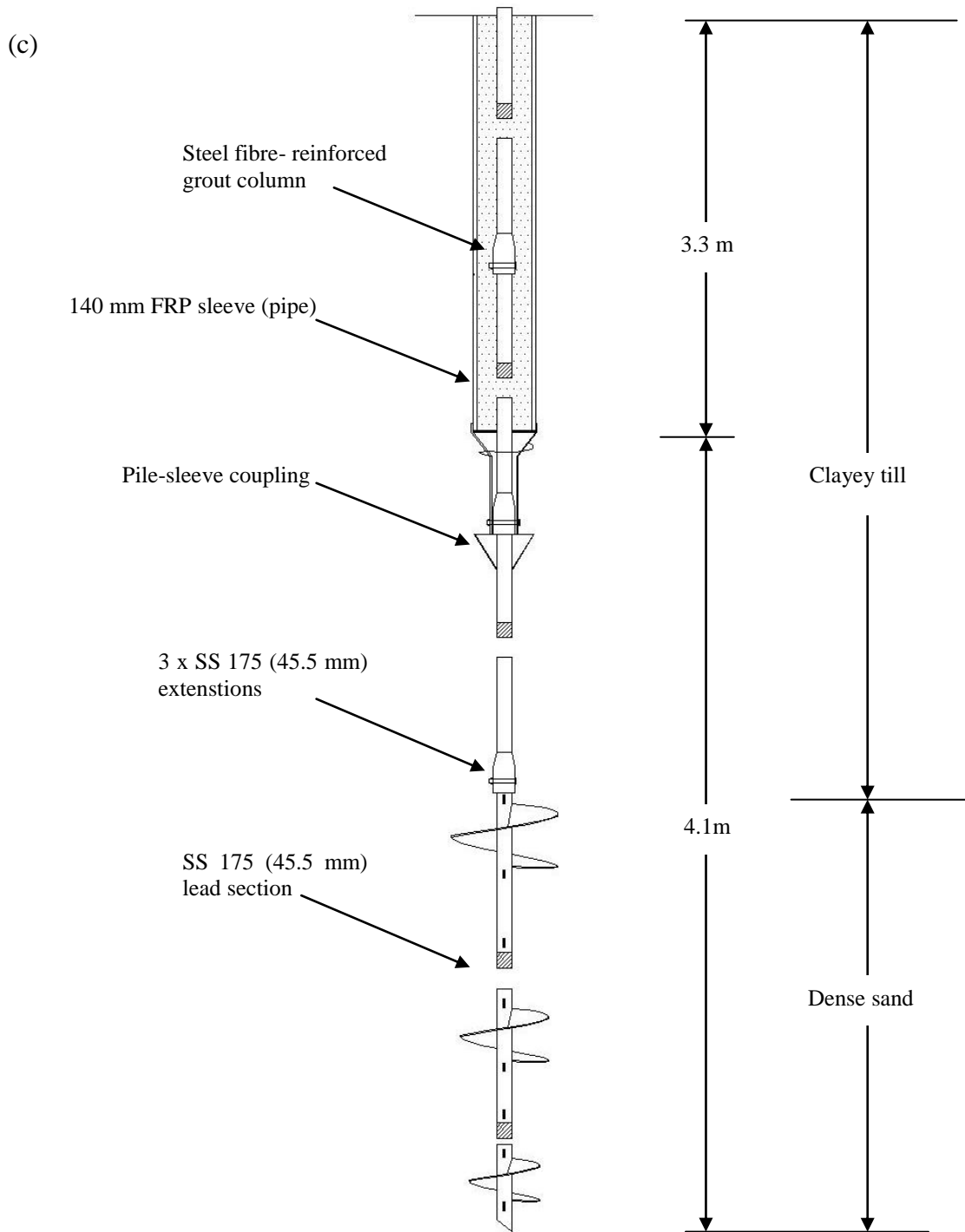


Figure 5.1. Dimensions and schematic of test piles used for FE verification: (a) Schematic of plain helical pile; (b) RHPM test pile profile; (c) FRP-RHPM test pile profile.

5.3 Geometry and Model Discretization

The pile system is simulated using a three-dimensional finite element model. The soil medium and piles are modelled using eight-noded hexahedron reduced integration elements, C38DR. These elements are chosen as opposed to fully integrated elements, to overcome the volumetric locking effect of the fully integrated elements when the material model is almost incompressible (Cook et al., 2002).

Due to symmetry, only one quarter of the pile and soil system is modelled. The model configuration is cylindrical (i.e. cross-section of soil medium is circular). The boundaries are located such that they have no effect on the results of analysis: the bottom boundary is placed below the pile tip more than 4.5 the average helix diameter or 5.5 the lead helix diameter (Elsherbiny 2011); and the radius of the soil medium is about 18 times the shaft diameter (analysis was conducted with radius up to 25 times the shaft diameter, and no change in response was found). The helices were approximated to planar plates. To ensure model accuracy, staged mesh refinement was carried out. A typical FE mesh is shown in Figure 5.2.

More than 25,000 C38DR elements are used to discretize the pile and soil medium. Staged mesh refinement is employed in order to achieve convergence within acceptable tolerance. The elements are most refined along the pile/soil interface and near the helices and a gradual size increase is applied as the distance increased radially from pile centre-line.

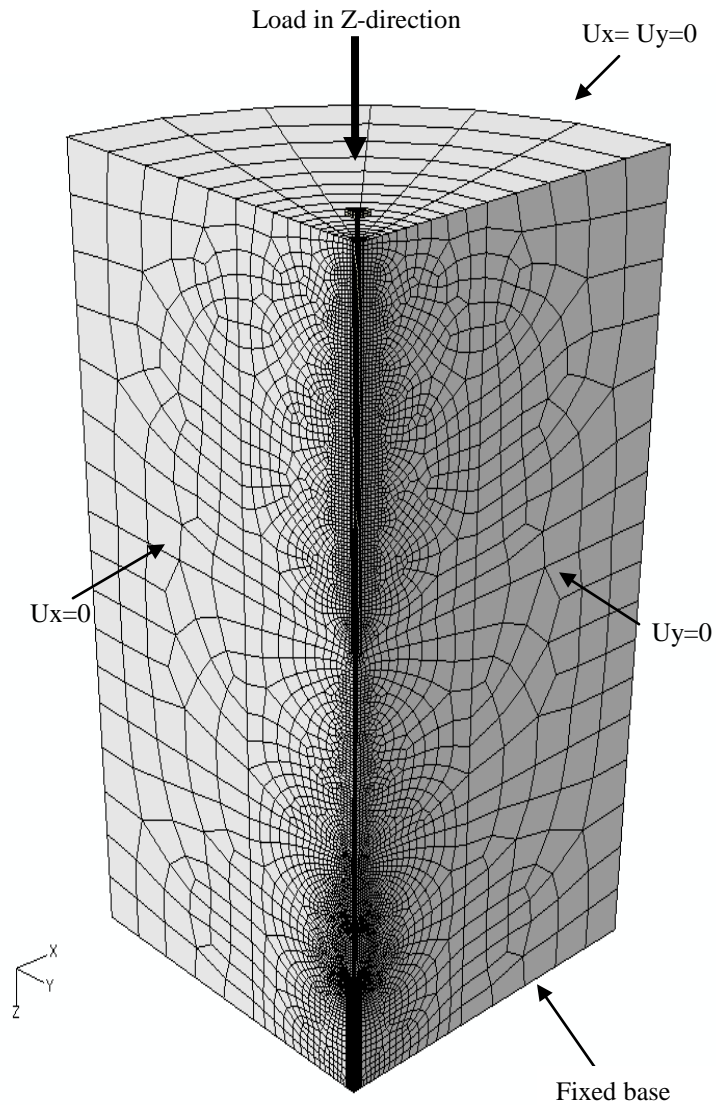


Figure 5.1. Typical finite element mesh.

5.4 Boundary conditions

The bottom of the soil medium is fully restricted. The elements along the perimeter of the soil medium are restricted in the lateral direction (x-any-direction). In addition, on the x-z symmetry plane, the out-of-plane movements in the y-direction are restricted, and on the

y-z symmetry plane, the out-of-plane-movements in the x-direction are restricted. At the pile head, only axial displacement (in the z-direction) is allowed.

5.5 Interaction modelling

Contact interaction between the pile and soil is modelled using the surface to surface algorithm available in ABAQUS (Habitt et al., 2011). Surfaces are considered in contact if the contact pressure at a slave node is positive (directed towards the master surface). Pressure will be transmitted only when the clearance between the contact surfaces is approaching zero.

Friction between the pile and soil is simulated through the friction Coulomb's model where a friction coefficient at the soil-pile interface is defined. In addition, limiting interface shear strength is provided.

5.6 Material model

The soil is modeled as elastic-perfectly plastic material with failure defined by the Mohr-Coulomb yield criterion. The grout column and the FRP tube are modelled as elastic materials. The Von-Mises plasticity criterion is used to define the yield and post yield behaviour of steel. The properties for pile components used for all the analyses are shown in Table 5.1. Soil properties are shown later in this chapter.

5.7 Loading and solution steps

Prior to load application, an initial geostatic step is applied in order to simulate in-situ stresses. At the end of the geostatic step, it is verified that deformation is negligible indicating appropriate modelling of the in-situ stressed. During this step, interaction

between the pile and surrounding soil is allowed. In other words, the pile maintained its equilibrium through its contact with the soil. This technique allowed proper simulation of in-situ stresses at the pile-soil interface.

For the case of the plain pile, the initial step is followed by the loading step. For the cases of simulating the RHPM and FRP-RHPM an intermediate step, before the loading phase, is included. The adhesion at the pile/soil interface is modelled as independent from the overburden pressure, where slippage would occur when the stress along the interface reaches the maximum adhesion strength. Therefore, pressure is applied at the pile/clay soil interface such that adhesion can be properly simulated.

The loading step followed the geostatic step (or the intermediate pressure step). Loading is displacement controlled applied at the pile head.

5.8 Limitations

Modeling the soil material as an elastic-perfectly plastic continuum using the Mohr-Coulomb yielding criterion could be a rough assumption at high levels of stresses and strains. The developed model ignores changes of soil stiffness with depth and the stiffness dependency on the strain level. In addition, the models do not account for the effect of pile installation, soil disturbance on the capacity of the piles and existence of couplings.

5.9 Verification of FE model

The finite element model was first verified against the results of the plain pile. In order to calibrate the model, a range of soil parameters was used, as shown in Table 5.2. The analysis commenced by assuming that the helices are within a layer of pure sand with a

modulus of elasticity of 50 MPa, and with an in-situ horizontal stress $K_o = 0.5$. The FE model predicted a much lower response and stiffness than the experimental results. Therefore, the modulus of elasticity and the in-situ horizontal stress values were revised. The in situ horizontal stress values as reported in Jeon and Kulhawy (2001) were considered. The modulus of elasticity value was chosen within the ranges reported in Kulhawy and Mayne (1990). A Closer match was achieved with $E = 63$ MPa and $K_o = 1.36$. Figure 5.3 shows the load-displacement curve of tested plain pile and the FE analysis. As can be seen, the FE results are in good agreement with the test results.

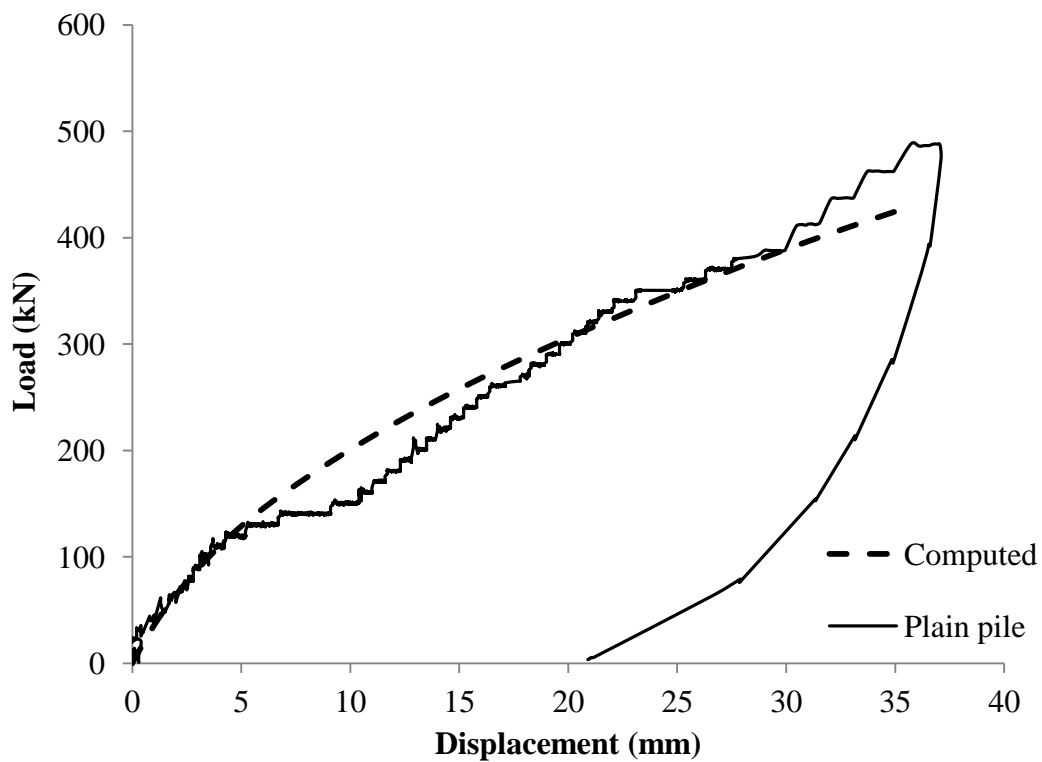


Figure 5.3. Comparison between computed and test load-displacement curves for plain helical pile.

After calibration of the model with the plain helical pile, the FE model was validated against the experimental results for the RHPM and the FRP-RHPM as well. Several

attempts were carried out. First, the same sand layer characteristics that provided reasonable agreement were chosen. The FE model significantly underestimated the piles' performance. Another attempt was carried out by increasing the angle of friction to 38° , modulus of elasticity to 110 MPa and the corresponding in-situ horizontal stress value to 1.58 (Kulhawy and Mayne, 1990). Table 5.2 shows the range of values used for calibration.

Figures 6.4a and b show the range of test results for the RHPM and FRP-RHPM, and the FE results. A favourable agreement between the FE results and the average of test results was achieved. The shaft friction shear strength for the RHPM was found to range from 60 kPa to 120 kPa and for the FRP-RHPM from 70 kPa to 130 kPa. The undrained shear strength values using the SPT count and the correlations proposed by Sivrikaya and Toğrol (2006) were on average 166 kPa and 132 kPa along Borehole-1 (BH-1) and Borehole-2 (BH-2), respectively. In addition, Abdelaziz and El Naggar (2012) reported undrained shear strength values obtained from lab tests to range from 84 kPa to 183 kPa. El Sharnouby and El Naggar (2012a) reported a value of 100 kPa from BH-1. The analysis also showed that the response of the system was quite insensitive to the undrained shear strength of the clay soil. Considering the minimum and maximum undrained shear strength in this site to be 100 kPa and 183 kPa, respectively, the friction coefficient for the RHPM was about 0.6 and for the FRP-RHPM was about 0.7.

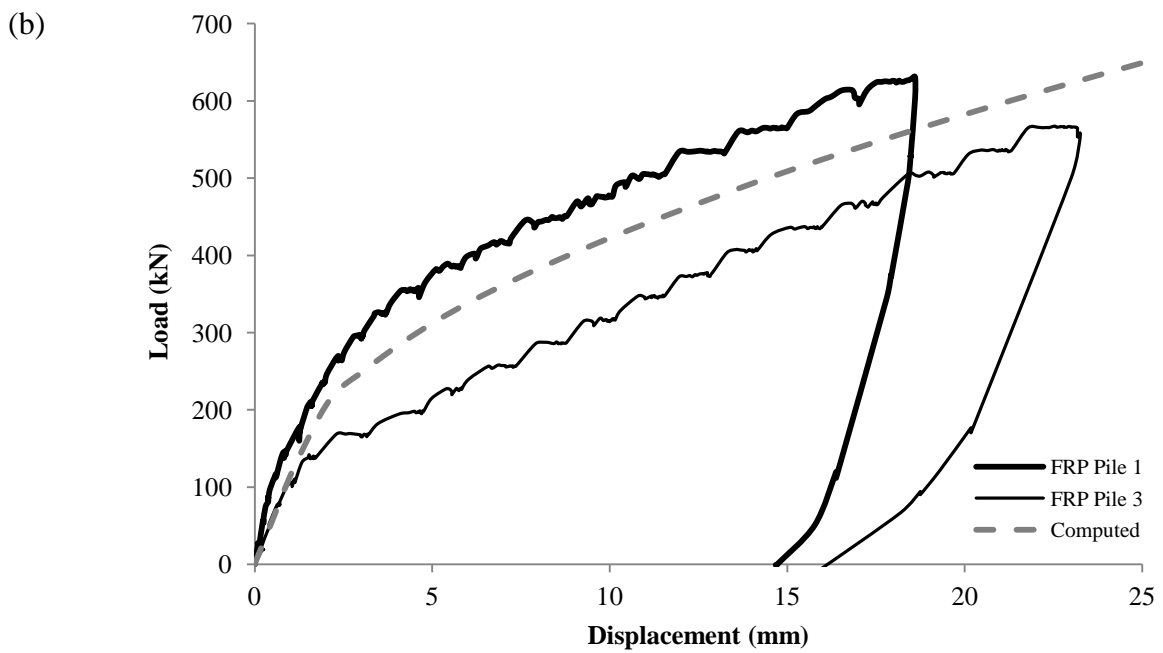
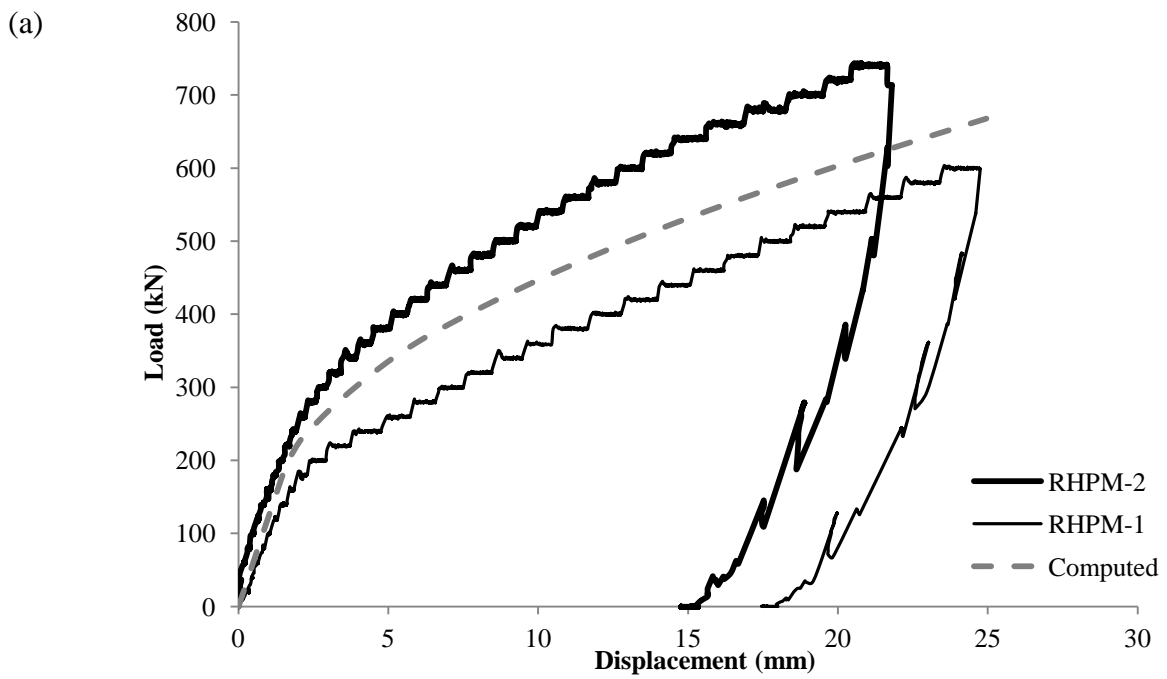


Figure 5.4. Comparison between computed and test load-displacement curves for: (a) RHPM; (b) FRP-RHPM.

5.10 Parametric Study

The experimental investigation revealed that the load transfer mechanism within the lead section is predominantly through individual bearing. In addition, it showed that the ultimate capacity is comprised of the ultimate shaft resistance and the total capacity of the lead section. In this section, a parametric study is conducted to investigate the effect of different soil conditions on the performance of the RHPM, and to attempt to establish recommendations for design of such systems. Chapter 4 revealed that the FRP-RHPM behaves in a similar manner to the RHPM under axial compression loads. Therefore, it is assumed that the results of the analysis herein apply to both piles.

5.10.1 Pile configurations and soil parameters

The pile consisted of the SS 175 and a grouted shaft with a 152.4 mm diameter. The grouted shaft extended from the ground surface to 457 mm (1.5 ft.) above the top helix, as typically constructed. The sand layer ranged from loose to dense, and the clay layer ranged from soft to stiff. The pile material properties were the same as in the calibrated model as discussed above. Figure 5.5 shows a schematic of pile dimensions and soil type considered in the parametric study and Table 5.3 shows the soil properties used.

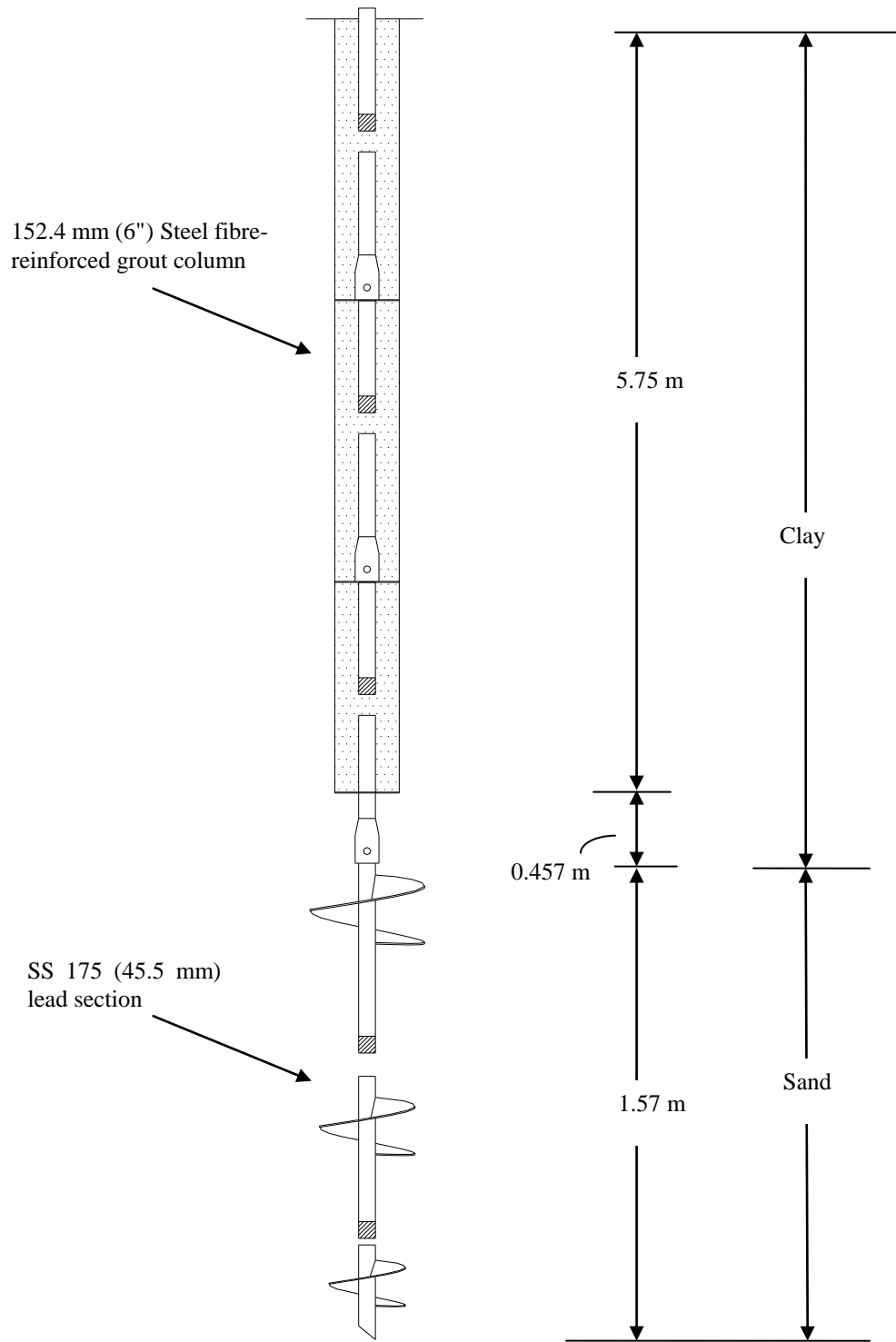


Figure 5.6. Schematic of pile dimensions and soil type along pile depth used for FE analysis.

5.10.2 Axial compression response

The load-displacement curves for all cases are plotted in Figure 5.7. As can be seen from Figure 5.7, the initial response up to the transition zone, for each sand condition, is dominated by the clay layer condition (soft, medium or stiff). As the resistance of the shaft is mobilized, the pile behaviour is controlled by the sand layer condition. For example, for the dense sand layer cases, the stiffness (slope) of the response beyond the transition zone is the same. These observations show that the load-transfer mechanism within the lead section is insensitive to the clay conditions surrounding the grouted shaft. This also means that the resistance of this pile system can be considered as the summation of the resistance of the shaft friction and lead section resistance.

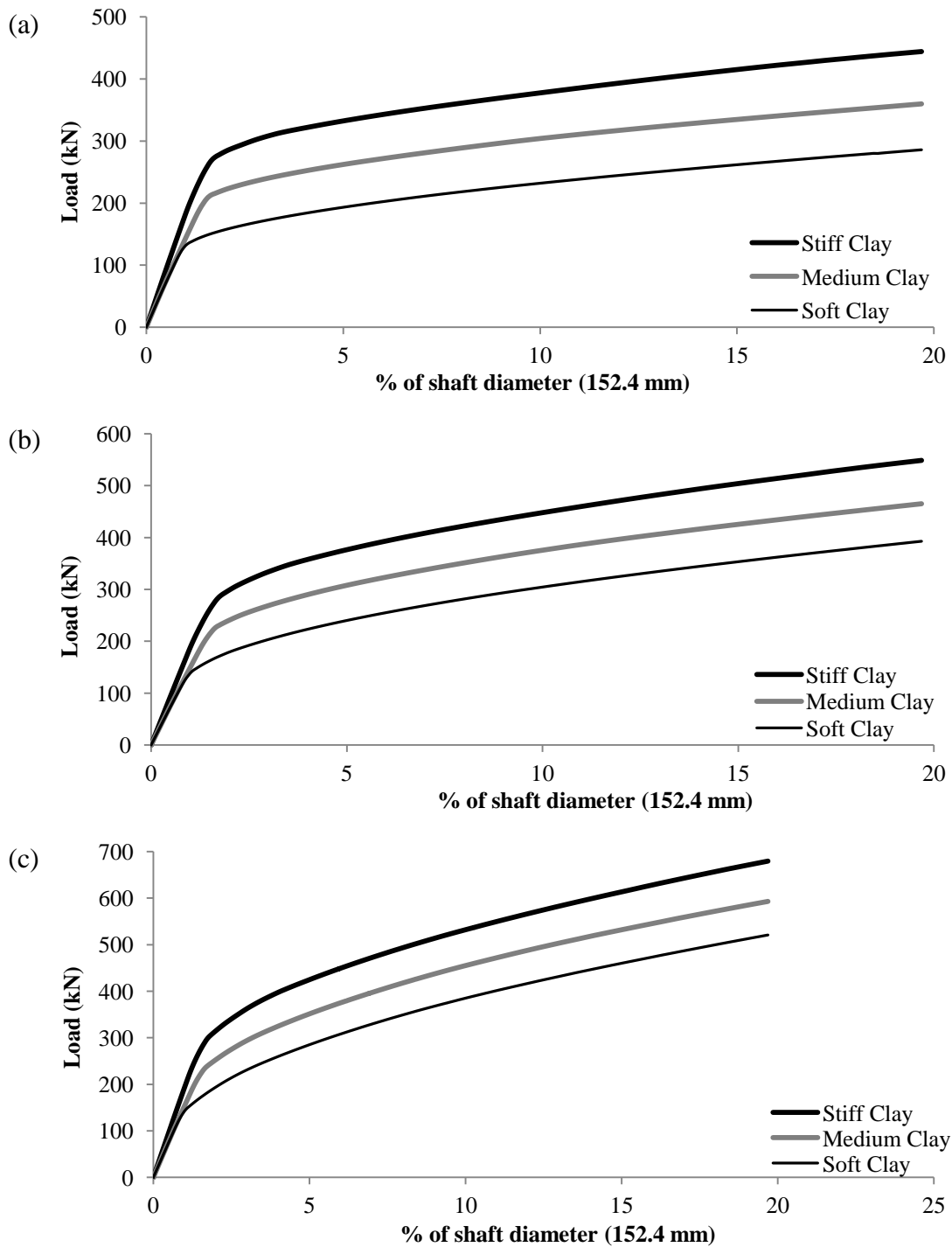


Figure 5.7. Load-normalized displacement (% of shaft diameter) response for RHPM for grouted shaft in Soft, Medium and Stiff clay and lead section in: (a) Loose Sand; (b) Medium sand; (C) Dense sand.

Figure 5.8 demonstrates the effect of sand conditions on the ultimate capacity of the pile system. It depicts the load-displacement response resulting from the FE analysis for RHPM with the grouted shaft embedded in soft clay and the lead section in loose, medium or dense sand. The initial slope is primarily similar as the pile shafts are within the same clay layer condition (and same shaft friction). However, the rate of change of slope within the transition zone is lowest for dense sand and highest for loose sand. The ultimate capacity at 25 mm of dense sand is about 31% and 78% higher than that for medium and loose sand, respectively. The non-linear behaviour occurs at 52%, 38% and 28.5% for the loose, medium and dense sand, respectively.

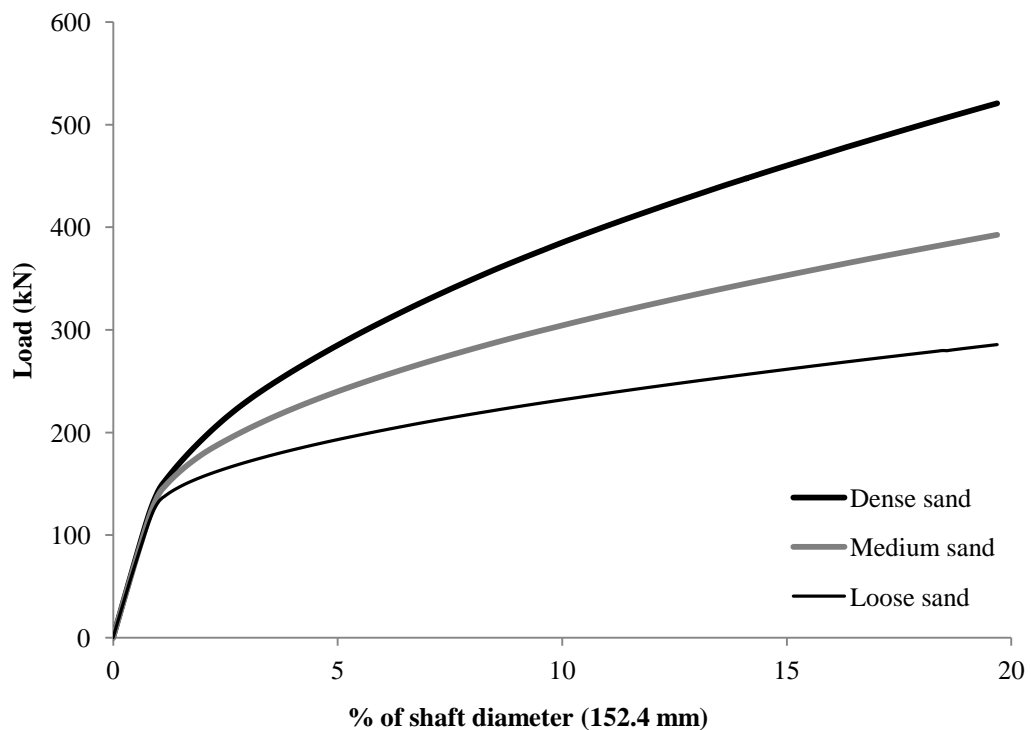
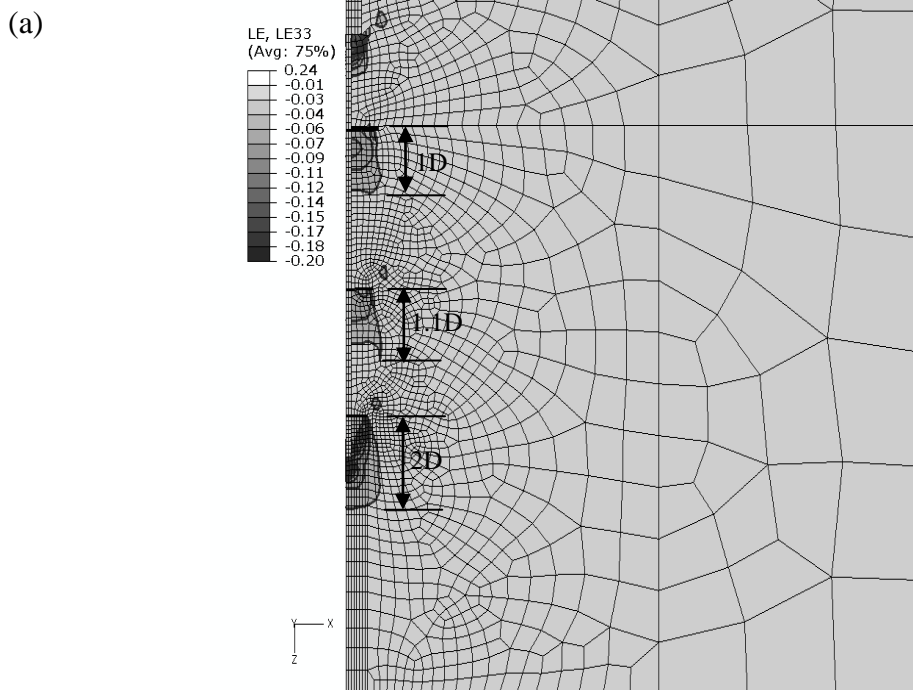


Figure 5.8. Computed load-normalized displacement (% of shaft diameter) response for RHPM; shaft in soft clay and lead section in loose, medium and dense sand.

Figure 5.9 shows the contours of axial strain concentrations below the shaft and helices at 25 mm pile head displacement for cases of lead section in dense, loose and medium sand, with the shaft in medium clay. The first observation from these contours is that the active resisting soil zone below the shaft base is about 1.6 D, (0.54 the distance from the shaft base to the top helix). This shows that the grout shaft is not interacting with the upper helix, indicating that placing the shaft at 457.2 mm (1.5 ft.) above the top helix seems adequate. Secondly, it is observed that the influence zone below the helices for the three sand cases considered is almost the same. The active resisting soil below the top helix, mid helix and bottom helix, in ratio to the helix diameter, is about 1D, 1.1 D and 2D, respectively. These ratios agree with previous findings by Elsherbiny (2011).



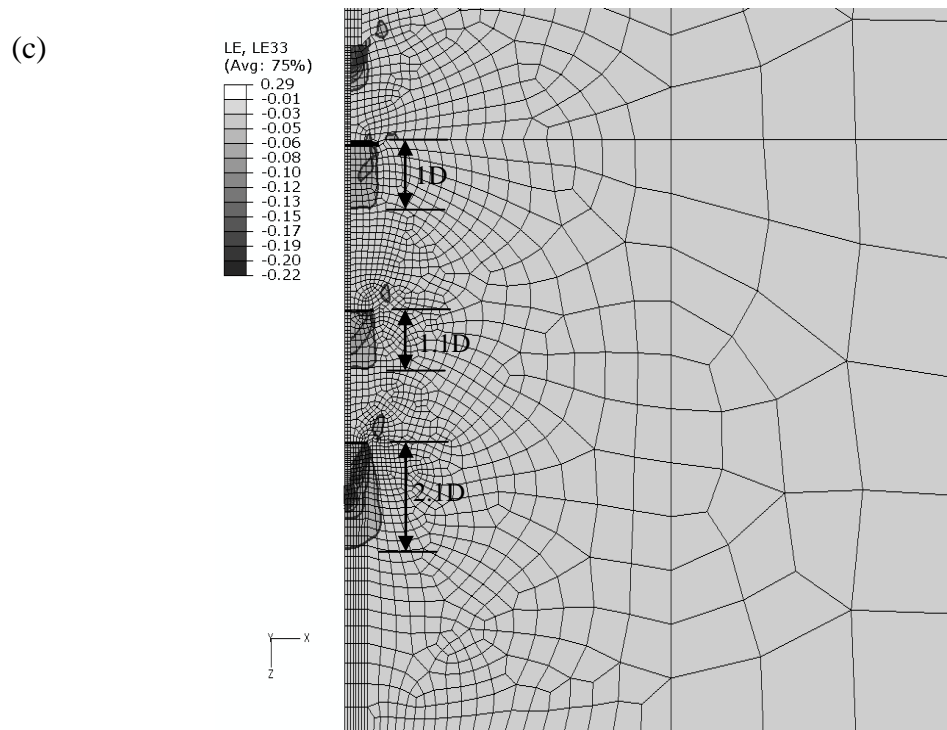
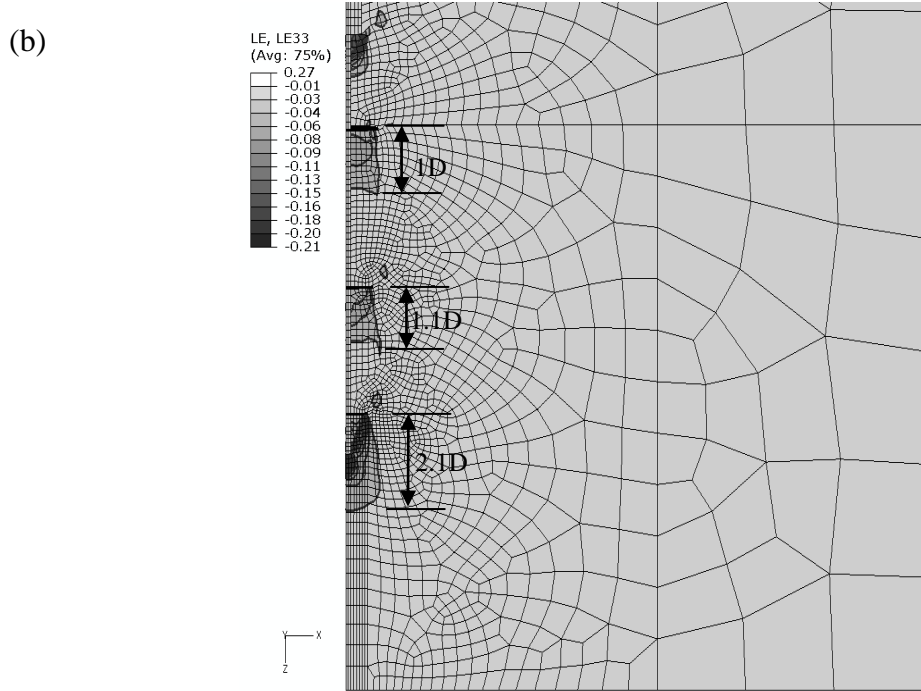


Figure 5.9. Contours of axial strains at 25 mm pile head displacement for RHPM with shaft embedded in soft clay and lead section in (a) dense sand; (b) medium sand; (c) loose sand.

5.10.3 Effect of helix thickness on the capacity of piles

Local deflection of the helices depends on the pressure below the helices and their flexural rigidity, which in turn is a function of the helix thickness. Therefore, the thickness of the helices may affect the pile capacity. It varies for the piles under consideration from 9.5 mm to 13 mm, and up to 25 mm for helical piles with circular shafts. The SS 175 (the pile under consideration) has a helix thickness of 9.5 mm. To investigate the feasibility of using larger thickness plates, FE analyses are conducted for RHPM piles with SS 200 (50.8 mm round-square shaft) that has a plate thickness $t = 13$ mm. All other dimensions are the same as for the SS 175. The cases considered are for lead section in loose, medium and dense sand, and shaft in soft clay. The detailed properties of the soil are as described in Table 5.4.

The load-displacement of the SS 175 (plate thickness $t = 9.5$ mm) is plotted along with the results for the SS 200 in Figure 5.10. As can be seen, minor increases in stiffness and capacity are observed due to the increase in helix thickness. The ultimate capacity in loose, medium and dense sand increased by 4%, 5.4% and 7.4%.

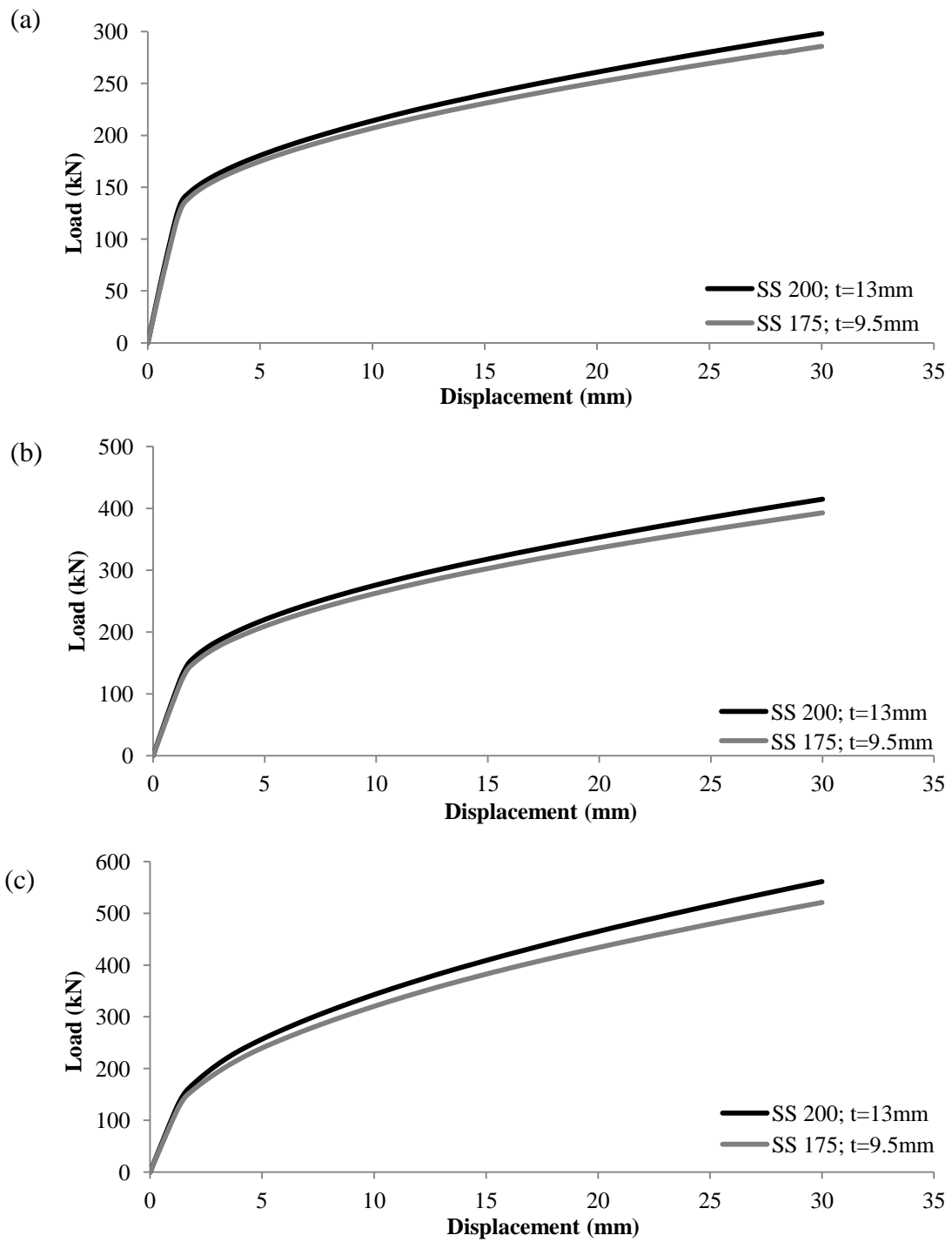


Figure 5.10. Load displacement curves for SS 175 (plate thickness 9.5 mm) and for SS 225 (plate thickness = 13 mm) for RHPM with shaft in soft clay and lead section in (a) loose sand; (b) medium sand; (c) dense sand.

5.11 Design Method for Axial Compressive Loading

Based on the experimental results and the numerical simulations, a design procedure for RHPM and FRP-RHPM is suggested.

5.11.1 Pile ultimate capacity

The experimental investigation showed that the pile resistance consists of the lead section resistance, Q_{lead} and the shaft friction resistance, Q_{shaft} :

$$[6.1] Q_u = Q_{shaft} + Q_{lead}$$

The construction of the shaft renders it as a Type A micropile where grout is poured by gravity to fill in the void created by the cutting disk (and by the pre-drilled hole if needed for the FRP-RHPM). The experimental investigation revealed that the shaft friction strength values given in the FHWA 2000 (Armour et al., 2000) are appropriate for RHPM and FRP-RHPM in stiff clay conditions. In addition, the FE analysis showed that the shaft resistance strength does not influence the stiffness of the pile system beyond the transition zone (for lead sections installed in sand). Therefore, the shaft friction resistance can be calculated as:

$$[6.2] Q_{shaft} = c_a A_s = \alpha c_u A_s$$

where c_a is the adhesion, α is the adhesion coefficient, c_u is the cohesion and A_s is the surface area of the soil-shaft interface. The shaft resistance strength values maybe adopted from the FHWA 2000 (Armour et al., 2000) for Type A micropile for stiff layer conditions. For undrained shear strength between 100 kPa and 185 kPa, a friction factor

of 0.7 is suggested. However, this value should be used with caution until test data from other sites are available. For soft clay conditions, the FHWA 2000 (Armour et al., 2000) may also be used or alternatively the CFEM 2006 design recommendation for shaft resistance in clays with undrained shear strength less than 100 kPa may be used.

The lead section capacity can be calculated as the sum of the individual capacity of the three helices, as

$$[6.3] \quad Q_{lead} = \sum_1^n Q_{bearing}$$

$$[6.4] \quad Q_{bearing} = A_h(qN_q)$$

where A_h is the projected bearing area, q is the unit bearing capacity below the helix, and N_q is the bearing capacity factor.

The individual capacity can be estimated directly from the SPT values or by using the conventional bearing capacity method. For estimating the bearing capacity directly via the SPT count, El Sharnouby and El Naggar (2012a and b) found that the Meyerhof's (1976) method as cited by the Canadian Foundation Manual (CFEM 2006) yields reasonable results, while, the Decourt's method overpredicted the ultimate capacity.

For estimating the bearing capacity using the bearing capacity factor, several equations exist in the literature. The CFEM (2006) defines the N_q for helical piles as that for local shear failure but does not provide specific values for design. The bearing capacity factors recommended by Meyerhof (1976), which are widely used for design of drilled shafts

(and helical piles), are recommended herein to be used for design of helical piles. Table 5.4 shows the computed capacity by the FE analysis at 25 mm displacement, compared to that predicted through the bearing capacity factor by Mayerhof (1976) and Terzaghi (1948) for local shear failure.

Table 5.4 shows that the Terzaghi's bearing capacity factors significantly underestimate the capacity of the lead section. Meanwhile, the Mayerhof's bearing capacity factors provide good predictions of the ultimate capacity for friction angles 34° and 38° . However, for friction angle of 30° , it underestimates the computed capacity by about 34%. It should be noted however, that this comparison is limited to the values of lateral earth pressure coefficient used, along with the modulus of elasticity.

5.11.2 Axial performance under one-way axial compressive cyclic loading

The field investigation included 15 one-way cyclic loading on RHPM and FRP-RHPM. The mean cyclic loading was 43% (45% for the RHPM) of the ultimate capacity and the cyclic load amplitude was about +/- 13% of the ultimate capacity. It was concluded that under such loading conditions and for piles installed in similar soil conditions, the ultimate capacity of piles subjected to cyclic loading can be conservatively estimated using the conventional available methods. However, more research is required to examine the effect of higher cyclic loading range on the pile ultimate capacity and performance.

5.11.3 Pile Spacing

Piles placed in groups experience interaction. The ultimate capacity of piles in groups can be defined as:

$$[6.5] Q_g = Q_e \cdot n \cdot Q_u$$

where Q_g = ultimate capacity of pile group, Q_e , is the group efficiency, n = number of piles in the group Q_u = ultimate capacity of one single pile.

The above analysis showed that at a distance of about 1.4 the average helix diameter, the soil experienced very negligible strains, i.e. less than 1×10^{-4} , indicating that at spacing of about 3 times the average helix diameter, the group efficiency may be high. Similar observations were made by Elsherbiny (2011). He conducted numerical analysis of pile in groups of 2 and 4 and found that the group efficiency was about 90% for piles spaced at three times the helix diameter, and almost 100% for piles spaced at five time the average helix diameter. Similar observations were made by Livneh and El Nagggar (2008).

Therefore, for typical pile group configurations for helical piles, i.e. spacing ration of three times the average helix diameter, the maximum value for group efficiency should be less than 90%.

5.11.4 Buckling

Helical piles with round-corner square shafts range in size from 42 mm to 57 mm. Therefore, buckling may be a concern for piles installed such that they have high slenderness ratio. In addition, helical piles may experience eccentric loading when used

for retrofitting applications. Hoyt et al. (1995) investigated the susceptibility of helical piles used in retrofitting applications to buckling through field and laboratory testing, and computer modeling using LPILE. They found that buckling is of practical concern only for long shafts in soft soils. Perko (2003) examined buckling susceptibility of helical piles in new foundations applications using L-Pile. Similar to the findings by Hoyt et al. (1995), he concluded that bulking is of concern only in very soft to soft clays and very loose to loose sand.

The slender shaft in the RHPM is encased in a fibre-reinforced grouted column and for the FRP-RHPM is encased in a fibre-reinforced grout column and a FRP casing. Therefore, the buckling resistance is expected to be significantly improved. As stated above, the construction of such system may render the grouted and the encased grouted shaft as Type-A micropile. FHWA 2000 (Armour et al., 2000) cites Bjerrum (1957), Mascardi (1970, 1982) and Gouvenot (1975) who concluded that buckling is only of a concern for micropiles in soils in the poorest mechanical properties. The FHWA 2000 (Armour et al., 2000) based on Caltrans (1993) also reports that for micorpiles encased in 178 mm casing, installed in 30 m of very soft clay over dense sand, the piles sustained 1775 kN without signs of buckling.

If it is desired to calculate the buckling capacity of a RHPM or FRP-RHPM, the Moment-Flexural Rigidity ($M-EI$) curves under a range of thrust loads can be calculated. The procedure can be similar to that used in Chapter 5 to obtain the $M-EI$ charts under zero

thrust loads. LPILE program can then be used similar to the procedure by Hoyt et al. (1995) and Perko (2003) to determine the buckling load.

5.12 Conclusions

A three-dimensional finite element analysis was conducted to simulate the RHPM and FRP-HPM. The model was verified by comparing the computed response to the test results. The developed model was then employed to analyze cases of lead sections installed in loose, medium or dense sand, and grouted shaft in soft, medium or stiff clay. Based on the results obtained from the analysis, the following conclusions can be made:

1-The load transfer mechanism within the lead section is insensitive to the clay conditions along the grouted shaft.

2-The FE analysis confirmed the conclusions from the experimental study that the RHPM and FRP-RHPM are composite pile systems whose resistance consists of shaft friction and lead section capacity.

3-No interaction was found to occur between the grouted shaft and the lead section.

4-The shaft friction coefficient for clay with undrained shear strength from 100 kPa to 166 kPa can be taken as 0.7.

4-The shaft friction for soft clays can be estimated based on the CFEM 2006 procedures or the FHWA 2000 (Armour et al., 2000) guidelines.

5-Using the SS 200 lead section and extension shaft increases the capacity slightly. The increase in the capacity of the lead section depends on both the plate thickness and the soil conditions.

5-The bearing capacity factors proposed by Mayerhof (1976) for drilled shafts were found to provide a very reasonable estimate for the lead section capacity for friction angles more than 34° and a conservative estimate for lesser friction angles.

Based on the FE analysis along with the experimental results, a design procedure for FRP-RHPM and RHPM under axial compression loading conditions is presented.

5.13 References

Armour, T., Groneck, P., Keeley, J., and Sharma, S. 2000. Micropile design and construction guidelines-implementation manual. Federal Highway Administration FHWA-SA-97-070, Washington, D.C.

Bjerrum, L., 1957. Norwegian Experiences with Steel Piles to Rock. *Geotechnique*, Vol. 7, pp. 73 - 96.

Caltrans, 1993. Caltrans pile load test results at a deep bay mud site using various pile types - I-280 San Francisco: Results and Seismic Design Guidelines. DFI and Caltrans Specialty Seminar, Sacramaneto, CA, October, p: 44.

Canadian Foundation Engineering Manual. 2006. Fourth edition. Canadian Geotechnical Society, 488 p.

Cook, R. D., Malkus, D. S, Plesha, M. E., and Witt, R.J. 2002. Concepts and applications of finite element analysis. John Wiley & Sons. Inc, USA.

El Sharnouby, M.M, and El Naggar, M.H. 2012. Field investigation of axial monotonic and cyclic performance of reinforced helical pulldown micropiles. Canadian Geotechnical Journal, 49(5): 560-573.

El Sharnouby, M.M, and El Naggar, M.H. 2012. Axial monotonic and cyclic performance of FRP-steel fibre-reinforced helical pulldown micropiles (FRP-RHPM).Canadian Geotechnical Journal, Accepted.

Elsherbiny (2011). Axial and lateral performance of helical pile groups. 2011. M.E.Sc thesis. The University of Western Ontario.

Gouvenot, D., 1975. Essais de chargement et de plambement de pieux aiguilles. Annals de ITdB et de Travau Publics, No. 334.

Ensoft Inc. 2011. LPILE PLUS 6: A program for the analysis of piles and drilled shafts under lateral loads. Version 6.0.27 [computer program]. Ensoft Inc., Austin, Tex.

Hibbitt, H.D., Karlsson, B.I., and Sorensen, E.P. 2011. General purpose finite element analysis program. version 6.9. Habbitt, Karlsson & Sorensen, Inc., Pawtucket, R.I.

Hoyt, R., Seider, G.; Reese, Lymon C., Wang, S-T. 1995. Buckling of helical anchors used for underpinning. Foundation Upgrading and Repair for Infrastructure Improvement. GSP (50), p 89-108.

Jeon, S.S., and Kulhawy, F. H. 2001. "Evaluation of axial compression behavior of micropiles." Foundations and ground improvement, GSP 113, T. L. Brandon, ed., ASCE, Reston, Va., pp. 460–471.

Kulhawy, F.H., Mayne, P.W. 1990. Manual on estimating soil properties for foundation design. Research Project 1493-6, Cornell University, Ithaca, New York.

Livneh, B., and El Naggar, M.H. 2008. Axial testing and numerical modeling of square shaft helical piles under compressive and tensile loading. Canadian Geotechnical Journal, 45(8): 1142-1155.

Mascardi, C. A. 1970. Comportamento dei Micropali Sottoposti a Sforzo Assiale, Momento Flettente e Taglio. Verlag Leeman, Zurich.

Mayerhof, G.G. 1976. Bearing capacity and settlement of pile foundations. Journal of the Geotechnical Engineering Division, ASCE, 102(GT3), pp. 225-244.

Perko, H. A. 2003. Lateral capacity and buckling of helix pier foundations. In proceedings of the helical foundations and tie-back seminar. Deep foundation institute.

Prakash, S., and Sharma, H.D 1990. Pile foundations in engineering practice. John Wiley & Sons, Inc., NY.

Sivrikaya O, and Togrol E (2006). Determination of undrained strength of fine-grained soils by means of SPT and its applications in Turkey. Journal of Engineering Geology, 86: 52-69.

Terzaghi, K. 1942. Discussion of the progress report of the committee on the bearing value of pile foundations. In Proceedings, Earth and Foundations, American Society of Civil Engineers, Vol. 59, No. 8, pp. 1363-1372.

Table 5.1. Material properties for pile components.

Property	Helix/ central shaft	Fibre-reinforced grout	FRP
Modulus of Elasticity (Gpa)	200	30.1	12.7
Yield Stress (Mpa)	550/620	-	
Ultimate Stress (Mpa)	621/760	-	
Poisson's ratio	0.3	0.2	0.45

Table 5.2. Range of soil parameters used for calibration of RHPM and FRP-RHPM.

Layer	Depth (m)	γ (kPa)	γ_{sub} (kPa)	E (Mpa)	C_u (kPa)	α_{bond} (kPa)	ν	ϕ ($^{\circ}$)	K_o
Stiff Clay; WT at 3.8 m	0-6 (along pile shaft)	17	10	40-65	85- 166	60- 120	0.49	0	1
Medium dense to dense sand	6-8.5 (lead section)	20	11	73- 110	-	-	0.3	36- 38	1.36- 1.58

Note: γ , unit weight of soil, γ_{sub} , submerged unit weight; E, Young's modulus; C_u , undrained shear strength; α_{bond} , shaft adhesion; ν , Poisson's ration ; ϕ , internal friction angle; K_o , coefficient of lateral earth pressure (estimated-soil along shaft; Jeon and Kulhawy 2004).

Table 5.3. Soil properties used for the parametric study.

Parameter	Soil along shaft			Soil below top helix		
γ_{sub} (kPa)	11	11	11	10	10	10
E (Mpa)	64.8	68.9	77	30	30	50
C_u (kPa)	-	-	-	35	60	121
C_a (kPa)	-	-	-	35	60	85
ν	0.3	0.3	0.3	0.49	0.49	0.49
ϕ (°)	30	34	38	-	-	-
K_o	0.707	1.123	1.58	1	1	1

Note: γ_{sub} , submerged unit weight; E, Young's modulus; C_u , undrained shear strength; C_a , shaft adhesion; ν , Poisson's ration ; ϕ , internal friction angle; K_o , coefficient of lateral earth pressure (estimated-soil along shaft; Jeon and Kulhawy 2004).

Table 5.4. Comparison between computed and predicted ultimate capacity for lead section in sand

Friction Angle	Ultimate capacity of lead section (kN)		Computed (kN)	% difference	
	Mayerhof (1976)*	Terzaghi (1948)**		Mayerhof (1976)	Terzaghi (1948)**
38°	396.1	166.8	387	-2.4	56.9
34°	217.8	115.6	272	19.9	57.5
30°	118.8	82.3	176	32.5	53.2

*Obtained from Prakash and Sharma (1990); N_q for drilled foundations.

**Terzaghi's modified factors to account for local shear failure.

***FIELD INVESTIGATION OF LATERAL MONOTONIC AND CYCLIC PERFORMANCE OF STEEL FIBRE-REINFORCED HELICAL PULLDON MICROPILES (RHPM) AND FIBRE GLASS-REINFORCED POLYMER-FIBRE REINFORCED HELICAL PULLDOWN MICROPILES (FRP-RHPM)**

6.1 Introduction

A Helical pile is a deep foundation system that is typically used to support light to medium load applications such as solar farm applications, pipelines, telecommunication and transmission towers, and low- and medium-rise buildings. They are installed using mechanical torque with minimal noise and vibration levels. They are suitable for applications involving expansive soils and ad-freeze conditions and are advantageous in limited access installations. In addition, it allows onsite quality control by monitoring installation torque. Helical piles can be used for both retrofitting existing foundations and for supporting new foundations. The segmented helical piles are examined in this study as a candidate for seismic retrofitting of existing foundations, which can also provide an efficient foundation option for new construction.

The segmented helical (screw) pile consists of relatively small galvanized central square shaft (SS) or rounded shaft (RS) fitted with one or more (up to 4) helices. Shaft sizes

*A version of part of this chapter has been published in the 36th Annual Conference on Deep Foundations.

range from 42 mm to 57 mm. The first segment (lead section) contains the helices and is installed to the desired depth by adding extensions connected onsite using bolted couplings. The helices diameters range between 150 mm to 400 mm. For multi-helix lead sections, larger diameter helices are placed near the top followed by smaller diameter helices at a spacing of about three times the helix diameter. Helices have standard pitch of 76 mm (3").

6.1.1 Steel fibre-reinforced helical pulldown micropile (RHPM) and fibre reinforced polymer-steel fibre-reinforced helical pulldown micropile (FRP-HPM)

To overcome the main drawbacks of the square slender shaft; buckling potential in relatively weak soils, Vickers and Clemence (2000) introduced the helical pulldown® micropiles (HPM). It consists of a helical pile installed with a grout column surrounding the pile central shaft along the extensions. Along with Vickers and Clemence, several studies focused on the axial capacity of the grouted helical pile (e.g. Abdelghany and El Naggar, 2010; Lutenecker, 2010) and reported a considerable increase in the axial capacity of the pile compared to the plain helical pile.

The RHPM differs from the HPM in that the grout mix contains steel fibres that are added during construction. Steel fibre reinforced concrete or grout has been increasingly used in the last decade for structural applications. The mix is made by adding steel fibres to fresh mix of concrete. The main advantage of addition of such fibres is that they enhance the tensile strength and provide ductility and therefore energy dissipation to the material, which are favorable characteristics for structures to resist cyclic and dynamic loads (de Oliveira Junior et al., 2010; Abbas and Mohsin, 2010). Despite the increased

use of steel fibre-reinforced concrete/grout in structural application, its use did not extrapolate yet from structural applications to foundation engineering. Expanding their use to foundation engineering, given the low associated cost, may result in a better performing foundations and more optimal design. Chapter 3 provides the details of the conducted full-scale testing on both pile systems under axial static and one-way cyclic loads. Test piles displayed a significant increase in axial resistance relative to the plain pile (no grout column). In addition, post-cyclic ultimate capacity was within the same range or higher than the static ultimate capacity.

The FRP-RHPM is the RHPM with an FRP tube encasing the steel-fibre reinforced grout column. The use of FRP composite materials in construction has increased significantly in the past few years. FRP materials are made of a polymer matrix reinforced with fibreglass (or other fibres). Their light weight, combined with corrosion resistance and minimum maintenance requirements make them an attractive option for deep foundations. Chapter 4 provides the details of the conducted full-scale testing on the FRP-RHPM under axial static and one-way cyclic loads and reported similar findings to that of RHPM.

6.1.2 Previous studies on lateral behaviour of helical piles

The square shaft pile requires less installation torque and can be constructed in hard soil conditions compared to the round shaft pile. However, the square shaft is more susceptible to buckling. In addition, the square shaft has a limited surface area in contact with the surrounding soil, which limits its lateral resistance.

Round square shafts have received more attention in the literature. Puri et al (1984) looked at various test data of piles in sand and clay. They concluded that helical anchors can develop significant resistance to lateral loads. Perko (2009) carried out LPILE Plus analysis, using the p-y curves approach, considering several pile types and found that the helical piles offer lateral capacity of the same order of magnitude as micropiles and small diameter drilled shaft piles having comparable diameters and installed in similar soil conditions. Prasad and Rao (1996) examined the behaviour of model scale piles in clayey soils. They found that the lateral capacity increases with increasing embedment depth and soil shear strength.

Several attempts have been made to study the effect of the helical plates on the pile's lateral resistance. Puri et al (1984) conducted full-scale and model tests, and concluded that the helices play a minor role in the lateral resistance if the extension is more than a certain limiting value. Similarly, Sakr (2009) conducted full-scale lateral tests on piles installed in oil sand. He observed that piles with one and with two helices behaved similarly. He concluded that the helices had a minor effect on the lateral resistance. Meanwhile, Prasad and Rao (1996), and Mital and Shekhbar (2010) found that helical piles offer more lateral resistance than that of single straight pile without plates, with resistance increasing with number of plates. A theoretical model was developed from both studies that attributed the capacity increase to the bearing resistance on the bottom of the plates, uplift resistance on the top of the helices and frictional resistance on their surface. The disagreement between the above studies may be due to the difference in soil-pile interaction and depth of the helices relative to the depth of the active soil resisting

zone, as well as if piles are behaving as rigid short piles where rotation activates the resistance on top and bottom of the plates, or as long piles where rotation doesn't take place considerably.

Helical piles behaviour under cyclic loading has received much less attention in the literature. The limited literature available has focused on behaviour under one-way cyclic loads. Prasad and Rao (1994) carried out one way sustained cyclic load model tests on helical piles embedded in clay and reported that helical piles performed better at relatively high cyclic load levels than piles without helical plates that had the same geometric dimensions. More recently, Abdelghany and El Naggar (2010) conducted one-way sustained lateral cyclic tests plain helical piles and HPM including the RHPM. They concluded that for all tested piles, the lateral capacity degraded due to the cyclic loading, with the RHPM presenting the most favorable performance during cyclic loading.

The primary objectives of this study are to (i) Evaluate the lateral capacity of RHPM and FRP-RHPM; (ii) Investigate their suitability for cyclic loading applications; and (iii) Determine the effect of lateral cyclic loading on their axial capacity.

6.2 Site Investigation

The experimental program was carried out at the environmental site of the University of Western Ontario, London, Ontario. As discussed in Chapter 3, two boreholes were conducted within the test area, 16.6 m apart, to a depth of 8.8 m. Standard penetration tests was performed for each borehole using an automatic hammer. The site consisted of stiff to very stiff clayey silt till underlain by dense sand. Retrieved samples showed that

the till layer was fissured, especially at shallow depth. The ground water table was found at an elevation of 3.7 m and 4.1 for BH-1 and BH-2, respectively.

All piles were installed such that the lead section was situated entirely within the dense sand, while the shaft (FRP shaft) was situated within the stiff clayey silt till, as shown in Figures 6.1b and c. More details on in-situ soil conditions and SPT count can be found in Chapters 3 and 4.

6.3 Test Pile Description and Installation

6.3.1 Description of RHPM and FRP-RHPM

The reinforced helical pulldown micropile consisted of two main parts: a plain helical pile; and a steel fibre-reinforced grout column surrounding all or part of the extensions. The plain pile consisted of a lead section and three extensions. The details of the lead section, as shown in Figure 6.1a, are as follows: 1.5 m long; 44.5 mm square shaft; 3 attached helices (diameters = 305 mm, 254 mm and 203 mm); 76 mm helix pitch, helix spacing 3 times helix diameter. Extensions were 44.5 mm square shafts, each was 2.1 m long. The grout column was 3.8 m depth and 150 mm in diameter. As the grout used to fill the shaft void was poured in by gravity, it can be classified as a Type A micropile according to the FHWA micropile design and construction implementation manual (Armour et al., 2000). A schematic of the reinforced helical pulldown micropile (RHPM) is shown in Figure 6.1b.

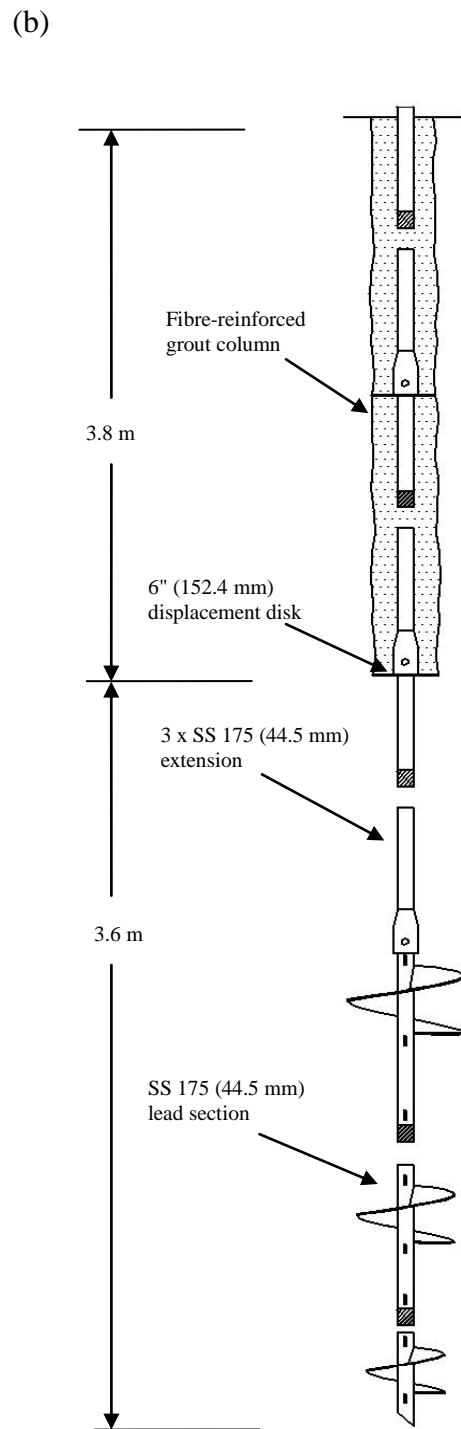
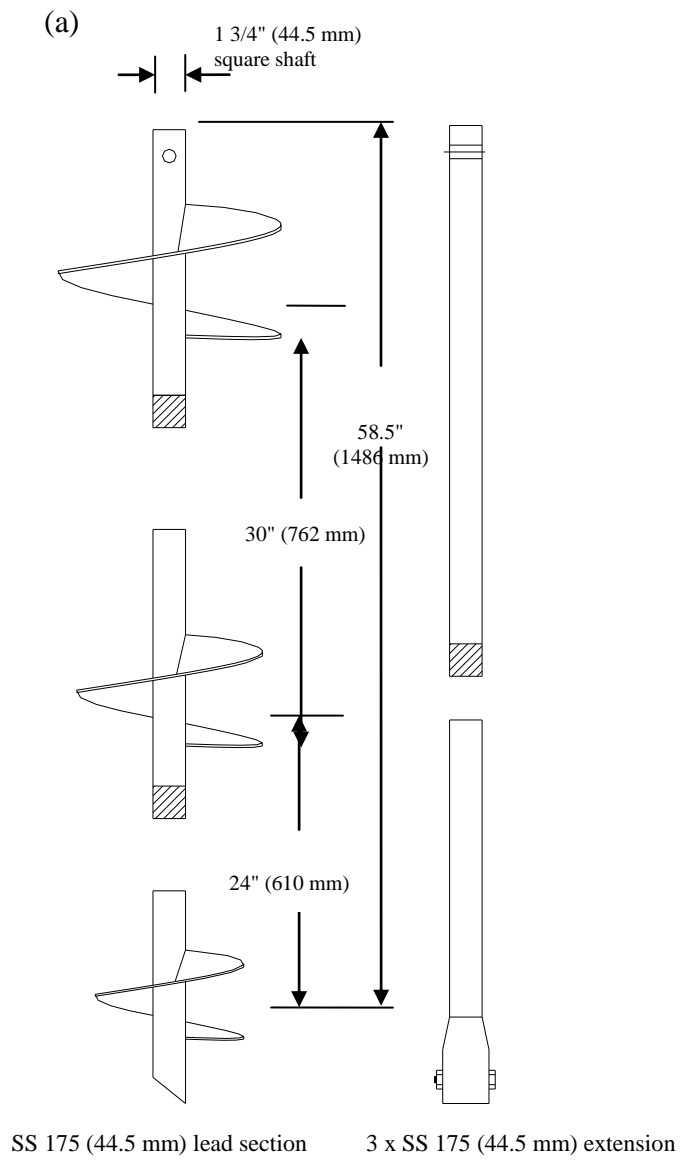
The tested composite pile system, the FRP-RHPM, (Figure 6.1c) was comprised of: a lead section, three extensions, and a cylindrical FRP tube (sleeve) that surrounded part of

the pile shaft, infilled with steel fibre-reinforced grout column. Lead section and extensions were as of the RHPM (Figure 6.1a). The FRP tube was 3.3 m long, a nominal outside diameter of 140 mm and wall thickness of 7.62 mm. An innovative technique was used in installation of FRP-RHPM to overcome the installation difficulties associated with excessive friction along the FRP tube. The new installation technique, provided minimal resistance along the FRP profile during installation, and minimized the stresses developed within the FRP tube and hence preserving its structural integrity. A detailed description of the installation technique was provided in Chapter 4.

All test piles were installed such that the lead section was situated entirely within the dense sand, while the shaft (grout shaft for RHPM or FRP sleeve infilled with grout for FRP-RHPM) was situated within the stiff clayey silt till, as shown in Figures 5.1b and c.

Compression and splitting tensile lab tests were conducted on the grout mix. The average compressive and tensile strength of three specimens, after 28 days, were found to be 47 MPa and 6.5 MPa, respectively. The steel fibres were 0.5 mm in diameter and 30 mm long. All piles were tested after 28 days.

To evaluate the improvements that the FRP-RHPM offers over the plain helical pile, one plain helical pile with the same lead section and extension configurations was installed to the same depth and tested under cyclic loading conditions.



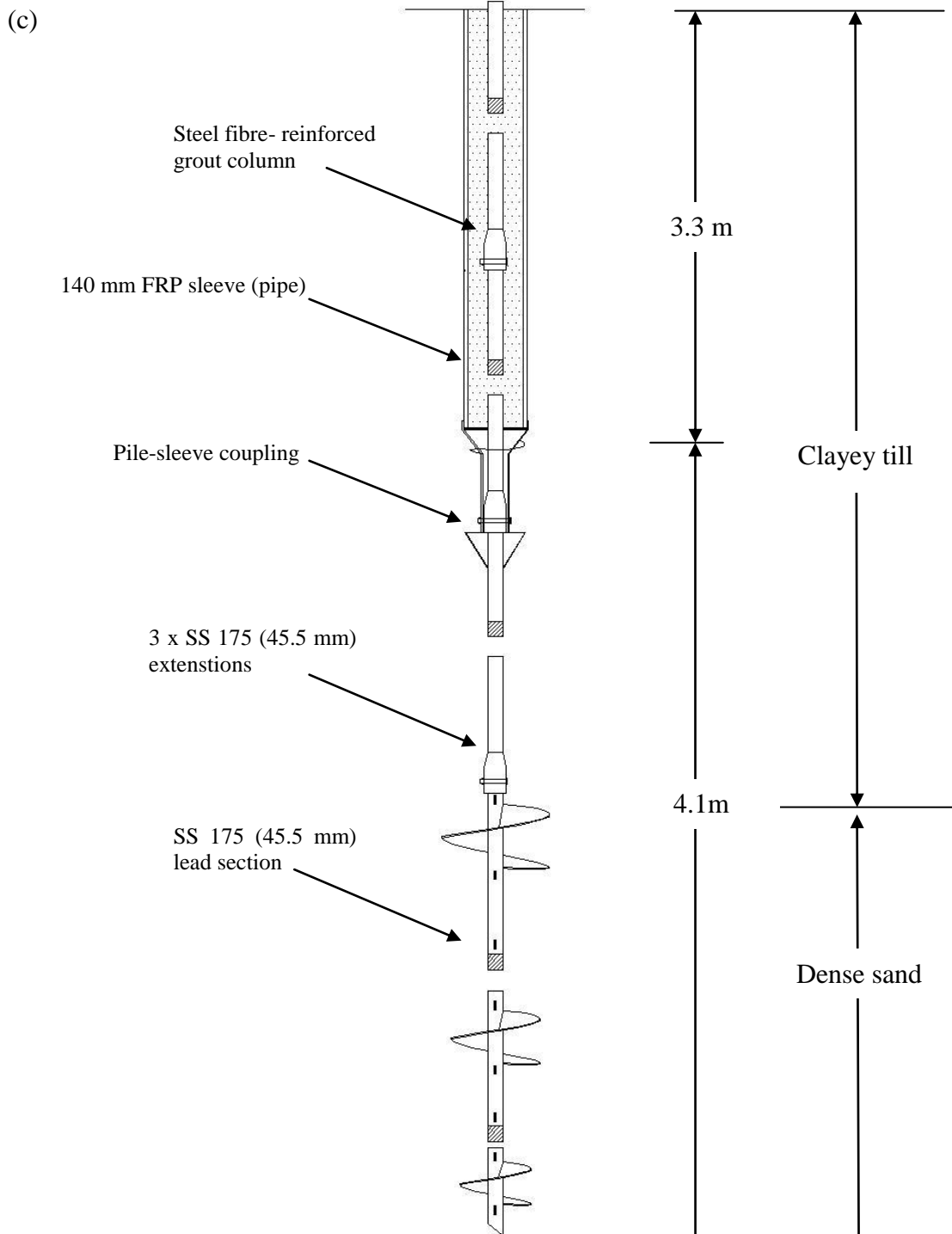


Figure 6.1. (a) Plain pile configurations; (b) RHPM test pile profile after installation; (c) FRP-RHPM test pile profile after installation.

6.4 Field Test Set-up

6.4.1 Monotonic Testing

Two different setups were used in the monotonic lateral loading experiments. The first setup can be used for monotonic and cyclic loading, as well as dual pile testing (testing piles in pairs). The second setup can be used for only monotonic testing and can be used for one test at a time.

Figure 6.2a shows the first lateral test set-up. It was designed and manufactured to be used for both monotonic and cyclic testing. For monotonic loading of a single pile, the system consisted of a loading plate that was pinned to a steel rod, threaded into the hydraulic jack, which in turn was clamped between two steel plates. The load cell was connected to the clamping steel plates through another steel rod threaded into the load cell from one side. Another steel rod was threaded into the load cell from the other side, and was bearing against a reaction beam. The reaction beam was anchored to the ground by two reaction helical piles and was laterally restrained by the 19500 kg installation machine.

Figure 6.2b shows the second set-up. The load cell was connected directly to the loading plate through a threaded collar. After the loading plate and the load cell were put in place, the hydraulic jack was installed. The gap between the main beam and the hydraulic jack was filled by an additional beam and a series of steel plates.

LDTs were used to measure the lateral displacement at four points on the loading plate. The load cell and linear displacement transducers (LDTs) were monitored through a data

acquisition system. Figure 6.2a shows the lateral monotonic set up and Figure 6.2b shows a close up of the loading system. The pile head was free to rotate during the test in both setups, and two or four (LDTs) were used to measure the pile head displacement.

The load was applied in increments of 5 kN every 2.5 minutes. The load was increased until continuous jacking was required to maintain the load or a minimum displacement of 30% of the grout shaft was reached.

(a)





Figure 6.2 (a) Lateral test set-up; first set-up; (b) Lateral test set-up; second set-up.

6.4.2 Cyclic testing

Cyclic test set-up is shown in Figure 6.3. The rod assembly apparatus was expanded for dual pile load testing. This was done by connecting the steel rods to the test piles from both sides through bearing plates. This system uses the test piles as reaction piles at the same time (dual pile testing). The system was assembled on site. Before the assembly, the hydraulic jack was pumped half way so that advancement and retraction can take place. All components were manufactured such that no yield would occur under applied load levels and that it would accommodate variations of spacing between different pairs of test piles. The pile head displacement was measured using two LDTs for each test pile.

The cyclic load test involved two-way cyclic loading. The piles were subjected to 5 cycles at every load level with an increment of 5 kN, as shown in Figure 6.4. The loading lasted until the maximum available stroke of the hydraulic jack was reached.



Figure 6.3. Cyclic test set-up.

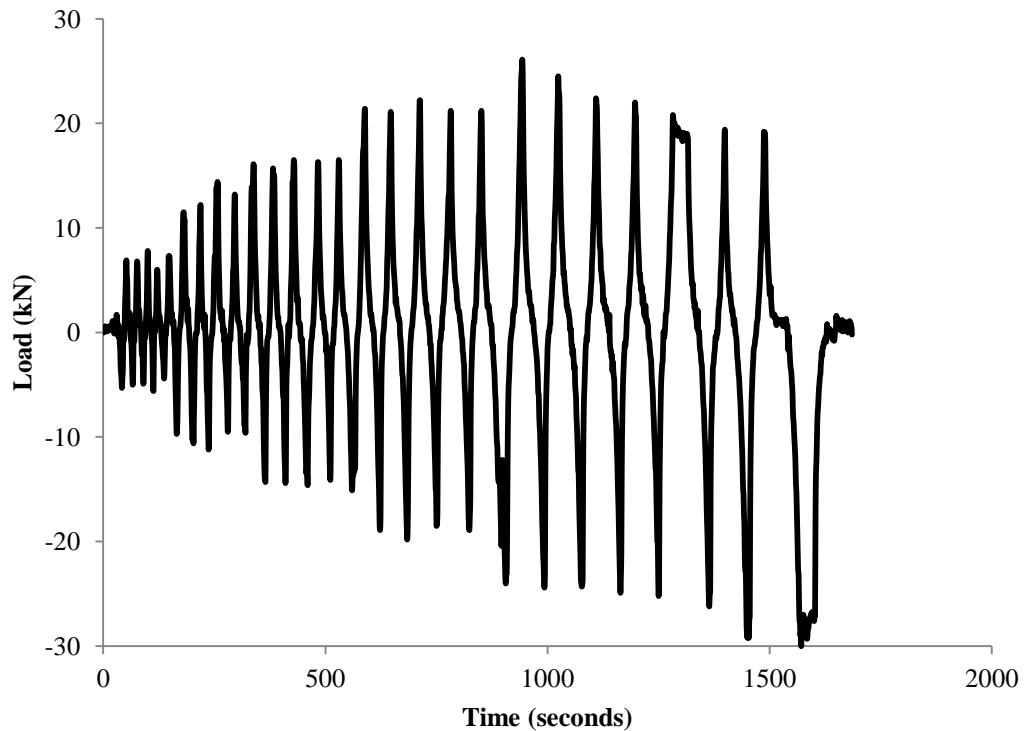


Figure 6.4. Cyclic test protocol.

6.5 Monotonic behaviour of RHPM

As mentioned above, 6 piles were subjected to static (monotonic) loading conditions. Table 6.1 shows the ultimate capacity for all test piles. Figure 6.5 shows the load-displacement response for two RHPM that envelop the observed response of all test pile. Thus, they are deemed to be representative of the range of results for all other piles. As can be noted from Figure 6.5, the piles' response can be characterized by an initial response with relatively high stiffness up to load levels between 15 kN and 25 kN and a corresponding displacement of 6 to 9 mm. After which, the piles displayed a non-linear response up to displacement levels of about 40 mm. At higher displacement levels, the response curve exhibits a semi-linear shape up until the end of loading. The piles sustained loads ranging from 54 kN to 70 kN at displacements of about 80 mm (52% of

pile shaft diameter). Upon unloading, the piles retrieved up to 67% of the displacement with a permanent displacement of about 10 mm or less.

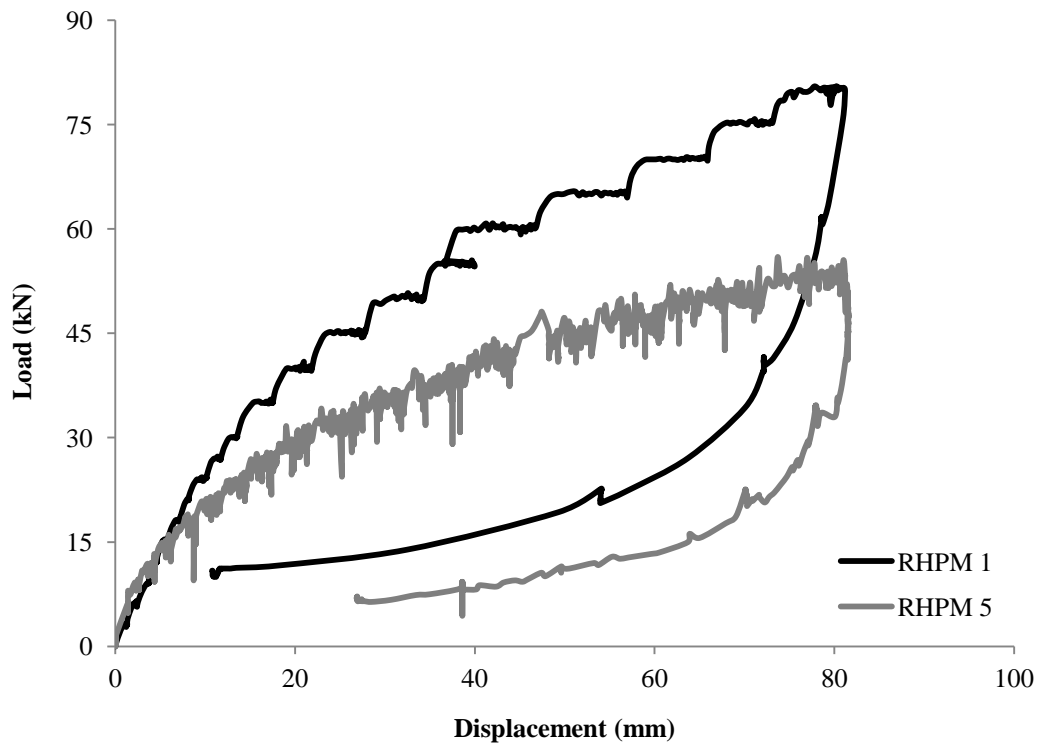


Figure 6.5. Load-displacement response for RHPM.

The observed displacement was caused by two mechanisms: a global mechanism and a local mechanism. In the global mechanism, the grout shaft displaces and rotates by punching through the soil, the so-called plowing. This process starts by separation/crack of the grout shaft (including the grout fill) at the back interface between the pile and soil (behind the load). The separation starts along the centre line of the pile. As the load increased, the separation propagated along the circumference, reaching the centre line of the pile as shown in Figure 6.6a. As load increases, cracks propagated radially through the surrounding soil. With further increase in the load, the separation/gap increased

vertically along the soil/pile interface. The measured gap depth at end of load (using a tape measure) was approximately 0.5 m. In the local mechanism, a series of radial and/or splitting cracks formed on the grout surface in front and/or behind the pile. These cracks were visible at relatively high load levels (> 33 kN). These cracks propagated outwards from the steel shaft, and widened with the increase of load. Figure 6.6b shows the splitting crack at the end of testing. The global mechanism was observed in all piles. The degree by which the local mechanism took place varied from pile to another. The variation is most probably due to the inherent variability of the steel-fibre orientation and the consistency of soil in the vicinity of test piles. Upon excavation at the site, cobbles were found at depth less than 1.8 m.

(a)



(b)



Figure 6.6: (a) Gap opening behind the pile-RHPM, static test; (b) Radial cracks profile at end of static test-RHPM.

6.6 Cyclic Behaviour of RHPM

Eight RHPM piles were tested under two-way cyclic loading. All piles were subjected to axial monotonic and cyclic loading prior to lateral testing. In general, the piles' behaviour was similar to that under monotonic loading. A gap formed behind the pile and propagated radially. As the load progressed and reversed, the entire perimeter of the pile was separated from the surrounding soil. Figure 6.7 shows the complete cyclic load-displacement response of one RHPM. The remainder of piles showed a similar shape of response curves. The general observation that can be made from Figure 6.7 is that the pile response was slightly stiffer in one direction than the other. This can be explained as follows. At the first cycle, if loading started in the leftward direction, a gap is created behind the pile (in the rightward side). As the loading is reversed, the pile doesn't offer resistance until the gap is closed. Therefore, the results produce a "preferential side" which displayed higher stiffness than the other side. For the remainder of loading, the gap in the direction of first loading cycle remained smaller than that in the other direction.

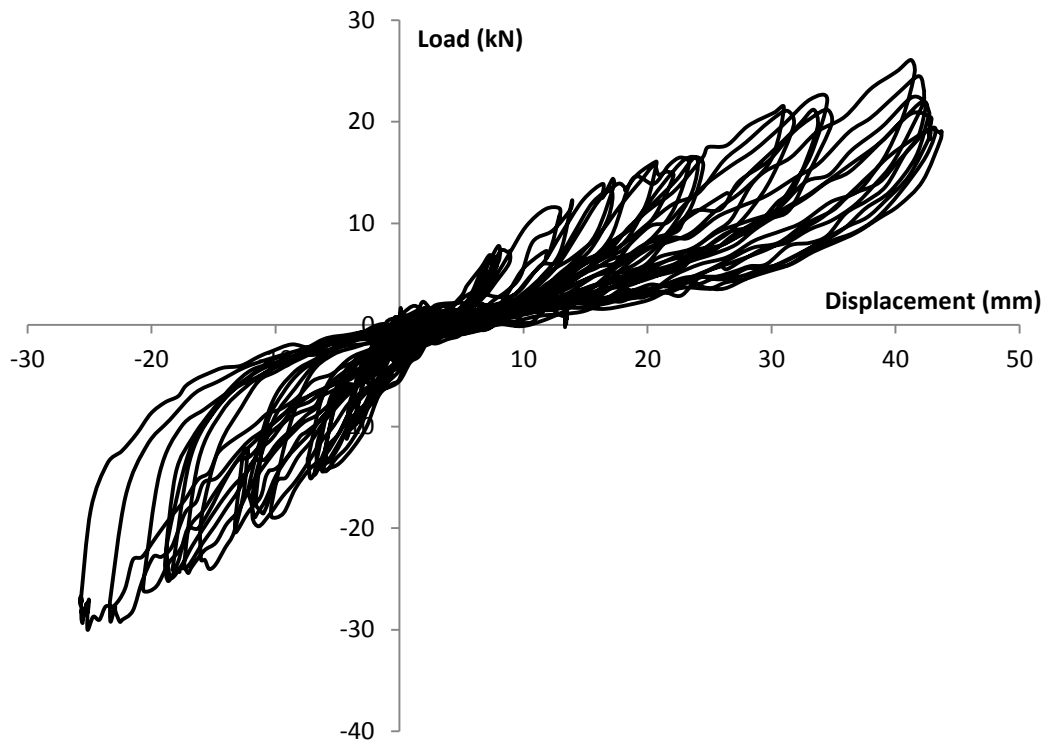


Figure 6.7. Cyclic load vs. displacement for RHPM 7.

To further illustrate the gap opening and closing process, the first full cycles at load levels 5, 10, 15, and 20 kN are plotted in Figure 6.8. As can be seen, the loading-unloading hysteretic curve can be characterized by three distinct branches that correspond to three phases. As the load is reversed, the piles first show near-zero resistance (pile behaved as a free column); then the response takes a concave-up shape representing the closing of the gap in the direction of loading, followed by a linear or non-linear shape (depending the displacement level) as contact was fully established and the soil in the direction of loading was full mobilized.

It can also be noted from Figure 6.8 that for all load levels, the stiffness of the loading branch in the preferred direction was higher than that of the other direction. Another

observation is that the response of the pile was shifting more towards the non-preferred side: as the load progressed, more displacement was required to mobilize the full soil resistance, compared to the preferred side, indicating that the gap was larger at any load level on the non preferred side.

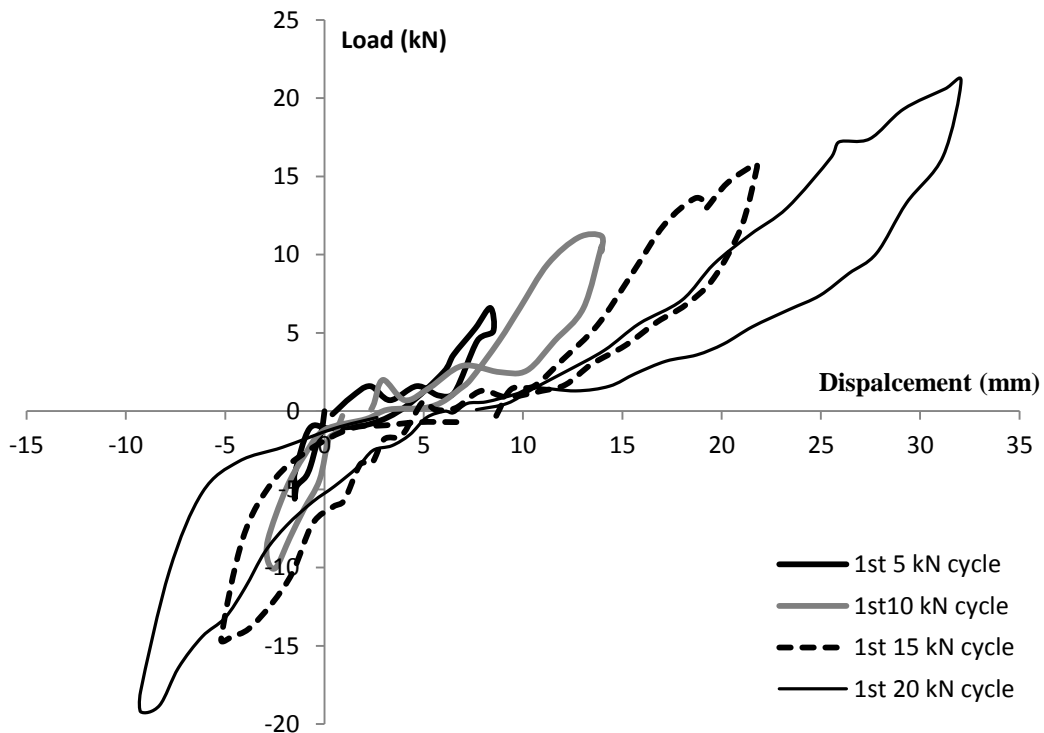


Figure 6.8. Cyclic load vs. displacement for first cycle at 5,10,15 and 20 kN for RHPM 7.

6.6.1 Effect of cyclic loading on stiffness and response (RHPM)

Degradation due to cyclic loading in stiff clay can be attributed to gap formation and/or degradation in soil resistance. Figure 6.9 shows the load-displacement in one direction for the first and last cycles for load levels 10, 15, 20 and 25 kN. As can be noted from Figure 6.9, for load levels 5 and 10 kN, no noticeable performance degradation was observed. At higher cyclic load levels (15, 20 and 25 kN), as loading was reversed, the concave-up

shape had a lower stiffness with progression of cycles, then it was parallel to that of previous cycles. That response indicates the widening of gap and increase in its depth with an increase of the number of cycles, which was observed visually during testing. At the higher load levels, it was observed that the pile was plowing into the soil, and hence creating increased separation depth at the soil/pile interface. The load-displacement curves remained parallel until the load reached the cyclic load level, which suggests that degradation didn't occur in soil strength but rather only due to increase of gap. This was manifested in that the stiffness within the last loading cycle was the same as the first load cycle (for the same load level). At load level of 30 kN, a degradation in pile stiffness (within the loading branch) was observed indicating degradation in soil resistance. It should be noted that degradation occurred gradually with the number of cycles.

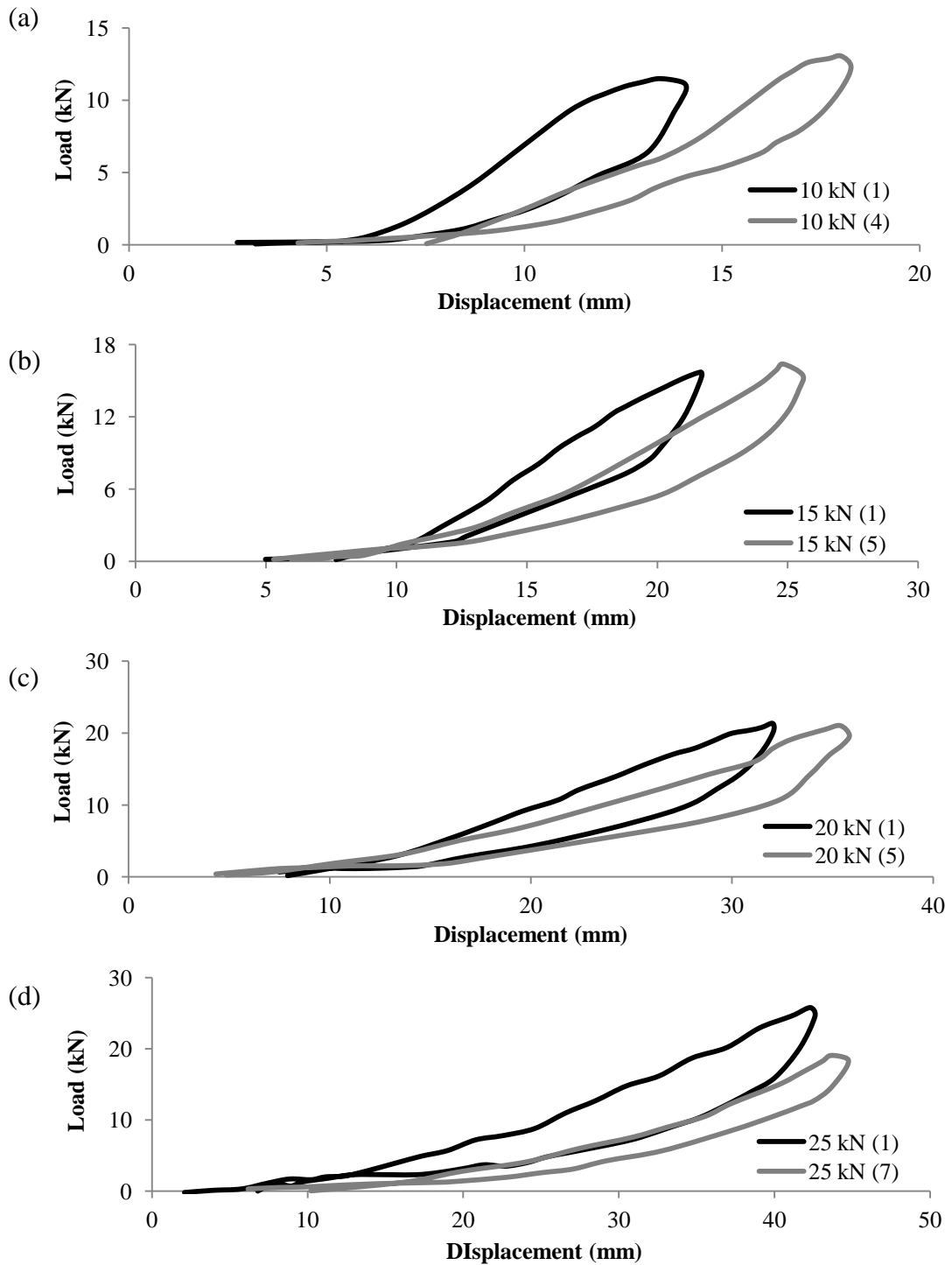


Figure 6.9. Load displacement for first and last cycle for (a) 10 kN; (b) 15 kN; (c) 20 kN; and (d) 25 kN [() = no. of cycles].

Figure 6.10 shows the envelope of resistance of two piles plotted along with the range of results obtained in the static tests. As noted above, at all loading stages, the pile cyclic response was biased towards the direction where loading occurred first. It can be seen that initially there was no degradation in one direction; however, the other direction experienced degradation from the beginning of loading. It can also be seen that the slopes of these envelopes were reduced compared to the slopes of the static piles, indicating that soil degradation due to cyclic loading was significant in this case. It can be also seen that the weaker side of the pile had an envelope with lower stiffness than the lower bound of the static results.

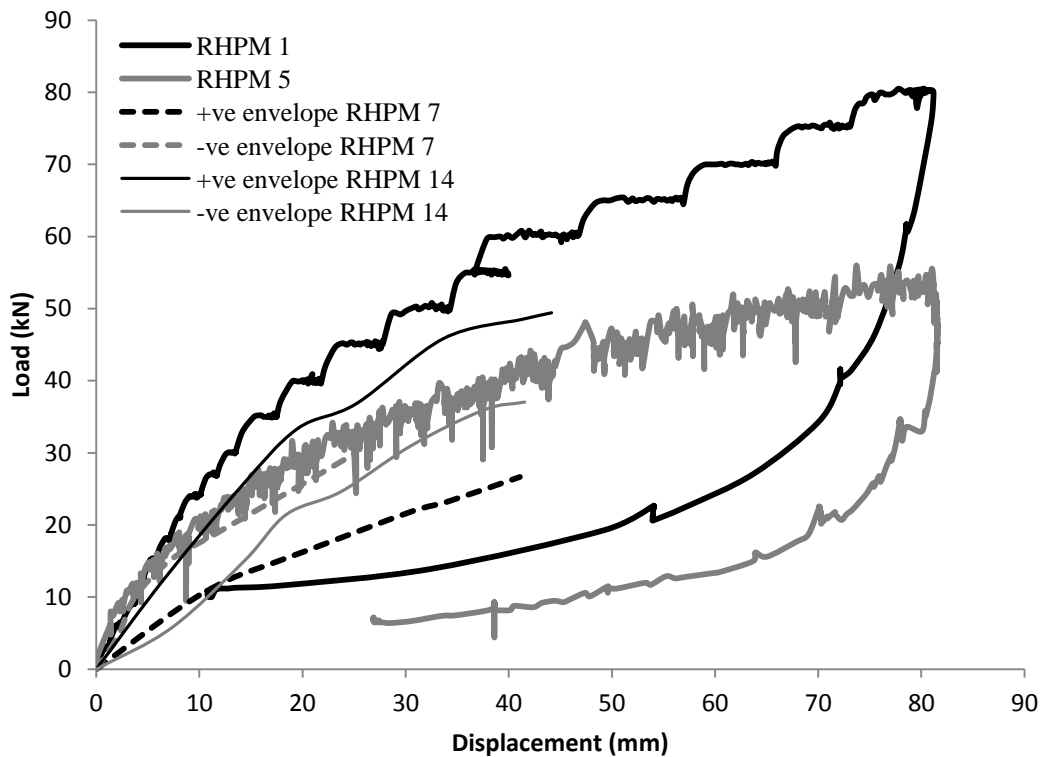


Figure 6.10. Static and backbone curves for RHPM.

6.7 Monotonic behaviour of FRP-RHPM

As mentioned above, 5 piles were subjected to static loading conditions. Table 6.1 shows the ultimate capacity for all test piles. Figure 6.11 shows the load-displacement response for two FRP-RHPM, representing the range of results for all other piles. The piles' response can be characterized by an initial high stiffness branch followed by a near-linear branch followed by a non-linear branch where an increase in the load was accompanied by non-proportional increase in displacement. The test piles sustained loads ranging from 80 kN to 101 kN at displacements ranging between 71 mm and 80 mm (52% of pile shaft diameter). Upon unloading, the piles retrieved more than 20% of the maximum displacement, resulting in permanent displacement of 15 mm or less.

The FRP-RHPM, in general, displayed similar failure progression as that of the RHPM. Cracks initiated behind the pile that evolved into gaps forming along the soil/pile interface. The exception in the FRP-RHPM performance was that no separation between the steel shaft and the grout was observed. Also, no crack radiating from the steel shaft (within the FRP tube) formed, showing that the FRP tube provided confinement to the grout column that prevented cracking and/or separation resulting in the pile system maintaining its structural integrity.

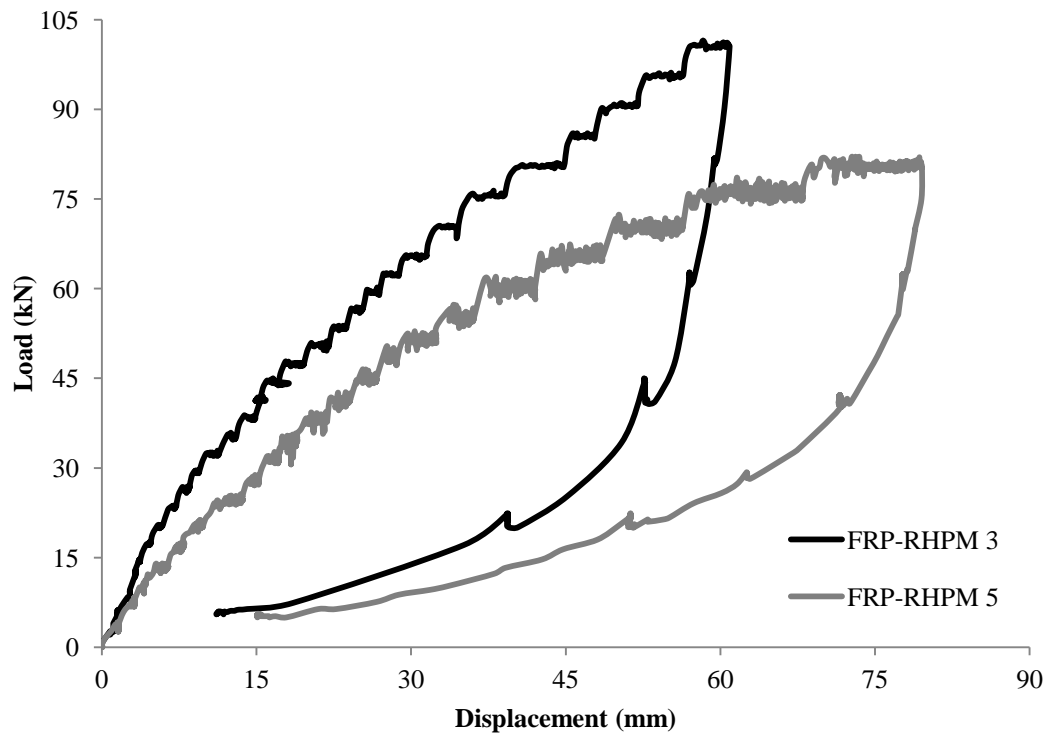


Figure 6.11. Load-displacement response for RHPM 3 and 5.

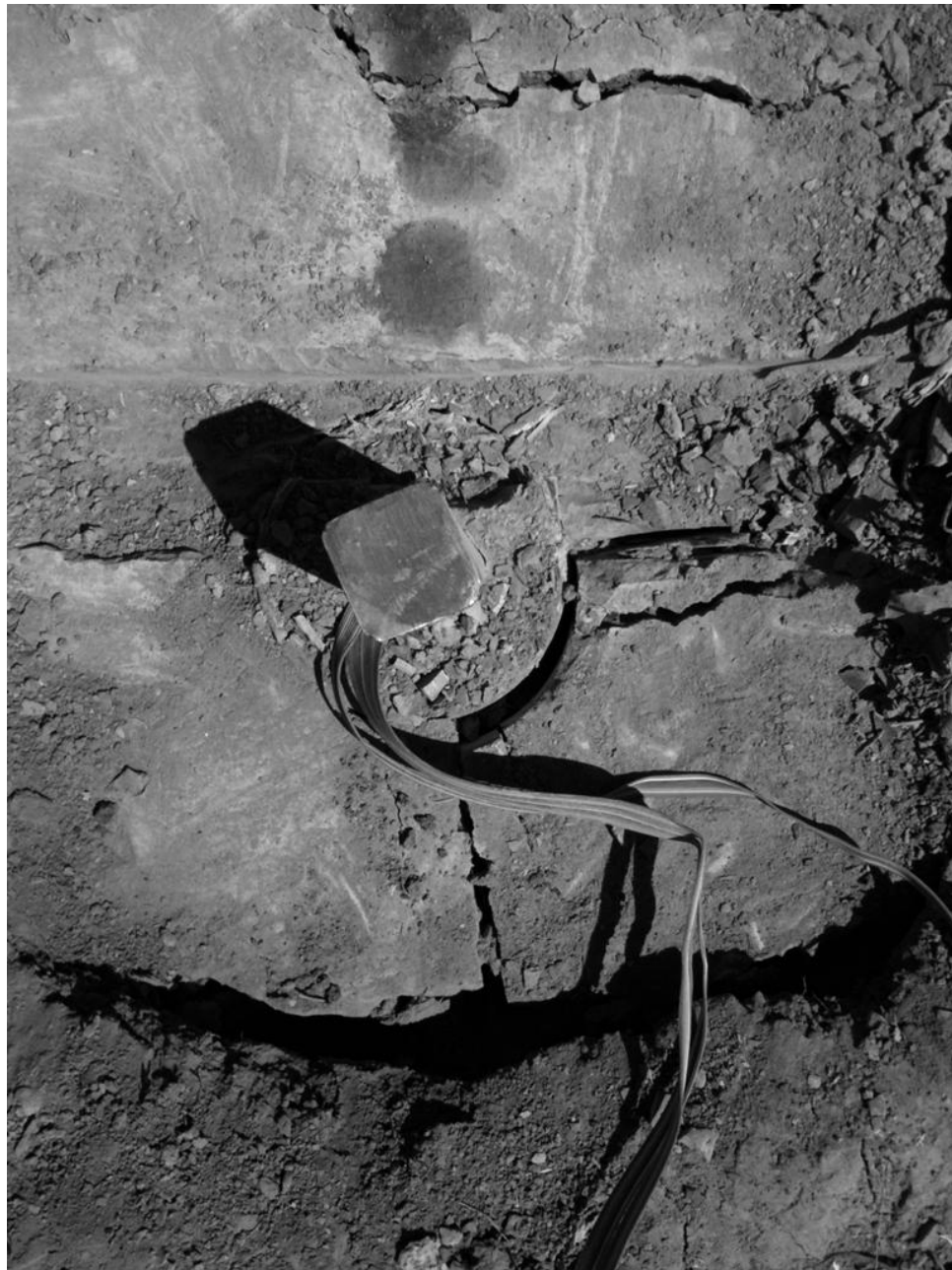


Figure 6.12. Gap opening at end of testing, FRP-RHPM static test.

6.7.1 Cyclic behaviour of FRP-RHPM

Figure 6.13 shows a typical cyclic load-displacement response of FRP-RHPM (FRP-RHPM 8). Similar to the RHPM, the pile displayed a preferred direction that offered in general higher resistance.

The overall behaviour of the pile under cyclic loading was similar to that under static loading. No cracks were observed within the FRP tube. As loading proceeded, gap behind the pile was observed. As loading was reversed, gaps in front of the pile started to form. Gaps along the soil-pile interface progressed radially and eventually separation between the pile and surrounding soil was observed.

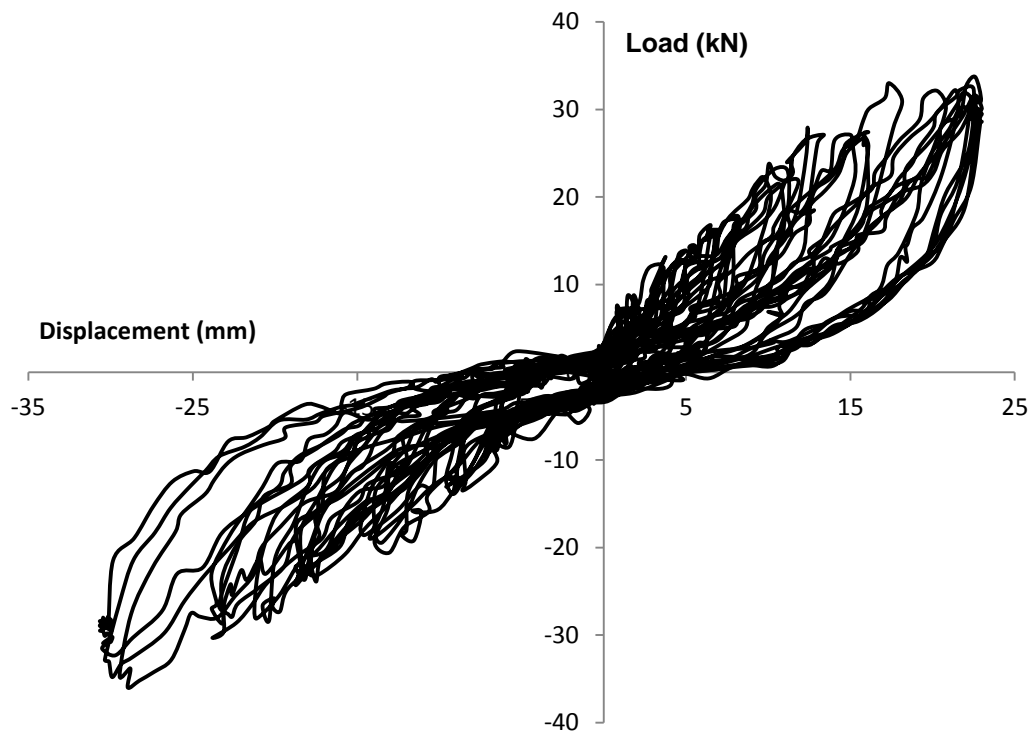


Figure 6.13. Cyclic load vs. displacement for FRP-RHPM 8.

Figure 6.14 shows the load displacement for the first and last cycles at different load levels. As indicated before, stiffness degradation can be due to soil degradation and/or formation of gaps. It can be seen that the response curve at the last cycle at a particular load level was parallel but slightly shifted to the response curve of the 1st cycle. In the last loading cycle, the transition to the concave-up shape occurs at a larger displacement,

after which the response curve was almost parallel to that at the first cycle. As can be seen from Figure 6.14, for both in front of and behind the pile, there was no noticeable degradation in its stiffness with as the number of cycles increased. However, there was stiffness degradation in comparison with initial loading cycle. That indicates that the stiffness degradation was due to larger gaps created during cyclic loading rather than soil resistance degradation. Even after 9 cycles at 30 kN (Figure 6.14), only a slight degradation was more pronounced.

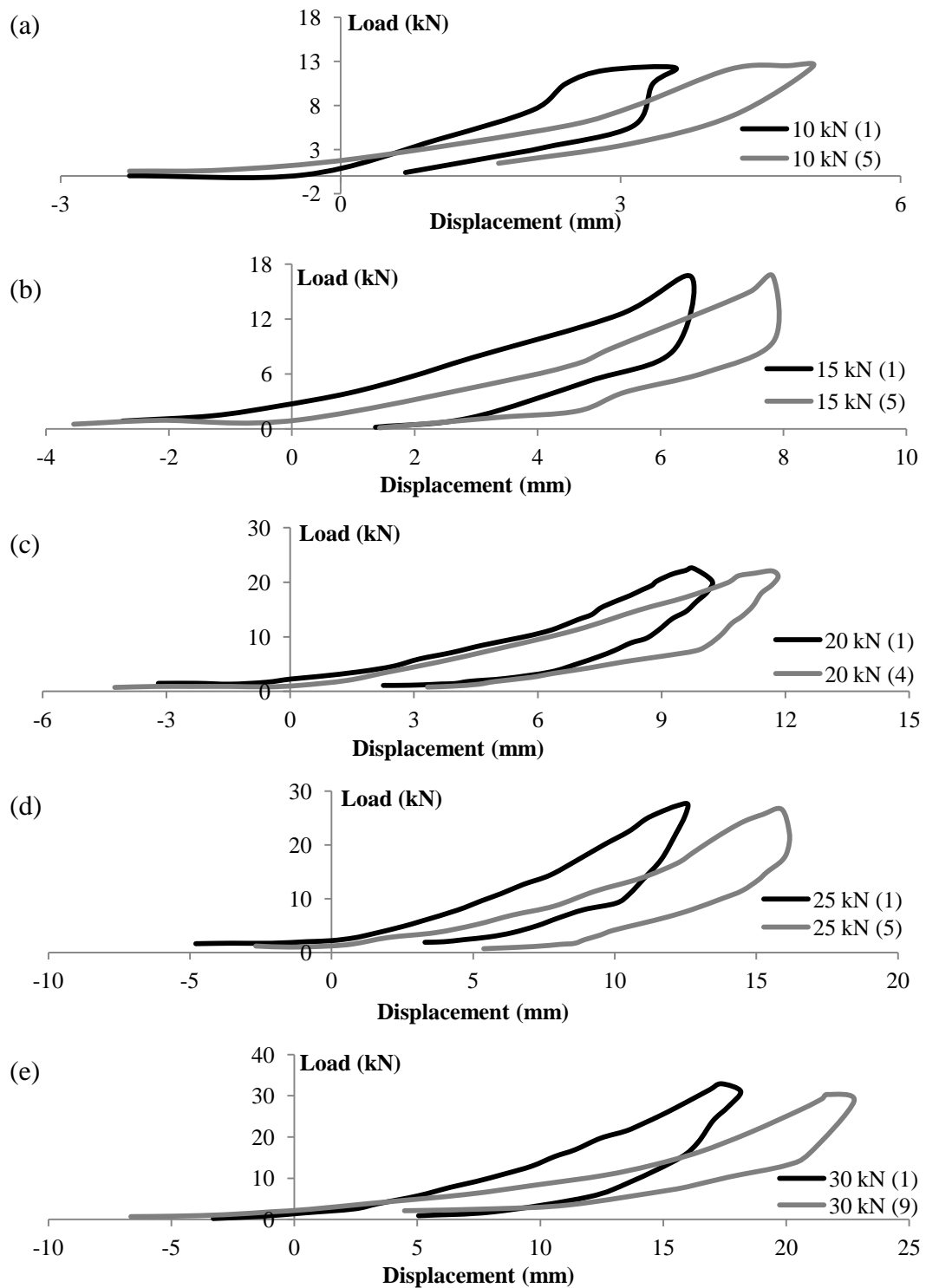


Figure 6.14. Load displacement for first and last cycle for (a) 10 kN, (b) 15 kN, (c) 20 kN, (d) 25 kN, and (e) 30 kN [() = no. of cycles].

Figure 6.15 shows the envelope of resistance of two piles plotted along with the range of results obtained in the static tests. At all loading stages, the pile cyclic response was biased towards the direction where loading occurred first. It can be noted from Figure 6.15 that initially there was no degradation in one direction; however, the other direction experienced degradation from the beginning of loading. It can also be noted that the slopes of these envelopes were comparable to the slope of the static piles, indicating that soil degradation due to cyclic loading was not significant in this case. It can also be seen that the weaker side of the pile had an envelope with lower stiffness than the lower bound of the static results.

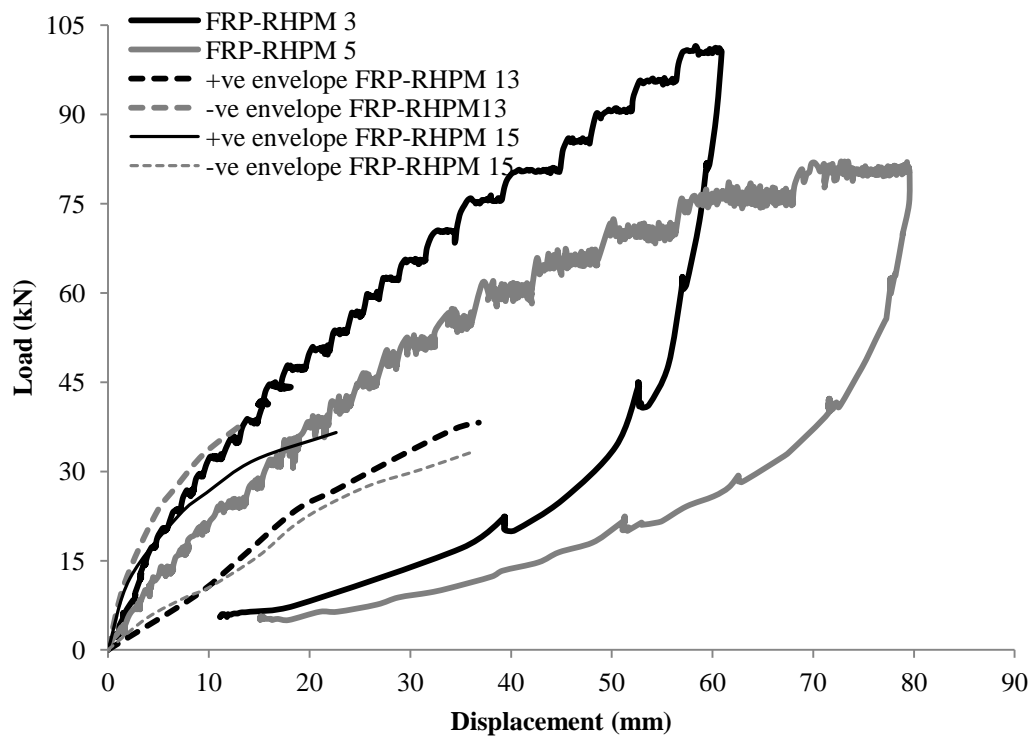


Figure 6.15. Static and backbone curves for FRP-RHPM.

6.7.2 Effect of Lateral cyclic load on axial capacity of FRP-RHPM

The experimental observations showed that lateral cyclic loading created gaps at the top portion of the pile. In order to examine the effect of lateral two-way cyclic loading on the axial capacity of the FRP-RHPM, three piles were subjected to axial loading after being tested under lateral cyclic loading. The load-displacement response is shown in Figure 6.16 along with the maximum response obtain from those tested under axial loading without prior lateral cyclic loading. The initial portion of the response depends primarily on the shaft friction. As can be seen, the piles displayed similar performance with no noticeable degradation in the initial stiffness. This may show that the gap depth was rather shallow, and had no effect on the axial pile performance. Piles 14, 15 and 16 were tested after LC; all other piles were tested axially only before LC.

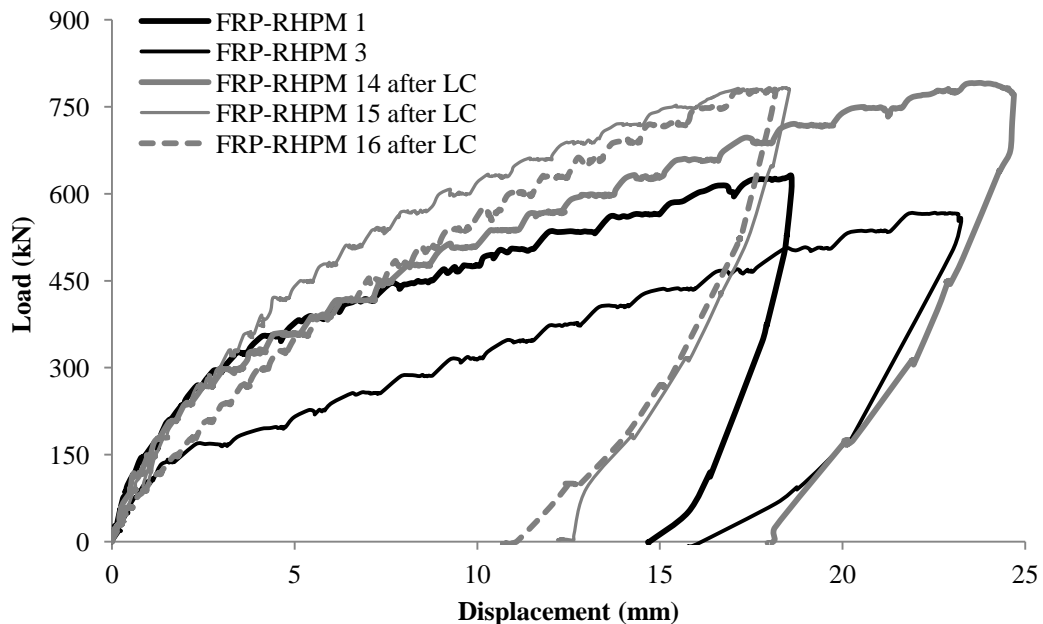


Figure 6.16. Load-displacement response for FRP-RHPM for piles with no prior lateral cyclic load (LC) and piles with prior lateral cyclic load.

6.8 Comparison between behaviour of FRP-RHPM and RHPM

6.8.1 Monotonic behaviour

Figure 6.17 compares the test results for one FRP-RHPM and RHPM. Both piles lie within the average response of their respective test group. As can be seen, the FRP-RHPM displayed higher initial stiffness, a longer slowly changing transition non-linear phase, and, unlike for the RHPM, no near-linear branch was observed until end of testing. The stiffness at any loading level was significantly higher for the FRP-RHPM than for the RHPM. Figure 6.17 clearly shows the significant improvement that the FRP tube provided to the soil-pile system. The FRP tube significantly increased the bending resistance of the pile, and hence reducing the stresses on the soil resisting the load. The FRP-RHPM consistently had 50% less displacement at the same load level throughout testing. Interestingly, the RHPM retrieved 70% upon unloading compared to 63% for the FRP-RHPM. On average, as can be seen in Table 6.1, the resistance of the FRP-RHPM was 35.7% higher resistance at 25 mm displacement.

It is note worthy that while both piles had similar axial ultimate capacities, their lateral capacity as percentage of their axial capacity was 7.5% and 5% for FRP-RHPM and RHPM, respectively.

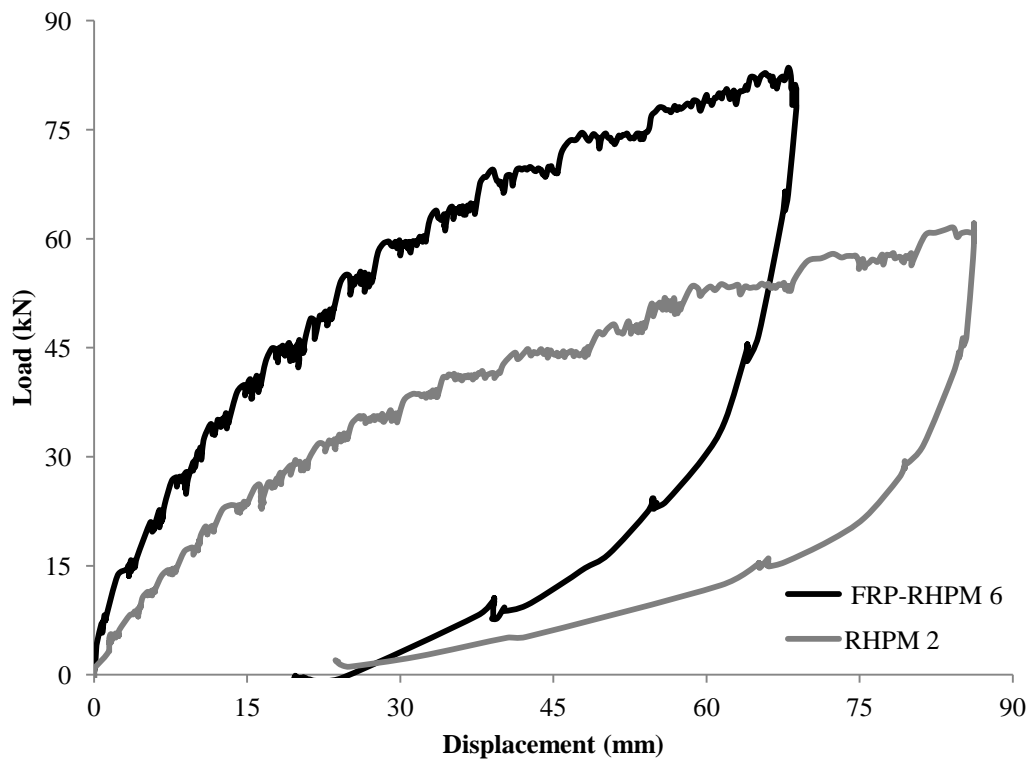


Figure 6.17. Load-displacement response for FRP-RHPM 6 and RHPM 2.

6.8.2 Cyclic behaviour

In order to investigate the effect of the fibre-reinforced grout column and/or the FRP sleeve, one plain helical pile was tested under cyclic loading and the results are compared with those for the RHPM and FRP-RHPM and the results for the last loading cycles are shown in Figure 6.18.. The comparison of results of other loading cycles demonstrated a similar trend. As can be seen from Figure 6.18, both the FRP-RHPM and RHPM provided significant improvement in capacity and stiffness over the plain pile. For instance, at 35 mm displacement, the FRP-RHPM provided 400% increase in resistance over the plain pile. It is also noted that the FRP-RHPM displayed better cyclic performance than the RHPM. The load carried by the FRP-RHPM was 60% to 100% higher than the load carried by the RHPM at relatively high displacement levels.

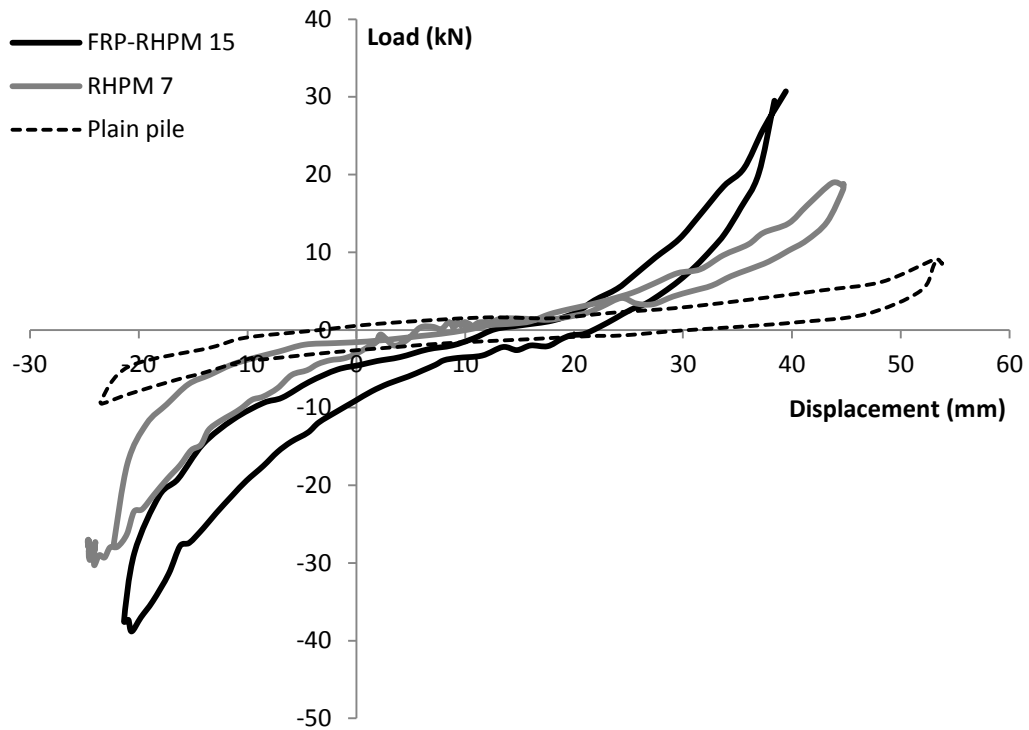


Figure 6.18. Cyclic load displacement for FRP-RHPM, RHPM and plain pile at last cycle of loading.

6.9 Ultimate capacity prediction

There are several methods reported in the literature for calculating the ultimate lateral capacity of a pile. Broms (1964a and b) proposed methods for estimating the ultimate capacity based on limiting equilibrium analysis. These methods predict the ultimate capacity for short and long piles. For short piles, the ultimate capacity corresponds to the maximum soil resistance, while for long piles it corresponds to the maximum moment resistance of the pile cross-section. Puri et al. (1984) provided one of the first attempts to estimate the lateral capacity of helical piles with circular shafts. They looked at field test data in sandy soil, clay fissured clay and fissured clay. In addition, they conducted 1/4-scale model tests on piles in dry sand with a lead section and one extension. Lead

sections with one, two and three helix anchors were considered, with helix diameter decreasing with depth. They observed that the ultimate capacity of test piles was the same, and concluded that the lateral load capacity was essentially governed by the extension shaft. They modified the equations developed by Reese and Matlock (1956) and Davisson and Gill (1963) by introducing a coefficient that reduced the ultimate capacity by the aforementioned methods by a factor of 3. They indicated that the modified factor provides reasonable estimates for loads higher than 1/3 of the load at 25.4 mm (1in.) displacement.

Currently, there is no available analytical method for estimating the lateral performance and ultimate capacity for RHPMs and FRP-RHPM. LPILE Plus (Ensoft Inc. 2011) program, which is based on the p-y curves approach, is widely used for lateral load applications. For proper modelling of the pile, the moment resistance versus the flexural rigidity of the pile cross-section should be adequately evaluated. The flexural rigidity is a function of the properties of steel-fibre reinforced grout shaft, where crack initiation and propagation is the main factor in its bending resistance. A ready-to-use embedded cross-section in LPILE Plus (Ensoft Inc. 2011) that incorporates steel-fibre reinforced piles (uncased or cased in a FRP tube) is not available. As such, a 3-dimensional FE model was developed using the program ABAQUS (Habitt et al., 2011).

6.9.1 Section properties estimation through FE analysis

The RHPM and FRP-RHP shafts system were simulated using a 3-D FE model comprised of eight-noded hexahedron elements, C38DR, to represent the reinforced grout, the steel shaft and the FRP pipe. The pile shaft system was modelled as a

cantilever beam fixed at the base, and load applied at its top. The round-square shaft was modelled as a circular shaft with a diameter calculated to provide the same moment of inertia by the 45 x 45 mm section.

As mentioned above, separation between the steel shaft and the grouted column was observed during field experiments. Therefore, the pile system was modelled such that separation between the grouted shaft and the steel shaft (extension), and between the grout column and the FRP pipe was allowed. The coefficient of friction between grout and steel, and between grout and FRP was taken as, $\mu = 0.43$.

Symmetry was exploited in order to reduce the computational time and effort, and the pile model was simplified to a half symmetric model. A fully fixed boundary condition was applied to the base of the pile. A typical mesh is shown in Figure 6.19.

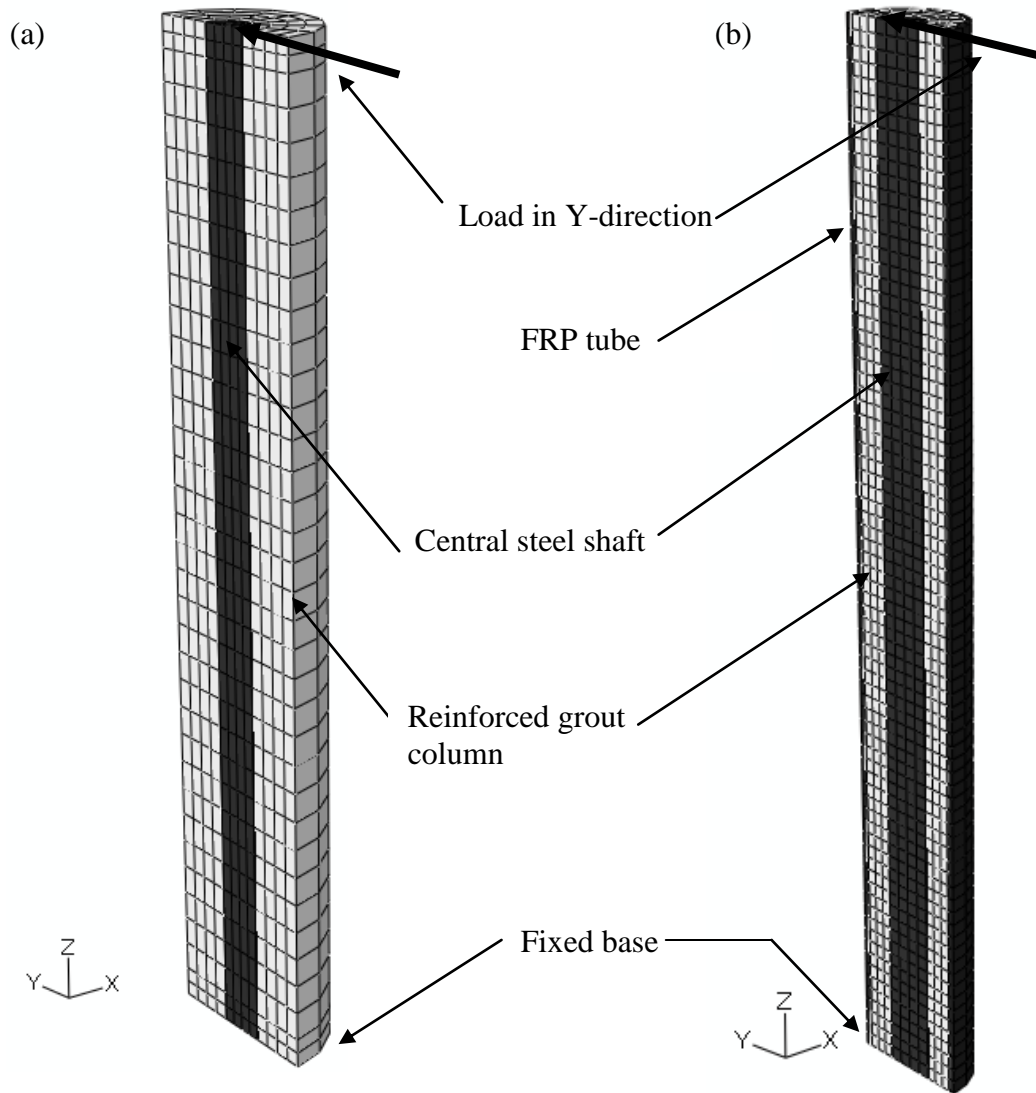


Figure 6.19. Typical finite element mesh, (a) RHPM, and (b) FRP-RHPM.

6.9.1.1 Concrete, steel and FRP parameters

The response of steel-fibre reinforced grout (or concrete) is characterized by its tensile softening behaviour (Abbas and Mohsin, 2010). The steel-fibre reinforced grout behaviour is described using a plastic-damage model. steel-fibre reinforced grout parameters used in this study are: compressive strength $f_c' = 47$ MPa, compression modulus of elasticity $E_{\text{grout}} = 30.1$ GPa, Poisson's ratio $\nu_{\text{grout}} = 0.2$, strain at ultimate stress

$\varepsilon_{cu} = 0.0036$, tensile strength $f_t = 4.23$ MPa ($= 9\% f_c'$ - surveyed literature indicated that f_t does not exceed $9\% f_c'$), biaxial to uniaxial compressive ratio $f_{bu}/f_{cu} = 1.16$ (Kupfer et al., 1969), and the ratio of the second stress invariant on the tensile meridian to that on the compressive meridian for a given value of the first stress invariant $K_C = 2/3$ (Lubliner et al., 1989).

The compression behaviour model proposed by de Oliveira Junior et al. (2010) was adapted as shown in Figure 6.20a, with the compressive damage parameter equal to zero. The tensile behaviour was described by a linear stress-strain curve until cracking, considering the tension modulus of elasticity $E_t = E_{grout}$, and damage parameter $d_t = 0.75$. Post cracking behaviour was described by a multi-linear stress-strain softening relationship based on Tlemat et al. (2005) was adapted as shown in Figure 6.19b.

The Von-Mises plasticity criterion was used to define the yield and post yield behaviour of steel. A bi-linear stress-strain relationship was adapted. The steel parameters were taken as: Young's modulus $E_s = 200$ GPa, Poisson's ratio $\nu_s = 0.3$, yield stress $f_{ys} = 621$ MPa, and ultimate strength $f_{uts} = 760$ MPa. The coefficient of friction between hardened grout and steel $\mu_c = 0.43$. The same criterion (Von-Mises) was used for the FRP pipe with a linear-perfect plastic stress-strain relationship assumed. The yield stress $f_{utFRP} = 80$ MPa, $E_{FRP} = 12700$ MPa, and Poisson's ratio $\nu_{FRP} = 0.45$.

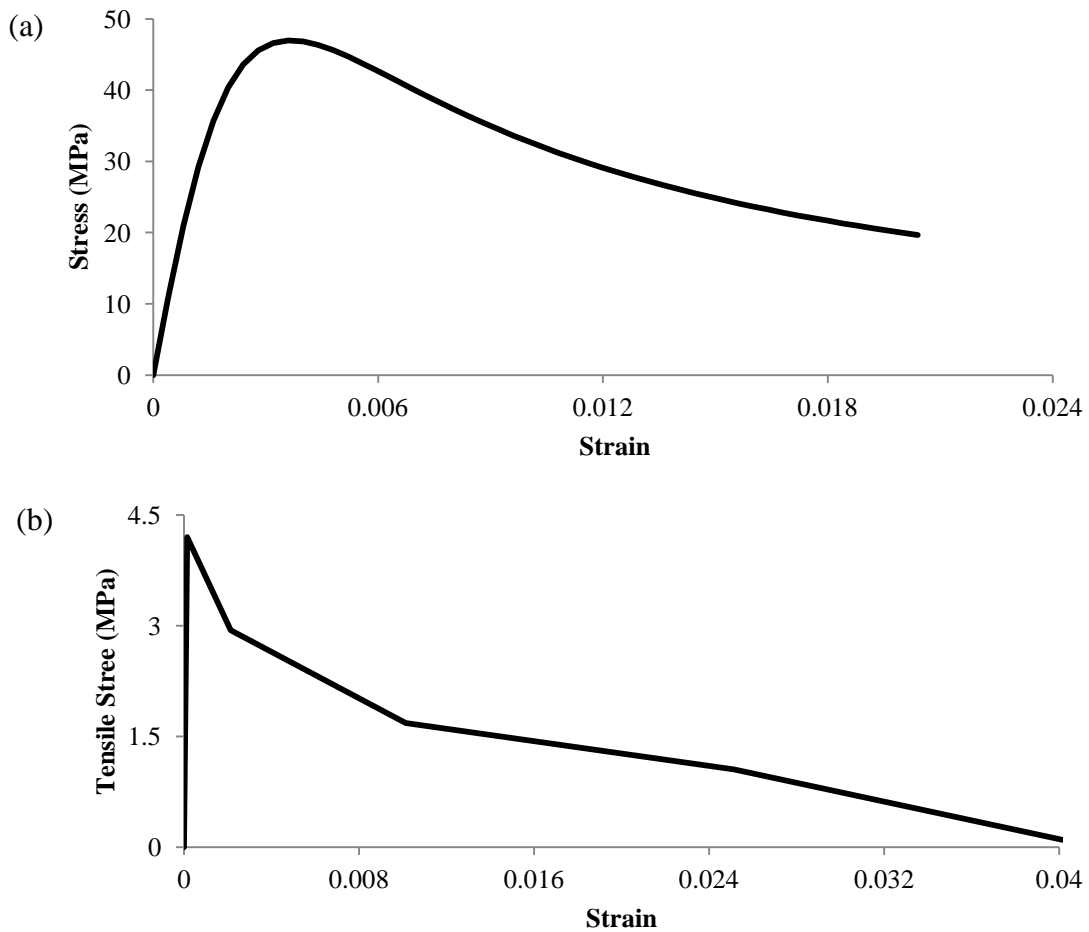


Figure 6.20. Fibre-reinforced grout model: (a) in compression; (b) in tension.

To estimate the M-EI curves, a simplified approach was employed. The moment at a cross-section was calculated as the resultant of the applied load times the distance to the cross-section under consideration. To calculate the curvature, the strain values in the steel shaft were used.

Computed M-EI curves are shown in Figure 6.21. The results show that while the RHPM has a higher initial stiffness (as predicted because of larger diameter), the FRP casing

results in slower rate of rigidity degradation as the load increases, and in higher moment capacity of the pile cross-section.

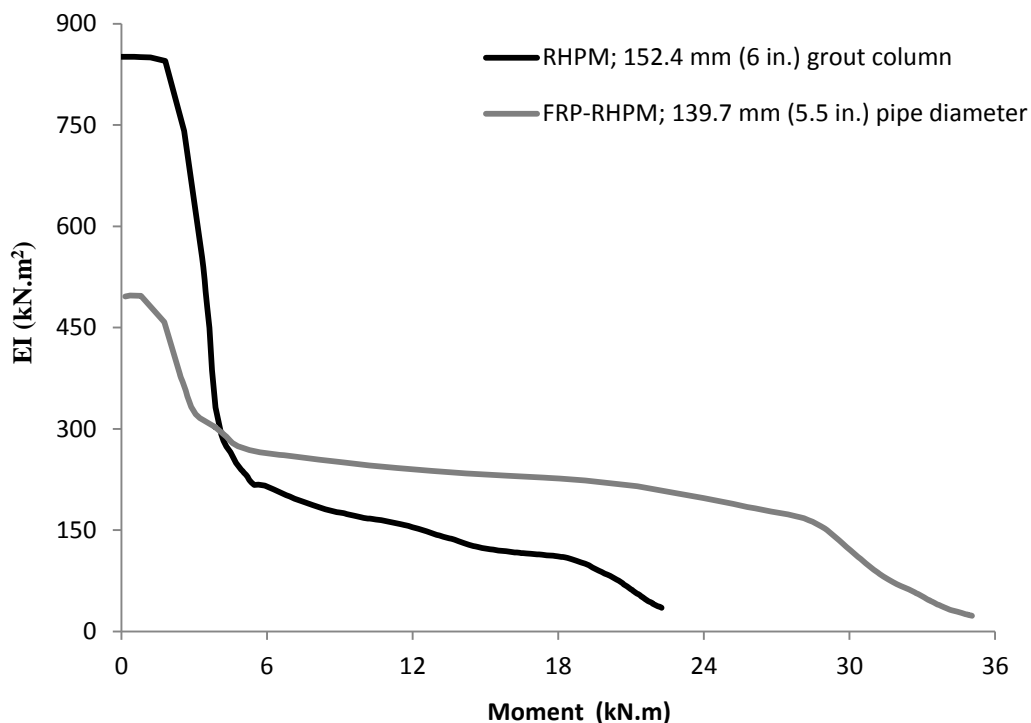


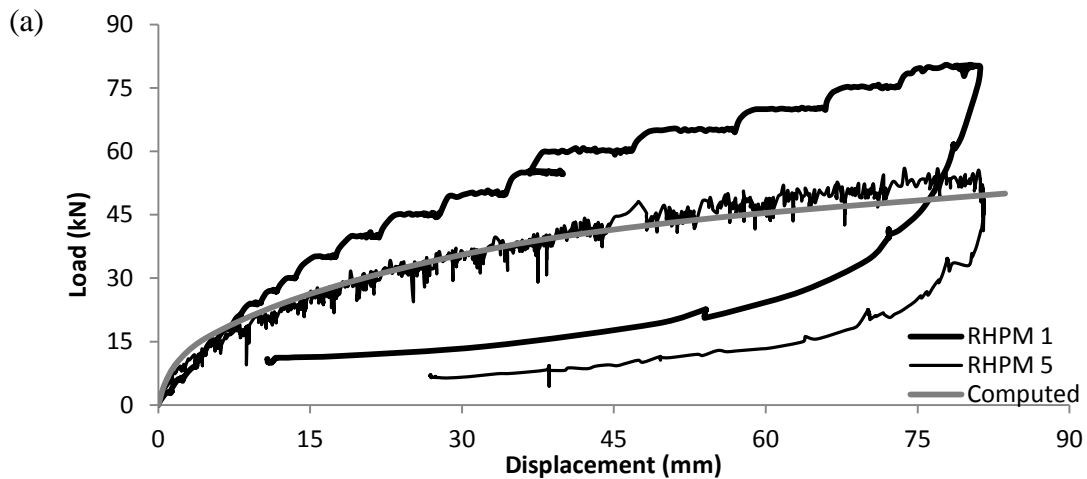
Figure 6.21. Computed M-EI for RHPM and FRP-RHPM test piles.

6.9.2 LPILE Plus Analysis and Results

The soil parameters used in the analysis are shown in Table 6.2. The soil along the shaft was modeled as stiff clay. These parameters were chosen based on the available SPT counts (Sivrikaya and Toğrol, 2006) and lab testing. The initial calculated response was stiffer than the test results. Therefore, the soil modulus was modified at ground level to 136,000 kPa. The pile steel shaft was above ground by 76 mm simulating the experiment conditions. The sectional properties for RHPM and FRP-RHPM were obtained from the

ABAQUS (M-EI) analysis as mentioned above. The steel shaft was represented using the existing built-in options in LPILE Plus.

Figure 6.21 compares the computed and the experimental results. As can be noted from Figure 6.21, the computed and measured responses for the RHPM are in good agreement (Figure 6.21a). However, the computed response for the FRP-RHPM was very flexible compared with the measured response (Figure 6.21b). This may be explained by the existence of a layer of grout surrounding the FRP pipe. This layer was observed (upon excavating) to have a minimum thickness of 50 mm at a depth of 1.8 m. To be on the conservative side, this layer was not accounted for in the M-EI analysis. It should be noted that better match between computed and test results was achieved by increasing the undrained shear strength in the top 1.8 m, simulating an equivalent soil layer comprised of the native soil and the layer of grout surrounding the FRP pipe.



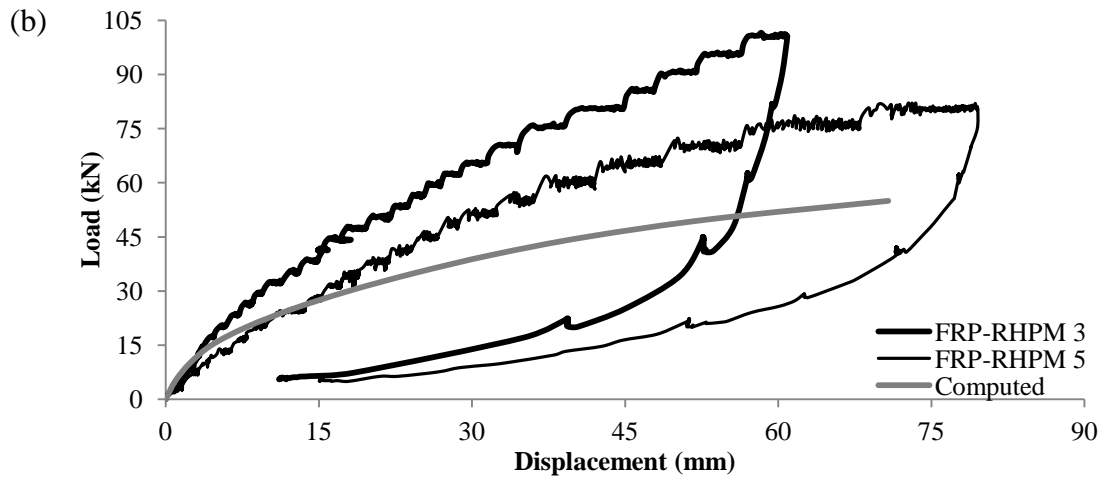


Figure 6.21 Comparison between computed and experimental results for (a) RHPM 3; (b) FRP-RHPM 5.

6.10 Development of Design charts

Moment-rigidity curves were developed using finite element analysis employing ABAQUS for steel shaft sizes: SS175 (45.5 mm) (dimensions?), SS200 (50.8 mm) (dimensions) and SS225 (57.15 mm) (dimensions) piles and grout shaft sizes 152.4 mm (6in.), 177.8 mm (7 in.) and 203.2 mm (8 in.), as shown in Figure 6.22. Such charts can be used in conjunction with LPILE Plus for design purposes of RHPM with different soil types. Figure 6.22 demonstrates that an increase in the diameter results in a considerable increase in the pile rigidity until cracking is sufficiently developed in the grout column. When cracking develops fully, the pile rigidity drops to an almost constant value for all grout diameters. However, piles with larger grout columns have higher moment capacities, as expected.

To further illustrate the effect of pile size on the later capacity, LPILE Plus analysis was conducted for three cases, 152.4 mm grout shaft encasing an SS175, 152.4 mm grout shaft encasing an SS200, and 177.8 mm grout shaft encasing an SS225. The results are

plotted in Figure 6.23, which clearly show that increasing the grout diameter from 152.4 mm, to 177.8 mm or increasing the steel shaft size from SS175 to SS200 had the same effect. It should be noted that, if constructible, increasing the grout column size may be more economical than increasing the steel shaft size.

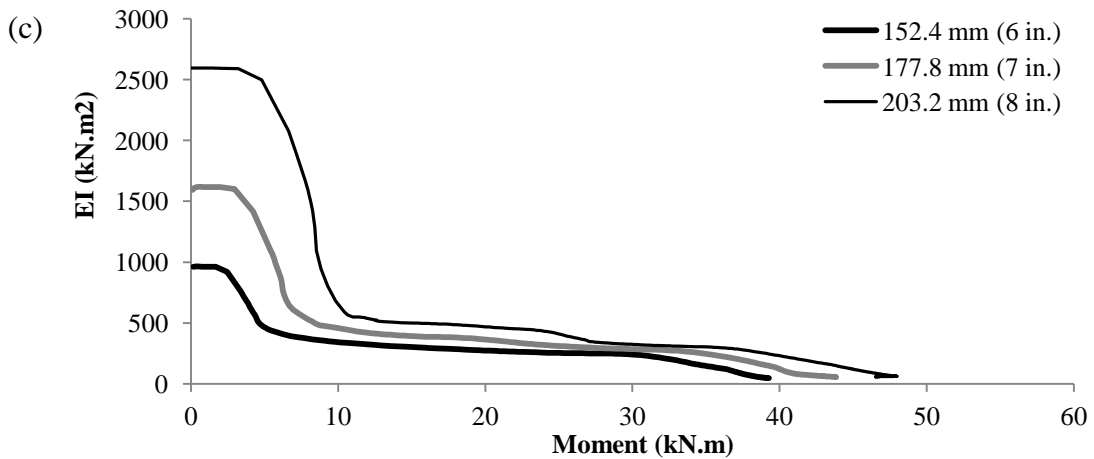
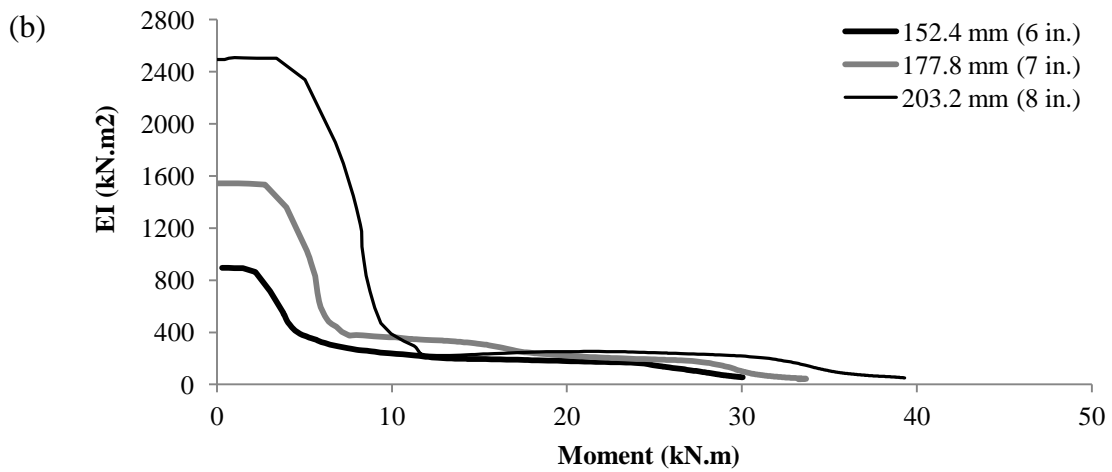
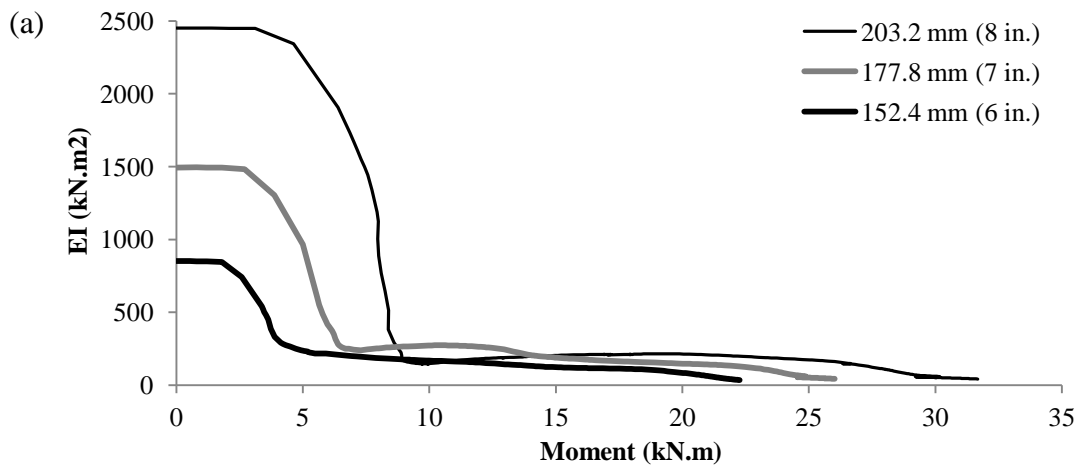


Figure 6.22. M-EI charts for 152.4 mm (6 in.), 178.8 mm (7 in.) and 203.2 mm (8 in.) grout shaft diameters for: (a) SS 175; (b) SS 225; (C) SS 225.

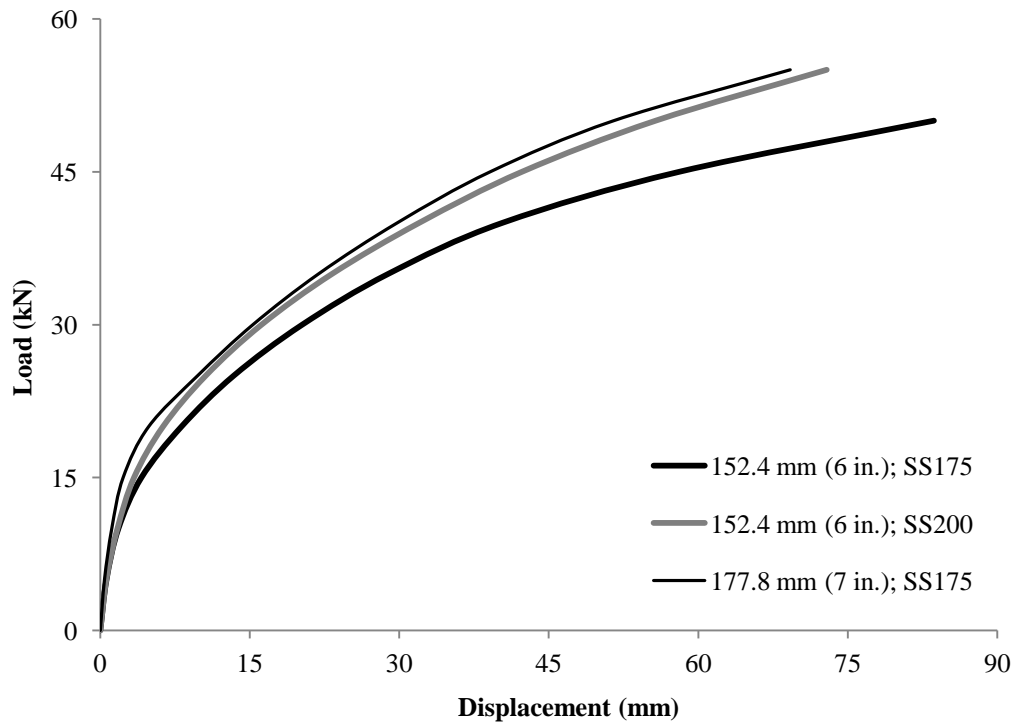


Figure 6.23. Computed load-displacement curves for RHPM with different shaft configurations.

M-EI charts were also developed for the FRP-RHPM considering some commercially available FRP pipes. The developed M-EI charts are presented in Figure 6.24. As mentioned earlier, using the developed M-EI without due consideration of potential grout layer around the FRP pipe may produce very flexible (overly-conservative) results, especially at high deflections. It is recommended that these M-EI charts to be used along with soil input data modifications to account for the grout layer surrounding the FRP pipe.

It can be seen that reducing the pipe size from 140 mm (5.5 in.-used in test piles) to 125 mm (5.0 in.) had a larger effect than reducing the pipe size from 125 mm in. to 116 mm

(4.5 in.). It should be noted that the pipe thickness for the 140 and 116 pipe is 7.62 mm, and for the 125 is 7.1 mm.

Figure 6.25 presents the results for different FRP-RHPM configurations. As can be seen from Figure 6.25, increasing the shaft size from the considered systems had a negligible effect on the pile lateral performance. However, increasing the pipe shaft diameter resulted in a noticeable improvement in performance (at 75 mm displacement, resistance increased by about 14%).

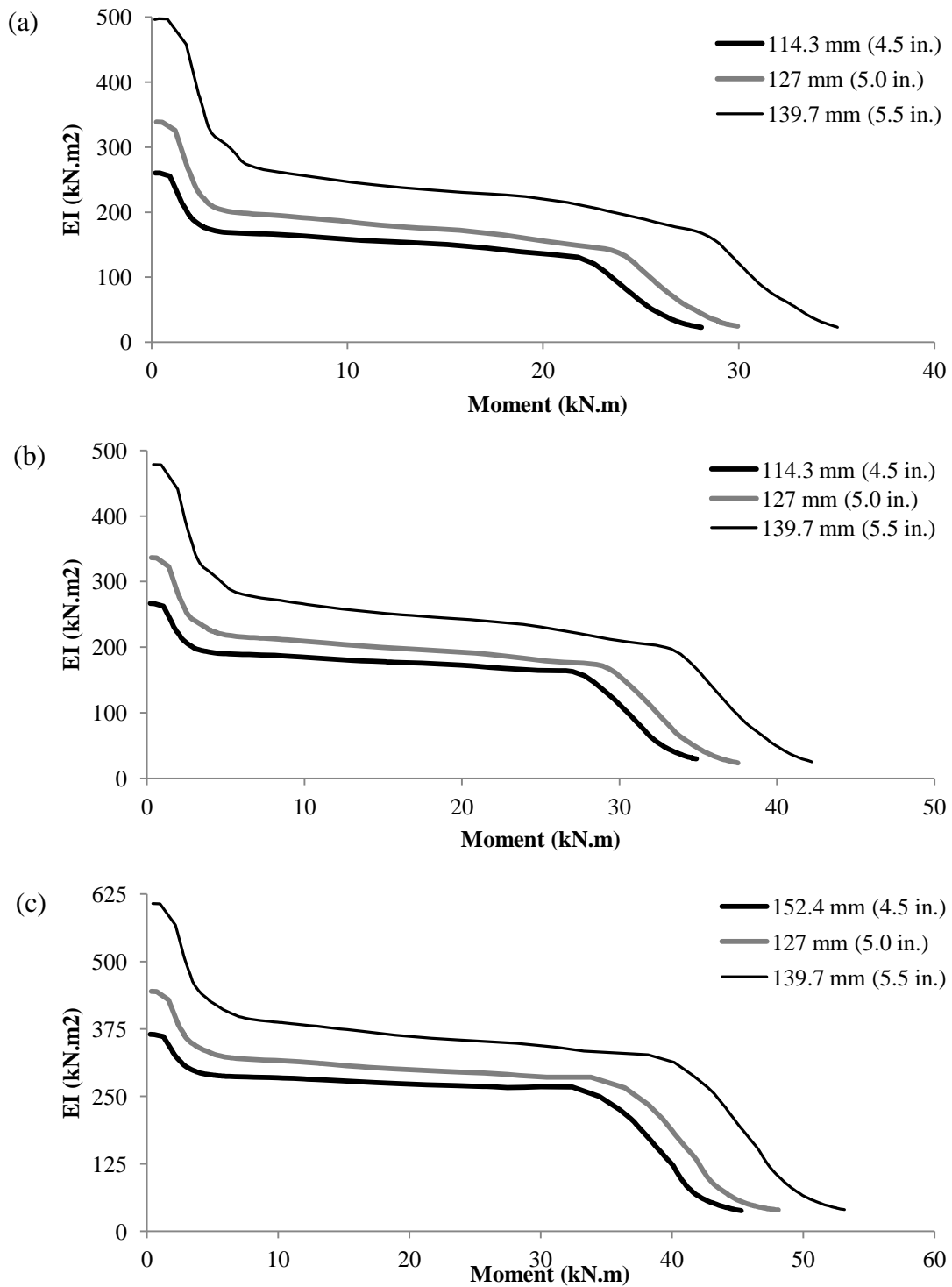


Figure 6.24. M-EI charts for 140 mm (5.5 in.), 125 (5 in.) and 116 (4.5 in.) FRP pipe diameter for: (a) SS 175; (b) SS 225; (C) SS 225.

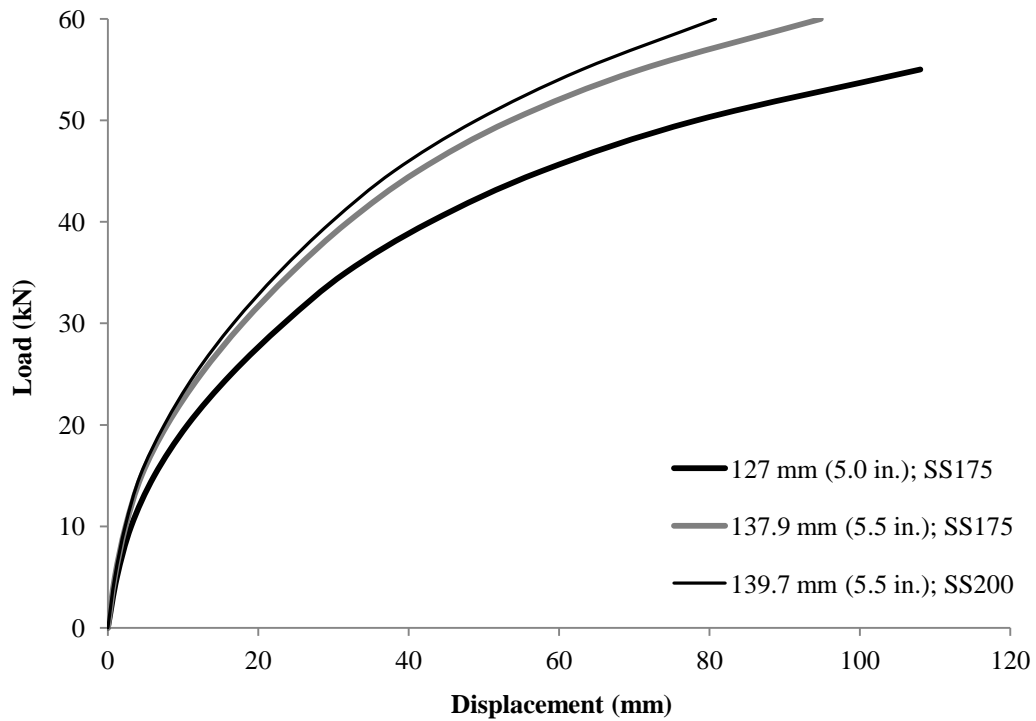


Figure 6.25. Computed load-displacement for different FRP-RHPM configurations.

6.11 Conclusions

A full-scale lateral load testing program was conducted on two innovative pile systems, namely, the steel fibre reinforced helical pulldown micropile (RHPM) and Fibre reinforced polymer-steel fibre reinforced helical pulldown micropile (FRP-RHPM). The piles were tested under lateral static and cyclic loads. In addition, the effect of lateral cyclic loading on the axial performance of FRP-RHPM was examined. Based, on the experimental observations, the following conclusions may be drawn:

- The steel-fibre grout column has considerably improved the pile ultimate capacity. In addition, the piles exhibited significant ductility (no sudden deflection up to 75 mm

displacement.-50% of pile diameter). However, separation between the steel shaft and the grout column was observed during testing.

- The composite FRP-RHPM pile had an improved capacity over the RHPM by 30-35%. In addition, no cracking was observed within the FRP pipe, preserving the structural integrity of the composite pile system, and further enhancing its ductility.
- The FRP-RHPM and RHPM displayed superior cyclic performance compared to the plain helical pile. Both piles showed significant ductility (i.e. sustained displacement of more than 50% of pile diameter). Also, the cyclic performance of the FRP-RHPM was superior to the cyclic performance of the RHPM (about 60-100% stiffer).
- Two-way cyclic loading resulted in overall degradation in pile stiffness and capacity. Degradation was found to stem from the formation of gaps rather than degradation of soil strength. It was found that the formation of gaps caused the piles to have a "preferential direction" with one side providing stiffer response than the other. The piles should be designed considering the softer response part.

The piles response in second and subsequent cycles displayed three distinct branches: pile behaving as a free cantilever, the pile moving through the gap; and linear or non-linear response after the gap is closed and the soil resistance is mobilized. The backbone curve (envelope) of the cyclic load-displacement has the same shape of the static response curve, but reduced stiffness and ultimate capacity.

- The FRP-RHPM axial behavior was not affected after being subjected to lateral cyclic loading; showing that the effect of cyclic loading was limited to a shallow length of the pile.

- RHPM and FRP-RHPM performance can be reasonably estimated using the developed EI-M charts along with the LPILE Plus (Ensoft Inc. 2011).
- Increasing the size of the steel shaft size or pile diameter increases the ultimate capacity of the RHPM. Meanwhile, the performance of the FRP-RHPM is dominated by the size of the FRP pipe.

6.12 References

Abbas, A., and Mohsin, S.S. 2010 Numerical modeling of fibre-reinforced concrete. In proceedings the international Conference on Computing in Civil and Building Engineering.

Abd Elaziz, A.Y., and El Naggar, M.H. 2012. Axial behaviour of hollow core micropiles under monotonic and cyclic loadings. *Geotechnical Testing Journal*, ASTM, 35 (2), 249-260.

Abdelghany, Y., and El Naggar, M.H. 2010. Full-scale experimental and numerical analysis of instrumented helical screw piles under axial and lateral monotonic and cyclic loadings-A promising solution for seismic retrofitting. In Proceedings of the 6th International Engineering and Construction Conference. American Society of Civil Engineers, Cairo, Egypt.

Armour, T., Groneck, P., Keeley, J., and Sharma, S. 2000. Micropile design and construction guidelines-implementation manual. Federal Highway Administration FHWA-SA-97-070, El Sharnouby, M.M, and El Naggar, M.H. 2012. Field investigation

of axial monotonic and cyclic performance of reinforced helical pulldown micropiles. Canadian Geotechnical Journal, 49(5): 560-573.

Davisson, M.T., and Gill, H.L. 1963. Laterally loaded piles in layered soil system. Journal of Soil Mechanics and Foundation Engineering Division, ASCE. part 1, 89(SM3): 63-94.

de Oliveira Junior, L.A., dos Santos Borges, V.E., Danin, A.R., Machado, V.R., de Lima Araujo, D., El Debs, M.KH., Rodrigues, P.F. 2010 Stress-strain curves for steel-fibre reinforced concrete in compression. Revista Materia. 15(2): 260-266.

El Sharnouby, M.M, and El Naggar, M.H. 2012. Axial monotonic and cyclic performance of FRP-steel fibre-reinforced helical pulldown micropiles (FRP-RHPM).Canadian Geotechnical Journal, Accepted.

Ensoft Inc. 2011. LPILE PLUS 6: A program for the analysis of piles and drilled shafts under lateral loads. Version 6.0.27 [computer program]. Ensoft Inc., Austin, Tex.

Hibbitt, H.D., Karlsson, B.I., and Sorensen, E.P. 2011. General purpose finite element analysis program. version 6.9. Habbitt, Karlsson & Sorensen, Inc., Pawtucket, R.I.

Kupfer, H., Hilsdorf, H.K., and Rusch, H. 1969. Behavior of concrete under biaxial stress. ACI Journal, 66(8): 656-66.

Lubliner, J., Oliver, J., Oller , S., and Onate, E. 1989. Plastic-damage model for concrete. International Journal of Solids and Structures, 124(8): 892-900.

Lutenegger, A.J. 2010. Shaft resistance of grouted helical micropiles in clay. In Proceeding of the 10th International Workshop on Micropiles. International Society of Micropiles, Washington, D.C., USA, pp. 22-25.

Mittal, S., Ganjoo, B., & Shekhar, S. 2010. Static Equilibrium of Screw Anchor Pile Under Lateral Load in Sands. *Geotechnical Geological Engineering*, 28: 717-725.

Perko, H.A., 2009. *Helical piles: a practical guide to design and installation*. John Wiley & Son, Inc., Hoboken, N.J., 512 p.

Prasad, Y., & Narasimha Rao, S. 1996. Lateral Capacity of Helical Piles in Clays. *Journal of Geotechnical Engineering* , 938-941.

Puri, V.K., Stephenson, R.W., Dziedzic. E., and Goen, L. 1984. Helical anchor piles under lateral loading. *Laterally Loaded Deep Foundations: Analysis and Performance (STP 835)*, American Society for Testing and Materials, pp. 194-213.

Reese and Matlock (1965). Non-dimensional solution for laterally loaded piles with soil modulus assumed proportional to depth. In proceedings, of the Eighth Texas Conference on Soil Mechanics and Foundation Engineering.

Sakr, M. 2009. Performance of helical piles in oil sand. *Canadian Geotechnical Journal*, 46(9): 1046-1061.

Tlemat, H., Pilakoutas, K., and Neocleous, K. 2006. Modelling of SFRC using inverse finite element analysis Tlemat, H. ; Pilakoutas, K.; Neocleous, K. Materials and Structures. 39: 221-233.

Vickers, R.A., and Clemence, S.P. 2000. Performance of helical piles with grouted shafts. In Proceedings of Sessions of Geo-Denver 2000 - New Technological and Design Developments in Deep Foundations. American Society of Civil Engineers, GSP 100, v 288, pp. 327-341.

Table 6.1. Test results for RHPM and FRP-RHPM.

Pile No.	Lateral resistance at 6.25 mm (kN)	Lateral resistance at 12.5 mm (kN)	Lateral resistance at 25 mm (kN)	Lateral deflection at end of test (mm)	Lateral resistance at end of test (kN)
RHPM					
1	17	29.6	45	81	80.3
2	12.6	22.7	34.4	86	61.4
3	24.6	40.1	66.4	45.9	95.6
4	13.7	23.4	32.5	46.7	52.7
5	14.5	22.6	31.6	81.5	56
6	10.5	18	27.4	91.5	56.9
Average	15.5	26	39.6	-	-
FRP-RHPM					
1	22.3	43.3	59.7	76.5	100.4
2	21.9	35	54.9	80.7	68.8
3	22.1	34.9	54.9	68	83.5
4	24.8	32.2	53.1	45.4	73.5
5	13.3	24.3	45.8	72.7	82.1
Average	20.9	33.9	53.7	-	-
% increase over RHPM	34.8	30.2	35.7	-	-

Table 6.2. Soil properties used in LPILE Plus (Ensoft Inc. 2011).

Soil layer	Depth (m)	Undrained shear strength (kPa)
Stiff clay	0-0.3	132*-166
Stiff clay	0.3-1.8	166
Stiff clay	1.8-4.0	166-155
Stiff clay	4.0-6.0	155-145

*Soil modulus parametrically chosen as 136,000 kPa/m

SUMMARY, CONCLUSIONS AND RECOMMENDATIONS

7.1 Summary and Conclusions

The main objective of this research program was to assess the performance of plain helical piles, fibre-reinforced helical pulldown micropiles (RHPM) piles, and FRP-steel fibre-reinforced helical pulldown micropiles (FRP-RHPM) FRP-RHPM piles under axial and lateral monotonic and cyclic loading conditions.

A full scale experimental program was conducted to evaluate one plain helical pile, 12 RHPM and 12 FRP-RHPM. Piles were tested under axial static and one-way cyclic loadings, and lateral static and two-way cyclic loadings. Strain gauges were mounted strategically located such that the load sharing and transfer mechanism under axial loading were evaluated.

Chapter 3 presents the results of a full-scale experimental program on steel fibre-reinforced helical pulldown micropiles (RHPM). Piles were subjected to axial monotonic and cyclic loads. The tested RHPM performs as a composite foundation system. Piles display the typical trend consisting of an initial branch, followed by a transitional branch than a near-linear branch. The results show significant shaft contribution to the total resistance. The load transfer mechanism for the lead section is through individual helices bearing.

The pile performance during 15 cycles of loading was found to be satisfactory. The shaft resistance decrease is accommodated by the lead section, where bearing of the top helix dissipating the excess load transferred to the lead section. One way axial cyclic loading slightly improved (up to 6%) the ultimate axial stiffness and axial capacity of tested piles.

The shaft friction ultimate resistance can be estimated by adapting typical design correlations for type A micropile. The bearing capacity can be estimated by considering the sum of individual bearing resistance for the helical plates. In general, the RHPM pile was shown to be a viable foundation system for axial monotonic and one-way cyclic loading applications.

Chapter 4 presents an innovative installation technique for constructing the FRP-RHPM that was developed to overcome the installation difficulties associated with excessive friction along the FRP tube. The novel installation procedure proved to be feasible and mitigated the shortcomings of previously used methods. The tested FRP-RHPM performs as a composite foundation system. The load-displacement curves of this pile system display the typical trend of conventional piles consisting of an initial branch, followed by a transitional branch followed by a near-linear branch.

The pile performance during 15 cycles of loading was found to be satisfactory. The displacement per cycle decreased with number of cycles. No notable degradation in the stiffness was observed. Uniform stable degradation of the pile shaft resistance was observed. The degradation was counter balanced by the stiffening effect from the lead

section. Cyclic loading may considerably improve the axial performance and capacity by up to 15% for pile installed in similar soil conditions.

The pile ultimate capacity for axial static or cyclic loading applications can be conservatively estimated using the conventional available methods. In general, the FRP-RHPM pile was shown to be a viable foundation system for axial monotonic and one-way cyclic loading applications.

Chapter 5 presents development and validation of three-dimensional finite element model that simulated the behaviour of plain helical piles, RHPM and FRP-RHPM under axial loading. No interaction was found to occur between the grouted shaft and the lead section. Estimation of pile capacity was examined against available methods in literature and most suitable methods are identified.

Based on the field testing and the numerical analysis conducted in this research, a design procedure for FRP-RHPM and RHPM under axial compression loading conditions is presented.

Chapter 6 contains the components of a specially designed and manufactured dual-testing system that allows testing two piles under lateral static and cyclic loading simultaneously. In this chapter, the test results on RHPM and FRP-RHPM under lateral monotonic and two-way cyclic loading are presented. The results showed that the steel-fibre grout column have drastically improved the ultimate capacity of the pile. In addition, the piles showed a significant ductility. The composite FRP-RHPM pile showed an improved capacity to the RHPM by 30-35%.

The FRP-RHPM and RHPM displayed superior cyclic performance compared to the plain helical pile. Two-way cyclic loading resulted in overall degradation in pile stiffness and capacity. However, degradation was found to stem from the formation of gaps rather than soil stiffness degradation for the load levels applied. Increasing the steel shaft size or the pile diameter increases the ultimate capacity of the RHPM. Meanwhile, the performance of the FRP-RHPM is predominantly affected the FRP pipe size. Finally, the FRP-RHPM axial behavior was not affected after being subjected to lateral cyclic loading; showing that the effect of cyclic loading was limited to a shallow length of the pile.

A parametric study was conducted that included typical pipe and grout sizes currently used in application. The study led to a series of design charts that can be used in conjunction with available numerical programs to design such systems under lateral loads.

7.2 Recommendations for future research

The current research revealed that some further studies on the RHPM and FRP-RHPM may be needed. The following are recommendations for future research:

1-Evaluate the performance of RHPM and FRP-RHPM soft and medium clay conditions to determine the frictional resistance along the pile shaft.

2-Examine the effect of higher cyclic loading range on the pile's performance and ultimate capacity.

3-Investigate the lateral performance of RHPM and FRP-RHPM under cyclic loading with large number of cycles may need to be investigated.

4-Investigate the buckling capacity of the RHPM and FRP-RHPM through field testing and numerical modelling.

5-Determine the performance of these systems under tension loading.

6-Perform full-scale testing on pile groups to examine the group effect on the piles' performance.

APPENDIX A

In this appendix, sample of the installation torque versus depth for the SS 225, SS 200 and SS 175 for are provided, as can be seen below.

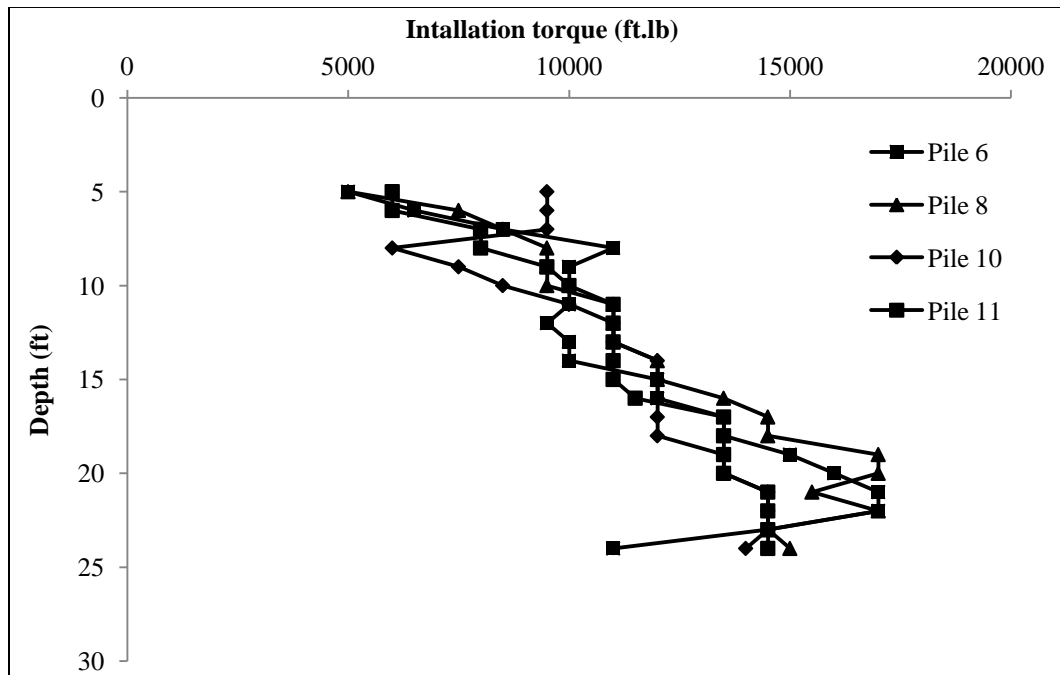


Figure A.1. Installation torque versus depth for SS 225 piles used for pre-drilling. Pile numbers correspond to same pile numbers in Chapter 3.

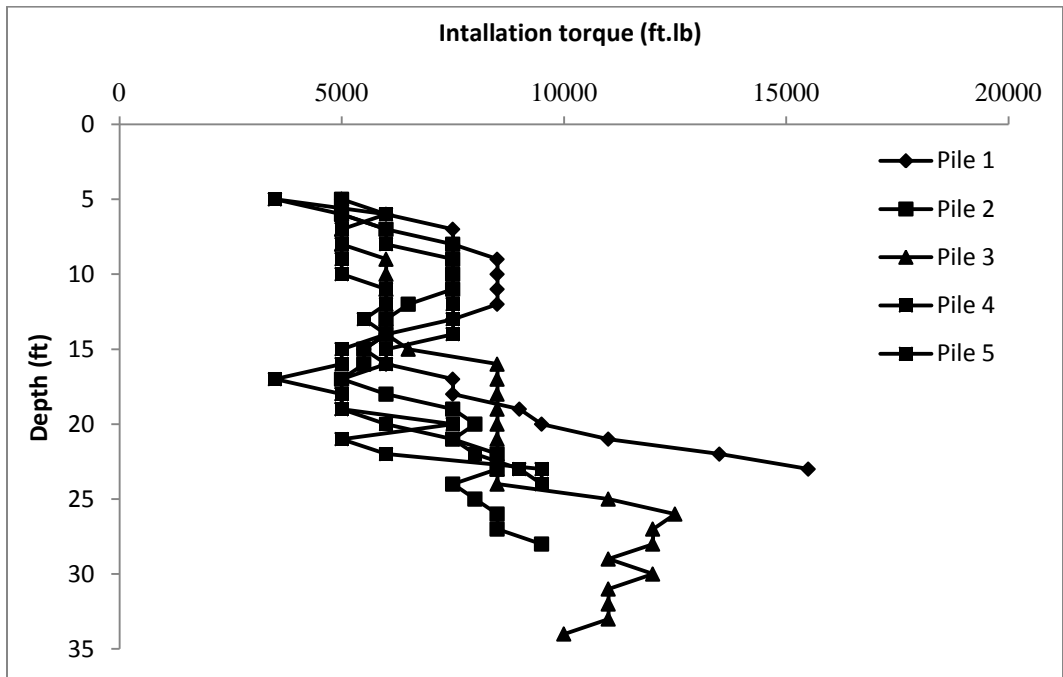


Figure A.2. Installation torque versus depth for SS 200 reaction piles.

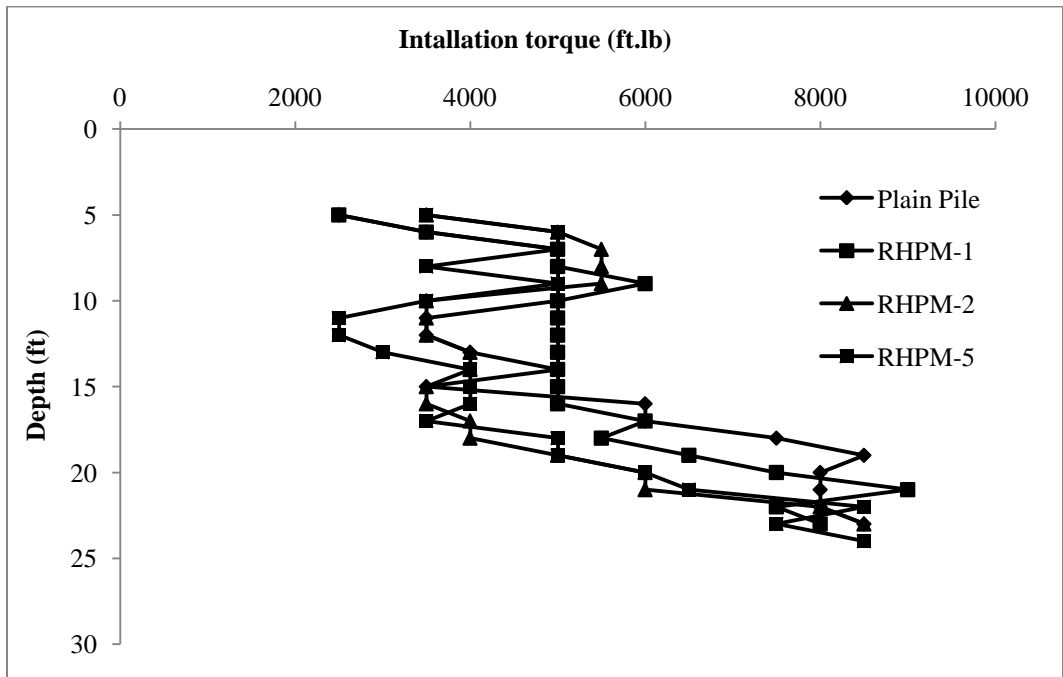


Figure A.3. Installation torque versus depth for RHPM.

CURRICULUM VITAE

M. Meckkey El Sharnouby

▪ Education

- Ph.D. Candidate in Civil and Environmental Engineering **2008-present**
Western University, London, Ontario
- Master of Engineering Science in Civil Engineering **2006-2008**
Western University, London, Ontario
- Bachelor's Degree in Civil Engineering with Distinction **1999- 2004**
Alexandria University, Alexandria; Egypt

▪ Relevant Work Experience

- AMEC (under supervision of M. Hehsam El Naggar, , Western University): **2007-2011**
Analysis of machine foundations using Dyna5 and SAP 2000
- Team leader: Supervised co-op and NSERC students (2) during PhD project. **Summer 2011**
- Naeema Consulting Office: Seismic analysis of structures according to Egyptian Code (using quasi-static analysis) **Winter-2005**
- Teaching Assistant at Western University: Finite Element Methods in Engineering; Structural Theory and Design I. **2006-present**
- Teaching Assistant at Alexandria University: Harbour Design and Analysis; Engineering Geology. **2004-2006**

Awards and Honours

- Natural Sciences and Engineering Research Council of Canada (NSERC CGS D **2010-2012**

- Canadian Geotechnical Society -SOS Graduate Presentation Student University Competition: 1st Place **2011**
- Ontario Graduate Scholarship (OGS) **2006-2007; 2007-2008; 2008-2009; 2009-2010**
- John Booker Award- Geotechnical Research Centre, Western University **2008**
- Nominated for the "Best Teaching Assistant Award" for five consecutive years (selection is based on students and faculty members' nominations), Western University.
2007-2008; 2008-2009; 2009-2010; 2010-2011

Publications

- El Sharnouby, M.M and El Naggar, M.H. 2012. Field investigation of axial monotonic and cyclic performance of reinforced helical pulldown micropiles. Canadian Geotechnical Journal, 49(5), pp 560-573.
- El Sharnouby, M.M and El Naggar, M.H. 2012. Axial monotonic and cyclic performance of fibre reinforced-polymer-steel reinforced-helical pulldown micropiles. Canadian Geotechnical Journal, in press.
- El Sharnouby, M. M. and El Naggar, M. H. 2011. Monotonic and cyclic axial full-scale testing of reinforced helical pulldown micropiles. In proceedings, 14th Pan-American Conference on Soil Mechanics and Geotechnical Engineering.
- El Sharnouby, M. M. and El Naggar, M. H. 2011. Monotonic and cyclic lateral full-scale testing of reinforced helical pulldown micropiles. In Proceeding, the 36th Annual Conference on Deep Foundations.
- El Sharnouby, M. M. and El Naggar, M. H. 2011. Shear behaviour of expansion anchors. In Proceeding, Computational Geomechanics, COMGEO II.
- El Sharnouby, M. M. and El Naggar, M. H 2010. Numerical Investigation of Response of Single and Double Expansion Anchors to Axial Load. Canadian Journal of Civil Engineering, 37 (6), pp 866-877.
- El Sharnouby, M. M. and El Naggar, M. H. 2009. Numerical analysis of expansion anchors. In Proceeding, Computational Geomechanics, COMGEO I.